https://doi.org/10.35662/unine-thesis-3098

Université de Neuchâtel

DEVELOPING THE BIOLOGICAL POTENTIAL OF ORGANOMETALLIC CAGES

Thesis submitted to the University of Neuchâtel,
for the title of Doctor in Science

by

Santiago Luis Pons Allés

Members of the jury:

Prof. Bruno Therrien – Thesis director, University of Neuchâtel

Prof. Stephan H. von Reuss – Internal examiner, University of Neuchâtel

Prof. Gilles Gasser - External examiner, Chimie ParisTech - PSL

Thesis defended on February 23rd, 2024

unine
Université de Neuchâtel
Faculté des sciences

Rue Emile-Argand 11
CH-2000 Neuchâtel
doctorat.sciences@unine.ch

IMPRIMATUR POUR THESE DE DOCTORAT

La Faculté des sciences de l'Université de Neuchâtel autorise l'impression de la présente thèse soutenue par

Monsieur Santiago Luis PONS ALLES

Titre :

"Developing the biological potential of organometallic cages"

sur le rapport des membres du jury composé comme suit :

- Ass. Prof. Bruno Therrien, directeur de thèse, Université de Neuchâtel, Suisse
- Prof. Stephan von Reuss, Université de Neuchâtel, Suisse
- Prof. Gilles Gasser, Chimie Paris Tech, Université PSL, France

Neuchâtel, le 4 mars 2024

Le Doyen, Prof. R. Bshary

Acknowledgements

First of all, I would like to thank Professor Bruno Therrien for giving me the opportunity of doing my PhD thesis in his group and guiding me through all this journey. Thanks for all the discussions and support, which helped me improve and develop as a scientist.

Thanks to Prof. Stephan von Reuss for his support during the final phases of my PhD and accepting to be part of my thesis jury.

I would like to thank as well Prof. Gilles Gasser, for accepting to be part of my thesis jury and all the remarks and discussion on my work.

Thanks to Dr. Arno Wiehe and Dr. Barbara for having me in their research labs during my secondments in Berlin and Bologna.

Thanks to all the members of the NOAH project, for all the meetings and all the scientific discussions.

Thanks to all my lab mates in Neuchâtel: Chrysanthi and Sirine, for everything we shared both in and outside of the lab, without your friendship and support I would have never succeeded. Manuel, for all the help and discussions in the lab. Alaa, Yueying, and Lou for making my final days in the lab much lighter and funnier.

Thanks to Désirée and Sarah, for all the games and moments. Thanks as well to all my colleagues from the faculty: Mareike, Antoine, Mathilde, Luana, Hanna, Yi-Ho. Thanks for all the laughs and lunch-breaks we shared.

Muchas gracias Daniel por todo lo compartido, hiciste que mis primeros meses en Neuchâtel y mi estancia en Bologna fueran mucho mas agradables.

Muchas gracias a todos mis amigos de Menorca, por hacerme sentir en casa cada vez que vuelvo y ayudarme a desconectar de todo lo demás.

Moltes gràcies Papa, Mama i Laura, per ser sa meva guia i exemple a seguir, voltrus sou sa sort mes grossa de sa meva vida.

Moltes gràcies a tu Maria, pel teu suport incondicional i per creure en mi més que jo mateix. Gràcies per estar al meu costat.

Abstract

Arene ruthenium metalla-assemblies are supramolecular structures which self-assemble through coordination forces. They are composed by different building blocks: clips and panels, the choice of which determines the final architecture of the assembly. This modular approach is what makes the functionalization of these systems most interesting, as different modifications can be introduced at the same time in a controlled manner. Three-dimensional structures such as prisms or cubes are possible, some of which possess a cavity capable of transporting hydrophobic molecules, making arene ruthenium assemblies relevant candidates for the design of novel drug delivery systems.

The aim of this thesis is to investigate the synthetic pathways to functionalize metalla-assemblies and to study their combination to obtain multi-functional platforms for biological applications. In a first approach, trigonal panels with different functional groups have been synthesized and used to form prisms. Then, those panels have been combined with double-arm pyrenyl derivatives, acting as guests, proving that prisms with functionalized panels are able to encapsulate functionalized guests. The same strategy has been applied in the synthesis of a set of third generation photosensitizers, based on assemblies with a biotinylated panel for targeting, and three different pyrenyl-photosensitizer guests for photodynamic therapy (PDT) applications. Their phototoxic activity has been tested on HCT116 human colorectal cancer cells.

Moreover, clips containing an oxamide spacer have been modified by introduction of functional groups such as alkylic chains with different amounts of hydroxyl groups or short PEG chains. These clips have been used in the synthesis of prisms and cubes to tune their water-solubility. Their hydrophilicity has been studied by calculating their octanol-water partition coefficient. Hydrophilic values have been obtained for both sets of samples.

Keywords

Arene ruthenium complexes, supramolecular chemistry, host-guest chemistry, photodynamic therapy, anticancer activity, phototoxicity, drug delivery

Résumé

Les métalla-assemblages d'arène ruthénium sont des structures supramoléculaires qui s'auto-assemblent grâce à des liaisons de coordination. Ils sont composés de différents éléments : clips et panneaux, dont le choix détermine l'architecture finale de l'assemblage. Cette approche modulaire est ce qui rend la fonctionnalisation de ces systèmes très intéressante, car différentes modifications peuvent être introduites en même temps et de manière contrôlée. Des structures tridimensionnelles telles que des prismes ou des cubes sont possibles, dont certaines possèdent une cavité capable de transporter des molécules hydrophobes, ce qui fait des assemblages arène-ruthénium des candidats pertinents pour la conception de nouveaux systèmes d'administration de médicaments.

L'objectif de cette thèse est d'étudier les voies synthétiques permettant de fonctionnaliser les métalla-assemblages et d'étudier leur combinaison afin d'obtenir des plates-formes multifonctionnelles pour des applications biologiques. Dans une première approche, des panneaux trigonaux avec différents groupes fonctionnels ont été synthétisés et utilisés pour former des prismes. Ensuite, ces panneaux ont été combinés avec des dérivés de pyrényle à double bras, agissant comme invités, prouvant que les prismes avec des panneaux fonctionnalisés sont capables d'encapsuler un invité. Cette même stratégie a été appliquée à la synthèse d'un ensemble de photosensibilisateurs de troisième génération, basés sur des assemblages avec un panneau biotinylé pour le ciblage, et trois invités pyrényl-photosensibilisateurs différents pour des applications de thérapie photodynamique (PDT). Leur activité phototoxique a été testée sur des cellules cancéreuses colorectales humaines HCT116.

En outre, les clips contenant un espaceur oxamide ont été modifiés par l'introduction de groupes fonctionnels tels que des chaînes alkyliques avec différentes quantités de groupes hydroxyles ou de courtes chaînes PEG. Ces clips ont été utilisés dans la synthèse de prismes et de cubes pour ajuster leur hydrosolubilité. Leur hydrophilie a été étudiée en calculant leur coefficient de partage octanol-eau. Des valeurs hydrophiles ont été obtenues pour les deux séries d'échantillons.

Mots clés

Complexes arène ruthénium, chimie supramoléculaire, chimie hôte-invité, thérapie photodynamique, activité anticancéreuse, phototoxicité, administration de médicaments

Table of contents

1. Introduction

1.1 Arene-ruthenium

Ruthenium is the element 44 of Mendeleev's periodic table and is one of the rare elements belonging to platinum group metals[1]. Its electronic configuration is [Kr] $4d^7$ $5s^1$ and it can have up to eight different oxidation states, among those, +2 and +3 being the most common. In the context of biological applications, Ru(II) complexes present advantages such as higher stability, as it has been observed that the activity of Ru(III) complexes is dependent on in vivo reduction to Ru(II) complexes[2,3]. In addition, stability of the +2 oxidation state can be easily improved by coordination with arene ligands. Arene ligands are hydrocarbons with a conjugated cyclic molecular structure, as they are strong π-acceptors, they enhance the stability of ruthenium's d orbitals, resulting in a very high stability against oxidation. As L_3 ligands, arenes occupy three of the six coordination sites of ruthenium forcing the complex to adopt a pseudo-octahedral geometry with the three remaining sites at 90° from each other, which is key for the formation of shape-controlled supramolecular assemblies[4].

The first arene ruthenium complex was a dinuclear benzene ruthenium chloride and it was synthesized in 1967 by Winkhaus and Singer[5], even if the correct dimeric structure was only confirmed in 1974 by Bennett[6], in which the two ruthenium centers are linked by two chlorides. It was obtained through a redox reaction by reacting $RuCl_3 \cdot nH_2O$ with 1,3-cyclohexadiene in ethanol, a method still employed nowadays for electronically poor dienes. Many different dienes such as *p*-cymene and 1-methyl-1,3-cyclohexadiene have been used to form arene-ruthenium dimers[6] (Figure 1), since not only they are very stable under atmospheric conditions but they also show good solubility in organic solvents and water thanks to their amphiphilic character.

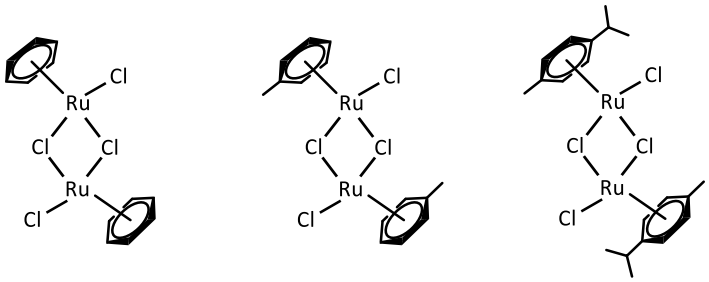

Figure 1. Some of the first arene ruthenium dimers synthesized.

The concept of molecular clip was first introduced by Stang in the early 2000's[7–9], in his work, they used the clip as a preconstructed shape-defining unit, as it contained two platinum centers fixed in a *cis* arrangement (Figure 2). Then, the clip was combined with rigid planar tritopic linkers to form highly symmetrical prismatic molecular cages[7]. During the same period, Fujita reported the use of similar tritopic ligands to form as well 3D coordination cases, baptizing these ligands as molecular panels[10–13] (Figure 2). It is from their pioneering work that the notation of clips and panels has been adopted and extensively used in the field of organometallic supramolecular assemblies.

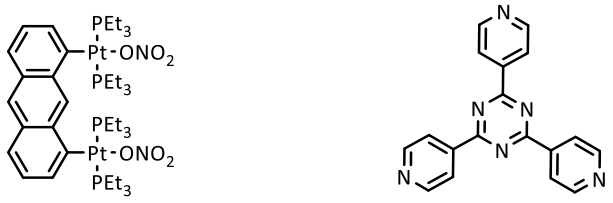

Figure 2. Stang's molecular clip (left), Fujita's molecular panel (right).

As it has been discussed above in this text, arene ruthenium complexes have their geometry fixed thanks to the arene group, for this reason, arene ruthenium dimers are perfect candidates to be used as clips to form different supramolecular structures. Furthermore, the two chloride bridging ligands are labile and easily replaceable with other donor groups, in general consisting in anionic ligands. A first example, is the substitution with the bis-bidentate oxalate ligand developed by Süss-Fink in 1997[14] (Figure 3). Bridging ligands connecting the two ruthenium centers are also known as spacers, as the use of ligands of different sizes allows to control the final length of the clip. Many different spacers have been used to form clips, the most common of them being quinones, but other groups like oxamides have also been explored[14–19] (Figure 3).

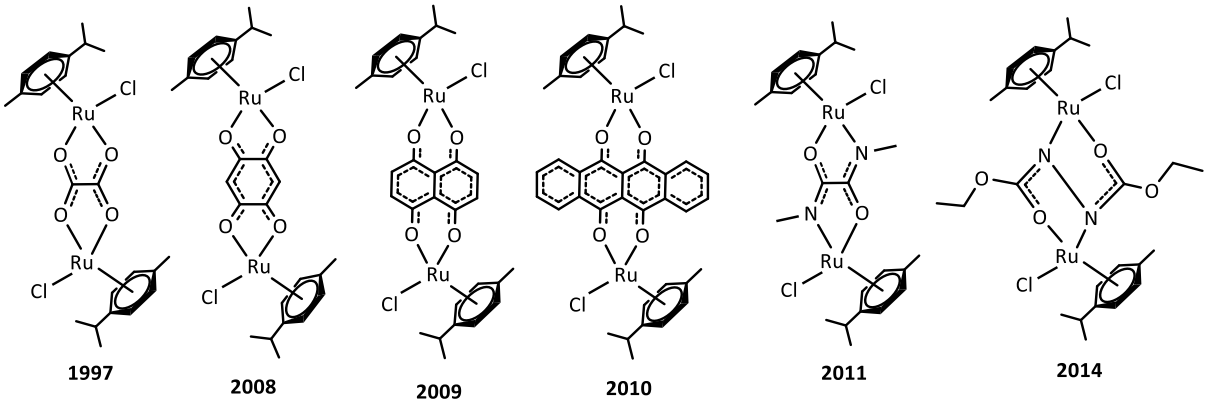

Figure 3. Examples of clips with different spacers with their publication date.

The final geometry of the metalla-assembly will be determined by the panel of choice. These ligands contain different amounts of coordination sites, and the angle between those may vary: ditopic ligands form rectangles, tritopic ligands form prisms and tetratopic ligands form cubes (Table 1).

Panel	Geometrical structure
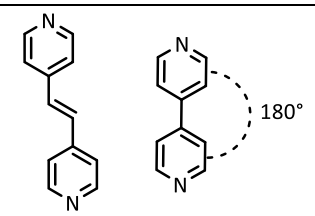	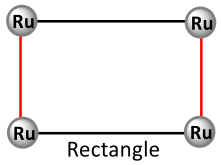
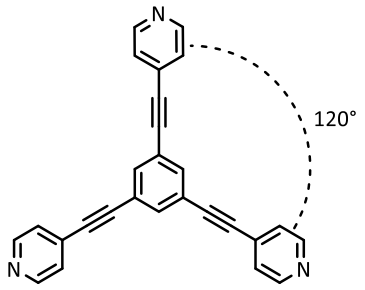	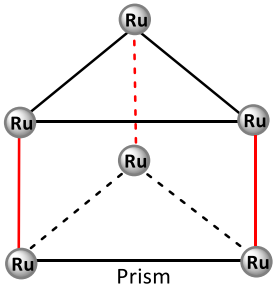
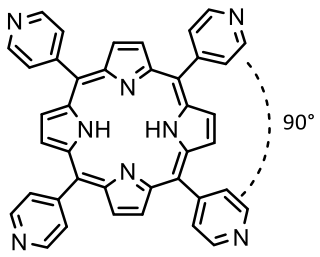	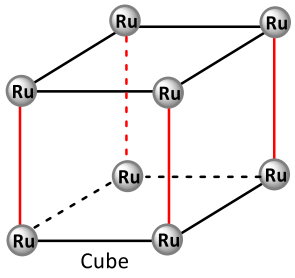

Table 1. Different panels with representations of the assemblies and geometries they form.

By combining different building blocks, the properties of the metalla-assembly can be tuned. For instance, metalla-prisms are able to encapsulate small aromatic molecules inside their hydrophobic cavity. The size of this cavity depends directly on the length of the clip used and by extension on the spacer used to build the clip, and will determine the capacity to form host-guest supramolecular systems. For example, the cavity of prisms with oxalate bridged clips was found to be too small to host a guest while prisms with quinone bridged clips resulted in very good hosts for molecules like pyrene, phenanthrene, triphenylene or coronene[15,20,21].

1.2 Functionalization of metalla-assemblies

The next step in the evolution of metalla-assemblies is their functionalization. There are many options due to the modular approach of their synthesis, in other words, any of the different building blocks (clips and panels) and even guests can be functionalized to design a final metalla-assembly with specific properties adequate to the application in mind. Furthermore, many different strategies or routes can be followed to derivatize the building blocks, for example, clips can be functionalized through their spacer or through the arene group. In Figure 4, a representation of a metalla-prism showing some of the functionalization spots is presented.

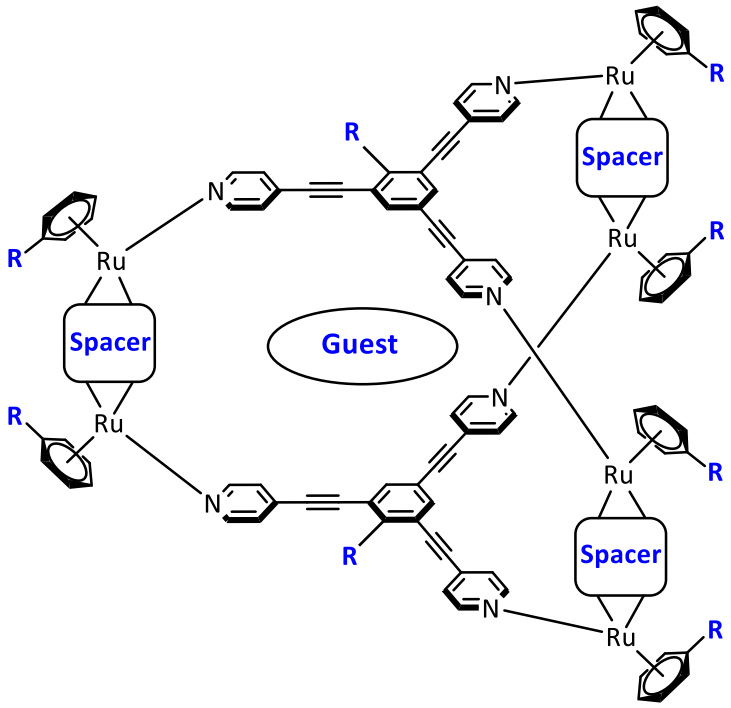

Figure 4. Metalla-prism with possible functionalization spots (blue).

1.2.1 Functionalization of metalla-clips

The use of different arene groups was a topic of study already in the 70's, Winkhaus and Singer's method was found to not be suitable for electronically rich arenes such as hexamenthylbenze. For this type of arenes, other methods were developed such as an arene exchange at high temperature (180 °C)[22] (Figure 5). During the following years, many substituted arenes were introduced by substitution[23,24].

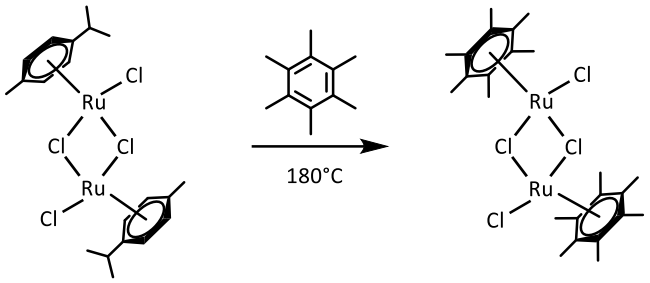

Figure 5. Synthesis by substitution of dimer with hexamethylbenzene[22].

A strategy that was found to be convenient to obtain functionalized derivatives consists in the pre-functionalization of the arene through conventional coupling methods, to then obtain the diene by Birch reduction. Then, the diene can be coordinated to ruthenium following the Winkhaus and Singer's method. This route was followed in our group to obtain functionalized arene ruthenium dimers in 2006[25], the synthesis of one of the two dimers from that work is shown in Figure 6.

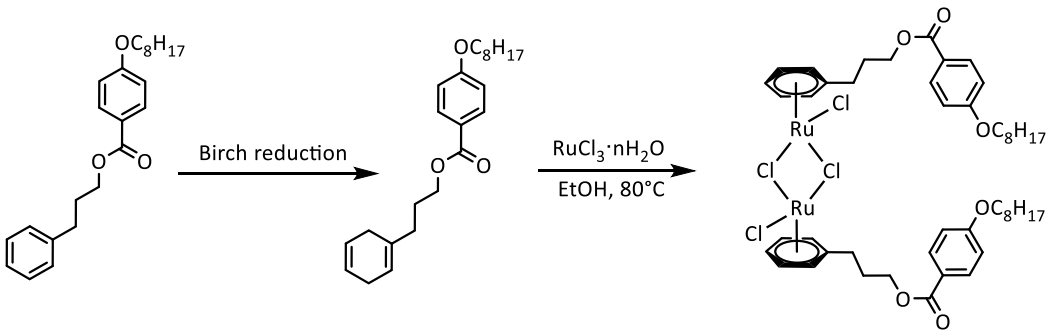

Figure 6. Synthesis of arene-ruthenium dimers with functionalized arenes[25].

The application of arene ruthenium complexes in the treatment of cancer was started and extensively studied by Dyson and Sadler[26,27], among the different compounds, it is specially remarkable RAPTA-C (Ruthenium Arene PTA) a compound first synthesized by Dyson in 2001[28]. RAPTA-C was found to be highly active in vivo, which caused an increased interest in the RAPTA family of compounds, one of the strategies to tune or improve the activity of RAPTA-C was the use of different arene ligands[26,29,30]. Even if these complexes are not used as clips, the functionalization strategy of the arene moiety is essentially the same, the chloride bridged dimer is initially formed and then it is transformed into the mononuclear RAPTA derivative by coordination to PTA (1,3,5-triaza-7-phosphaadamantane). Not only solubility can be tuned through arene functionalization, for example, derivatives containing a formyl linker to be linked to human serum albumin (HSA)[31] or derivatives with ethacrynic acid[32], an inhibitor for glutathione transferase (Figure 7).

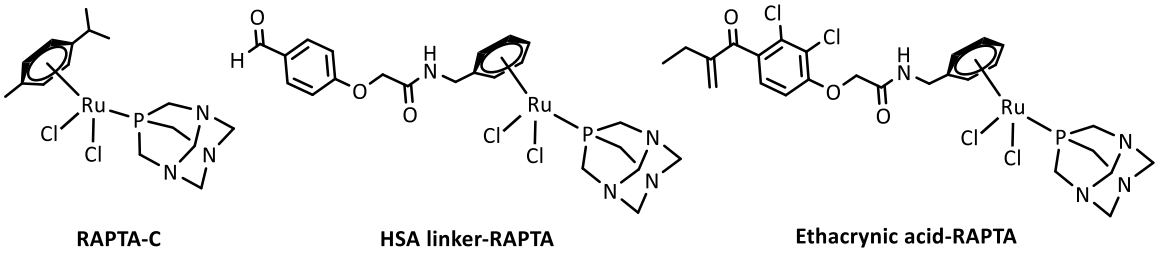

Figure 7. RAPTA-C and RAPTA based derivatives with functionalized arenes[28,31,32].

Following the same strategy, a RAPTA derivative containing a pyrene attached to the arene was synthesized in our group in 2012 (Figure 8)[33]. Here, the pyrene is used to be encapsulated inside an arene-ruthenium metalla-prism as it has been discussed above, pyrene is a very good guest for this type of assemblies. Pyrene fits very well inside the hydrophobic cavity of the prism and it is further stabilized by π interactions with the 2,4,6-tris(4-pyridyl)-1,3,5-triazine (4-tpt) panels, while the side alkylic chain and RAPTA moieties stand outside of the cavity into the solvent. The goal was to combine the cytotoxic properties of the RAPTA derivatives with the water solubility of the metalla-cage, to increase cellular uptake. The cytotoxicity of the empty metalla-assemblies and the host-guest system was similar, but kinetic studies revealed that the intracellular accumulation of the pyrenyl guest was improved by a factor of two when forming part of host-guest assemblies, demonstrating the transport capacity of the metalla-prism.

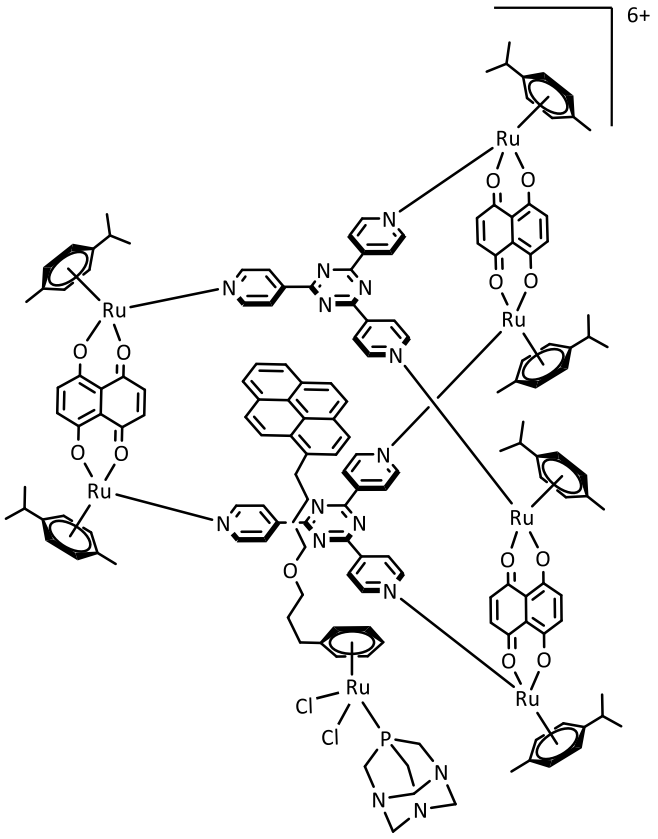

Figure 8. Metalla-prism with the pyrenyl-RAPTA derivative as guest[33].

Dinuclear metalla-clips can be functionalized as well through their bridging spacer. As it has been discussed above, spacers can consist in many different molecules, which gives rise to many possibilities for functionalization. Benzoquinone spacers have been functionalized mainly by Suzuki-Miyaura coupling reactions, for example, they have been used to tune the size of the portals of prismatic metalla-prisms[34]. Another approach is the functionalization of oxamides, as their two nitrogen centers offer the possibility to attach other moieties, with this strategy oxamides with PEG[35] or alkylic[36] linkers have been obtained. Both of these strategies are studied in more detail in chapter 4 of this thesis. Another family of compounds that have been used as spacers are thiolate derivatives, a first set of arene ruthenium dimers with thiolate bridging groups and different arenes was synthesized in 2010[37]. The following years, similar dimers containing different substitution at the thiol group and *p*-cymene as the arene were used as clips in the synthesis of metalla-assemblies[38] (Figure 9). Their cytotoxicity was tested against human ovarian cancer cells, specifically on *cis*platin-resistant cell line A2780cisR, obtaining IC_{50} values down to 0.25 μM.

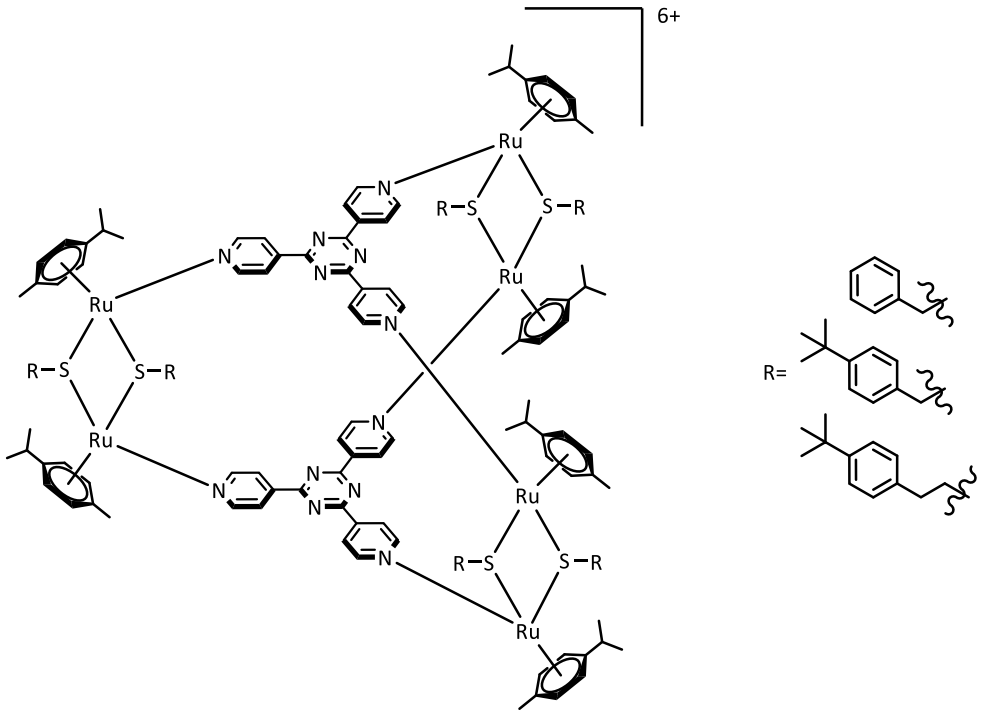

Figure 9. Hexanuclear metalla-prism with thiolato-bridged clips[38].

1.2.2 Functionalization of panels

The functionalization of assemblies through the panel ligand has been studied mainly in rectangles, as ditopic ligands are easier to be modified. Metalla-rectangles have been studied for many different applications, the versatility of these compounds is in part thanks to the modification of the building blocks. Sensing of relevant analytes is one of the fields studied mainly by Stang and Chi, in their work, they designed a panel with fluorescent properties for the detection of nitro aromatics[39] (Figure 10, left). The detection of other analytes such as polyanions oxalate, citrate and tartrate was also proved by combining dipyridyl panels based on amide donors, whose hydrogen bonding capabilities are key in the detection of these species[40,41] (Figure 10, right).

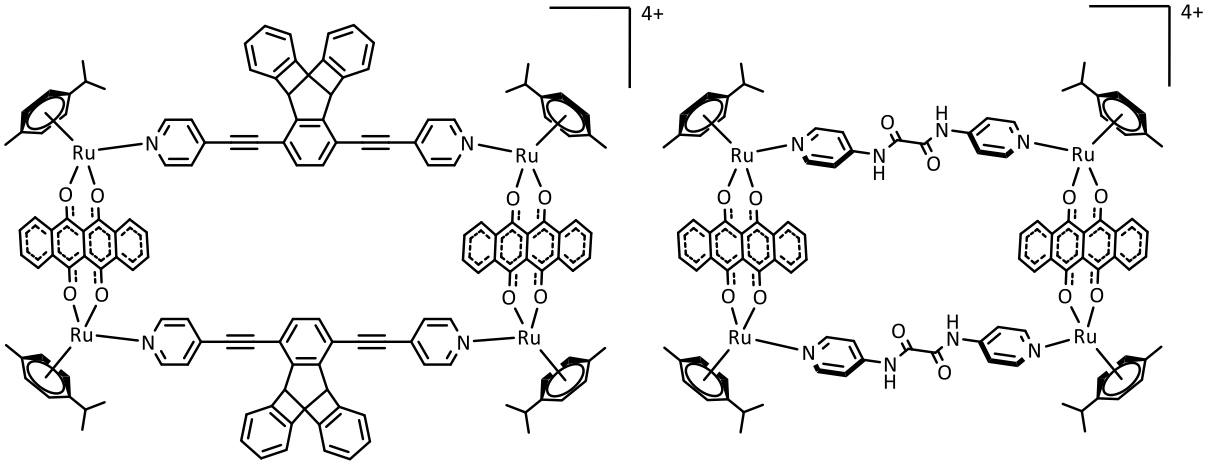

Figure 10. Metalla-rectangles with sensing properties[39,40].

Biological applications of these assemblies have been as well explored, as the amphiphilic properties of the arene-ruthenium compounds make them suitable for interactions with cells or biomolecules. Assemblies with a panel designed to bind to EGFP (enhanced green fluorescent protein) were synthesized by Chin[42] (Figure 11), the complex proved to be able to quench the fluorescence on the protein, which could be interesting for targeting or biosensing. This same panel was used to form a set of rectangles using different benzoquinone bridged clips[43], their anticancer properties were studied obtaining IC_{50} values in the low micromolar scale.

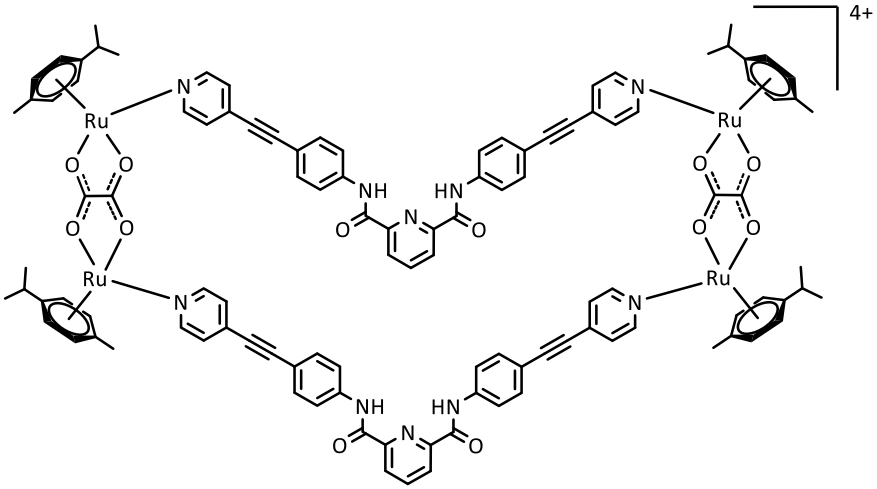

Figure 11. Metalla-assembly with EFGP binding properties[42].

Photodynamic therapy (PDT) is a medical treatment in which a photosensitizer (PS) is irradiated at a specific wavelength, generating reactive oxygen species (ROS) which can induce cell death by oxidative stress. Metalla-rectangles incorporating BODIPY (Boron-dipyrromethene), a well-known photosensitizer, in their panels have been synthesized[44] (Figure 12, left), BODIPY was used in this work to localize the assemblies in the cancer cells thanks to its fluorescent properties. Another approach to PDT is the use of oxygen-carriers such as anthracenyl derivatives, as cancerous tissues are known to be hypoxic environments[45–47] which hinders the efficiency of the therapy. With this in mind, metalla-rectangles with anthracenyl panels were recently designed in our group[48] (Figure 12, right).

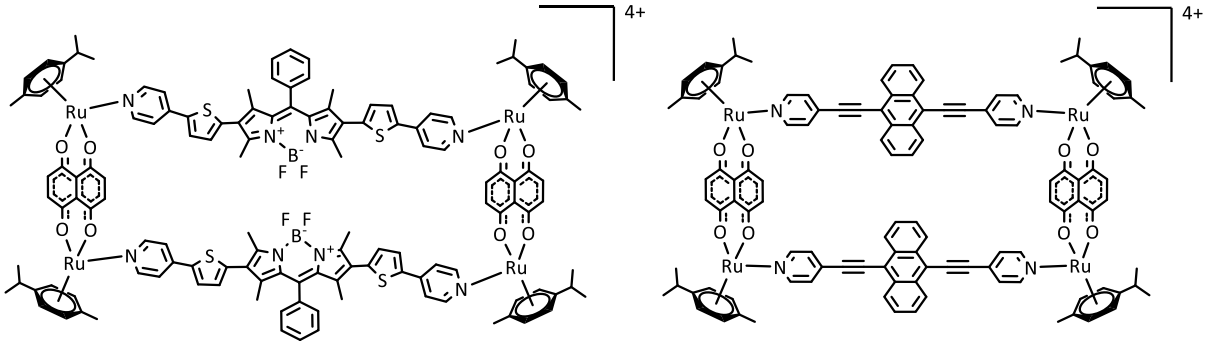

Figure 12. Metalla-rectangles with potential applications in PDT[44,48].

In the panels discussed until now, the functional group forms part of the direct structure of the ligand itself. Another strategy is the attachment of the group as a side chain to an already known panel, in a way that the coordination of it is not altered by the presence of the new groups. Using this strategy, panels based on 1,4-di(4-pyridinyl)benzene containing two poly(arylester) dendritic branches carrying cyanobiphenyl mesogens was obtained[49]. The supramolecular rectangle obtained by the coordination of this panels to arene-ruthenium clips displayed thermotropic liquid-crystalline properties (Figure 13). This assembly is specially interesting as the functional groups are quite big even compared to the basic structure of the rectangle, since the complexation was not hindered by them it suggests that it can be a suitable approach to tune the size of the supramolecular structure.

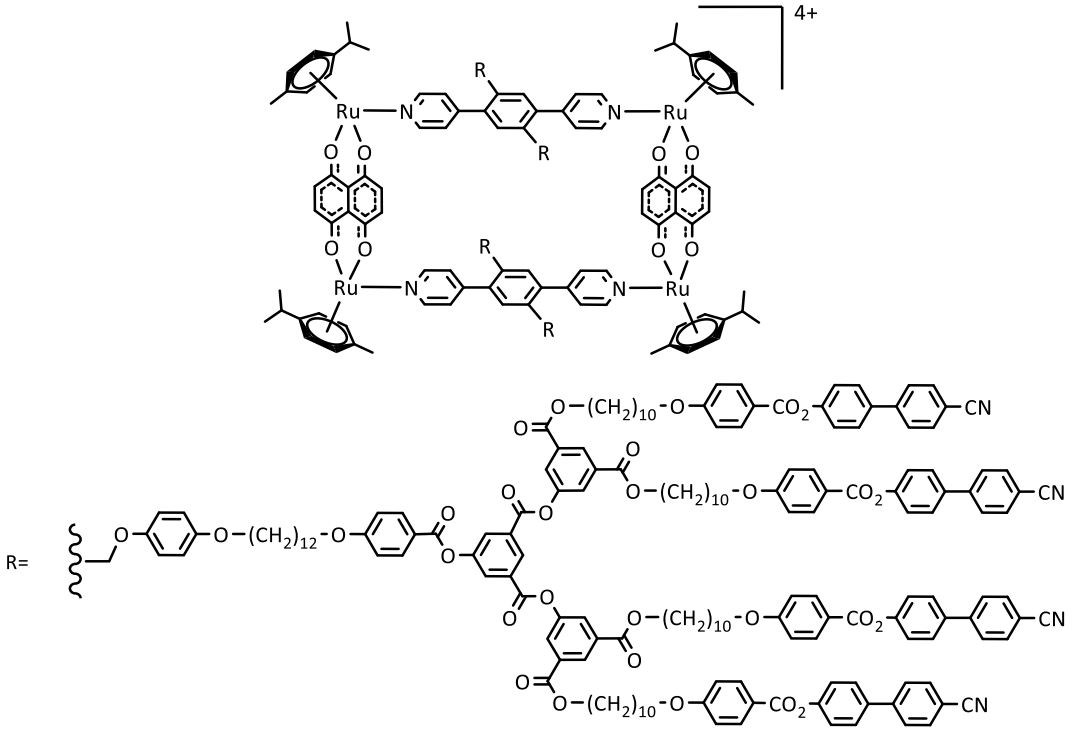

Figure 13. Metalla-rectangle containing dendrimeric side-chains[49].

Functionalization of tritopic and tetratopic panels for the formation of bigger 3D structures still remains to be explored, only recently studies on metalla-cubes were performed in our group. Functional tris-pyridyl porphyrins were designed incorporating technetium-99m (a radioactive tracer used in diagnostic imaging procedures[50]) in their core and a cellulose nanocrystal to target the enhanced retention and permeability effect (EPR) (Figure 14)[51], obtaining a theranostic system with PDT applications. This system, can be thought of something similar to an "opened-cube" since it contains only three arene-ruthenium metalla-clips. The *in vitro* PDT effect of these photosensitizers showed IC_{50} values in the nanomolar range in human ovarian cancer cells.

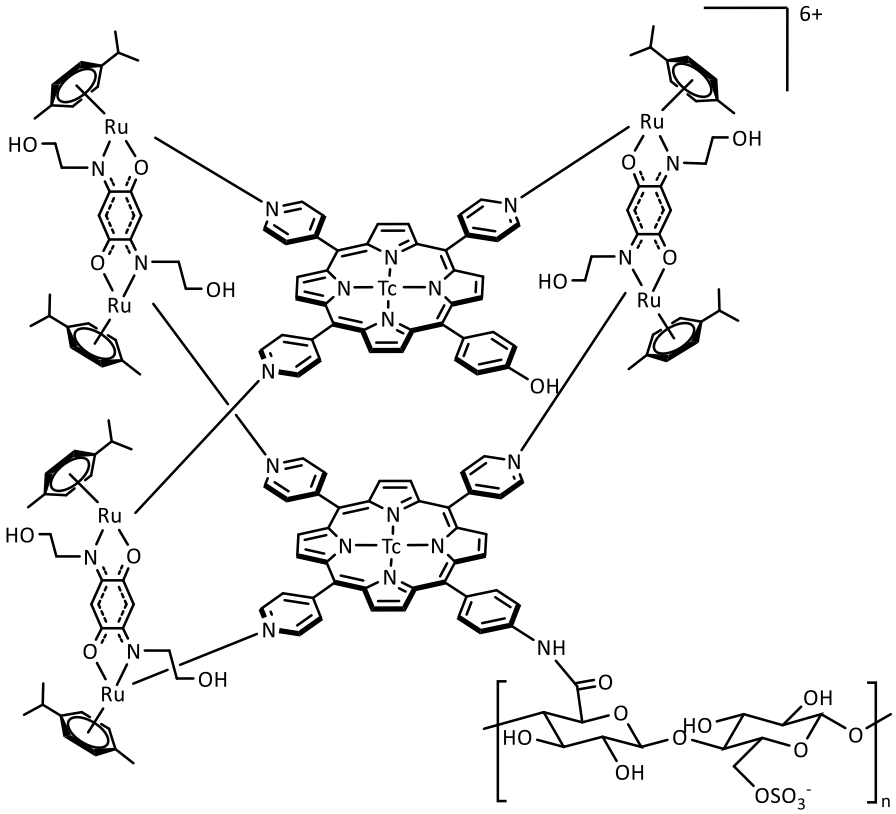

Figure 14. Open metalla-cube incorporating technetium-99m and a cellulose nanocrystal

1.3 Designing metalla-assemblies: the importance of the second coordination sphere

First coordination sphere (FCS) refers to the ligands directly attached to the metal while second coordination sphere (SCS) refers to ligands interacting through noncovalent forces (electrostatic, hydrogen-bonding, charge transfer, van der Waals, hydrophobic, π-π stacking). The concept of second coordination sphere was first introduced in 1912 by Alfred Werner[52], to explain a number of experimental observations that could not be understood only on the basis of first-sphere coordination[52,53].

While the FCS determines mainly the structure and general properties of the complex, the SCS plays a key role on in their potential applications. In the context of arene-ruthenium metalla-assemblies, it is crucial to think on a proper functionalization of the building blocks through the strategies described above in this chapter. At the same time, the formation of host-guest systems depends as well directly on the SCS, as the aromatic guests are mainly stabilized inside the assemblies by π-π stacking interactions. Many are the examples of functional building-blocks, for example, inclusion of a targeting agent may improve the biological activity of new metallodrugs. This is case of the RAPTA derivative containing ethacrynic acid[32] (Figure 7) is able to inhibit the activity of glutathione transferase (GST) by binding to their active site, GST P1-1 is targeted as its overexpression after exposure to antitumor drugs has been reported[54,55]. Another example of targeting is the rectangle designed to bind to EGFP interacting through the panel[42].

Arene-ruthenium metalla-cubes have been found to stabilize DNA quadruplexes[56]. G-quadruplexes are composed of guanine tetrads intercalated by cations and they possess a planar aromatic surface, which make them good candidates for interactions with metalla-cubes: π-stacking interaction with the porphyrinic panels and electrostatic interactions thanks to their cationic nature[57] (Figure 15).

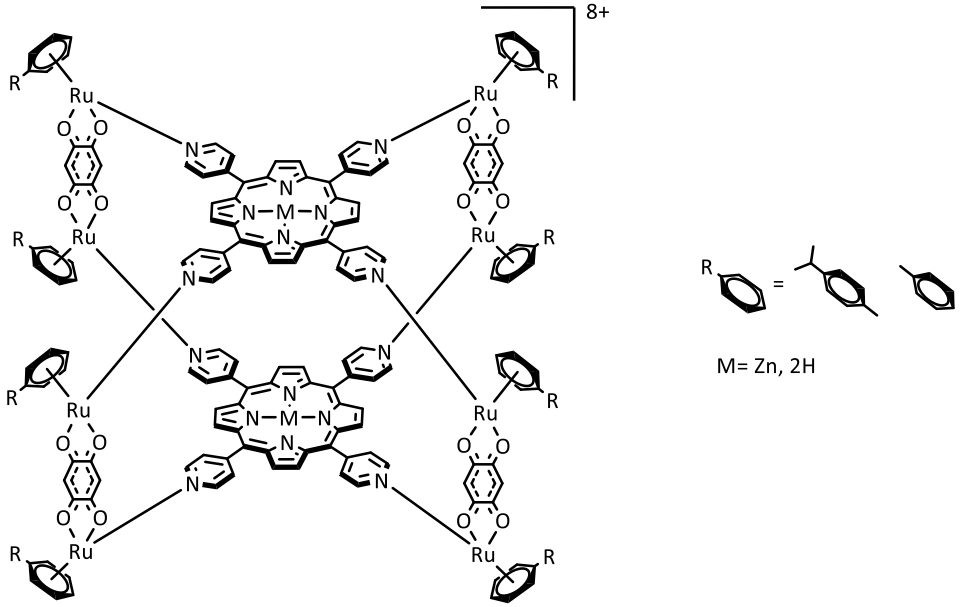

Figure 15. Metalla-cubes with G-quadruplex interaction capabilities[56].

Interest in the SCS is not only limited to biological applications, for instance, it is studied as well for catalysis[58–61] or sensing (Figure 16). The SCS is essential in sensing applications, as the detection of the analytes is performed through the weak interactions. Different sensing strategies are possible, mainly depending on the type of analyte and the interaction that will give rise to the response. The two rectangles described in Figure 10 are two good examples, one is able to detect nitroaromatics by fluorescence quenching, while the other is able to detect polyanions thanks to the ability of the panel to form hydrogen bonds with the analytes, resulting in a large fluorescence enhancement.

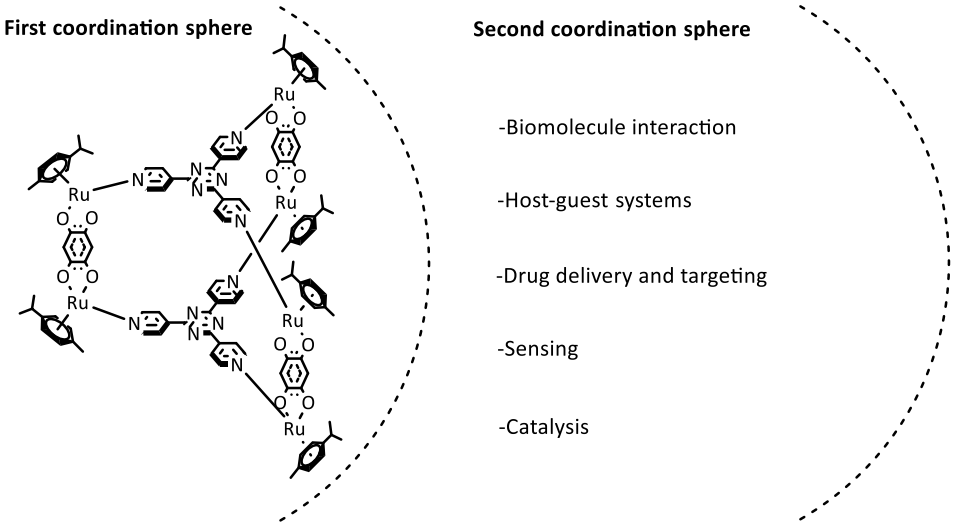

Figure 16. Representation of coordination spheres for an arene-ruthenium metalla-prism

In chapter 2 of this work some strategies to functionalize metalla-prisms and their combinations are investigated, then, in chapter 3 these same strategies are employed in the synthesis of multifunctional assemblies taking into account SCS interactions: a targeting moiety (biotin) is inserted for tumor targeting and different photosensitizers are included by insertion of a pyrenyl derivative in the cavity (for PDT applications). Chapter 4 is centered in the synthesis of functional metalla-clips to tune the water solubility of the resulting assembly.

1.4 Enhanced Permeability and Retention effect (EPR)

Enhanced Permeability and Retention (EPR) effect was first described by Maeda and Matsumura in 1986[62], where they observed that polymer conjugated anticancer protein neocarzinostatin (NCS) accumulates more in tumor tissues as compared to non-conjugated NCS. This effect is caused by the unique pathophysiological characteristics of most solid tumors[63]:

- Increased angiogenesis (formation of new blood vessels) resulting in hyper vasculature[64,65].
- Defective architecture of endothelial cells[66,67].
- Impaired lymphatic drainage[68,69].
- Highly expressed inflammatory factors and vascular mediators such as bradykinin, nitric oxide and vascular growth factors[70–73].

In consequence, large molecules are accumulated and retained in the tumor for longer periods than in healthy tissues. This effect has been extensively studied as a passive targeting for nanomedicines. Figure 17. is a representation of this effect, malignant tissue contains gaps between its endothelial cells, allowing macromolecules to go through them. On the other hand, smaller molecules are not accumulated, as they are removed through the lymphatic system.

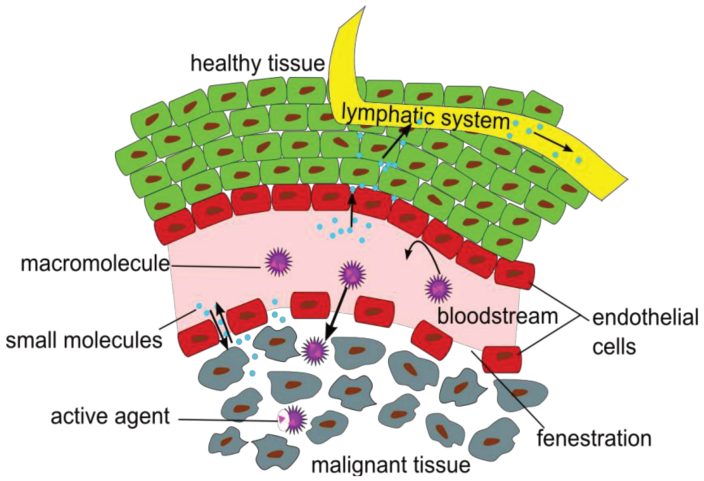

Figure 17. Representation of the EPR effect in tumoral tissue (bottom) compared to healthy tissue (top)[74].

Polymeric structures is only one example of the many different drug delivery systems that have been tested to exploit the EPR effect, other possibilities are nanoparticles[75], liposomes[76], proteins[77] or antibodies[78]. The perfect size of a drug delivery system for the EPR effect is a topic of debate. It has been stated by Maeda and coworkers that the ideal size is above 40 kDa and 5 nm of hydrodynamic radius[79,80]. Other studies show EPR effect in pegylated molecules as small as 5 kDa, even if results are optimal at 20 kDa[81].

1.5 Aim of the present thesis

Arene ruthenium metalla-assemblies have been proved to be very versatile systems thanks to the modular approach of their synthesis, which allows to tune the properties of the final assembly by modification of the different building blocks. In this project, different functionalization strategies are investigated aiming for biological applications. In the first chapter, modification of panels, guests and the combination of both is studied from the synthetic point of view, proving the viability of this method to obtain multifunctional assemblies. Parallelly to adding functionalities, the final molecular weight of the assembly is as well increased, which can be helpful to exploit the EPR effect. Another strategy to obtain bigger systems is to combine more than one assembly, this approach is studied by combining a porphyrinic central core that contains up to four metalla-prisms.

In the second chapter, the same methods are used to prepare multifunctional metalla-prisms containing a pyrenyl-photosensitizer guest and a biotinylated panel. This assemblies are applied in PDT combining the photosensitizing properties of the guests and the targeting properties of biotin. Their PDT efficacy is studied in Human HCT116 colorectal cancer cells.

In the third and final chapter, the functionalization of oxamide clips and their use in the formation of metalla-prisms and metalla-cubes is studied. These clips modify the water solubility of the final compound, as they are based on chains with varying number of hydroxyl groups or PEG chains. The hydrophilicity of the metalla-assemblies is studied by calculation of their octanol-water partition coefficient.

2. Investigating the functionalization of metalla-assemblies

2.1 Functionalization of guests

An important feature of arene-ruthenium metalla-prisms is their hydrophobic cavity. The cavity allows encapsulation of guests, one of the first examples of this, is the encapsulation of square-planar complexes giving rise to "complex-in-a-complex" cations[82] (Figure 18, left). The best guests were found to be planar poly-aromatic molecules such as pyrene, triphenylene or coronene. These aromatic systems are very good guests since they can interact with the panels of the assemblies by π-π stacking, and in combination with hydrophobic effect, it results in the formation of carceplex systems (carceplex being defined as host molecules that permanently encapsulate their guests[83]).

These aromatic molecules can be used as a platform to incorporate functionalities into the assemblies. Pyrene is the guest that has been studied the most in the context of metalla-assemblies, pyrene will sit inside the hydrophobic cavity while its functional group will hang out of the cage. The encapsulation of methyl 4-(pyren-1-yl)butanoate was the first system of this family[84] (Figure 18, right).

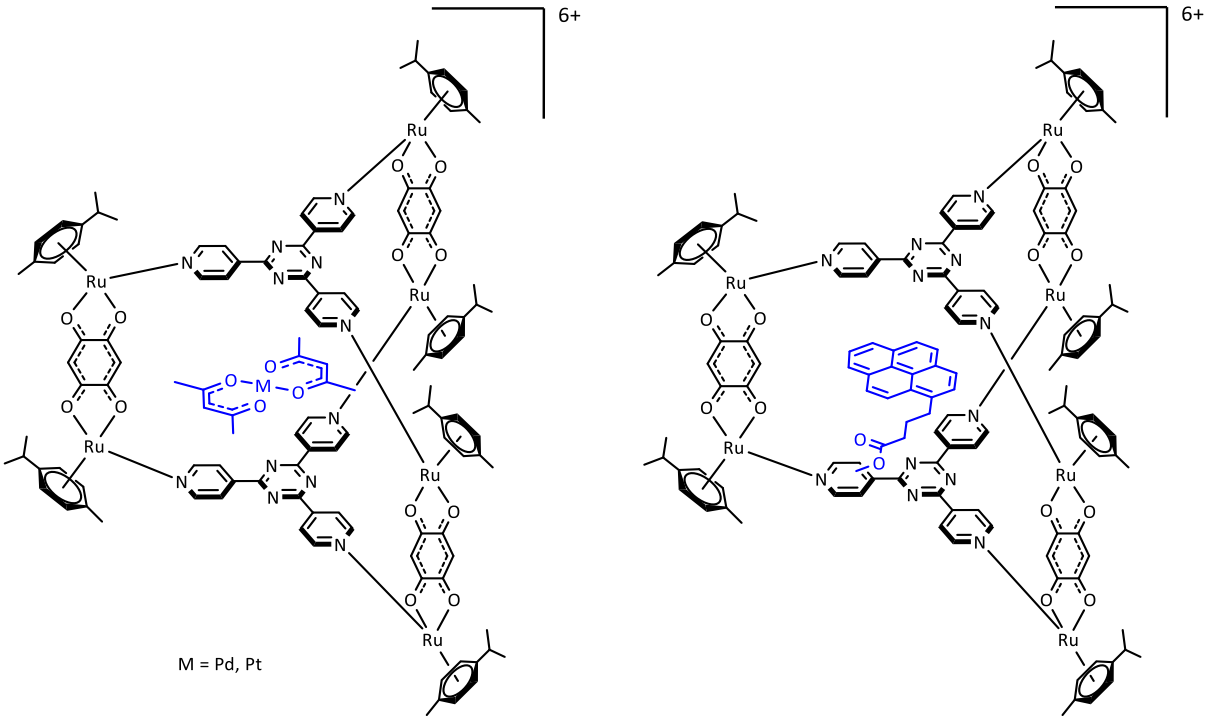

Figure 18. Complex-in-a-complex cation (left) and pyrenyl derivative as guest (right).

Many different pyrenyl derivatives have been prepared and encapsulated over the years, containing a range of functionalities such as floxuridine derivatives[85], different types of dendrimers[86–89] or even other arene-ruthenium compounds[90]. When aiming to increase the molecular weight of the assemblies to exploit the EPR effect, functionalization of the guest is one of the easiest approaches. Trying to achieve a higher molecular weight, pyrenyl derivatives containing two functional arms instead of one would represent an advantage. There have been only few examples, but a pyrenyl derivative containing two straight arms has been successfully encapsulated in the past[91]. Following this approach, double-armed pyrenyl derivatives were designed, synthesized and their encapsulation was studied.

2.1.1 Synthesis and characterization

Pyrenyl derivatives containing two arms should initially contain a rigid bond, which will help to stick out of the metalla-assemblies. Two different strategies were explored, connection through triple bonds by Sonogashira coupling, and connection through double bonds by Heck coupling. Both of these reactions are done in presence of palladium catalysts. For alkyne derivatives, the synthesis starts from 1,6-dibromopyrene, which is coupled to trimethylsilylacetylene in the presence of $Pd(PPh_3)_4$, CuI and triethylamine under inert conditions. Then, it is deprotected in methanol in the presence of K_2CO_3 to afford the free alkyne (Scheme 1). Functional groups containing bromide or iodine can then be attached through a second Sonogashira coupling reaction.

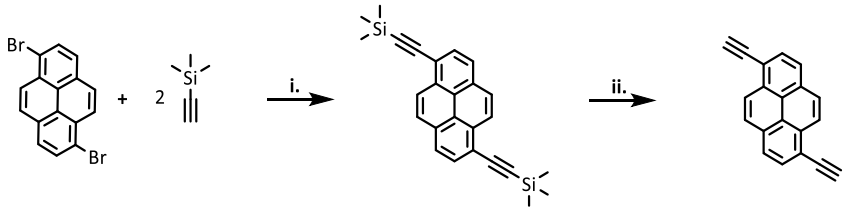

Scheme 1. Synthesis of pyrenyl derivatives with alkynyl arms i) $Pd(PPh_3)_4$, CuI, dry Et_3N:Toluene 1:1, 60 °C, overnight, 32% ii) K_2CO_3, DCM, 81%

In the case of alkene derivatives, the starting material is again 1,6-dibromopyrene, but in this case it is coupled to *tert*-butyl acrylate in the presence of $Pd(PPh_3)_4$ and triethylamine to afford **Pyr1**. In the next step, protecting group is removed in DCM in presence of trifluoroacetic acid (TFA) to afford the diacid derivative (Scheme 2), which can as well be further functionalized by either amide or ester couplings.

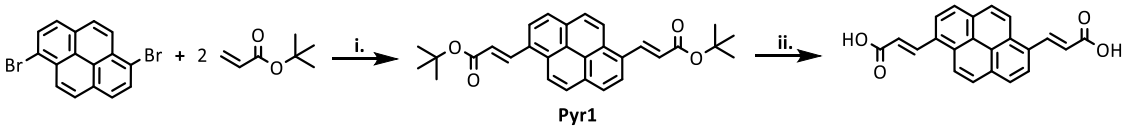

Scheme 2. Synthesis of pyrenyl derivatives by Heck coupling, i) $Pd(PPh_3)_4$, Et_3N, dry DMF, 90 °C, 48 h, 83% ii) TFA, DCM, 85%

Comparing the two methods, Heck coupling was chosen for next reactions as it presented two main advantages over the Sonogashira coupling in the context of our project. First, the copper co-catalyzer used in Sonogashira coupling favors the formation of homocoupling products, also known as Glaser byproducts[92], which makes the workup and purification more laborious; and second, by using amide/ester coupling to attach the next functional groups gives some polarity to the arms, which will potentially help them stick out of the assemblies and help the solubility in aqueous media. Heck coupling was also tested to form other pyrenyl derivatives, for example, it was coupled to 4-hydroxybutyl acrylate using the same conditions, but in that case, both mono and disubstituted products were obtained (**Pyr2** and **Pyr3**) (Scheme 3).

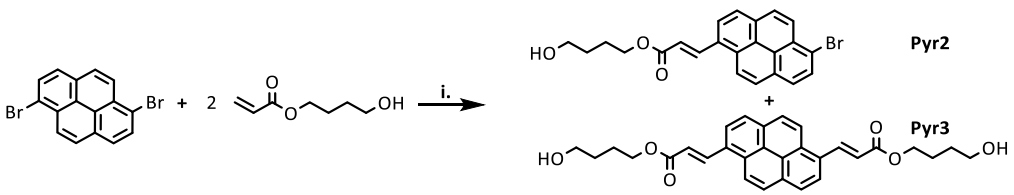

Scheme 3. Synthesis of **Pyr2** and **Pyr3**, i) $Pd(PPh_3)_4$, Et_3N, dry DMF, 90 °C, overnight, 73% total yield.

In a final step, Pyr1 was coupled to N-Boc-2,2'-(ethylenedioxy)diethylamine, a short PEG chain, through amide coupling in the presence of EDCl (1-ethyl-3-(3-dimethylaminopropyl)carbodiimide), HOBt (1-

hydroxybenzotriazole) and DMAP (4-dimethylaminopyridine) in dry DMF under inert conditions (Scheme 4) to afford **Pyr4**. This PEG chain increases the hydrophilicity of the arms, and helps as well to extend them in case a bulkier group has to be attached, minimizing possible steric interactions with the assembly.

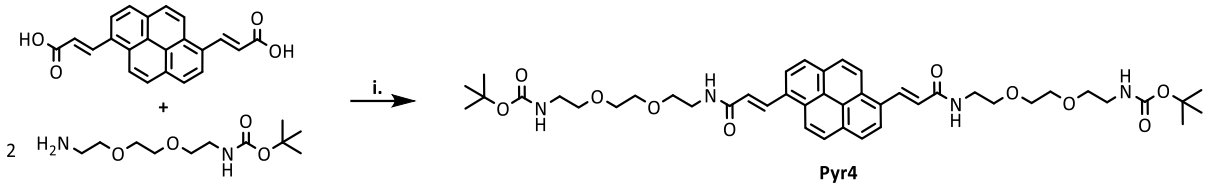

Scheme 4. Synthesis of **Pyr4**, i) EDCl, HOBt, DMAP, dry DMF, 48 h at RT, 44%.

Pyrene has been extensively studied as it has interesting fluorescent properties[93]. For this reason, pyrenyl derivatives **Pyr1-Pyr4** photochemical properties were studied through UV-Vis and fluorescence spectroscopy. In Figure 19, absorption spectra of the different derivatives are presented. All pyrenyl derivatives show red-shifting of their bands compared to pyrene. **Pyr-2** presents small differences on the shapes of the bands, but this result is expected as it contains a single side-chain and a bromine atom.

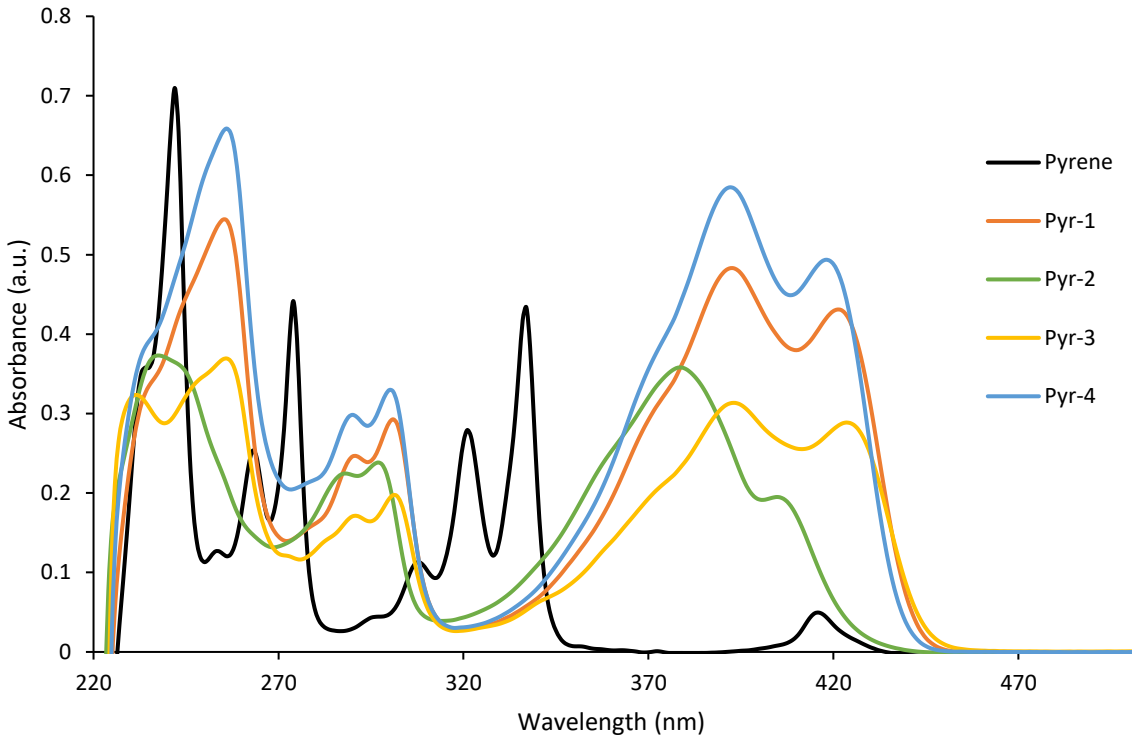

Figure 19. UV-Vis absorption spectra of pyrenyl derivatives (10^{-5} M in DCM)

Emission spectra of the four pyrenyl derivatives and pyrene was as well performed at the same concentration, at an excitation wavelength of 310 nm. Spectra obtained can be seen in Figure 20. It can be observed that all four pyrenyl derivatives present similar shape of the emission bands, with a significant redshifting compared to pyrene. Note that changes in intensity between derivatives in this representation should not be interpreted as fluorescence quantum yield differences, as their absorbance at the same excitation wavelength is not exactly equivalent even if similar.

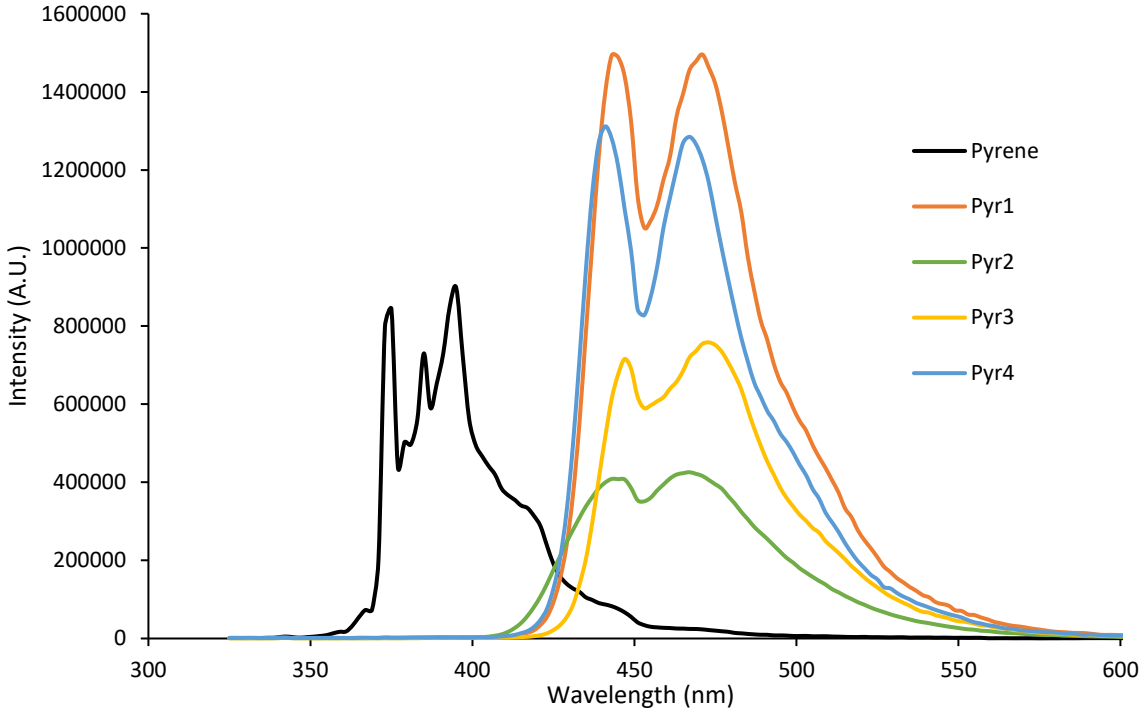

Figure 20. Emission spectra of pyrenyl derivatives (10^{-5} M in DCM, λ_{exc} 310 nm)

2.1.2 Encapsulation of double-arm pyrenyl derivatives

Pyrenyl derivatives containing two arms have been encapsulated into metalla-prisms by inserting them during the assembly. The synthesis of metalla-prisms starts with the activation of the metalla-clip, which takes place in MeOH in the presence of a halogen scavenger like silver triflate ($AgCF_3SO_3$). Once activated, the solution is filtered to remove AgCl and panel and guest are added in the correct stoichiometric amount. Finally, host-guest systems are isolated as trifluoromethanesulfonate salts. **Pyr2** and **Pyr3** encapsulation was first studied, since they are very similar derivatives, only that **Pyr3** has a second arm. Both guests were successfully encapsulated in good yields, suggesting that 1,6-disubstituted pyrenes are still very good guests for metalla-prisms (Scheme 5).

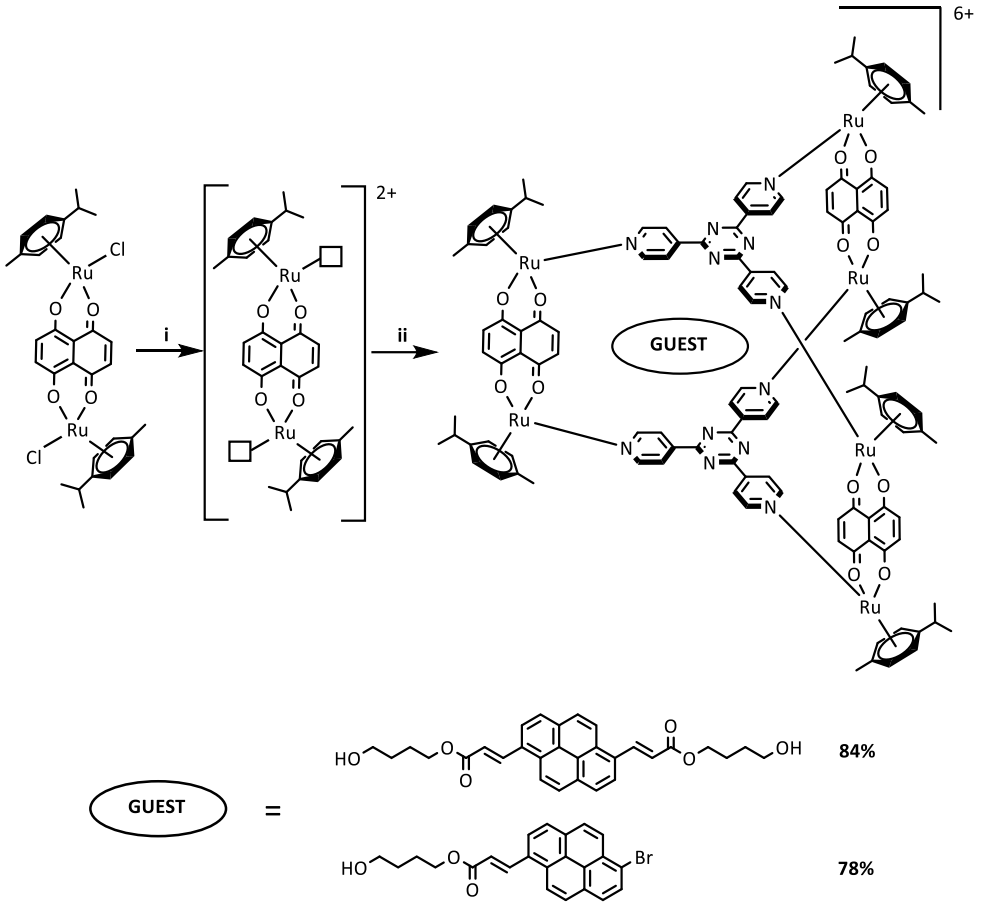

Scheme 5. Synthesis of host-guest metalla-assemblies, i) $AgCF_3SO_3$, MeOH, RT, 4 h. ii) Panel, guest, MeOH, 60 °C, overnight.

Characterization for **Pyr3⊂Prism** will be discussed as an example. ^{1}H-NMR spectrum can be seen in Figure 21. Alkylic signals from the guest can be identified, but aromatic pyrenyl signals are broadened (*). This broadening supports the idea that there is interaction between host and guest, suggesting a strong π-stacking with the panels. On the other hand, the encapsulation is a dynamic process, if the timescale of this dynamic process is similar to the NMR time-scale this may as well lead to disappearance of the signals of the protons involved. Side-chain signals can still be seen, as their shifts probably are less influenced by the encapsulation in the assembly.

Diffusion ordered spectroscopy (DOSY) is a well established NMR method that reports diffusion coefficients for individual species in solution[94]. In the context of our work, this technique allows us to correlate the signals from the ^{1}H-NMR of the different building blocks to diffusion coefficients. In the case the complex is formed, all signals have the same diffusion coefficient. This same principle is applied as well to the host-guest systems, since encapsulated guests will diffuse with the same coefficient as their hosts. In the case of **Pyr3⊂Prism**, signals corresponding to clip, panel and guests are aligned to the same diffusion coefficient, confirming the encapsulation of the guest inside the metalla-cage (Figure 21).

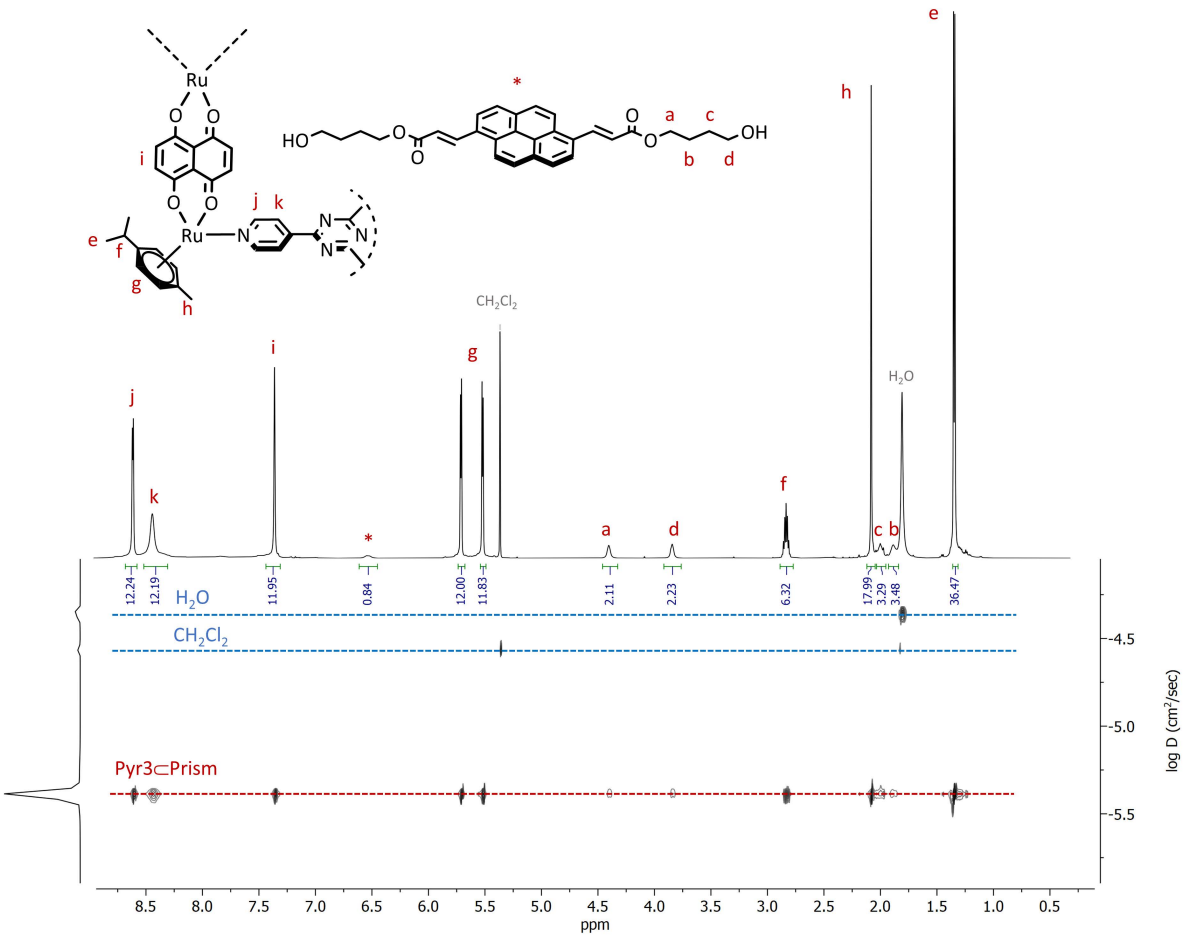

Figure 21. ^{1}H and DOSY NMR spectra of **Pyr3⊂Prism**

Further confirmation of the formation of the inclusion system is obtained by ESI-MS. In the case of arene-ruthenium metalla-prisms, the MS spectrum shows major peaks corresponding to the main assembly with different amounts of the triflate counterion. Depending on the amount of triflates lost, the charge of the fragment varies. For **Pyr3⊂Prism**, the fragment corresponding to [**Pyr3⊂Prism** – $4CF_3SO_3$]$^{4+}$ can be identified (Figure 22). The isotopic pattern of multinuclear ruthenium assemblies is very characteristic, in the same figure, it can be observed that the theoretical pattern fits perfectly the experimental.

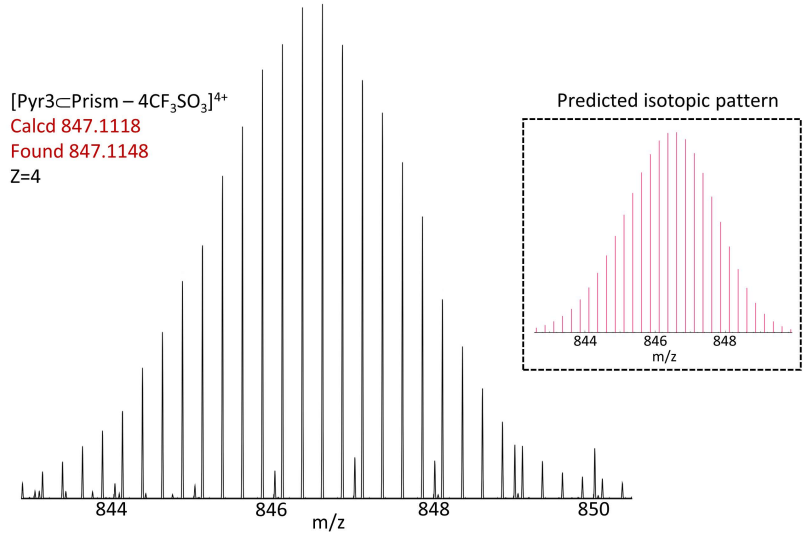

Figure 22. Excerpt of the ESI-MS spectrum corresponding to [**Pyr3⊂Prism** – $4CF_3SO_3$]$^{4+}$

Photophysical properties were also studied. UV-Vis spectra of **Pyr3⊂Prism** and its building blocks (**Prism** and **Pyr3**) are presented in Figure 23. The UV-Vis spectrum of the empty prism is characterized by a high energy band at 240 nm attributed to ligand localized or intraligand π-π* transition[95], together with a set of broad low-energy bands associated to metal-to-ligand charge transfer (MLCT) transitions appearing at 450, 640 and 695 nm, which are characteristic of metalla-prisms containing 5,8-dioxydo-1,4-naphtoquinonato (donq) as spacer in the clip[95]. In **Pyr3⊂Prism**, the UV-Vis spectrum presents bands associated to the empty prism overlapped with the characteristic bands of the pyrenyl derivative.

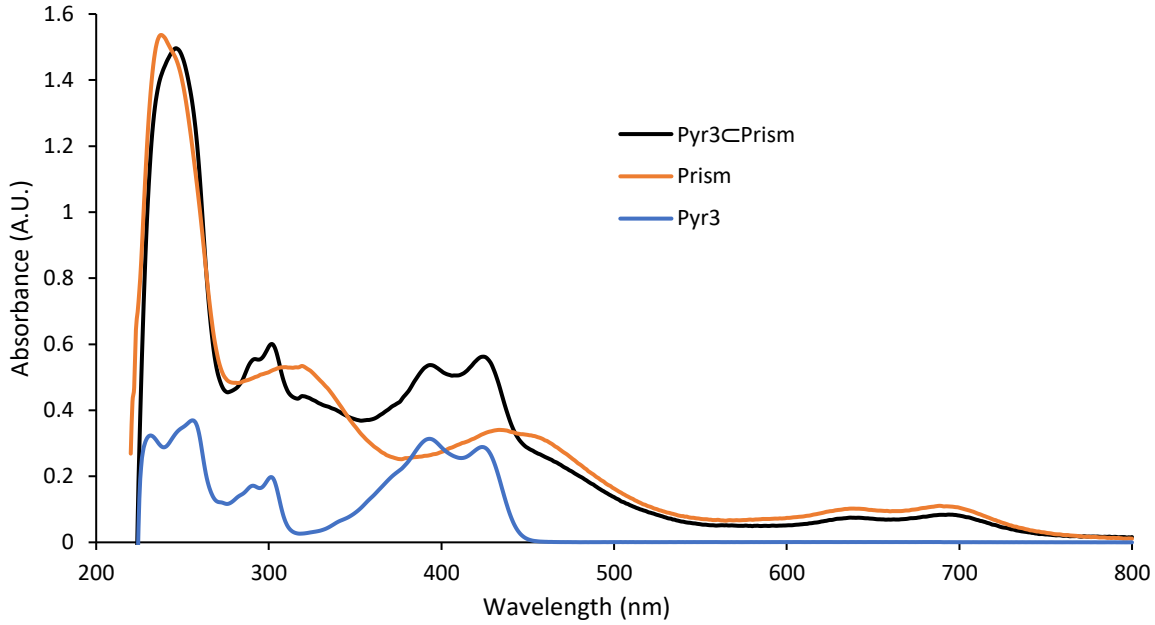

Figure 23. UV-Vis spectra of **Pyr3⊂Prism** and its building blocks (10^{-5} M in DCM).

In order to study the fluorescence of the guest when forming an assembly, emission of iso-absorbing solutions of **Pyr3** and **Pyr3⊂Prism** were compared in Figure 24. Partial quenching of the pyrene emission can be observed (prism and its components are non-emissive). Quenching of pyrenyl guests emission has been commonly observed when encapsulated in metalla-prisms[96,97], one of the reasons being the overlap of the emission of the guest with the absorbance of the prism.

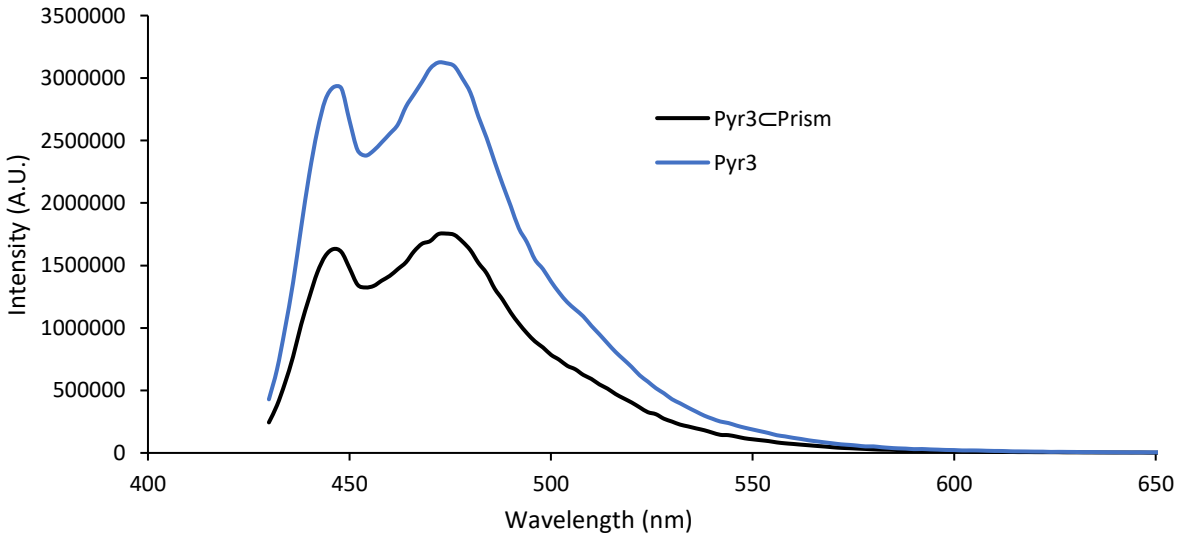

Figure 24. Emission spectra of **Pyr3⊂Prism** and **Pyr3** (DCM, λ_{exc} 395 nm)

2.2 Functionalization of panels

Arene-ruthenium metalla-assemblies geometry is determined by the choice of the building-blocks involved. When forming three dimensional assemblies, arene-ruthenium dinuclear metalla-clips are combined with rigid planar ligands of different denticities known as panels. Bidentate ligands form rectangles[98], tridentate ligands form prisms[99,100] and tetradentate ligands form cubes[101,102] (Figure 25). In all cases, the metalla-assemblies are isolated as their trifluoromethanesulfonate salts.

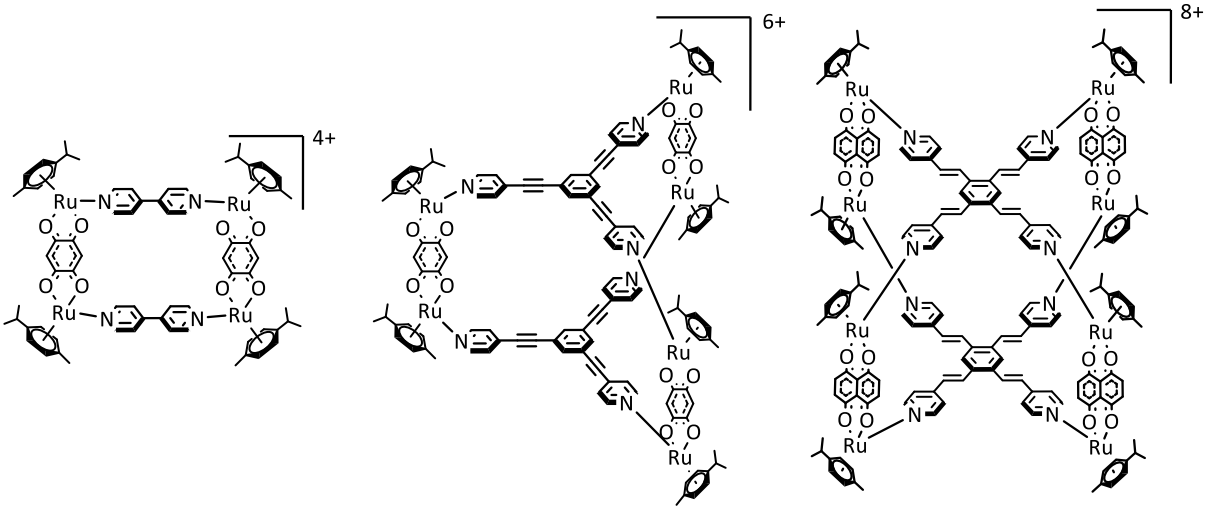

Figure 25. Metalla-assemblies with different geometries: rectangle, prism and cube.

One of the strategies possible for the functionalization of metalla-assemblies is the functionalization of its building blocks. In order to functionalize panels, it is important to design a strategy in which the coordinating ability of the ligand is not lost. For this reason, trigonal panels based on 1,3,5-tris(pyridin-4-ylethynyl)benzene (4-tpe) seem to be a good candidate, as their central aromatic ring presents three free positions that can be potentially functionalized, while keeping a distance from the coordinating pyridine.

With this in mind, we designed and synthesized a first set of trigonal panels with different functional groups such as alkylic and PEG chains (Figure 26). The ability of these panels to form metalla-prisms has been studied.

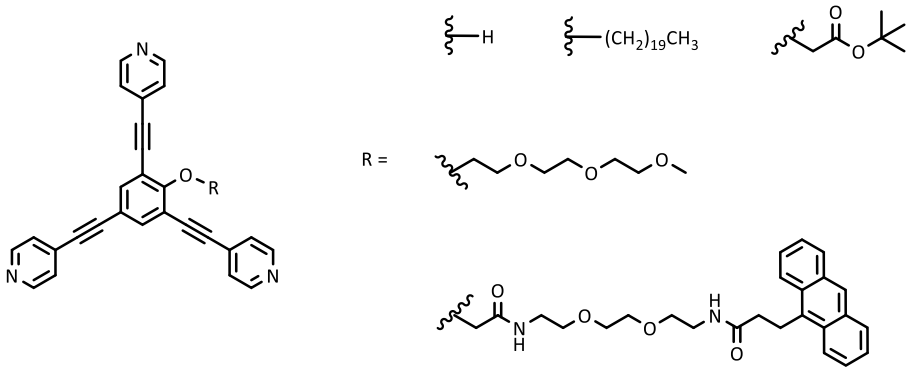

Figure 26. Functionalized panels synthesized

2.2.1 Synthesis and characterization

Functionalization of trigonal panels is based on the functionalization of 2,4,6-triiodophenol using a Williamson's ether synthesis reaction, followed by the formation of the panel through Sonogashira coupling using 4-ethynylpyridine. Scheme 6 shows reaction conditions for the two steps of the first four derivatives, **L1-L4**. Note that **L1** is prepared directly from 2,4,6-triiodophenol in a single step.

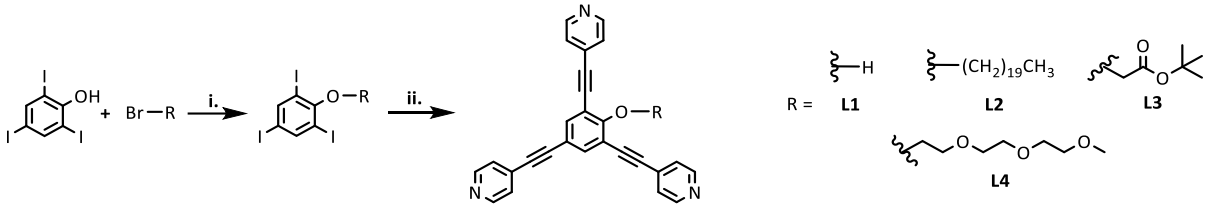

Scheme 6. Synthesis of functionalized trigonal panels, i) K_2CO_3, DMF, reflux overnight ii) 4-ethynylpyridine, $Pd(PPh_3)_4$, CuI, dry Et_3N:THF 1:1.5, 75 °C 48 h.

As it has been discussed for pyrenes, yields for Sonogashira couplings tend to be moderate, as the copper co-catalyzer induces the formation of homocoupling products. On the other hand, the functionalization through ether synthesis results in higher yields. Yields for both steps are compared in Table 2.

Panel	Ether synthesis (Yield, %)	Sonogashira coupling (Yield, %)
L1	-	35
L2	95	31
L3	96	78
L4	62	39

Table 2. Yields for the synthesis of panels.

Tert-butyl 2-(2,4,6-triiodophenoxy)acetate was further modified by deprotection of its carboxylic acid in DCM in the presence of an excess of TFA. Then, the free acid can be used to couple it to another group through an amide bond. It was coupled to N-Boc-2,2'-(ethylenedioxy)diethylamine, a short PEG linker, in the presence of EDCl, HOBt and DMAP in dry DMF under inert conditions to obtain **TriPEGboc** (Scheme 7).

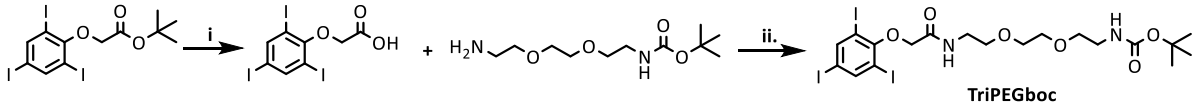

Scheme 7. Synthesis of **TriPEGboc**, i) TFA, DCM, RT, 4 h, 74%. ii) EDCl, HOBt, DMAP, dry DMF, 2 h at 0 °C, 48 h at RT, 69%.

Following the same strategy, **TriPEGboc**'s terminal amine is deprotected in DCM in the presence of TFA and it is then coupled to 9-anthracenepropionic acid under the same conditions (Scheme 8) to afford **TriPEGAnth**. Anthracene was the molecule of choice as it can act as an oxygen carrier [45–47]. In recent studies, arene-ruthenium complexes were combined to anthracene moieties to be used for PDT applications in hypoxic environments[48].

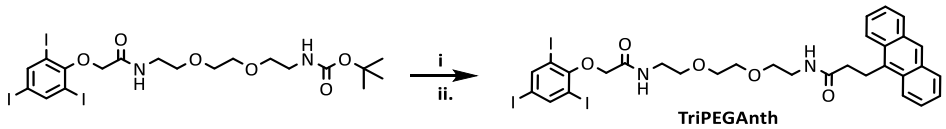

Scheme 8. Synthesis of **TriPEGAnth** i) TFA, DCM, RT, 4 h, 79%. ii) EDCl, HOBt, DMAP, dry DMF, 2 h at 0 °C, 48 h at RT, 69%.

Finally, formation of the panel was performed under Sonogashira conditions as described above, to obtain **L5** (Scheme 9). The formation of this panel suggests that this strategy might be suitable to add extra functionalities to the metalla-assemblies.

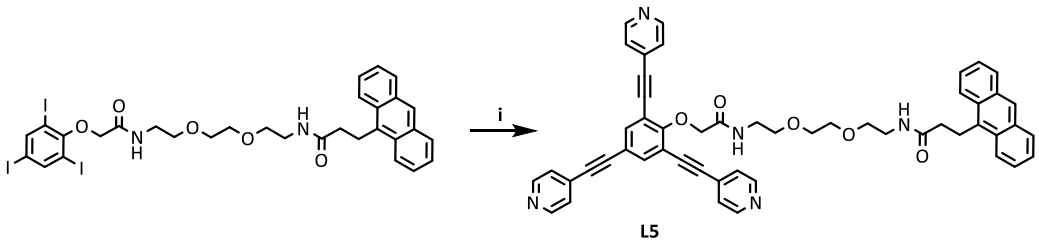

Scheme 9. Synthesis of **L5**, i) 4-ethynylpyridine, $Pd(PPh_3)_4$, CuI, dry Et_3N:THF 1:1.5, 75 °C 48 h, 56%.

Functionalized panels are characterized by a loss in symmetry compared to 4-tpe trigonal panels. This loss of symmetry, can be observed in their ^1H NMR as a splitting of their pyridine signals is observed. In Figure 27, assigned ^1H NMR spectrum of the anthracene derivative is presented.

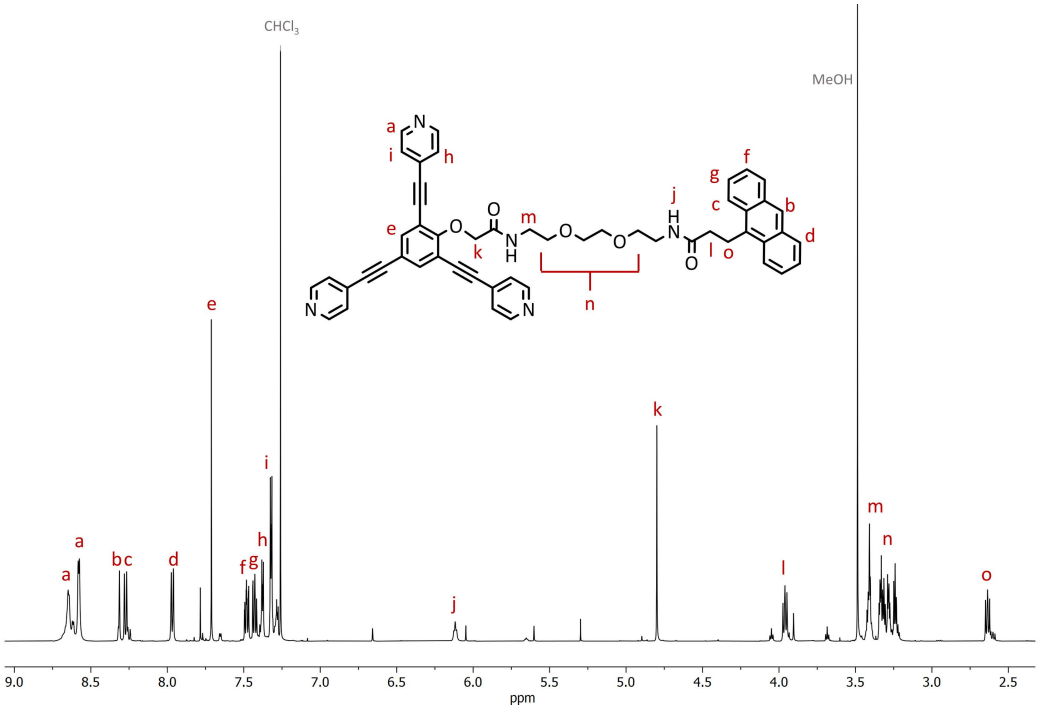

Figure 27. Assigned ^1H NMR spectrum of **L5**.

2.2.2 Formation of metalla-assemblies containing functionalized panels

The formation of metalla-assemblies with functionalized panels is performed using similar conditions to those used in the encapsulation of pyrenes. First, three equivalents of metalla-clip ($[Ru_2(p\text{-cymene})_2(dobq)Cl_2$ for **Pr1-Pr3**, $[Ru_2(p\text{-cymene})_2(donq)Cl_2$ for **Pr4** and **Pr5**) are activated using six equivalents of silver triflate in methanol, then, the solution is filtered to remove AgCl and two equivalents of the corresponding panel (**L1-L5**) are added and the solution is stirred overnight at 60 °C overnight (Scheme 10). All metalla-assemblies are isolated as their trifluoromethanesulfonate salts.

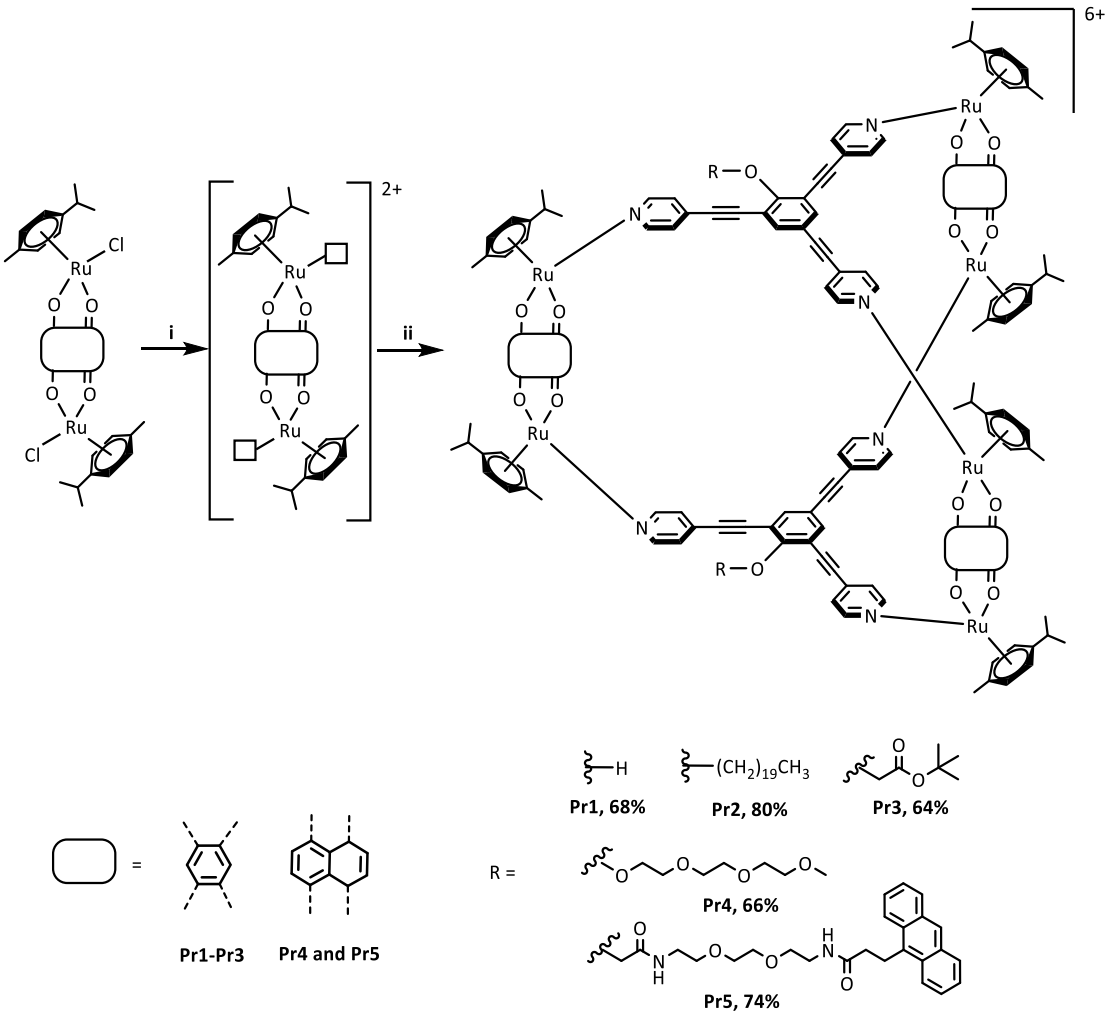

Scheme 10. Synthesis of metalla-assemblies with functionalized panels, i) $AgCF_3SO_3$, MeOH, RT, 4 h. ii) Panel (**L1-L5**), MeOH, 60 °C, overnight.

^{1}H and DOSY NMR for **Pr2** are presented in Figure 28 as an example. The splitting of the signals involving the panel (a and c) due to the presence of the functional group is noticeable. Not only there is less symmetry, but it gives rise to different isomers, which results in further splitting of some of the signals not belonging directly to the panels such as the ones coming from the *p*-cymene aromatic protons (d). DOSY NMR suggests that a single metalla-assembly is formed, since all signals (from panels, clips and side chains) correlate to a single diffusion coefficient. However, the presence of different isomers cannot be excluded as their diffusion coefficient would be equivalent or very similar.

ESI-MS is a further confirmation of the formation of the metalla-assembly. For **Pr2**, a peak corresponding to the assembly plus two triflate ions can be found (Calculated for [**Pr2** - $4CF_3SO_3$]$^{4+}$ 870.7100; Found 870.7144). Such peaks, maintaining some of the counterions, are typically found in arene-ruthenium metalla-assemblies.

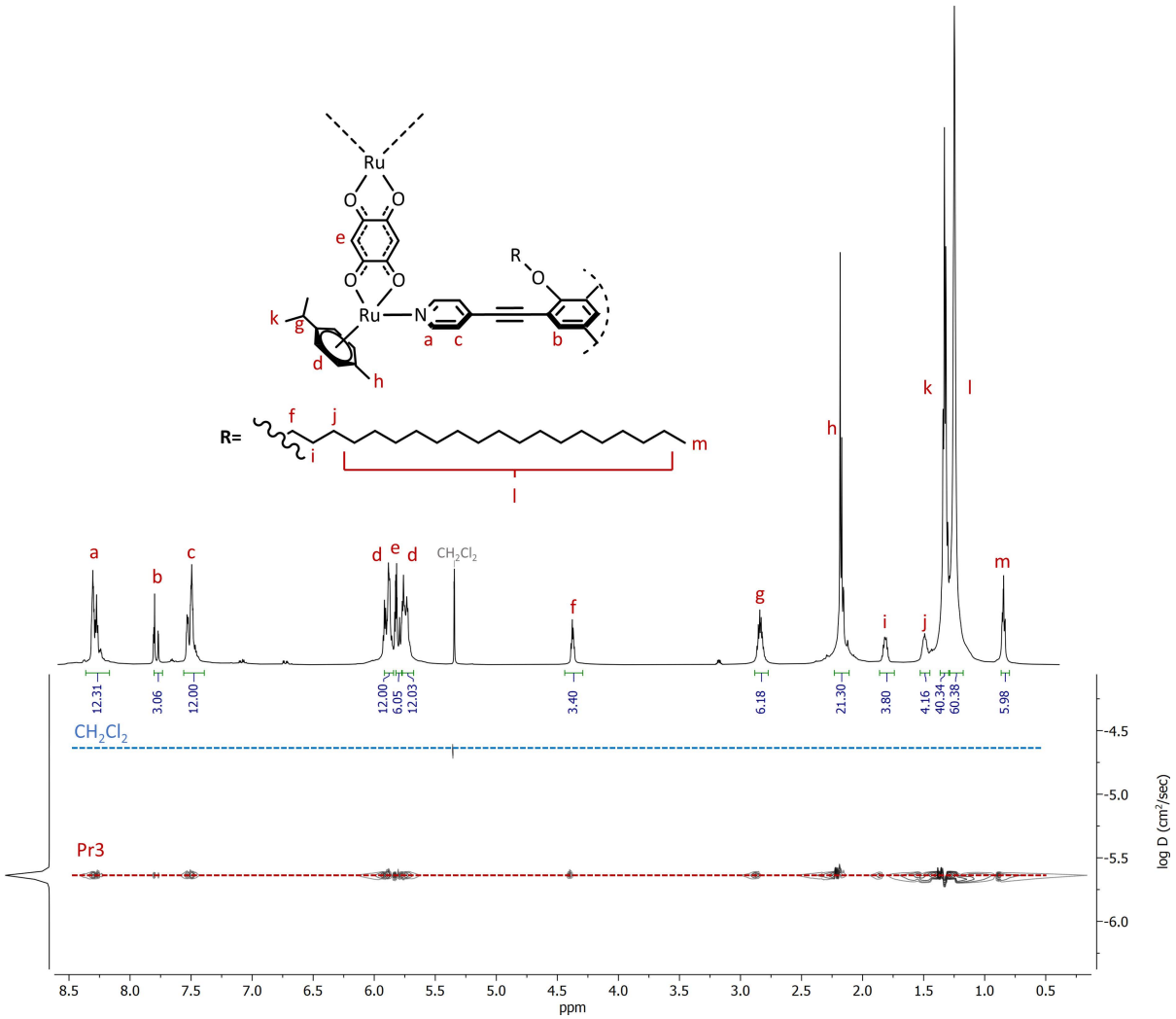

Figure 28. ^{1}H and DOSY NMR spectra of **Pr2**

2.3 Combining functionalized panels and guests

After exploring some of the different methods to functionalize metalla-assemblies, the following step was the combination of those. The functionalization of the building blocks and/or guest is performed before the formation of the metalla-assembly, this allows to keep control on the final structure while combining different functionalities. As it has been discussed, high molecular weight assemblies might be suitable to exploit the EPR effect[103], on this application, being able to control the size of the metalla-assembly through more than one strategy may present an interesting advantage.

Following this idea, one of the pyrenyl derivatives with two side arms described before in this chapter (**Pyr4**) was encapsulated inside a metalla-assembly with functional panels (**Pr6**). **Pr6** contains same panel as **Pr3** but with a different clip, it was decided to use clip with donq spacer as it results in a bigger cavity of the assembly, which can be helpful to accommodate the different building blocks. Synthesis goes through similar steps as the other metalla-assemblies, activation of the clip (3 eq.) in MeOH with $AgCF_3SO_3$ (6 eq.), then filtration and addition of panels **L3** (2eq.) and guest **Pyr4** (1 eq.) (Scheme 11). The final product (**Pyr4⊂Pr6**) is obtained as its trifluoromethane sulfonate salt.

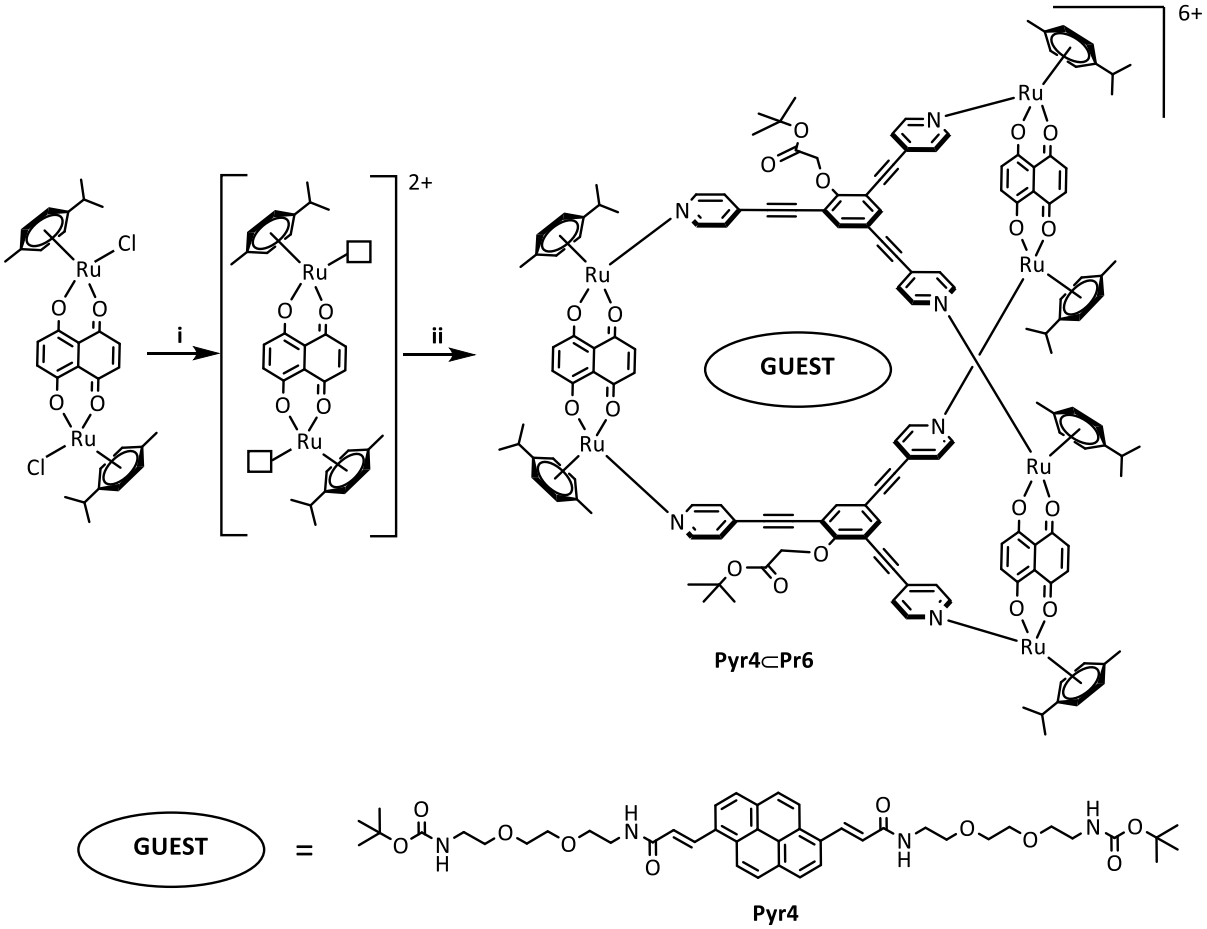

Scheme 11. Synthesis of a host-guest metalla-assembly with functionalized panels, i) $AgCF_3SO_3$, MeOH, RT, 4 h. ii) **L3**, **Pyr4**, MeOH, 60 °C, overnight, 77%.

The ^{1}H and DOSY NMR of **Pyr4⊂Pr6** are presented in Figure 29. The DOSY suggests formation of a single species, as signals from clips (c, h, k, d and i), panels (a, b, e and l) and pyrenyl guest (*, f, g, and j) are all aligned. It is again interesting to see the effect of the encapsulation on the aromatic signals of the pyrene, a similar result to what was observed for assemblies with 4-tpe panels can be seen: they broaden and spread over the spectrum. This effect could be explained by the π-stacking interaction with the panels once encapsulated, signals from side-chains (f and j) do not seem to be affected, as in solution they are sticking outside of the metalla-assembly into the solvent.

Photophysical properties of **Pyr4⊂Pr6** were studied through UV-Vis and fluorescence spectroscopy. UV-Vis spectrum (Figure 30a) of the empty metalla-prism is characterized by two high energy bands at 225 and 326 nm attributed to intra/intermolecular π–π* transitions[104], together with two broad and low-energy bands at 642 and 697 nm associated to MLCT transitions (similar to the ones observed in non-functionalized prisms). Absorbance spectrum of **Pyr4⊂Pr6** is characterized by an overlap of the bands coming from the pyrenyl guest (between 220 and 450 nm) with the bands described for the prism. To study the fluorometric properties of the host-guest metalla-assembly, iso-absorbing solutions (at absorption maximum of the guest, 390 nm) of **Pyr4** and **Pyr4⊂Pr6** were prepared. Emission spectra are presented in Figure 30b. A similar result to non-functionalized prisms is observed, only fluorescence from the guest is observed with partial quenching.

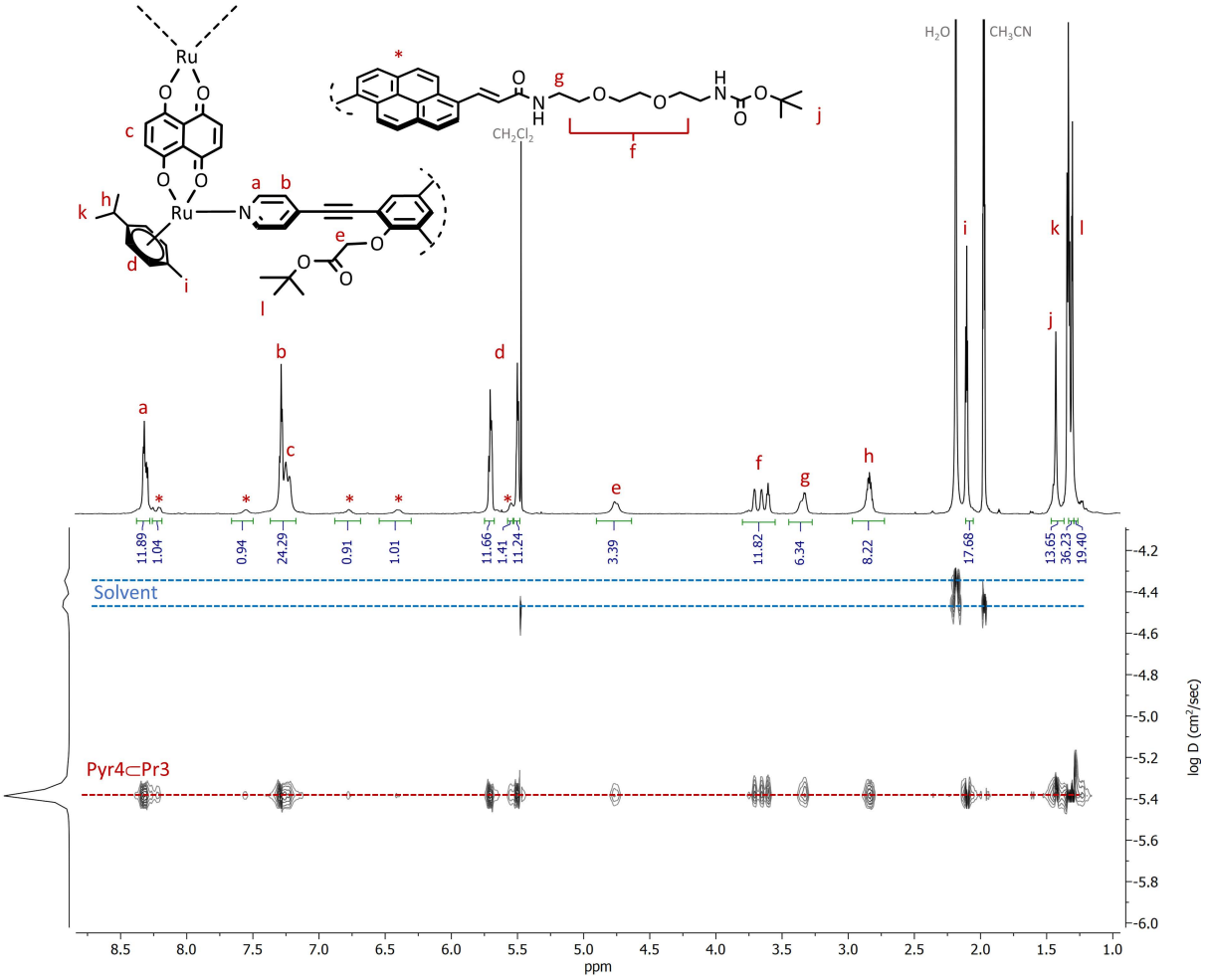

Figure 29. ^{1}H and DOSY NMR spectra of **Pyr4⊂Pr6**

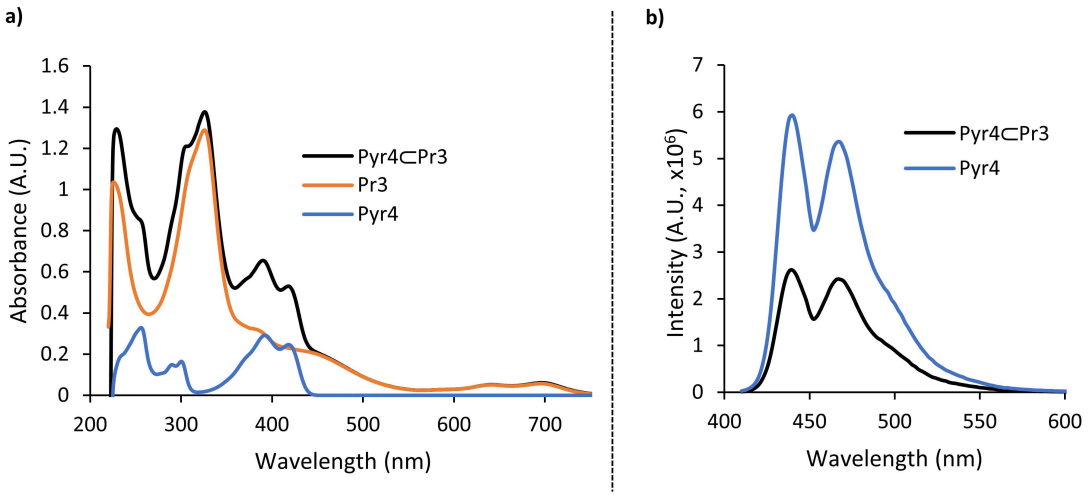

Figure 30. a) UV-Vis spectra of **Pyr4⊂Pr6** and its building blocks ($5x10^{-5}$ M in DCM) b) Emission spectra of **Pyr4⊂Pr6** and **Pyr4** (DCM, λ_{exc} 390 nm)

2.4 Systems with several cages

Thinking of a strategy to increase the weight of metalla-assemblies, another possibility is the formation of a bigger system interconnecting several cages. With this in mind, a scaffold based on a porphyrinic core with four flexible PEG chains, each of them ending with a pyrenyl was designed. Then, the four pyrenyl groups were encapsulated inside an arene-ruthenium metalla-prism, resulting in a large supramolecular system of up to 16 kDa (Figure 31). This system, not only aims to exploit the EPR effect, but since it is based on a central porphyrin, a photosensitizer, it could potentially be used for PDT applications.

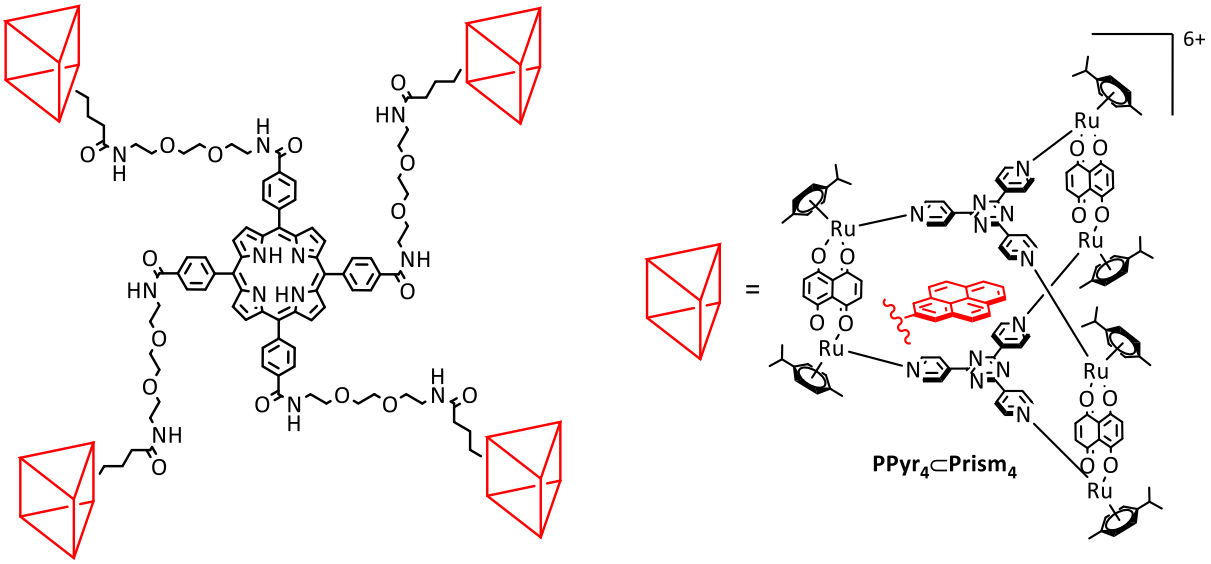

Figure 31. Supramolecular system containing up to 4 metalla-assemblies surrounding a PS.

2.4.1 Synthesis and characterization

Synthesis of the porphyrinic core starts from 5,10,15,20-(tetra-4-carboxyphenyl)porphyrin, to which N-Boc-2,2'-(ethylenedioxy)diethylamine is coupled through amide bonding. The reaction was performed in DMF under inert atmosphere and protected from light, 1 eq. of the porphyrin was mixed with 4 eq. of the PEG derivative in the presence of HOBt (6 eq.), EDCl (6 eq.) and DMAP (4 eq.) (Scheme 12), following a previously published strategy[105].

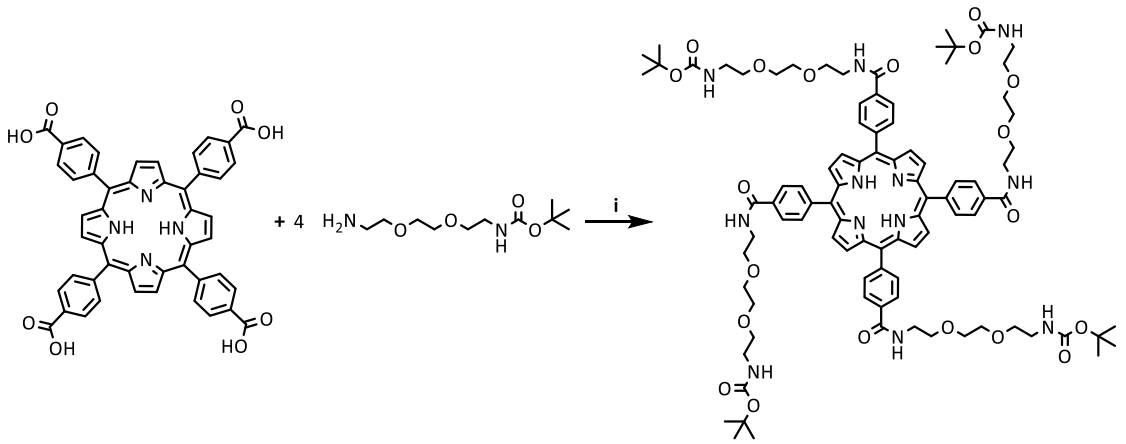

Scheme 12. Coupling of PEG linker through amide bonding, i) EDCl, HOBt, DMAP, dry DMF, RT, 48 h, 80%.

Terminal amine groups were then deprotected in anhydrous DCM in the presence of TFA, and on the next step pyrenebutyric acid was coupled using again an amide bond and similar conditions in the presence of the same coupling agents to afford **PPyr$_4$** in a moderate yield (Scheme 13).

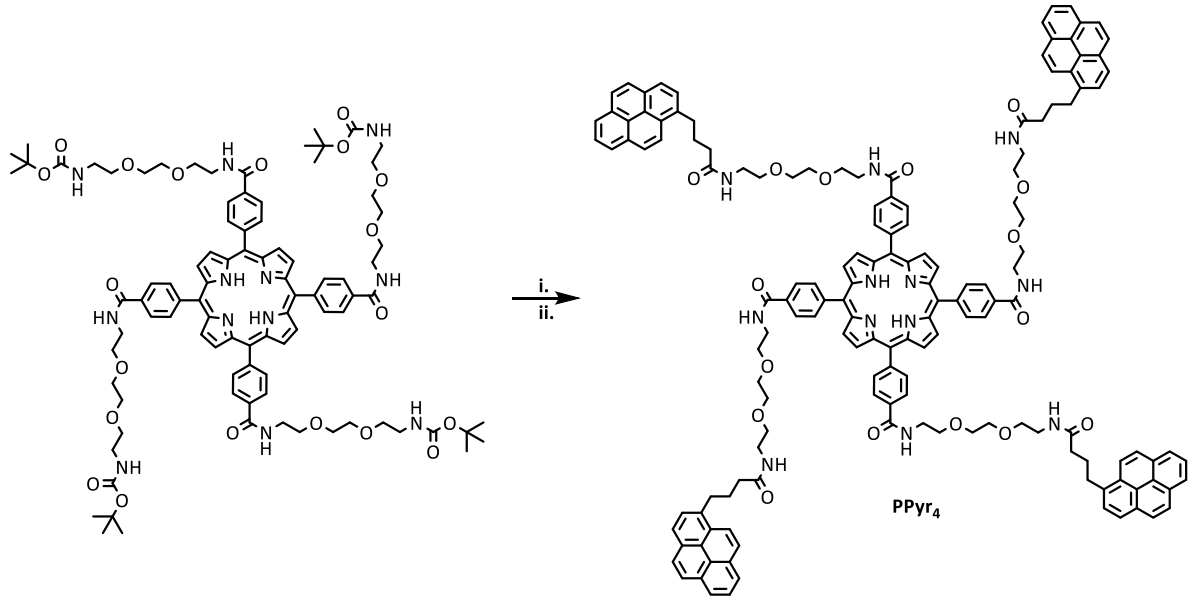

Scheme 13. Synthesis of **PPyr$_4$** i) TFA, DCM, RT, 2 h, 91%. ii) EDCl, HOBt, DMAP, dry DMF, RT, 24 h, 41%.

^{1}H NMR spectrum of **PPyr$_4$** is presented in Figure 32. Aromatic region contains signals from the porphyrin core (a, b and c) and pyrene (d). Between 6 and 7 ppm's the two signals corresponding to the NH protons of the amide groups can be found (e and f). Signals from the PEG chains appear between 3.5 and 3.75 ppm (g, h, I and j). Signals from the alkylic chain that connects to the pyrene appear in the lower region as two triplets (k and l) and one quintuplet (m). Finally, NH protons from the porphyrin can be found in their characteristic spot, close to -3 ppm (n).

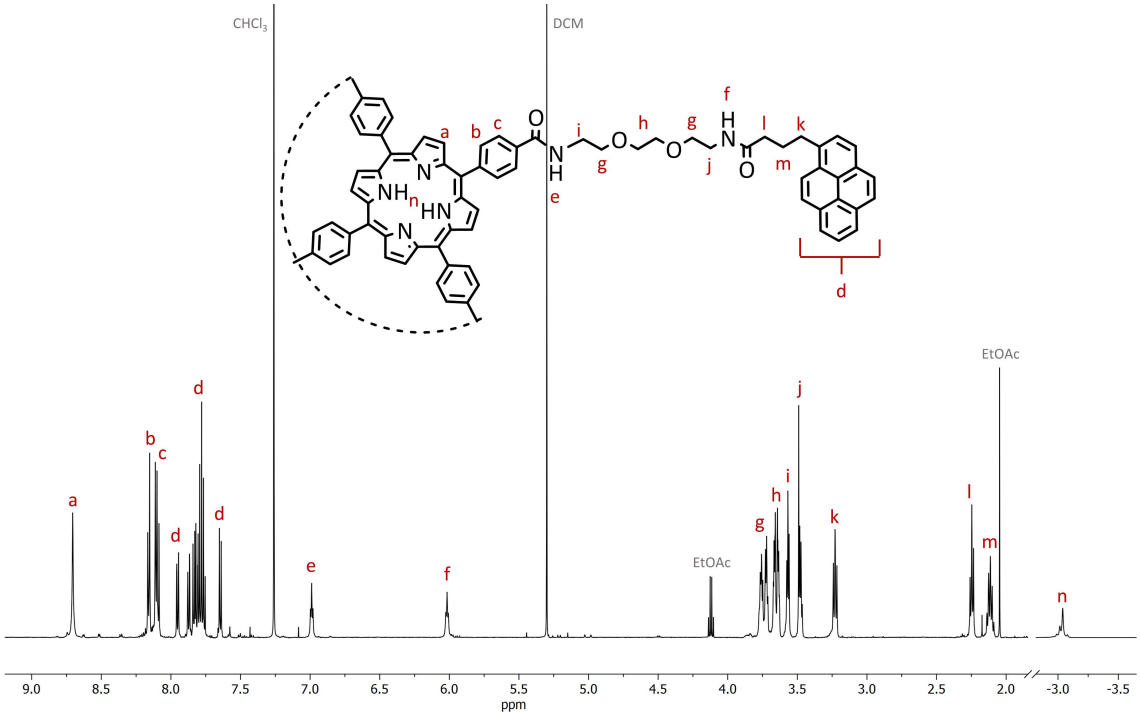

Figure 32. Assigned ^{1}H NMR spectrum of **PPyr$_4$**.

To encapsulate the four terminal pyrenes, the strategy followed the same procedure as in other host-guest metalla-assemblies, using the appropriate amount of every building blocks in order to have a final proportion of four metalla-assemblies to one porphyrin center. Metalla-clip [Ru_2(*p*-cymene)$_2$(donq)Cl_2] (12 eq.) was activated in MeOH with $AgCF_3SO_3$ (24 eq.) for 4h at RT. Then, the solution was filtered and 4-tpt (8 eq.) together with **PPyr$_4$** (1 eq.) were added. The solution was stirred at 60 °C overnight (Scheme 14), solvents were evaporated, and the resulting solid was redissolved in minimum amount of DCM and precipitated with diethylether to afford the final product.

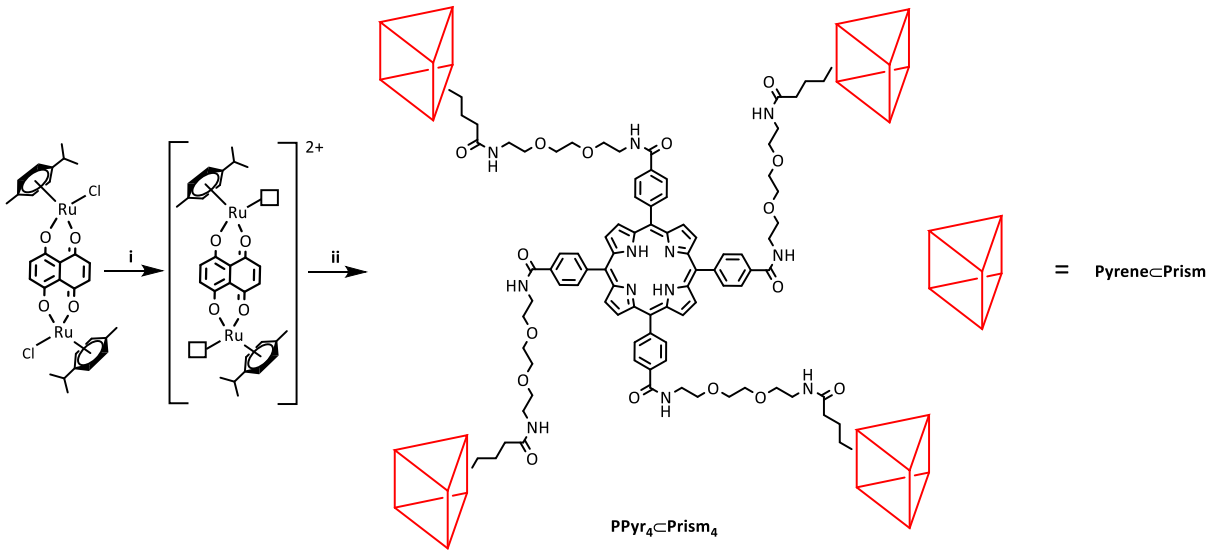

Scheme 14. Synthesis of **PPyr$_4$⊂Prism$_4$**, i) $AgCF_3SO_3$, MeOH, RT, 4h. ii) 4-tpt, **PPyr$_4$**, MeOH, 60 °C, overnight, 64%.

Characterization of **PPyr$_4$⊂Prism$_4$** through ^{1}H NMR was found to be complicated as it is a very big system, with a total weight of over 16 kDa (assuming four assemblies are formed). Not only that, it goes through up to four different encapsulations in which the host-guest dynamics might be different for each one, as the system needs to adapt and in the space for every metalla-assembly added. For this reasons, DOSY NMR was used to study this system (Figure 33). It can be appreciated that there is presence of one main species, with correlated signals that suggest the formation of host and guest systems:

- Aromatic region a contains proton signals coming from the porphyrin, pyrene and 4-tpt panels.
- Region b contains signals from aromatic protons from the *p*-cymene.
- Region c, contains protons from the PEG chain linkers.
- Regions d, e and f contain alkylic protons from the *p*-cymene.

On the other hand, there are other minor species (* in Figure 33) that potentially belong to free metalla-assemblies or clips, as these signals seem to belong to *p*-cymene.

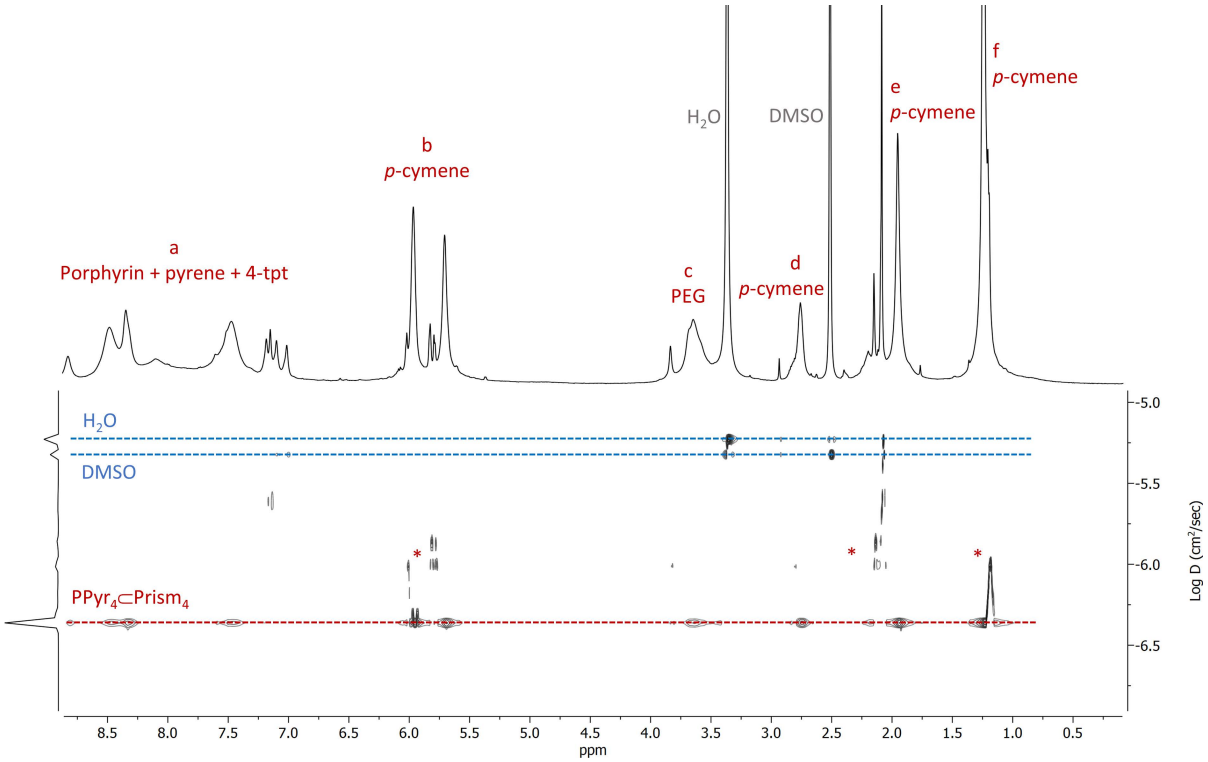

Figure 33. ^{1}H and DOSY-NMR of **PPyr$_4$⊂Prism$_4$**.

Photophysical characterization of **PPyr$_4$⊂Prism$_4$** was performed and compared to **PPyr$_4$** and **Prism** as well as with the building blocks of **PPyr$_4$** (Pyrene and TPP) and those of the prism (4-tpt panel and [Ru$_2$(*p*-cymene)$_2$(donq)Cl$_2$] clip). In Figure 34, absorption spectra of **PPyr$_4$** and **Prism** are compared to those of their building blocks. In the case of **PPyr$_4$** (Figure 34 left), the spectrum matches the model with slight differences, suggesting weak electronic interactions between the units: Soret band is broadened, and pyrene bands appear red-shifted about 5-8 nm. As for **Prism**, there is indication of strong interactions among the units of the cage (Figure 34 right), as the spectrum of **Prism** presents big differences from the model.

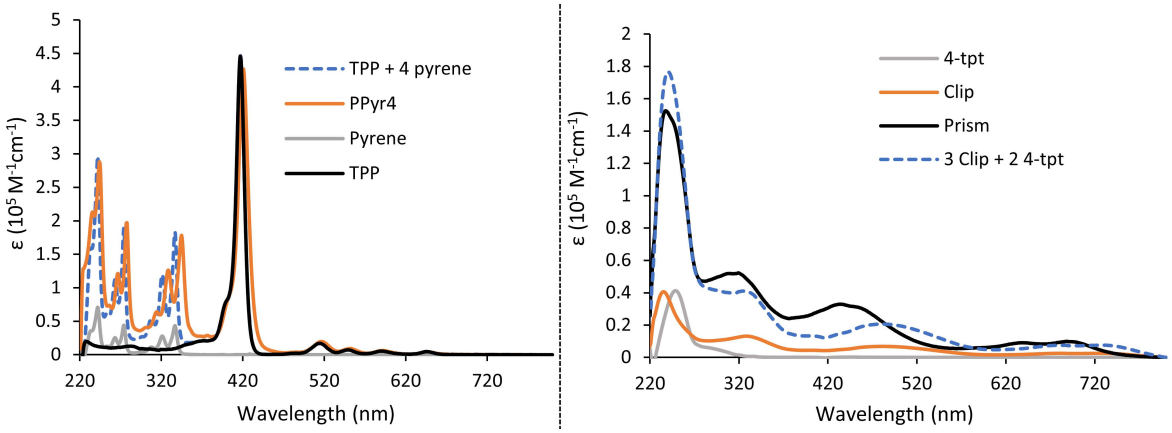

Figure 34. Absorption spectra in DCM of **PPyr$_4$** (left) and Prism (right) each of them containing as well their respective components. Weighted sum of the spectra of the components is also presented.

Absorption spectra of **PPyr$_4$⊂Prism$_4$** is presented in Figure 35 and it is compared to the building blocks. The spectrum matches the weighted sum of the spectra of the components, only a decrease can be observed in the porphyrins Soret band and in pyrene bands, which suggests there is an interaction between them and the coordinated cages.

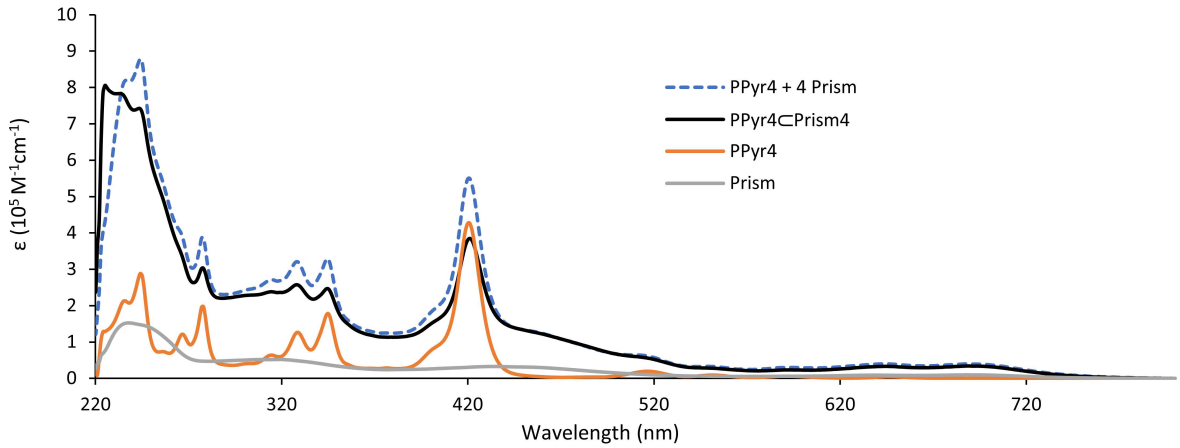

Figure 35. Absorption spectra of **PPyr$_4$⊂Prism$_4$** and its building blocks in DCM. Weighted sum of the spectra of the models is also presented.

Emission studies of the systems were performed in DCM. As it has been observed for other metalla-assemblies, **Prism** and its building blocks proved to be non-emissive. **PPyr$_4$** displays typical porphyrin fluorescence when excited at 515 with a quantum yield of 0.11 and a lifetime of 9.2 ns (Figure 36 left, Table 3), comparable to those of model TPP. In opposition, when **PPyr$_4$** is excited at 345 nm (where there is only absorbance of the pyrene units) the fluorescence of the pyrene is completely quenched while still conserving similar emission from the porphyrin (Figure 36 right). This result suggests that there is a highly efficient energy transfer from the pyrene to the porphyrin. Same experiment results for **PPyr$_4$⊂Prism$_4$** can be observed on the same figure, in this case, emission of the pyrene is also totally quenched, but the porphyrin emission is partially quenched due to photoinduced processes involving the **Prism** components. This quenching can be observed as well on the quantum yield of **PPyr$_4$⊂Prism$_4$**, which was found to be ten times lower than that of the model TPP (Table 3). This reduction of the fluorescence quantum yield might be a good indication thinking on potential PDT applications: fluorescence is a direct energetic decay from the singlet state into the ground state, therefore, a lower ϕ_{fl} suggests that more energy decays through other methods, potentially intercrossing to triplet state and producing reactive oxygen species (ROS). An enhancement of this singlet-to-triplet intersystem crossing is one of the desirable properties in photosensitizers[106,107].

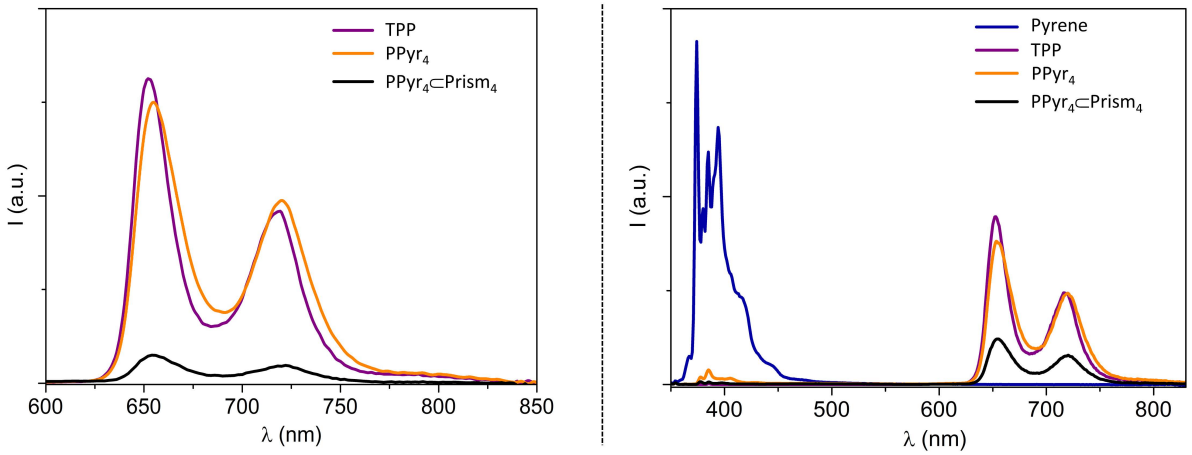

Figure 36. Left: Corrected emission spectra of iso-absorbing solutions of TPP, **PPyr$_4$** and **PPyr$_4$⊂Prism$_4$** in DCM, excitation at 515 nm (A_{515} = 0.13); Right: Corrected emission spectra of iso-absorbing solutions of **PPyr$_4$**, **PPyr$_4$⊂Prism$_4$** and models Pyrene and TPP in DCM; excitation at 345 nm (A_{345} = 0.11).

	λ_{max} (nm)[a]	ϕ_{fl}[b]	τ (ns)[e]
Pyrene [f]	374, 385, 394	0.063[c]	26.3
TPP	652, 718	0.091[d]	8.2
PPyr$_4$	654, 720	0.10[d]	9.2
PPyr$_4$⊂Prism$_4$	654, 720	0.010[d]	0.4 (10%); 9.1 (90%)[g]

Table 3. Emission data at RT for **PPyr$_4$⊂Prism$_4$** and its models. [a] Emission maxima from corrected spectra. [b] Fluorescence quantum yields. [c] Measured with reference to α-NPO in aerated cyclohexane (ϕ_{fl} = 0.94), excitation at 321 nm[108]. [d] Porphyrin emission quantum yield, measured with reference to TPP in aerated toluene (ϕ_{fl} = 0.11)[109], excitation at 515 nm. [e] Excited state lifetimes, excitation at 465 nm for the porphyrin component and 331 nm for pyrene (in brackets: fractional intensities). [f] Data in line with those reported in ref.[110g] Lifetimes measured with single photon counting technique. An ultrafast component is also identified by means of transient absorption analysis (see text).

2.5 Conclusion

A new set of pyrenyl derivatives containing two arms has been synthesized and characterized. Their encapsulation in arene ruthenium metalla-prisms has as well been studied through ^{1}H and DOSY NMR, HRMS, UV-VIS and emission spectroscopy. The presence of a second side-chain does not hinder the yield of the encapsulation, which suggests that this strategy might be suitable to obtain higher molecular weight host-guest systems.

Functionalization of trigonal panels through their central aromatic ring has been explored, obtaining a set of derivatives with alkylic or PEG chains. These panels have been used to form metalla-prisms obtaining yields similar to non-functional panels. Functional panels have been combined with the double-arm pyrenyl guests to form host-guest systems, proving that the combination of these two methods to obtain multifunctional assemblies is possible.

Finally, a new system based on a porphyrinic core attached to up to four metalla-prisms has been synthesized and characterized. Photophysical properties of this system have been studied through UV-Vis and emission spectroscopies. This system of up to 16 kDa could be used to target the EPR effect, as it falls close to the size needed for this application while at the same time, the central porphyrin ring can act as a photosensitizer for PDT applications.

3. Design and synthesis of multifunctional metalla-assemblies

3.1 Targeted drug delivery

One of the properties that are the most interesting when talking about drug delivery is selectivity, which can be enhanced by using targeting agents, thus helping deliver drugs specifically to cancer cells while minimizing the effect on healthy cells. Cancer cells express many tumor-specific receptors, which can be targeted to deliver cytotoxic agents into tumors, such as monoclonal antibodies[111], vitamins[112,113], fatty acids[114], aptamers[115] and oligopeptides[116]. Among those, vitamins are specially interesting due to their nature. As small molecules, they can be easily modified and linked to form vitamin-drug conjugates[117]. The most studied vitamins in this context are folic acid, vitamin B12 and biotin[117], from which biotin is especially interesting as targeting agent.

Biotin, also known as vitamin H, is an essential water-soluble vitamin crucial for many cellular functions, such as growth and metabolism of nutrients. The main transporter for biotin has been found to be the sodium-dependent multi-vitamin transporter (SMVT), which is generally overexpressed in several aggressive cancer cell lines, such as leukemia (L1210FR), ovarian (OV 2008, ID8), colon (Colo-26), mastocytoma (P815), lung (M109), renal (RENCA, RD0995), and breast (4T1, JC, MMT06056)[117]. Also, the overexpression of its receptor has been found to be superior to that of folate[118].

For these reasons, biotin was selected as the targeting agent to be attached to the panels of the metallaprisms presented in this chapter. In order to attach the biotin to the panel, a linker had to be chosen, and one of the best candidates was found to be a polyethylene glycol (PEG) chain. PEG is a hydrophilic and neutral molecule that has been widely used to improve solubility and biocompatibility of small molecules or proteins[119]. It is also known as a "stealth" molecule, since it helps avoid phagocytosis, increasing its biocirculation time[120]. Moreover, it is generally regarded as safe by the FDA and there are currently 10 FDA-approved PEG–protein conjugates and one PEG–aptamer conjugate with diverse applications as therapeutics in the clinic[119].

3.2 Photodynamic therapy (PDT)

Cancer chemotherapy still presents many drawbacks: it has plenty of side effects on human health, and its efficacy is conditioned by many factors giving rise to what is known as multidrug resistance[121,122]. One of the strategies developed to overcome these problems is Photodynamic Therapy (PDT), in which a photosensitizer (PS) is activated with light at a specific wavelength, thus allowing the PS to reach a higher energy triplet state, which can react with neighboring oxygen to produce reactive oxygen species (ROS)[123] (Figure 37)

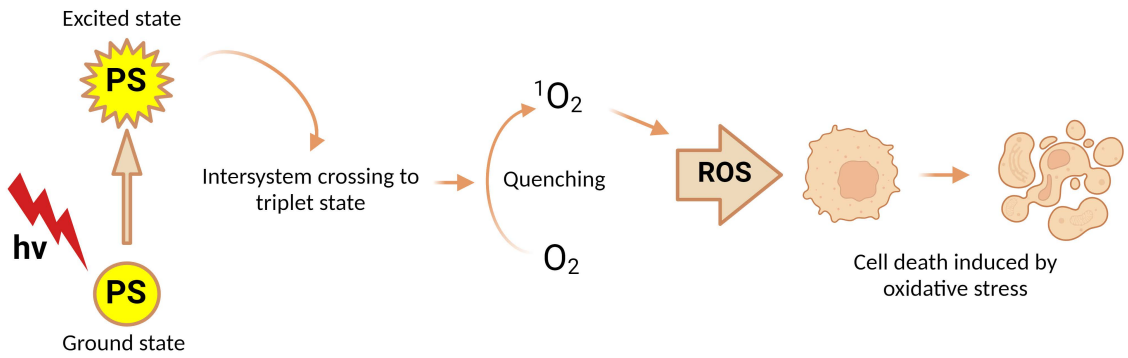

Figure 37. Simplified mechanism of PDT

As an anticancer therapy, PDT presents many advantages, among them are its minimal invasiveness and high spatiotemporal accuracy with minimum side effects. The first clinically approved PS is commercially known as Photofrin®, and has been involved in treating several types of cancer[124,125], even if nowadays it has been withdrawn from use in the European union, it remains an important player in PDT. Second generation of PSs are purely synthetic compounds based on an aromatic macrocycle similar to Photofrin® (porphyrins, chlorins, phthalocyanines, BODIPYs)[126]. Some second generation PSs have been clinically approved, such as temoporfin (Foscan®, Biolitec, Gina, Germany), verteporfin (Visudyne®, Novartis, Basel, Switzerland) and talaporfin (Laserphyrin®, Meiji Seika, Tokyo, Japan)[124]. However, their major drawback comes from their poor water solubility, which leads to aggregation behavior in biological media, and administration limitations[127].

The hydrophobic nature of 1st and 2nd generations of PSs has stimulated the development of third-generation PSs, which are usually composed of a second-generation PS conjugated or encapsulated in a drug delivery system, resulting in a higher affinity for the target cells, and better solubility. Many properties are improved in these systems: stability and hydrophilicity of PSs, pharmacokinetics, pharmacodynamics and biodistribution *in vivo* as well as unwanted side-effects [128,129].

In this project, three different second-generation PSs (Figure 38) from three different families were selected:

- Tetraphenyl porphyrin: As stated before, porphyrins are one of the most well-known and studied PSs, their main drawback being their low water solubility.[130]
- Pheophorbide a: A chlorophyll derivative, also formed by a tetrapyrrolic macrocycle. What makes this molecule especially appealing is that it presents an intense Q-band at 670 nm[131], and a wavelength which belongs inside the ideal therapeutic window for PDT[132]. Wavelengths in this region (650-800 nm) have been proved to be the ones penetrating deepest through human skin[132].
- Boron-dipyrromethene (BODIPY): BODIPYs have been found to possess interesting properties for PDT, such as high extinction coefficients in the red region and resistance to photobleaching[133,134].

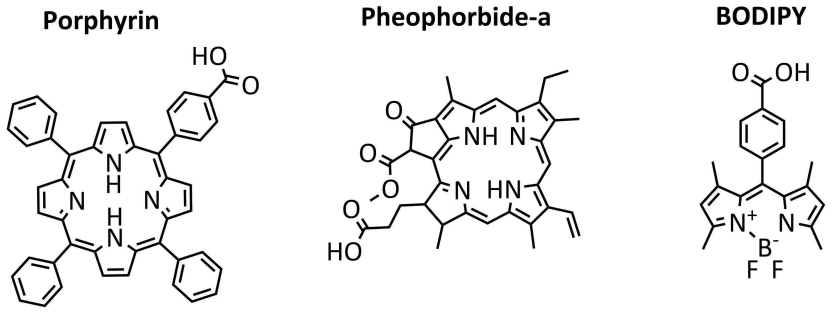

Figure 38. Photosensitizers used in this project

3.3 Multifunctional metalla-assemblies

As it has been discussed in the introduction, one of the best guests for arene-ruthenium metallaprisms is pyrene. The functionalization of this molecule has been used in the past as an anchor to introduce different functionalities to the metalla-assemblies[135–137]. For this reason, pyrene is the base molecule used in this project to introduce the PSs. The strategy used to form these pyrenyl-PS derivatives is the same as the one proposed for the biotin, using a PEG linker.

With this in mind, a new set of third-generation photosensitizers has been developed, based on pyrenyl-PS guests encapsulated inside biotinylated metalla-prisms (Figure 39). This multifunctional system combines the water-solubility capabilities of arene-ruthenium prisms and PEG linkers with the targeting properties of biotin, aiming to improve the PDT efficacy. Indeed, the presence of a targeting moiety is expected to help achieve a higher accumulation of the metalla-assembly in cancer cells, thus, helping to achieve an effective therapy, essential in drug-resistant cancer cells[138,139]. Photodynamic properties have been studied *in vitro* on HCT116 colorectal cancer cells.

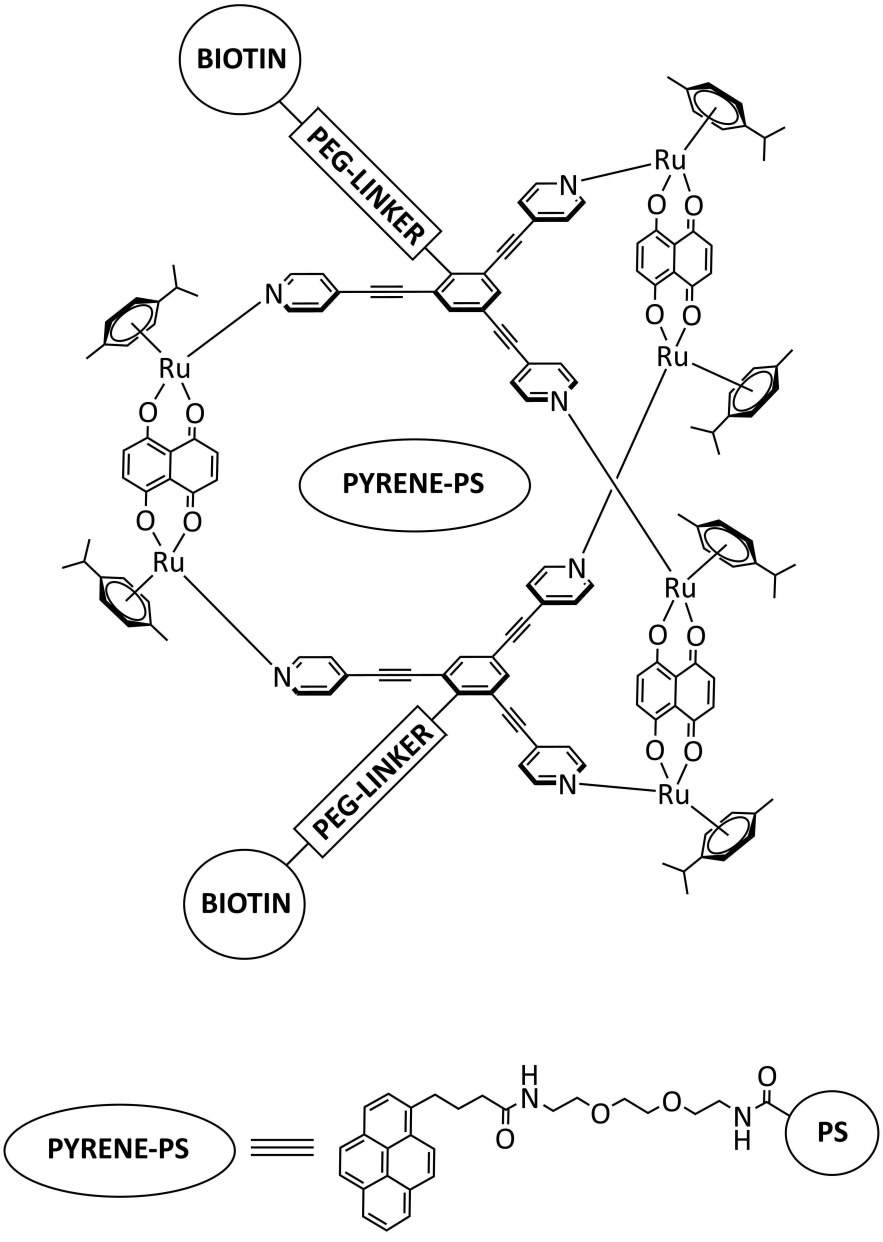

Figure 39. Schematic representation of the multifunctional metalla-assemblies.

3.4 Synthesis and characterization

3.4.1 Biotinylated panel

The functionalization of the trigonal panel starts by the functionalization of the central aromatic ring. The first step is a Williamson ether synthesis reaction, coupling *tert*-butyl bromoacetate to the hydroxyl group of 2,4,6-triiodophenol. This reaction is performed under reflux in acetone in the presence of an excess of potassium carbonate (K_2CO_3). The following step is to obtain the free carboxylic acid by deprotection of the *tert*-butyl group, using trifluoroacetic acid (TFA) in DCM (Scheme 15).

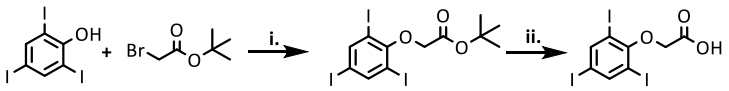

Scheme 15. Synthesis of *tert*-butyl 2-(2,4,6-triiodophenoxy)acetate i) K_2CO_3, DCM, reflux overnight, 67%. ii) TFA, DCM, RT, 3 h, 74%.

Next, the PEG linker (with one of the terminal amines protected) is attached by an amide coupling reaction in the presence of EDCl, HOBt and DMAP in dry DMF under inert conditions (Scheme 16). This type of reaction was chosen as the main strategy to bring the different building blocks together, as amide bonds are the most prevalent structures found in organic molecules and various biomolecules such as peptides, proteins, DNA, and RNA[140].

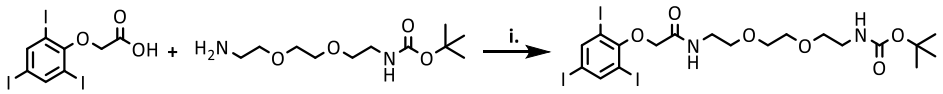

Scheme 16. Synthesis of 2-(2,4,6-triiodophenoxy)-PEGboc, i) EDCl, HOBt, DMAP, dry DMF, 2 h at 0 °C, 48 h at RT, 69%.

The formation of the panel is performed by Sonogashira coupling with 3 equivalents of 4-ethynylpyridine, using $Pd(PPh_3)_4$ and CuI in catalytic amounts and a mixture of dry triethylamine and dry THF 1:1.5 under inert conditions (Scheme 17). This reaction is the main limiting step in the formation of new panels, as yields tend to be moderate.

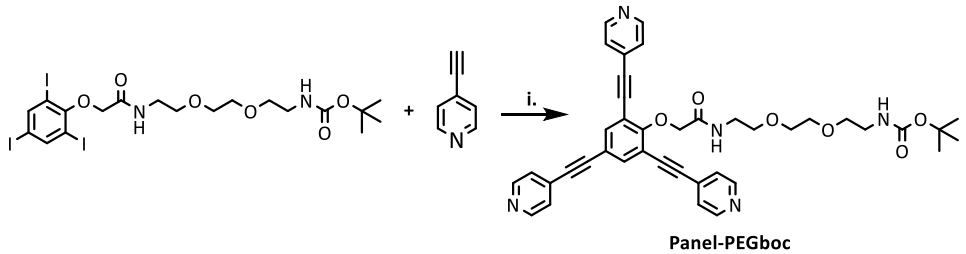

Scheme 17. Synthesis of **Panel-PEGboc**, i) $Pd(PPh_3)_4$, CuI, dry Et_3N:THF 1:1.5, 75 °C 48 h, 43%.

Finally, the terminal amine from the PEG is deprotected in DCM in presence of TFA, and biotin is coupled using the exact same conditions as for the previous amide coupling reaction (Scheme 18).

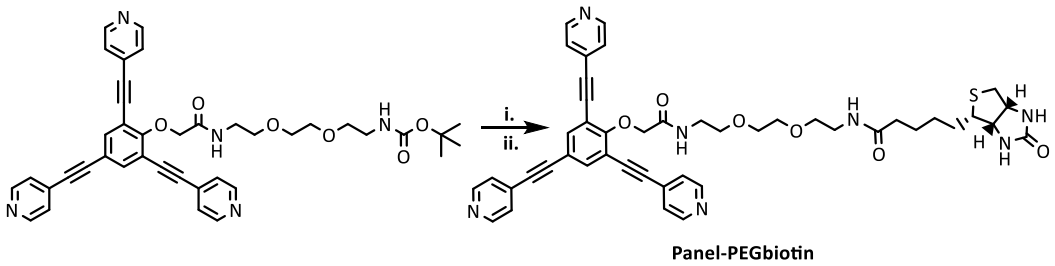

Scheme 18. Synthesis of **Panel-PEGbiotin**, i) TFA, DCM, RT, 4 h, 92%. ii) EDCl, HOBt, DMAP, dry DMF, 2 h at 0 °C, 48 h at RT, 61%.

Regarding the characterization of the biotinylated panel, the most interesting feature is the loss of symmetry originated from the introduction of the linker in the central ring. This loss of symmetry is translated in the ^{1}H-NMR spectrum with a splitting of the signals in the aromatic region (Figure 40). When building metalla-prisms on the next chapters this feature will become more relevant, since it will have a role in the characterization of these metalla-assemblies. The formation of the panel was further confirmed by electrospray ionization mass spectrometry (ESI-MS), which displays a molecular peak at 812.3232, the signal corresponding to [**Panel-PEG-biotin** + H]$^{+}$ (m/z, calc for $C_{45}H_{46}N_7O_6S$ 812.3230)

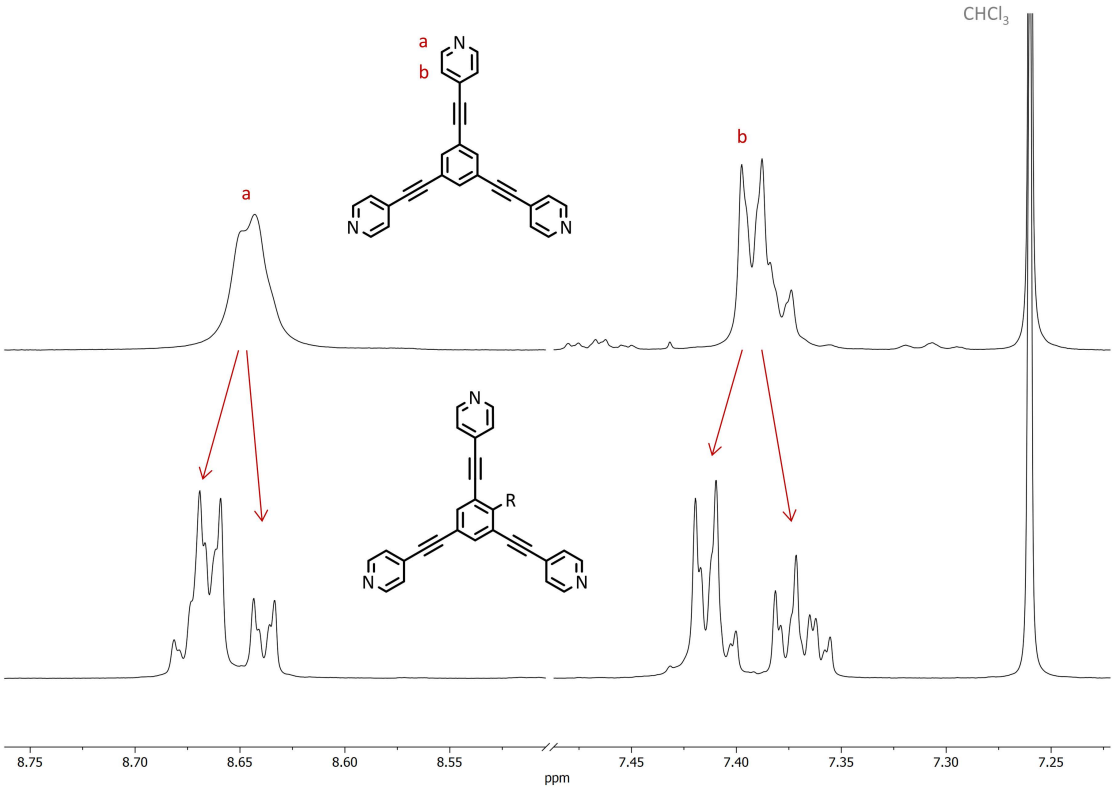

Figure 40. NMR comparison between 4-tpe and biotinylated panel.

3.4.2 Pyrenyl-PS derivatives

In the synthesis of the pyrenyl derivatives, the same short PEG linker was used. In a similar strategy, the PEG linker is initially coupled to 1-pyrenebutyric acid through an amide coupling reaction, same conditions as before but in this case in DCM. The following step is again the removal of the BOC protecting group in DCM in the presence of TFA (Scheme 19).

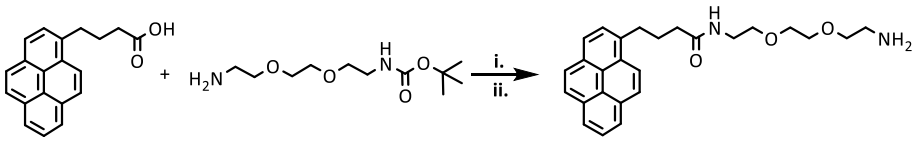

Scheme 19. Coupling of 1-pyrenebutyric acid with PEG linker, i) EDCl, HOBt, DMAP, dry DCM, 2 h at 0 °C, 48 h at RT, 90%. ii) TFA, DCM, RT, 4 h, 94%.

The synthesis of BODIPY derivatives has been extensively studied[133,141], in this specific case, the procedure published by Rampazzo et. al.[141] was used. In the first part, 2,4-dimethylpyrrole is reacted with methyl 4-(chlorocarbonyl)benzoate in dry DCM in the presence of $MgSO_4$ under inert conditions, going through a non-isolated intermediate. In the second step, N,N-diisopropylethylamine (DIPEA) and boron trifluoride diethyl etherate are added. Finally, the methyl protecting group is removed in THF solution in the presence of lithium hydroxide (Scheme 20).

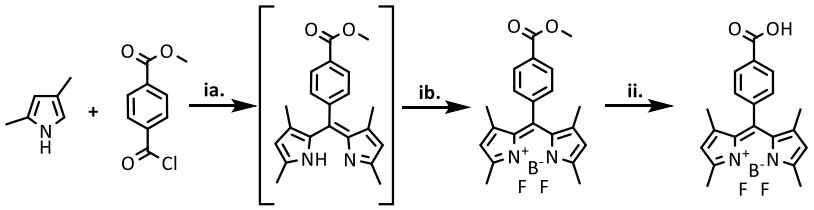

Scheme 20. Synthesis of BODIPY, ia) $MgSO_4$, dry DCM, 50 °C, 4 h ib) DIPEA, boron trifluoride diethyl etherate, 50 °C, overnight, 37% ii) LiOH, THF, RT, overnight, 33%.

As for pheophorbide-a, it is bought as the methyl derivative and deprotected in acetone in the presence of HCl[142] (Scheme 21), prior to the coupling to pyrene.

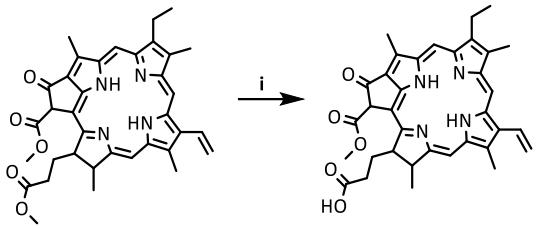

Scheme 21. Deprotection of methyl pheophorbide-a, i) HCl, acetone, RT, overnight, 82%.

Finally, together with the commercially available 5-(4-carboxyphenyl)-10,15,20-(triphenyl)porphyrin, all three photosensitizers are coupled through an amide bond to the Pyrenyl-PEG derivative, using the same conditions as before in DCM (Scheme 22).

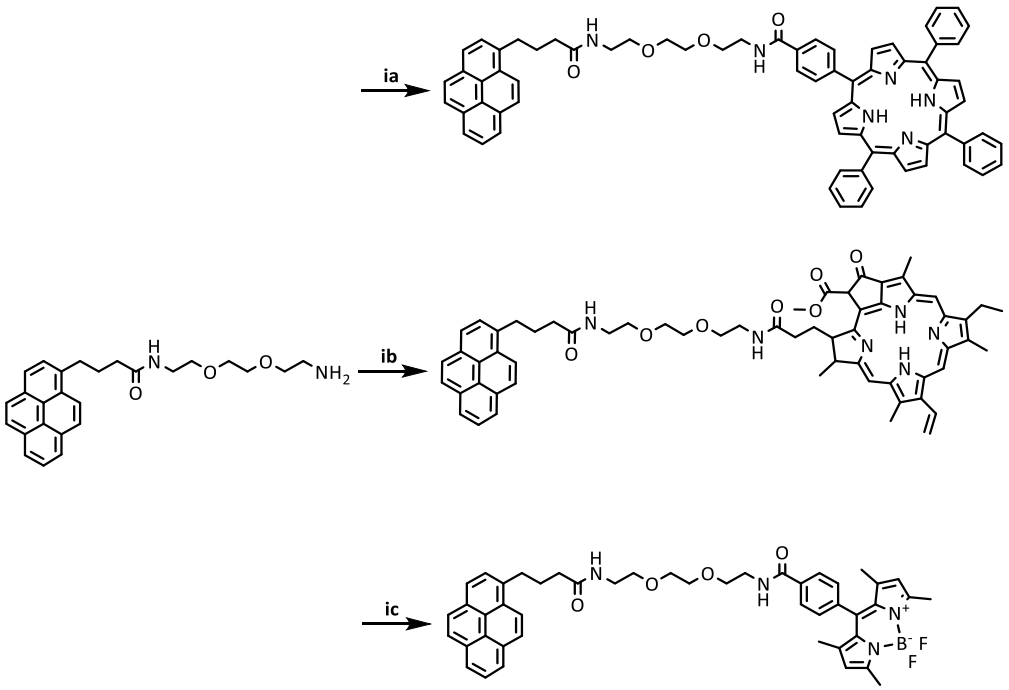

Scheme 22. Coupling of the photosensitizers, i) EDCl, HOBt, DMAP, dry DCM, 2 h at 0°C, 48 h at RT ia) 5-(4-carboxyphenyl)-10,15,20-(triphenyl)porphyrin, 91%. ib) pheophorbide-a, 72%. ic) BODIPY, 89%

All three final compounds have been fully characterized by ^{1}H-NMR, ^{13}C-NMR, ESI-MS and UV-Visible spectroscopy. Their ^{1}H NMR spectra are characterized by a set of aromatic signals corresponding to the pyrene, in the case of **Pyrene-TPP** and **Pyrene-PheoA**, some of the peaks from the photosensitizer fall as well in the same region. Also, all three pyrenyl derivatives show a similar set of PEG signals. In Figure 40, assignation of **Pyrene-BODIPY** ^{1}H NMR spectrum can be seen as an example. All the characterization data for final compounds and intermediates can be found in the experimental section.

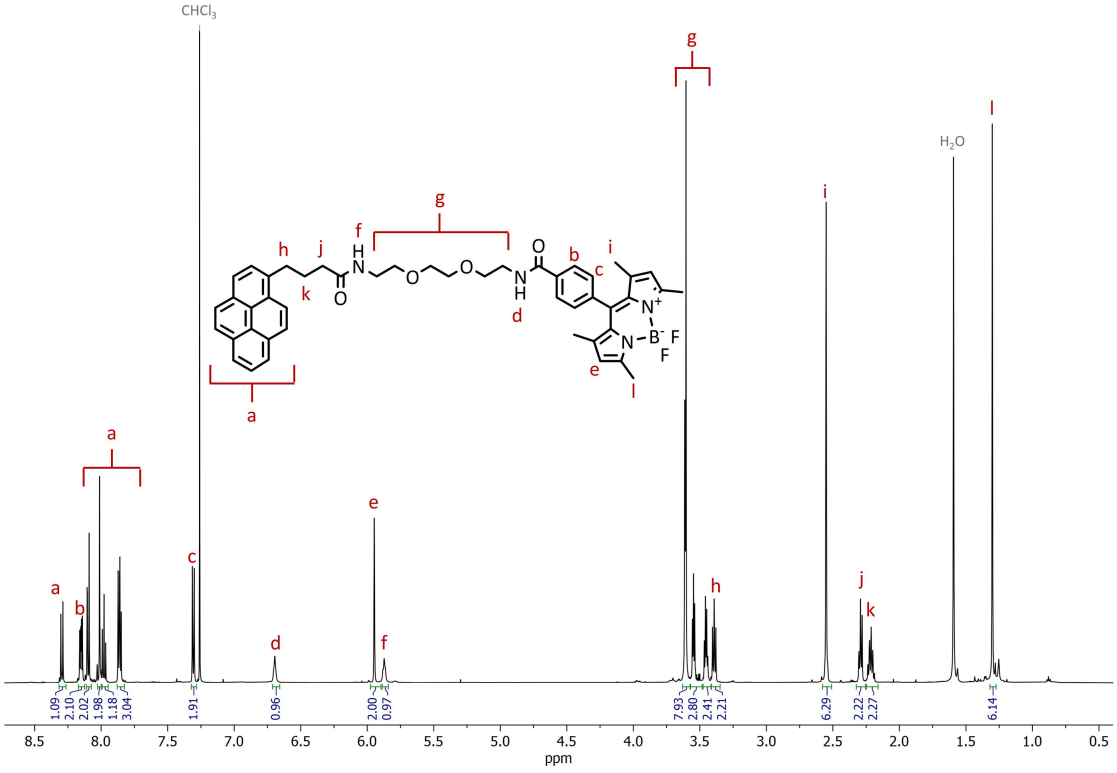

Figure 40. Assigned ^{1}H NMR spectrum of **Pyrene-BODIPY**

3.4.3 Metalla-assemblies

The synthesis of the metalla-prisms follows a simple one-pot strategy, in which the dinuclear arene-ruthenium metalla-clip (in this chapter, always [Ru_2(*p*-cymene)$_2$(donq)Cl_2]) is initially activated in MeOH using silver triflate as a halogen scavenger. After 4h, the solution is filtered to remove AgCl, and the panel is added to the solution. In the case of the host-guest systems, the guest is added with the panel to the mixture (Scheme 23).

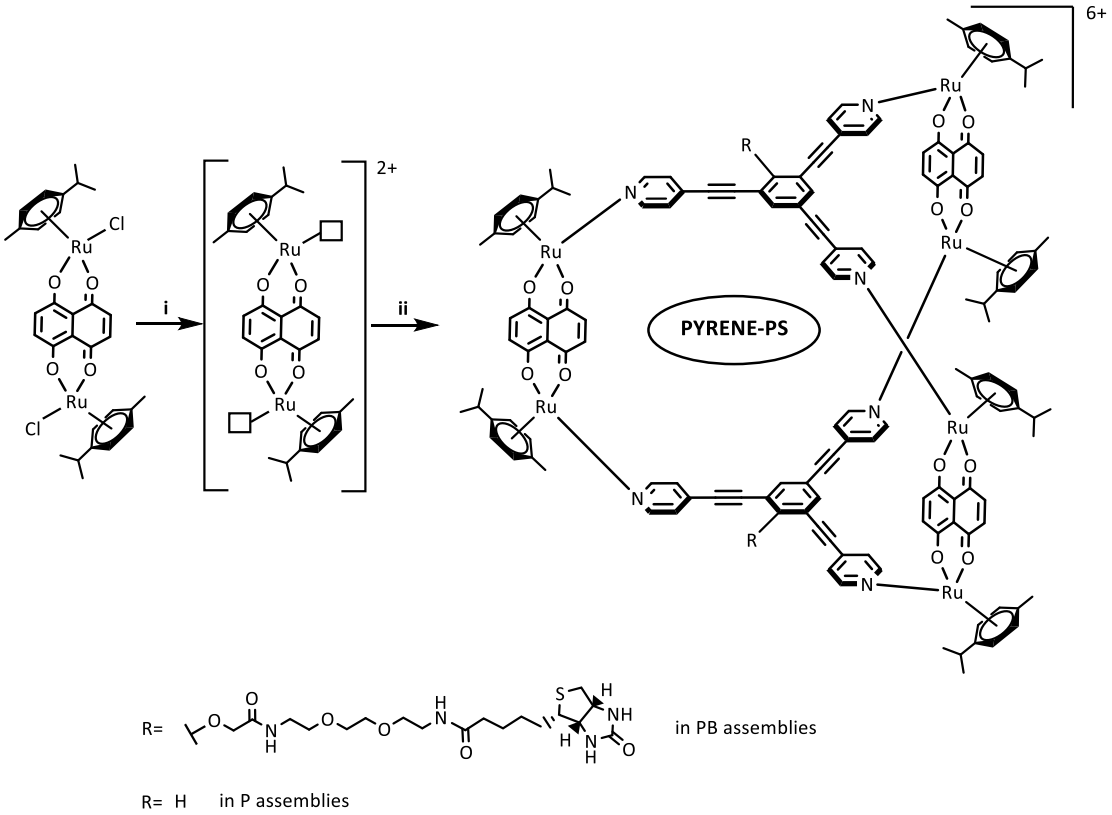

Scheme 23. Synthesis of metalla-assemblies, i) $AgCF_3SO_3$, MeOH, RT, 4 h. ii) Panel, guest, MeOH, 60 °C, overnight.

All combinations of host-guest assemblies were prepared, first using 4-tpe panels (empty cage, and pyrenyl-functionalized guests) and a second set using the biotinylated panel and guests, to afford a total of 8 different assemblies (Table 4).

Compound	Panel	Guest	Yield (%)
P	4-tpe	-	83
Pyrene-TPP⊂P		Pyrene-TPP	89
Pyrene-PheoA⊂P		Pyrene-PheoA	74
Pyrene-BODIPY⊂P		Pyrene-BODIPY	91
PB	Biotinylated	-	79
Pyrene-TPP⊂PB		Pyrene-TPP	81
Pyrene-PheoA⊂PB		Pyrene-PheoA	76
Pyrene-BODIPY⊂PB		Pyrene-BODIPY	79

Table 4. List of host-guest assemblies.

The characterization of the assemblies containing biotinylated panels by ^{1}H-NMR proved to be challenging. The main reason is that the panel shows a lower symmetry, which already was appreciated in the spectrum of the panel alone as discussed before. When the panel is introduced in a prismatic

assembly, this loss of symmetry is accentuated, due to the formation of two isomers, depending on the position of the central PEG-functionalized chain: One isomer being more statistically probable than the other (Figure 41).

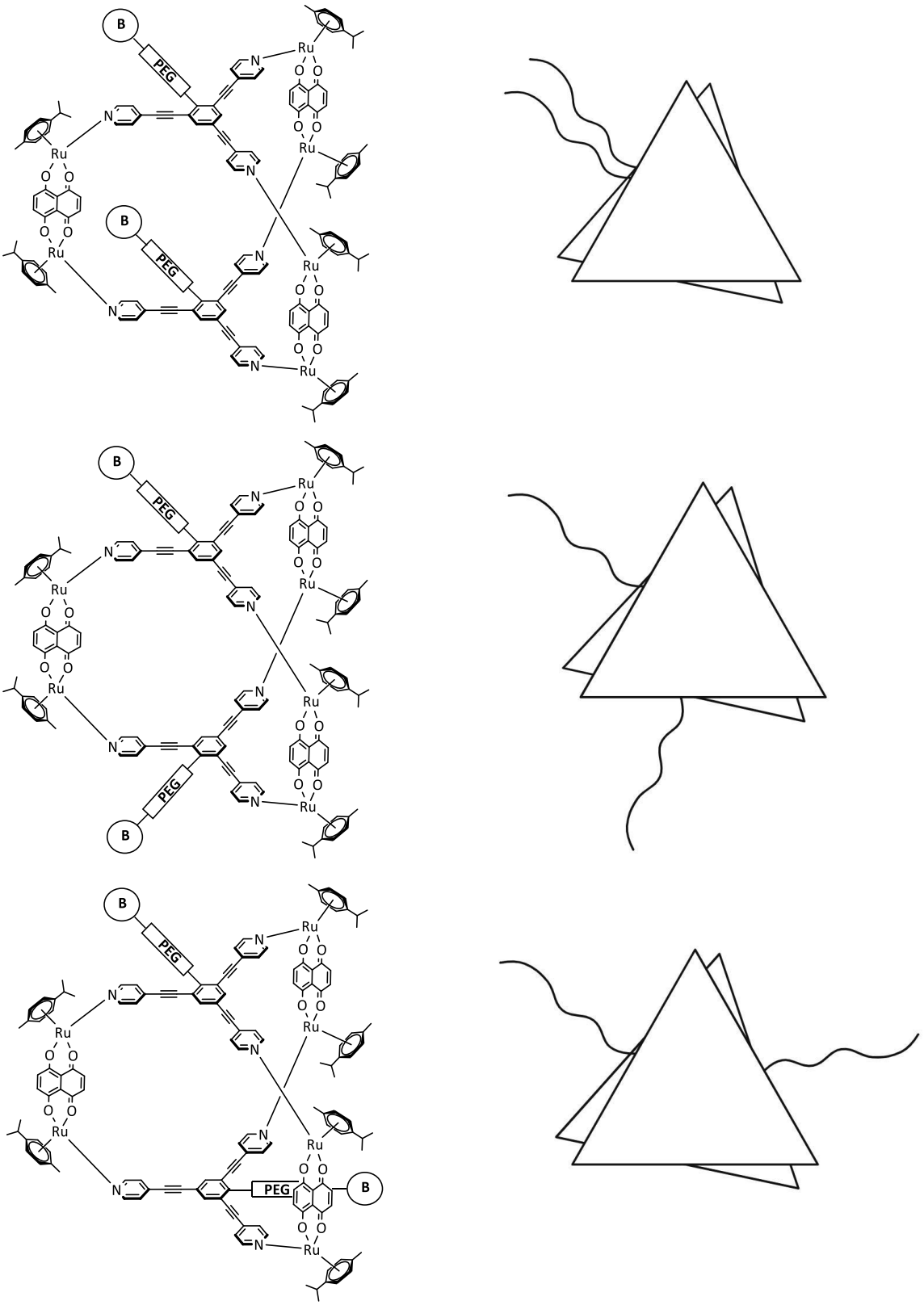

Figure 41. Schematic representation of the different isomers (left), top-view (right).

Two different isomers can be observed in Figure 41, the one at the top is called the eclipsed conformation, where the two PEG chains are on the same side of the panels. The other isomer (middle and bottom of Figure 41) is more statistically probable (two different positions resulting in the same isomer) and it is known as the staggered conformation, where the two PEG chains sit on different sides of the panels. In practice, other factors than statistics can influence the formation of one isomer or the other, for example, steric hindrance may disfavor the eclipsed conformation (top of Figure 41).

Comparing the ^{1}H NMR of **P** and **PB**, the effect of this loss of symmetry can be observed as a broadening of the signals. Specially, it strongly shrinks the signal corresponding to the protons in the central ring, since they are the closest ones (c in Figure 42). Nevertheless, this effect is also observed in the other aromatic protons, in all cases resulting in much broader peaks.

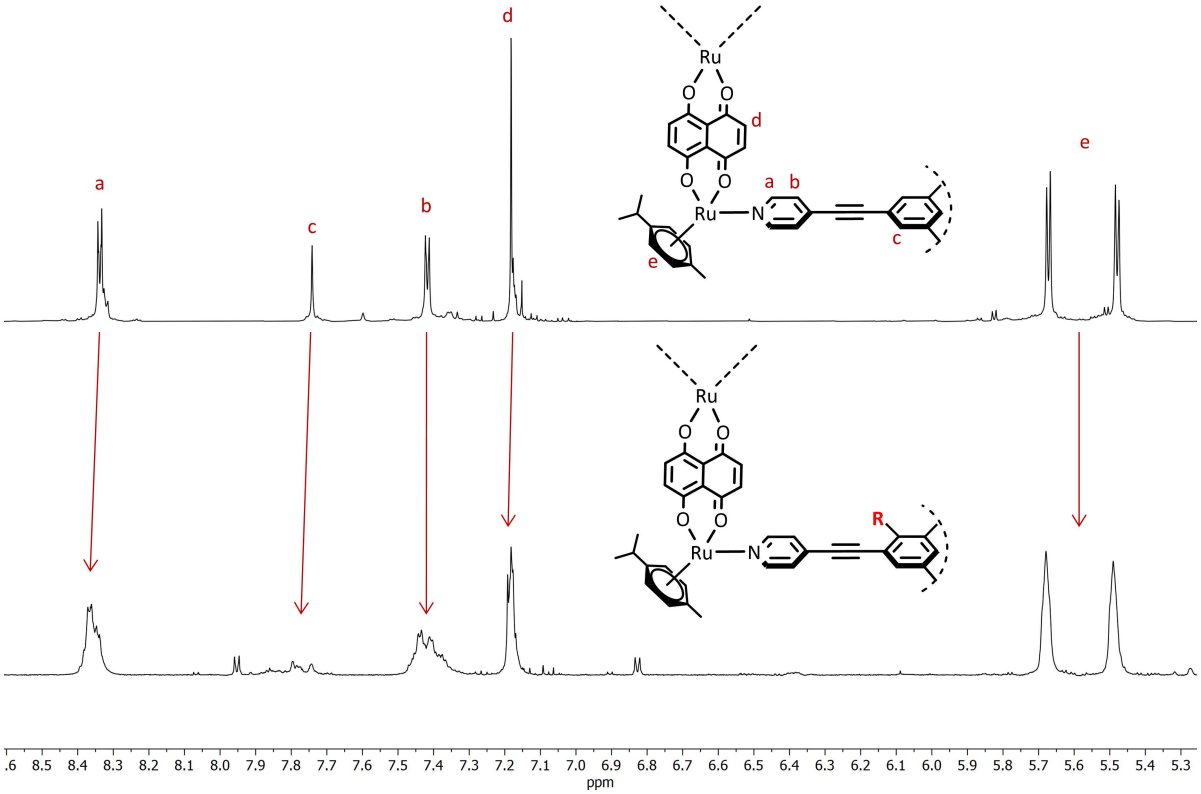

Figure 42. ^{1}H-NMR spectra of P and PB, broadening is observed in PB.

Diffusion ordered spectroscopy (DOSY) is a well established NMR method that reports diffusion coefficients for individual species in solution[94]. In the context of our work, this technique allows us to correlate the signals from the ^{1}H-NMR of the different building blocks to diffusion coefficients. When the assembly is formed, all signals have the same diffusion coefficient. This same principle is applied as well to the host-guest systems, since encapsulated guests will diffuse with the same coefficient as their hosts, if strongly bind.

As an example, DOSY-NMR of both P and PB can be observed in Figure 43. Here, it is possible to correlate signals from the panels with signals of the clips. For PB, it is interesting to see the correlation not only in the aromatic part, but also on the PEG signals. Signal corresponding to biotin itself is hard to identify, as it is mainly masked by the alkylic protons of the *p*-cymene.

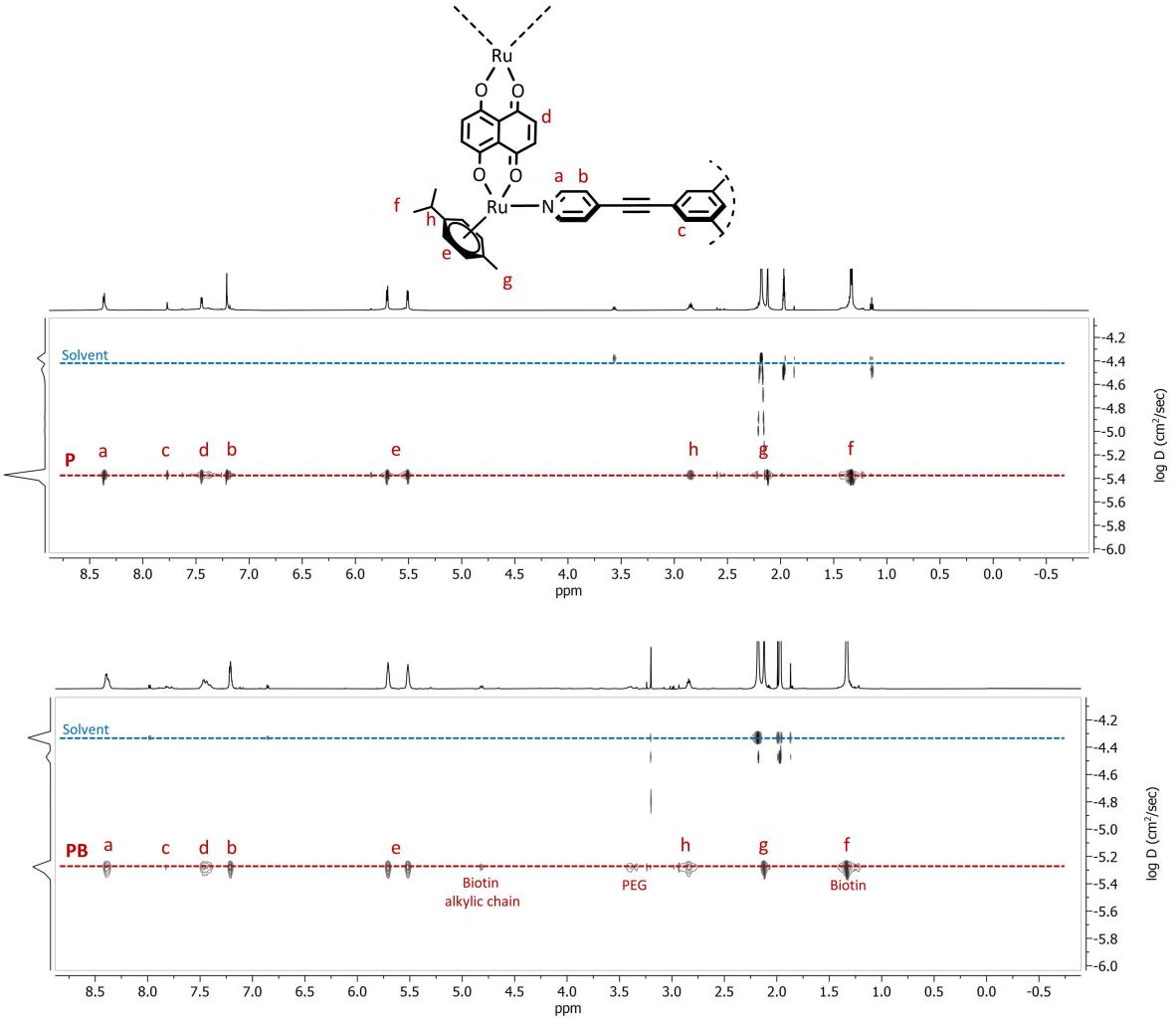

Figure 43. DOSY NMR spectra of both **P** and **PB**

ESI-MS analysis was also performed on the empty and host-guest assemblies. The MS spectra show major peaks corresponding to the main assembly with different amounts of the triflate counterions. Depending on the number of triflates, the charge of the fragment varies. In the case of our hexanuclear prisms, the most common peaks are those corresponding to the loss of three and four triflates, in the case of **P** and **PB** the main fragments are $[\mathbf{PB} - 3CF_3SO_3]^{3+}$ and $[\mathbf{PB} - 4CF_3SO_3]^{4+}$ (Figure 44). Also, the theoretical isotopic pattern is in good agreement with the experimental signal, which is very characteristic of multi-nuclear ruthenium assemblies.

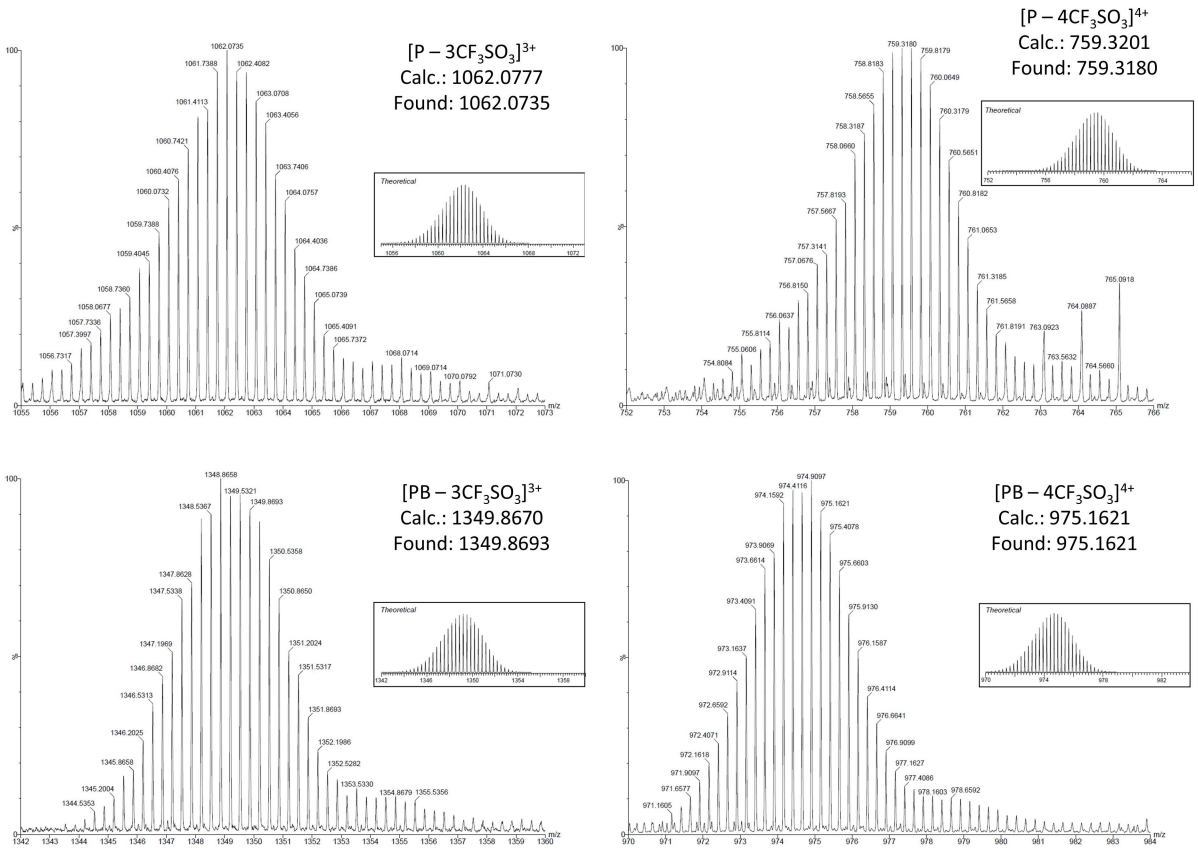

Figure 44. ESI-MS main peaks from **P** (top) and **PB** (bottom).

In the case of host-guest systems containing 4-tpe as panels, the characterization is very similar, their ^{1}H NMR show some broadening due to the presence of the guest, but in that case, the signals can still be distinguished and assigned to a certain extent, even if not totally. The aromatic region is specially complicated, as signals from panels, clips and guest fall in that region. As an example, characterization data for **Pyrene-BODIPY⊂P** will be discussed. The formation of the host-guest is confirmed by DOSY, ESI-MS and UV-Vis. In the DOSY spectrum, it can be appreciated that all peaks have the same diffusion coefficient, so even in the case of doubt of assignation, it is certain that they correspond to the same supramolecular structure. Taking a look at the ^{1}H-NMR in this same figure, it can be seen that most non-aromatic signals can be assigned: all peaks from the *p*-cymene (b, d, g, f), PEG chain from the guest (c) and the alkylic chain also from the guest (e) (Figure 45).

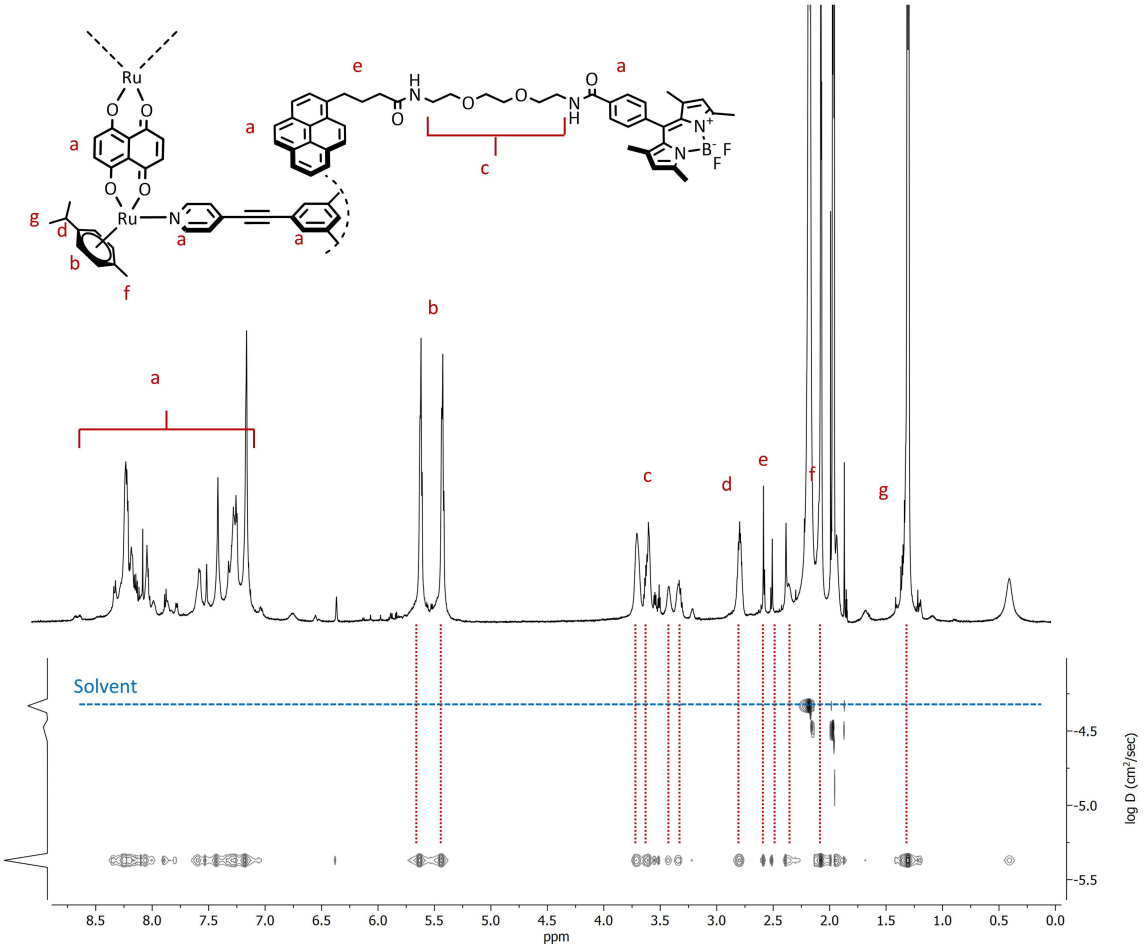

Figure 45. ^{1}H and DOSY NMR spectra of **Pyrene-BODIPY⊂P**

As for ESI-MS, same characteristic peaks described for the empty metalla-cage can be found, consisting in the loss of three or four triflate ions, but in this case, including the addition of the guest. In Figure 46, the two main peaks [**Pyrene-BODIPY⊂P** – $3CF_3SO_3]^{3+}$ and [**Pyrene-BODIPY⊂P** – $4CF_3SO_3]^{4+}$ are presented. It can be as well appreciated that the theoretical isotopic patterns fit very well to the shape of the experimental peaks.

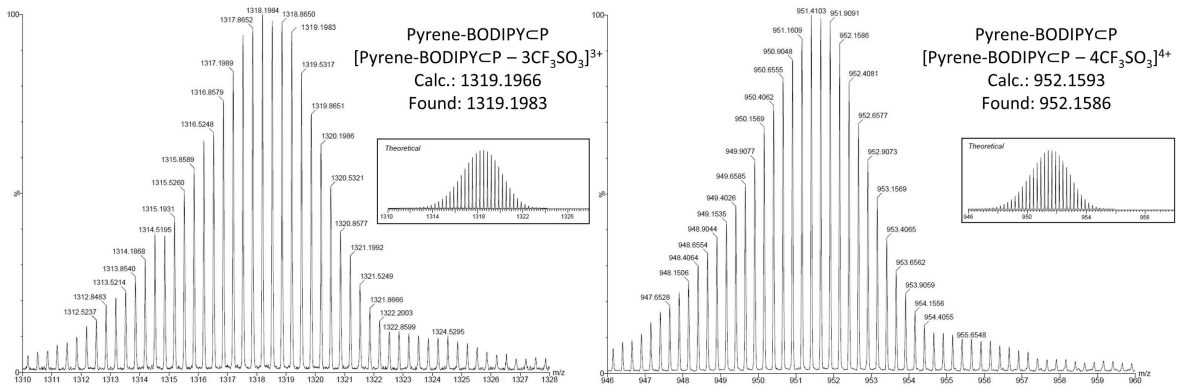

Figure 46. ESI-MS main peaks of **Pyrene-BODIPY⊂P**.

UV-Vis spectroscopy is interesting in this case because the signals of the guests are very characteristic and easily distinguishable from the absorption of the assembly, so it is a further confirmation of the presence of the guest. Pyrene (non-encapsulated) UV-Vis spectrum consists in a set of peaks of

recognizable pattern between 230 and 350 nm[143,144]. As for BODIPY, its main absorption band is at 500 nm[145]. In summary, guest bands can be identified, overlapping the absorption band of the cage (Figure 47).

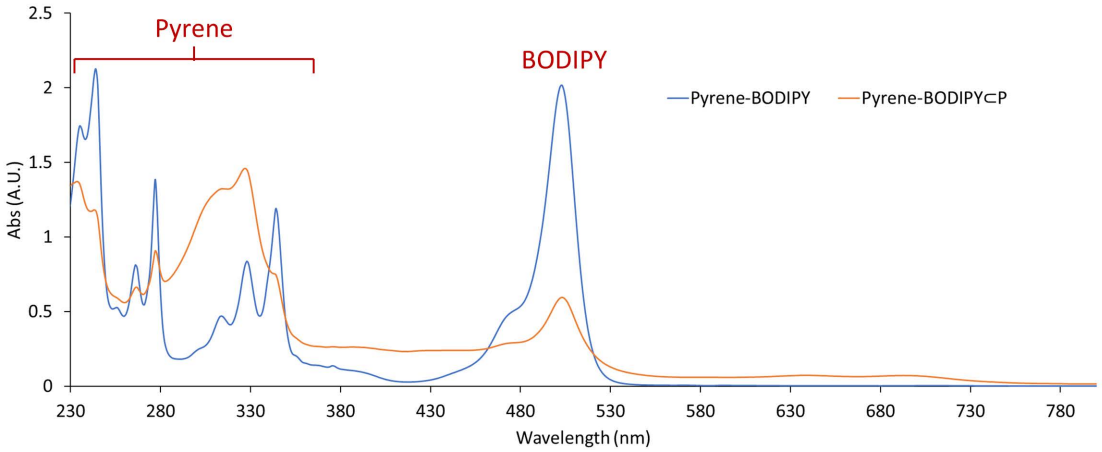

Figure 47. UV-Vis spectrum of **Pyrene-BODIPY⊂P** (DCM, 10^{-5} M).

The most advanced systems are the ones containing biotinylated panels and a guest. As it has been discussed before, the asymmetry introduced by the functionalization of the panel leads to a broadening of the signals in ^{1}H-NMR. When adding as well a guest to these assemblies, this broadening is accentuated. Assignation in this case cannot be done peak by peak, only by regions, by comparison to the previous cases, as an example, **Pyrene-BODIPY⊂PB** is further discussed (Figure 48). In the aromatic region (a), there is again a set of signals coming from panels, guest and clips. The signals of the *p*-cymene (b) can still be recognizable, even if broad these are the almost only signals appearing in this region. Between 3 and 4 ppm, is the region where signals from the PEG chains appear (c), both guest and panels contain PEG, which contributes to the broadening. Region e contains mainly alkylic protons from biotin and the *p*-cymene (methyl). Finally, region f corresponds mainly to the isopropyl protons from the *p*-cymene, together with biotin. Even if assignation of signals is hardly reliable, DOSY shows that there is formation of a single species.

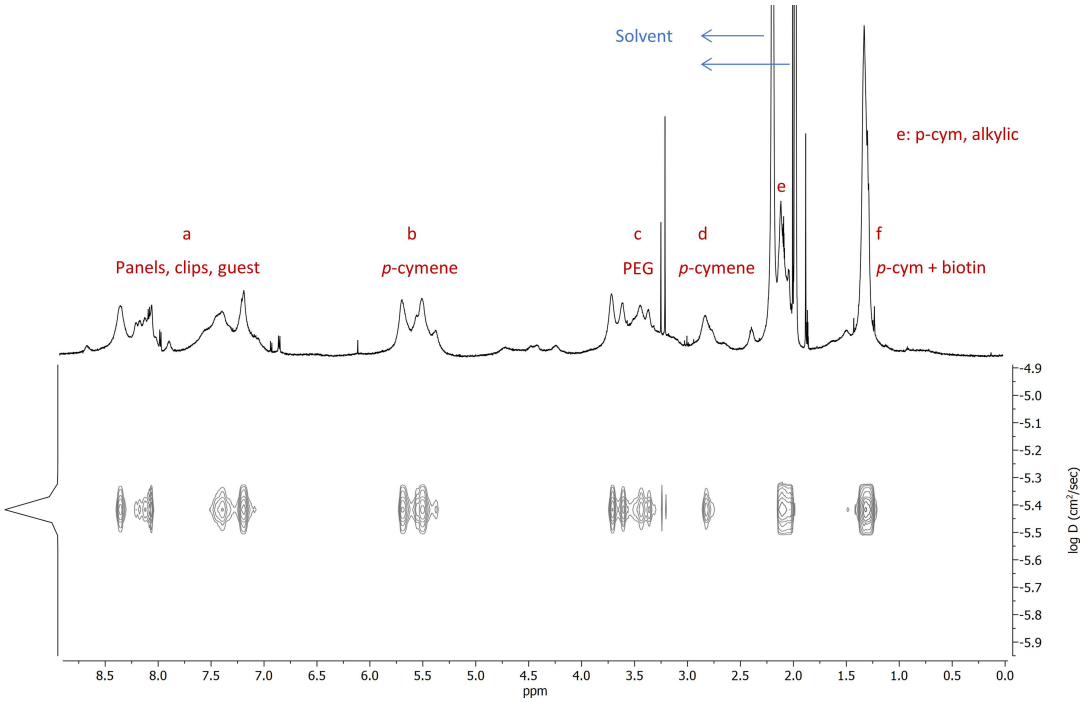

Figure 48. ^{1}H and DOSY-NMR spectra of **Pyrene-BODIPY⊂PB**

Other techniques are more revealing in these host-guest systems. ESI-MS was performed for all of them. The results obtained with this technique confirm the formation of a single host-guest species, thus confirming as well the encapsulation of the pyrenyl guests. As an example, peaks corresponding to [**Pyrene-BODIPY⊂PB** – $3CF_3SO_3$]$^{3+}$ and [**Pyrene-BODIPY⊂PB** – $4CF_3SO_3$]$^{4+}$ are presented in Figure 49. Table 5 summarizes the MS data for the three host-guest systems.

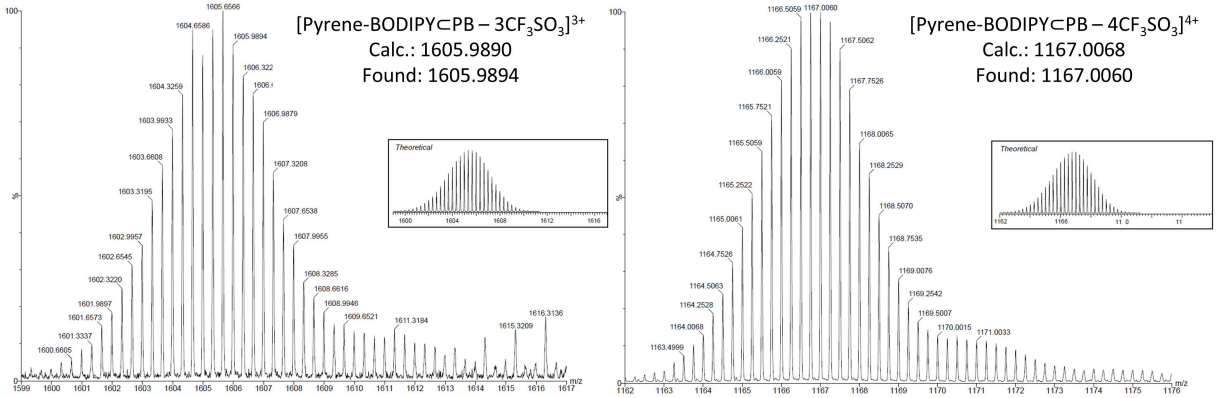

Figure 49. ESI-MS peaks of **Pyrene-BODIPY⊂PB**

Compound	Fragment	m/z calc.	m/z found
Pyrene-TPP⊂PB	[Pyrene-TPP⊂PB – $3CF_3SO_3$]$^{3+}$	1702.6843	1702.6851
	[Pyrene-TPP⊂PB – $4CF_3SO_3$]$^{4+}$	1239.7751	1239.7733
Pyrene-PheoA⊂PB	[Pyrene-PheoA⊂PB – $3CF_3SO_3$]$^{3+}$	1680.6949	1680.6912
	[Pyrene-PheoA⊂PB – $4CF_3SO_3$]$^{4+}$	1233.2830	1223.2853
Pyrene-BODIPY⊂PB	[Pyrene-BODIPY⊂PB – $3CF_3SO_3$]$^{3+}$	1605.9890	1605.9894
	[Pyrene-BODIPY⊂PB – $4CF_3SO_3$]$^{4+}$	1167.0068	1167.0060

Table 5. ESI-MS characterization data of host-guest systems.

We have seen that finding a specific ^{1}H signal belonging only to the guest is complicated in these final host-guest systems. In this context, UV-Vis spectroscopy is a helpful support to confirm the presence of the guest. In Figure 50, spectra from **Pyrene-BODIPY** (blue), **PB** (grey) and **Pyrene-BODIPY⊂PB** (orange) are compared. The complex is characterized by a strong high energy band between 300 and 330 nm, attributed to ligand localized or intraligand π-π* transition[146], broad low-energy bands associated to metal-to-ligand charge transfer (MLCT) transitions[146] are also observed at around 640 and 690 nm, characteristic for complexes containing 5,8-dioxydo-1,4-naphtoquinonato (donq) as spacer in the clip[147]. In the host-guest complex, it is possible to see the presence of the peaks from the pyrene, even if partially masked by the absorption of the cage, in addition to the peak corresponding to BODIPY.

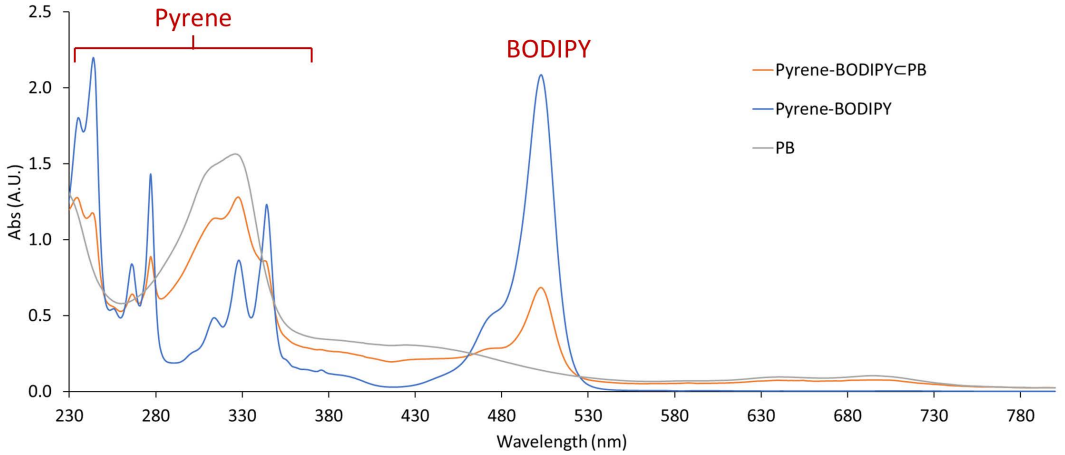

Figure 50. UV-Vis spectrum of **Pyrene-BODIPY⊂PB** (DCM, 10^{-5} M)

3.5 Phototoxicity studies

Phototoxicity of guests, metalla-prisms and host-guest systems was studied *in vitro* on HCT116 colorectal cancer cells in the laboratory of Prof. Bertrand Liagre at the University of Limoges (France). Cells were irradiated at 630-660 nm with a light dose of 75 J/cm^2. Cell viability was evaluated by MTT assays on irradiated (after 24 h) and non-irradiated HCT116 cells, obtaining IC_{50} values (concentration of compound necessary for 50% inhibition of cell viability). From these results phototoxic index (PI) can be calculated as the ratio between IC_{50} in the dark and IC_{50} irradiated with light (Table 6). A high PI value means the activity of the compound is higher upon irradiation as compared to the same compound in the dark. Red irradiation was chosen as it falls inside the therapeutic window[148] (600-800 nm), which is the range in which light best penetrates the tissue and photodamage is reduced[149].

Guest	Compound	IC_{50} dark (μM)	IC_{50} light (μM)	PI
-	P	1.3±0.1	1.2±0.2	1
-	PB	1.3±0.2	1.4±0.4	1
Pyrene-TPP	Pyrene-TPP	>10	1.20±0.02	>8
	Pyrene-TPP⊂P	1.02±0.08	0.6±0.2	2
	Pyrene-TPP⊂PB	1.0±0.3	0.4±0.1	2
Pyrene-PheoA	Pyrene-PheoA	0.19±0.06	0.02	9
	Pyrene-PheoA⊂P	1.6±0.5	0.01±0.03	160
	Pyrene-PheoA⊂PB	0.23±0.06	0.04±0.04	6
Pyrene-BODIPY	Pyrene-BODIPY	>50	>50	-
	Pyrene-BODIPY⊂P	1.3±0.09	1.3±0.1	1
	Pyrene-BODIPY⊂PB	1.30±0.02	1.4±0.3	1

Table 6. MTT results on HCT116 colorectal cancer cells, calculated phototoxic index (PI=IC_{50} dark/IC_{50} light) is also presented. Cells were irradiated at 630-660 nm, 75 J/cm^2.

As it was expected, cytotoxicity of both empty metalla-assemblies (**P** and **PB**) does not change with irradiation, as there is no photosensitizer present. Even if they are not phototoxic, they still present cytotoxic activity in the low micromolar range, as it has been seen in similar arene-ruthenium assemblies[150]. It is noticeable that the presence of biotin in the cage structure (**PB**) does not seem to neither improve or reduce the cytotoxicity, suggesting that cell internalization of the drug is not influenced by the presence of the targeting moiety.

In the case of guests, **Pyrene-TPP** and **Pyrene-PheoA**, both present phototoxic activity under the conditions tested, obtaining similar PI values but on different degrees of phototoxicity. From the two, **Pyrene-PheoA** seems to be the most active, showing an IC_{50} value down to the nanomolar scale (20 nM), while **PyreneTPP** remains in the low micromolar scale (1.20 μM). On the other hand, **Pyrene-BODIPY** does not present photoactivity under the conditions used, this result is not surprising as this guest does not absorb at the 630-660 nm range where it has been irradiated (Figure 50). In future studies a more suitable wavelength around 500 nm will be used to study the photoactivity of this compound, another possibility would be to study its two-photon absorption properties, as many different two-photon activated BODIPY derivatives are present in the literature[151,152] and this approach would allow red-NIR light to be used.

Both host-guest metalla-assemblies containing **Pyrene-TPP** as guest display a very slight increase in their cytotoxicity in the dark compared to the empty metalla-assemblies. Once irradiated, their cytotoxicity increases obtaining modest PI values of 2 in both cases, which suggests that their photoactivity is not compromised by the encapsulation and most probably there is a synergistic effect between the cytotoxicity of the metalla-assembly and the phototoxicity of the guests, as the irradiated IC_{50} of the host-guest systems is doubled compared to the free porphyrin. This effect is in part what

conditions the low PI values, as cytotoxicity in the dark is already high if compared to the guest alone. In a similar way as in the empty metalla-assemblies, the presence of biotin does not seem to have a relevant effect on their PDT efficacy.

Host-guest metalla-assemblies containing **Pyrene-PheoA** present the most promising results. Metalla-assembly **P** decreases the cytotoxicity of the photosensitizer in the dark by a factor of 8, while at the same time improving slightly their cytotoxicity after irradiation. The combination of both of these effects, results in a PI of 160, a PI around 18 times higher than the pyrenyl guest alone. On the other hand, metalla-assembly **PB** does not succeed at reducing the toxicity in the dark and at the same time the activity after irradiation is slightly reduced, still, the IC_{50} remains in the nanomolar scale. This results in a slight decrease of the PI as compared to the guest alone.

Finally, metalla-assemblies with **Pyrene-BODIPY** present very similar results to the empty metalla-cages as expected, as the guest alone already did not present any photoactivity. The only thing that can be inferred from this result is that the presence of a guest does not seem to always influence the cytotoxicity of the assembly in which is hosted.

3.6 Conclusion

A series of 3rd generation photosensitizers based on the combination of well known 2nd generation PSs and arene-ruthenium metalla-assemblies have been synthesized. Metalla-assemblies have been functionalized with Biotin through their panels as a targeting strategy. Multifunctionalization has been achieved by combining biotinylated assemblies and pyrenyl-PS derivatives as guests. At a synthetic level, the use of functionalized panel ligands does not seem to affect the encapsulation of the guests, but on the other hand makes the characterization of these systems more laborious as it gives rise to different stereoisomers.

Phototoxicity of the different compounds was studied. The use of functionalized panels does not seem to affect the activity of the compounds *in vitro*. Metalla-prisms containing **Pyrene-PheoA** show the best phototoxicity, showing a phototoxic index of 160 and an IC_{50} after irradiation of 10 nM.

4. Synthesis of metalla-assemblies with functionalized metalla-clips

4.1 Introduction

Arene-ruthenium metalla-assemblies are composed by two main building blocks: dinuclear arene-ruthenium metalla-clips and rigid planar ligands of different denticities known as panels. Metalla-clips contain two ruthenium centers linked by bis-chelating tetradentate ligands such as oxalates[153], oxamides[154], benzoquinones[155] or naphthoquinones[156] (Figure 51). Combination of metalla-clips with panels determine the geometry of the final assembly, shapes like rectangles, prisms or cubes are possible and they are commonly isolated as trifluoromethanesulfonate salts.

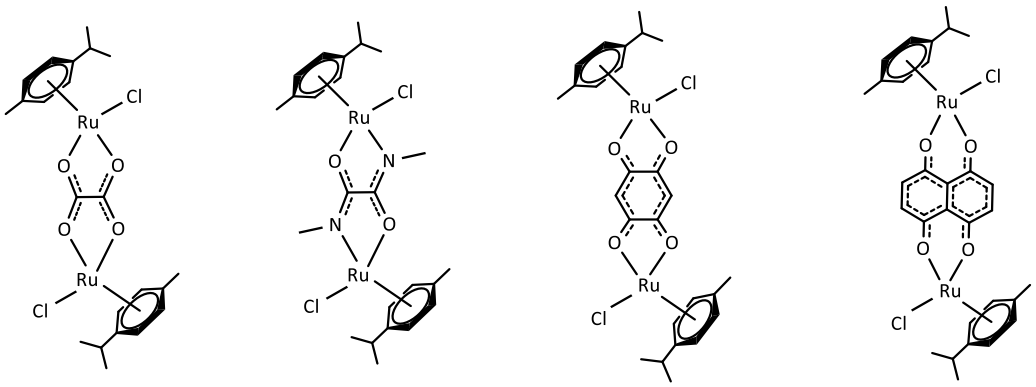

Figure 51. Metalla-clips with oxalate, oxamide, benzoquinone and naphthoquinone spacers.

The properties of arene-ruthenium metalla-assemblies can be tuned by functionalization of their building blocks, one of the different possibilities is the modification of the spacer in metalla-clips. Different strategies have been followed in the past to modify spacers, among the different ligands, the most studied ones for this purpose are benzoquinones and oxamides. Embelin is a phenolic lipid extracted from plants of the *Myrsinaceae* family[157], and it's composed by a dihydroxybenzoquinone unit with an undecyl chain on one side. It is one of the first benzoquinone derivatives studied to form functionalized metalla-clips, which allowed to obtain stimuli-responsive metalla-prisms when combined with 4-tpt[158]. These assemblies, adopted different conformations depending on the polarity of the solvent, with the aliphatic chains being inside or outside the cavity. Other benzoquinone derivatives were synthesized containing longer alkylic chains[103] or other aromatic substituents[159] (Figure 52).

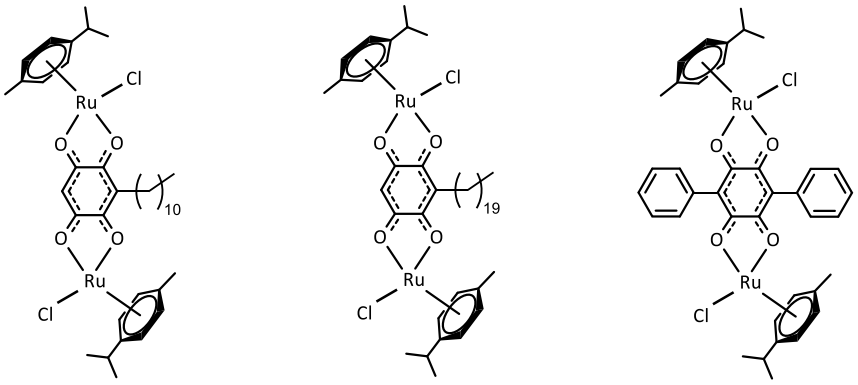

Figure 52. Examples of functionalized benzoquinone metalla-clips.

Oxamides present another opportunity for the synthesis of functional metalla-clips. The presence of the two nitrogen atoms allow the introduction of two substituents, by functionalization of the oxamide

previous to the clip formation. Some examples of functionalized oxamide clips contained short PEG chains[19] or alkylic chains[103] (Figure 53), and these clips were used in the formation of rectangles and prisms, thus modulating the solubility of the final assembly.

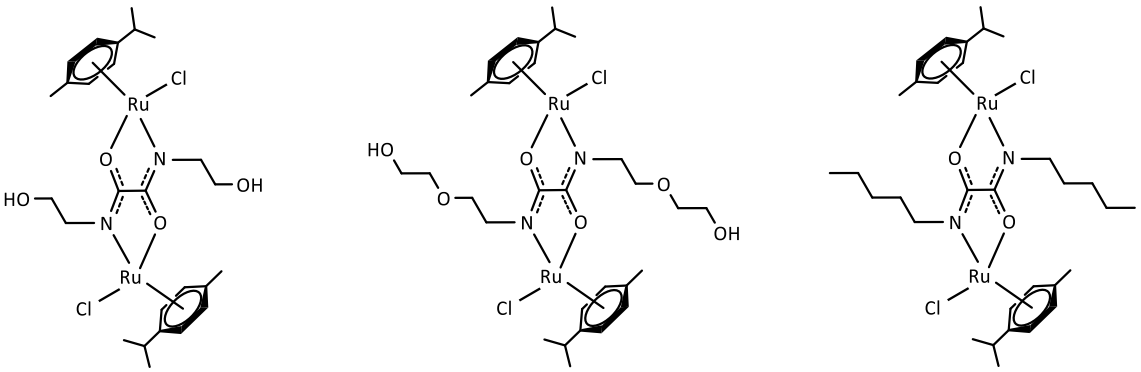

Figure 53. Examples of functionalized oxamide metalla-clips.

Arene-ruthenium assemblies have been widely used in biological applications as they possess interesting features such as water solubility[160], good anticancer activity[161] and interaction with DNA[56]. Among these, water solubility is a property that can be easily tuned by functionalization of oxamide clips. Hydrophilic substituents such as PEG chains or chains containing hydroxyl groups can be attached to the oxamides, improving significantly the solubility of the final assemblies in water.

Tetrapyridyl porphyrin (tpp) can be used as a panel in the formation of octa-nuclear arene-ruthenium metalla-assemblies. Porphyrin derivatives are one of the most well-known photosensitizers, and have been extensively used in Photodynamic therapy (PDT). The use of these porphyrins as panels, allows to combine the properties of arene-ruthenium metalla-assemblies with their own photosensitizing ability. Metalla-cubes have been tested for photodynamic treatment of cancer[162,163] and rheumatoid arthritis[164] (Figure 54), proving that the photosensitizing ability of the porphyrin still remains when being part of an assembly, even if the efficacy differs depending on the metalla-clip used.

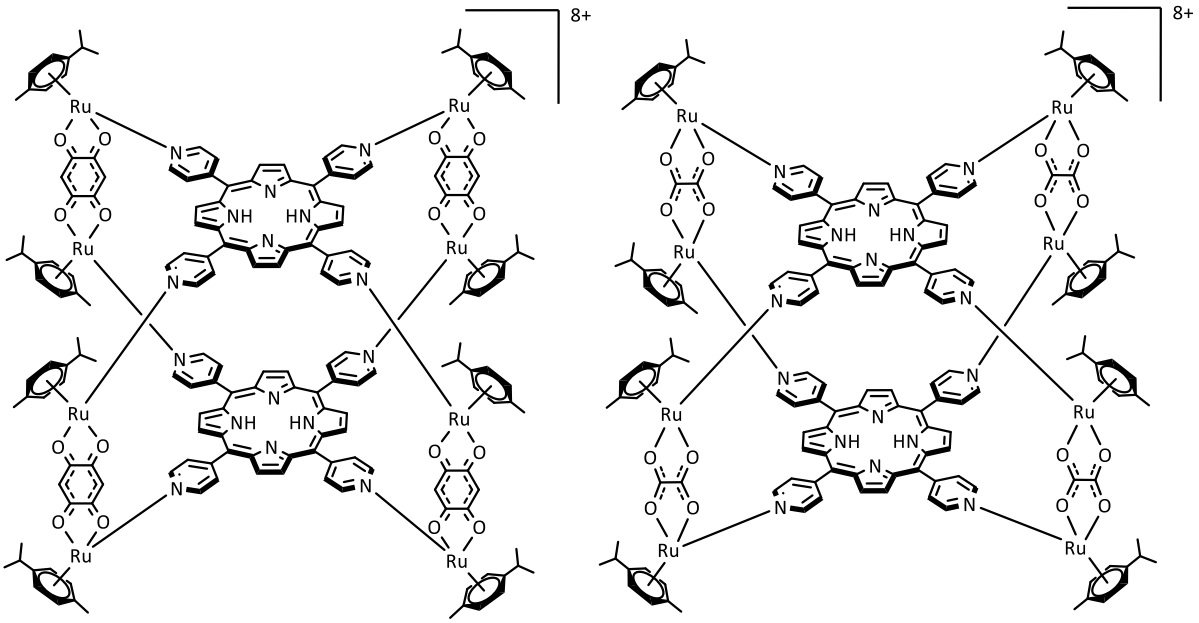

Figure 54. Cubes used in the PDT treatment of rheumatoid arthritis[164].

In this work, a new set of oxamide based metalla-clips has been designed and synthesized, containing chains of varying amounts of hydroxyl groups or PEG chains. The combination of the six metalla-clips and two panels has allowed the construction of twelve different metalla-assemblies: six hexa-nuclear metalla-prisms and six octa-nuclear metalla-cubes (Figure 55). The improvement of the water solubility is expected to improve the cytotoxicity of prisms and cubes, as well as the photodynamic efficiency of the latter.

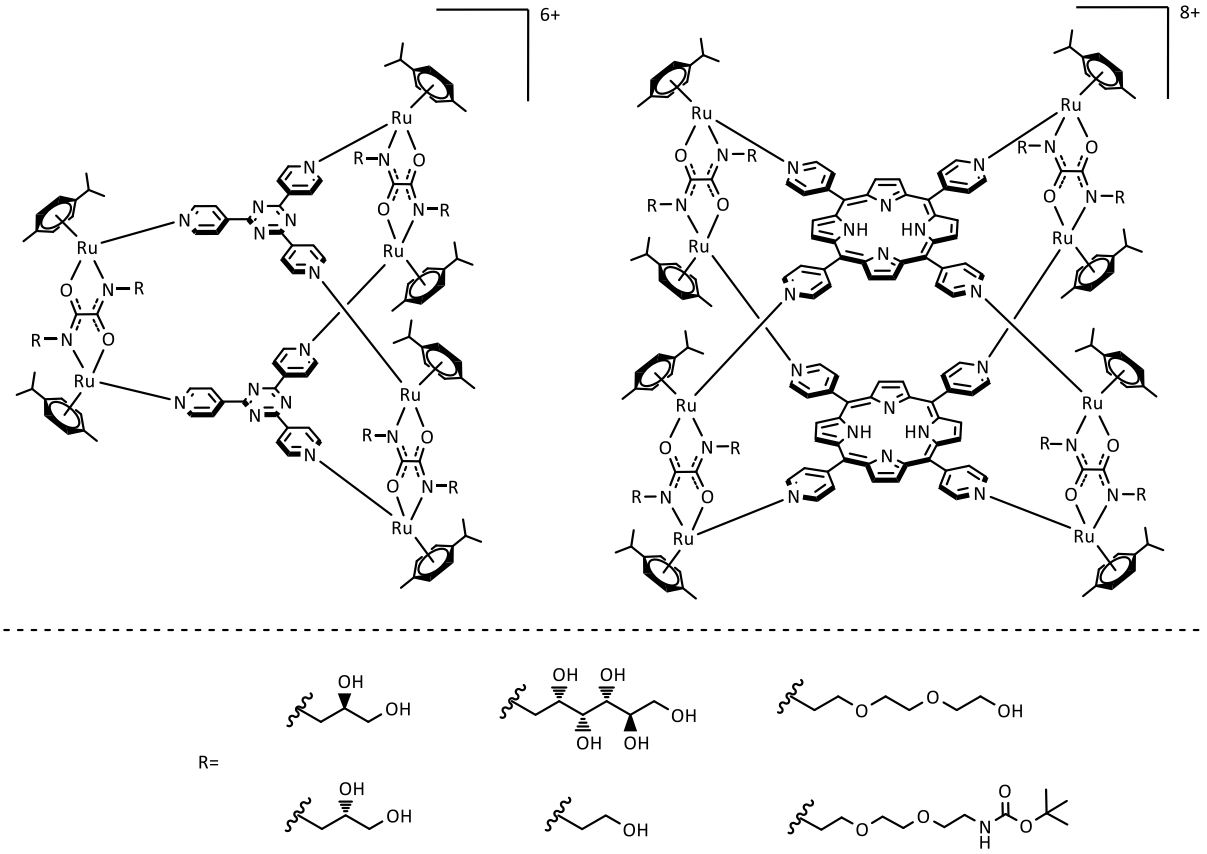

Figure 55. Prisms and cubes with functionalized oxamides.

4.2 Synthesis and characterization

4.2.1 Oxamides and metalla-clips

The functionalization of ON∩NO bridging linkers starts by reacting diethyl oxalate with the desired amino derivative in toluene, obtaining directly the product as a precipitate[165]. This strategy has been applied to obtain a set of six different linear oxamides, four based on alkylic chains with different amounts of hydroxyl groups, and two based on short PEG chains (**Ox1**, (*R*)-3-amino-1,2-propanediol; **Ox2**, (*S*)-3-amino-1,2-propanediol; **Ox3**, D-glucamine; **Ox4** was commercially available; **Ox5**, 2-[2-(2-Aminoethoxy)ethoxy]ethanol; **Ox6**, N-Boc-2,2'-(ethylenedioxy)diethylamine) (Scheme 24). In general, high yields were obtained in general for this reaction, ranging from 80 to 90%.

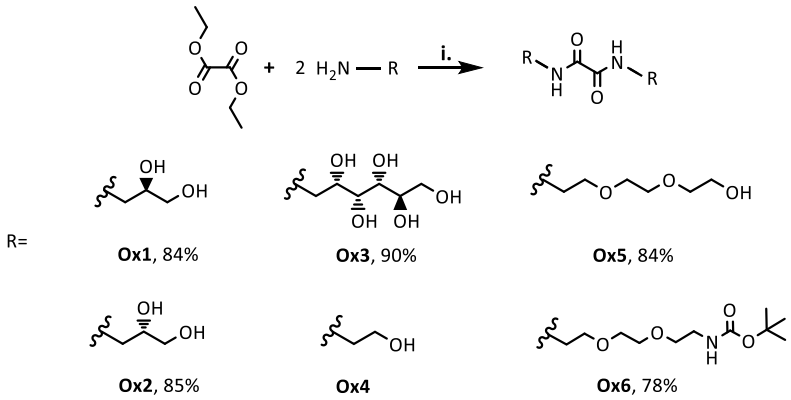

Scheme 24. Synthesis of oxamides, i) Toluene, RT, overnight.

Synthesis of the dinuclear arene-ruthenium metalla-clips of the general formula [(*p*-cymene)$_2$Ru$_2$Cl$_2$(μ-ox)] was performed in methanol by reacting the corresponding oxamide (**Ox1-6**) with [(*p*-cymene)$_2$Ru$_2$Cl$_2$(μ-Cl)] in the presence of two equivalents of triethylamine at reflux (Scheme 25).

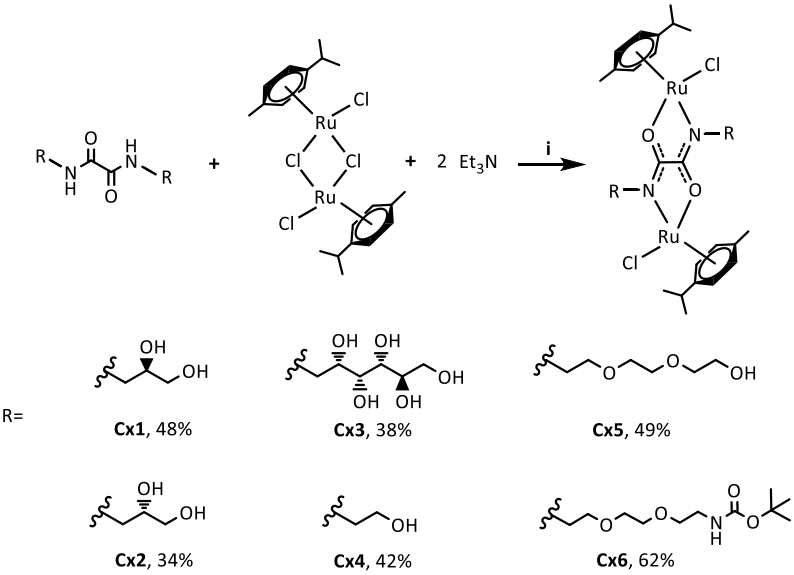

Scheme 25. Synthesis metalla-clips, i) Methanol, reflux, overnight.

The dinuclear metalla-clips were characterized by ^{1}H and ^{13}C NMR and ESI-MS (see experimental section for details). Metalla-clips containing an oxamide linker show two stereogenic ruthenium centers, forming racemic and meso stereoisomers (Figure 56). However, their ^{1}H and ^{13}C NMR are characterized by the presence of a single set of signals, suggesting formation of only the achiral meso form. In past studies with similar metalla-clips, this hypothesis was confirmed by single-crystal structure analyses, finding an inversion center perfectly positioned halfway between the two metals[166].

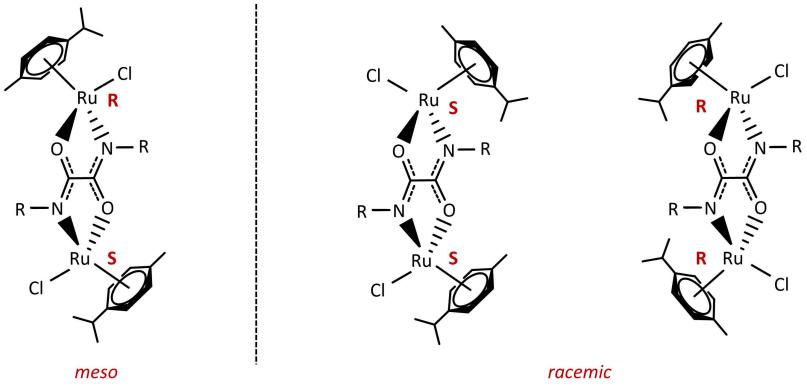

Figure 56. Possible metalla-clip stereoisomers.

4.2.2 Metalla-assemblies

All six different metalla-clips were used in the formation of prisms and cubes, resulting in a total of twelve assemblies. The synthesis of both types of assemblies go through the same synthetic procedure, only changing the number of equivalents of its components, clip:panel ratio being 3:2 for prisms and 4:2 for cubes. Metalla-clip is initially activated in methanol in the presence of silver triflate, then, panel (4-tpt for prisms, tpp for cubes) is added and the solution was refluxed overnight (Scheme 26). All assemblies were obtained in moderate to high yield (Table 7).

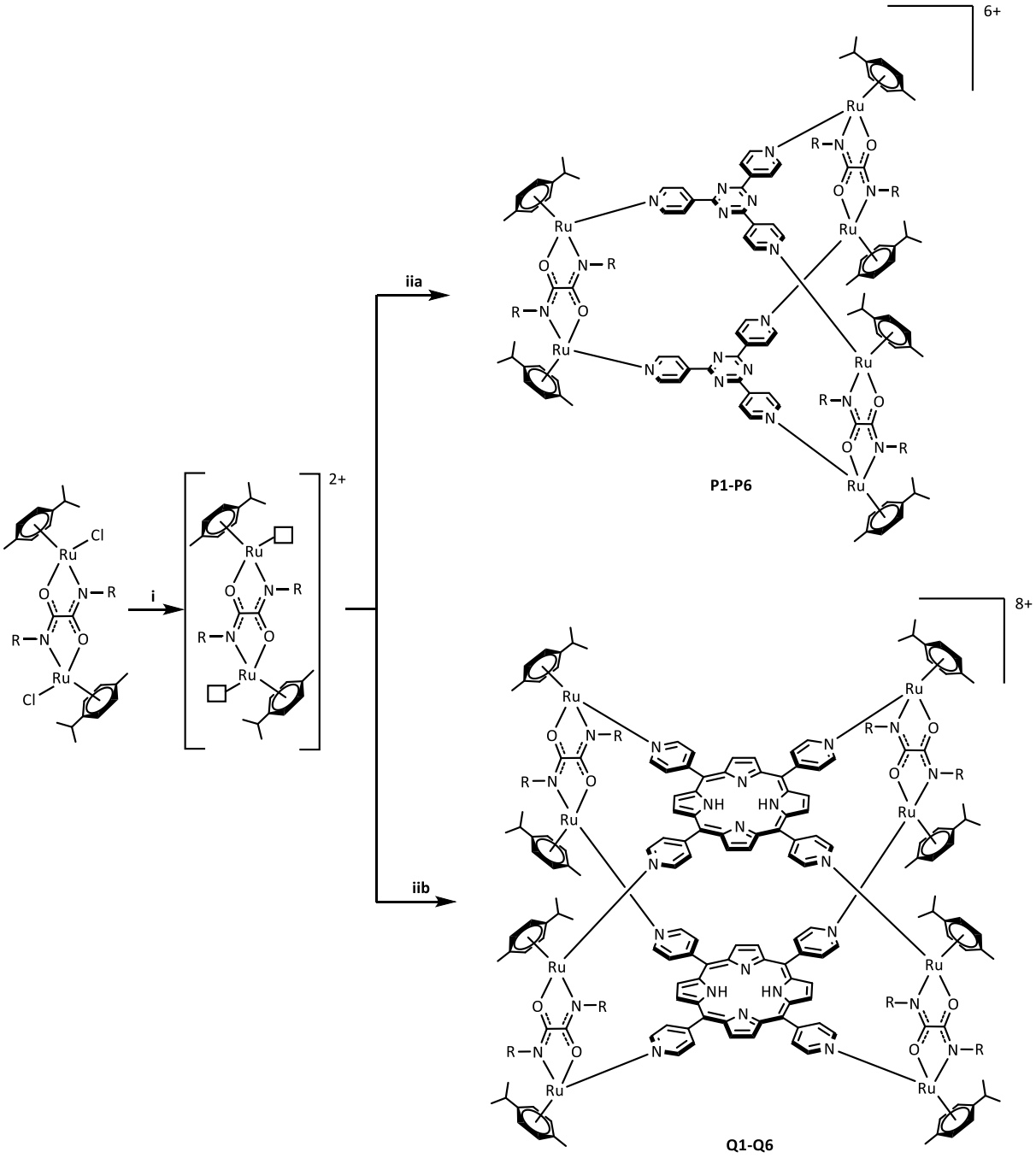

Scheme 26. Synthesis of assemblies, i) $AgCF_3SO_3$, MeOH, RT, 4 h. ii) Panel, MeOH, 60 °C, overnight. iia) 2,4,6-tris(4-pyridyl)-1,3,5-triazine (4-tpt) iib) 5,10,15,20-tetra(4-pyridyl)-21H,23H-porphyrin (tpp)

Compound	Clip	Yield (%)	Compound	Clip	Yield (%)
P1	Cx1	74	Q1	Cx1	81
P2	Cx2	85	Q2	Cx2	77
P3	Cx3	89	Q3	Cx3	85
P4	Cx4	93	Q4	Cx4	92
P5	Cx5	73	Q5	Cx5	87
P6	Cx6	63	Q6	Cx6	52

Table 7. Yields obtained for the different assemblies.

4.2.3 Metalla-prisms

All metalla-prisms were characterized by NMR (^{1}H, ^{13}C, DOSY), ESI-MS and UV-Vis spectroscopy. Fully assigned ^{1}H and DOSY NMR spectra of **P1** can be seen in Figure 57. All signals corresponding to the *p*-cymene (f, e, g, d) show some degree of splitting, even if DOSY suggests that they all belong to a single species with the same diffusion coefficient. This splitting can be explained by the formation of different enantiomers.

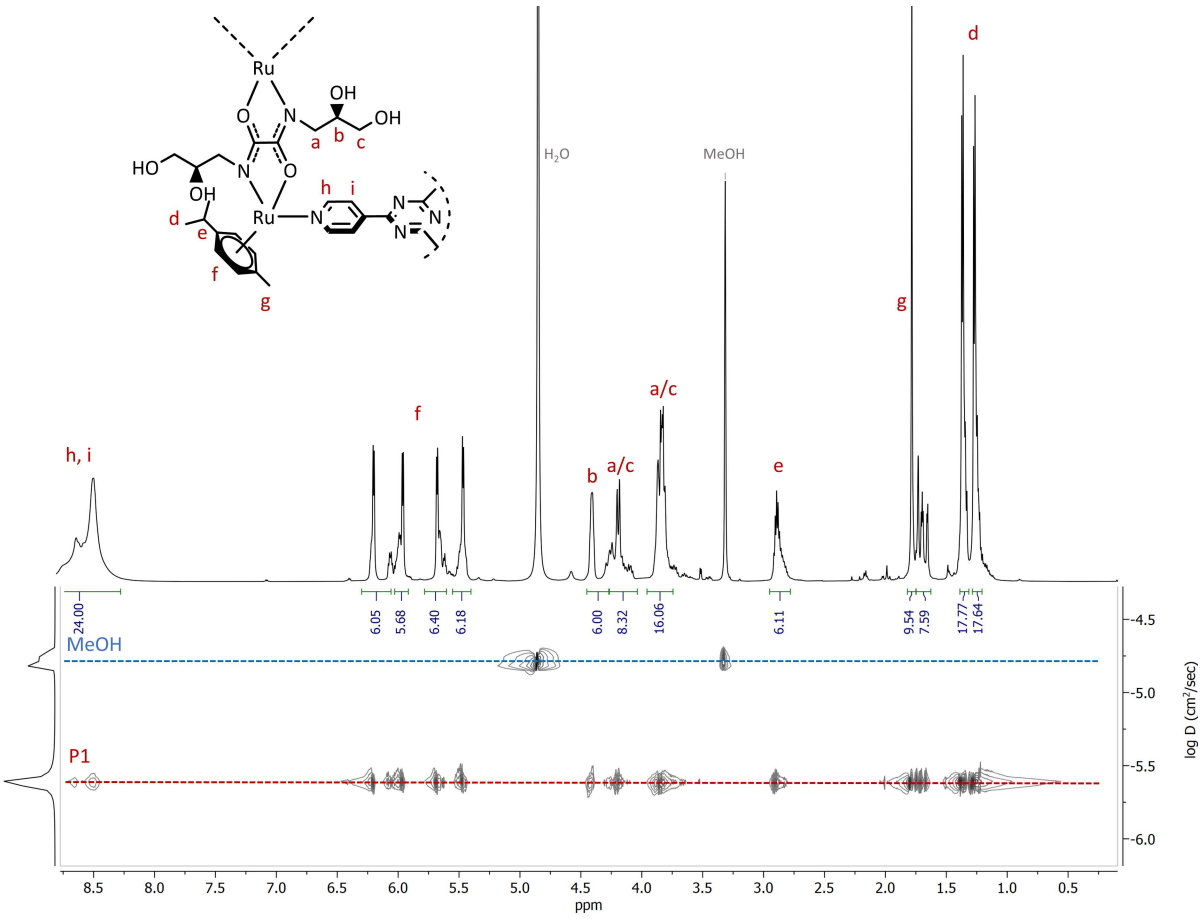

Figure 57. ^{1}H and DOSY NMR spectra of **P1**.

Even if the initial metalla-clip is isolated in the meso form, when forming a metalla-assembly a cis conformation with the connecting panel is necessary, thus fixing the configuration of the metalla-clips into *R,R* and *S,S* isomers. By combination of these, only two pairs of enantiomers are possible: homochiral *R,R-R,R-R,R* and *S,S-S,S-S,S* enantiomers or the mixed enantiomers *R,R-R,R-S,S* and *S,S-S,S-R,R*. It is as well clear that there is not a statistical distribution of the different isomers, most probably, one of them is favored by steric factors due to the presence of the side chains. The predominance of one isomer is confirmed as well through ^{13}C and HSQC NMR (Figure 58), where a single set of carbon

signals can be observed in the *p*-cymene aromatic region. One possible explanation is that the homochiral enantiomer might be able to organize the side-chains in a more favorable way, improving interactions between them and minimizing steric hindrance.

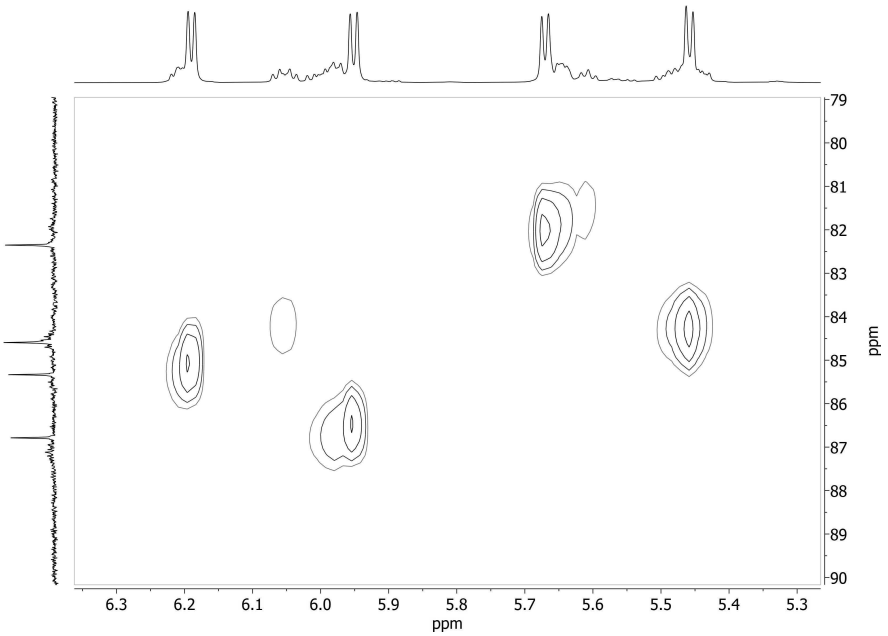

Figure 58. ^{13}C, ^{1}H and HSQC NMR spectra of **P1** in the *p*-cymene region.

The formation of one or more isomer has been found to be highly dependent on the characteristics of the side-chain. In fact, other metalla-clips give rise to a more remarkable splitting of the signals in both ^{1}H and ^{13}C NMR when forming metalla-assemblies. This is the case for **P5**, in which the side chain is a short PEG chain. Here, there still seems to be a predominant isomer, but ^{13}C and HSQC (Figure 59) display the presence of not only two sets of signals, but up to four. This additional chirality can be explained by the conformation adopted by the panel, which results in helical chirality, a common phenomenon in arene-ruthenium metalla-prisms[167].

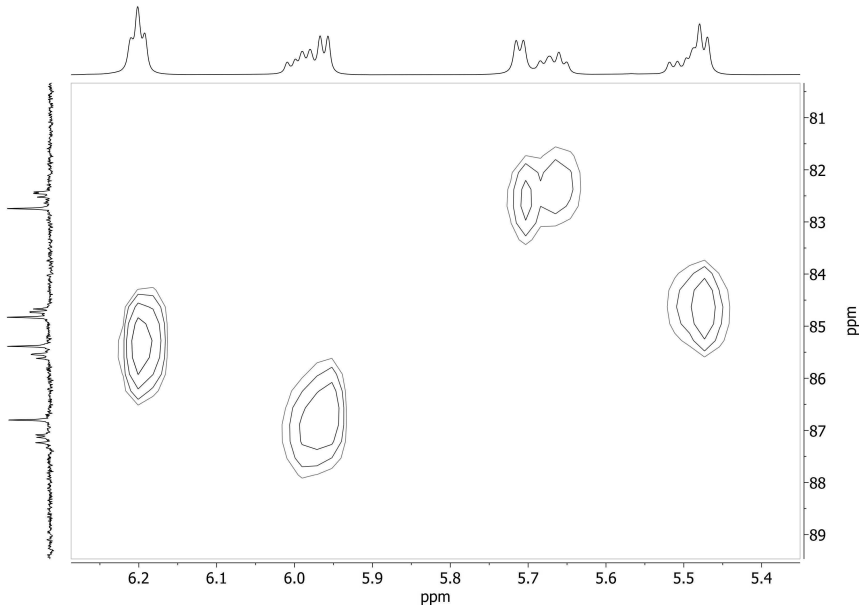

Figure 59. ^{13}C, ^{1}H and HSQC NMR spectra of **P5** in *p*-cymene region.

The ESI-MS spectra of metalla-prisms is characterized by a main peak assigned to the assembly minus three triflate ions ([**P1** – $3CF_3SO_3$]$^{3+}$), with fragments containing four ([**P1** – $2CF_3SO_3$]$^{2+}$) and two ([**P1** – $4CF_3SO_3$]$^{4+}$) triflates being also present, even if less intense. As an example, analysis for **P1** is shown in Figure 60.

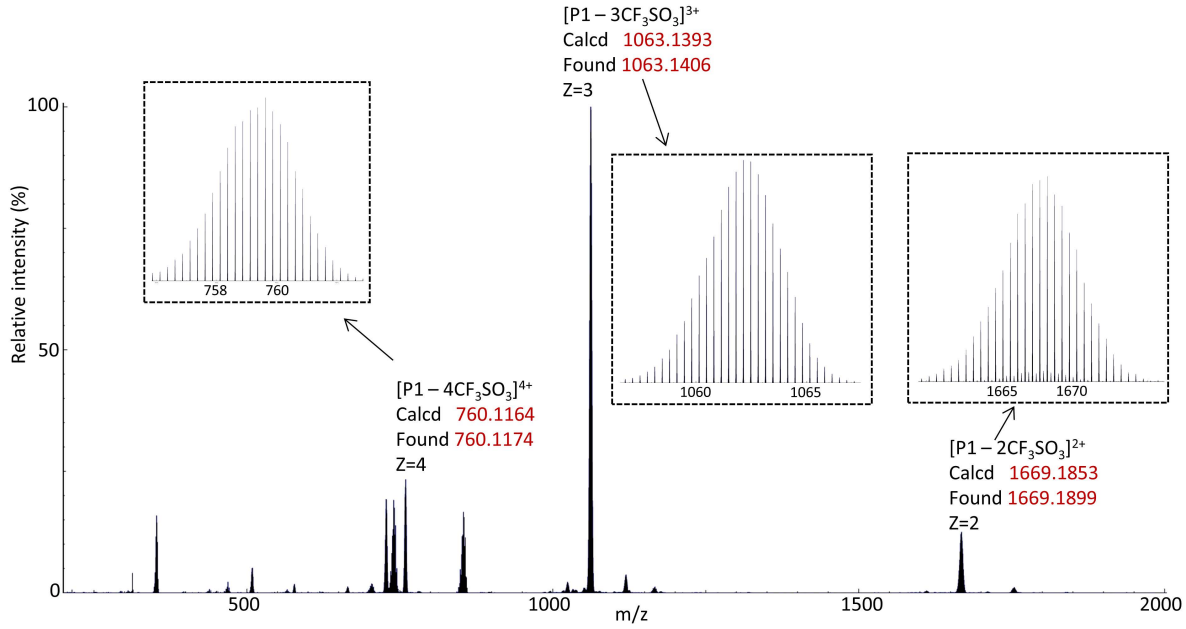

Figure 60. ESI-MS spectrum of **P1**

Ruthenium has seven stable isotopes, which results in very characteristic isotopic patterns in multi-nuclear assemblies. In Figure 61, the predicted isotopic pattern for one of the peaks of hexa-nuclear prism **P1** is compared to the experimental pattern. It can be seen that they match perfectly, showing a total overlap of the two. This characteristic isotopic pattern suggests the formation of the metalla-assemblies containing six ruthenium centers.

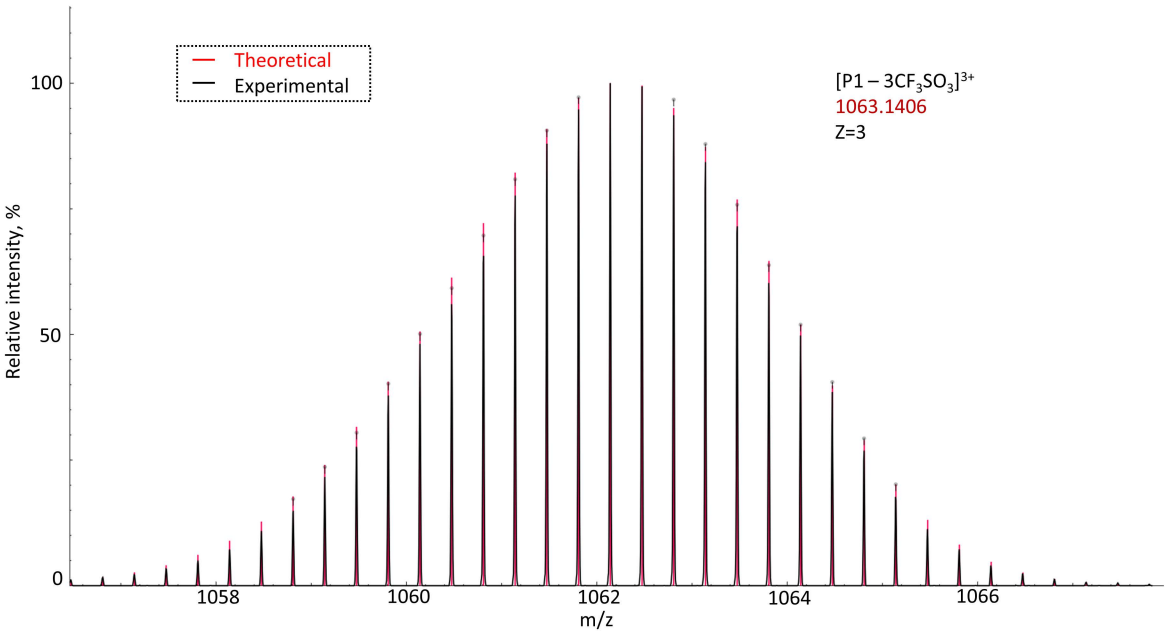

Figure 61. Comparison of predicted (red) and experimental (black) isotopic patterns for [**P1** – $3CF_3SO_3$]$^{3+}$

Lipophilicity of a molecule can be correlated to cellular uptake, which at the same time plays a role in their therapeutic efficacy. For this reason, the octanol-water partition coefficient (expressed as log P) was determined by the shake-flask method[168]. Log P is positive for lipophilic molecules and negative for hydrophobic molecules. Results obtained for **P1-P6** can be seen in Table 8.

Metalla-prism	Log $P_{o/w}$
P1	-1.90±0.03
P2	-1.91±0.01
P3	-1.94±0.01
P4	<-2.01
P5	-2.01±0.03
P6	0.01±0.02

Table 8. Log P values obtained for **P1-P6**

Metalla-prisms **P1** to **P5** all display a hydrophilic value of Log P. **P1** to **P3** have very similar values, their side-chains are based on alkylic chains with varying number of OH groups, with **P3** being the one with the most OH which results in a slight increase of the hydrophilicity. On the other hand, **P4** has the smallest side-chain and the most hydrophilic value (under the limit of the detection), from what we can infer that a longer side-chain with higher number of OH groups is not necessarily an advantage regarding the hydrophilicity. Metalla-prism **P5** has a short PEG3 chain as side-chains which results in a hydrophilic log P, slightly better than **P1-P3** and worse than **P4**.

Finally, prism P6 presents an amphiphilic behavior, as its log P is close to 0. This behavior can be attributed to the nature of its side-chain, it contains a short hydrophilic PEG chain terminated by a *tert*-butyloxycarbonyl (BOC) protecting group, which is a bulky hydrophobic group.

4.2.4 Metalla-cubes

All metalla-cubes were characterized by NMR (^{1}H, ^{13}C, DOSY), ESI-MS and UV-Vis spectroscopy. The study through ^{1}H NMR of these assemblies is more challenging than that of the prisms. They are composed by a total of four metalla-clips, resulting in an increased number of possible isomers. In addition, similar cubic systems have been found to display as well helical chirality[169]. Finally, their size is as well significantly bigger, thus allowing more conformational flexibility. All these factors explain the broadening of the signals in their NMR spectra. Nevertheless, relevant groups of signals can still be identified and assigned in ^{1}H NMR, while correlated to a same diffusion coefficient through DOSY NMR. In Figure 62, ^{1}H assignment for **Q1** is presented.

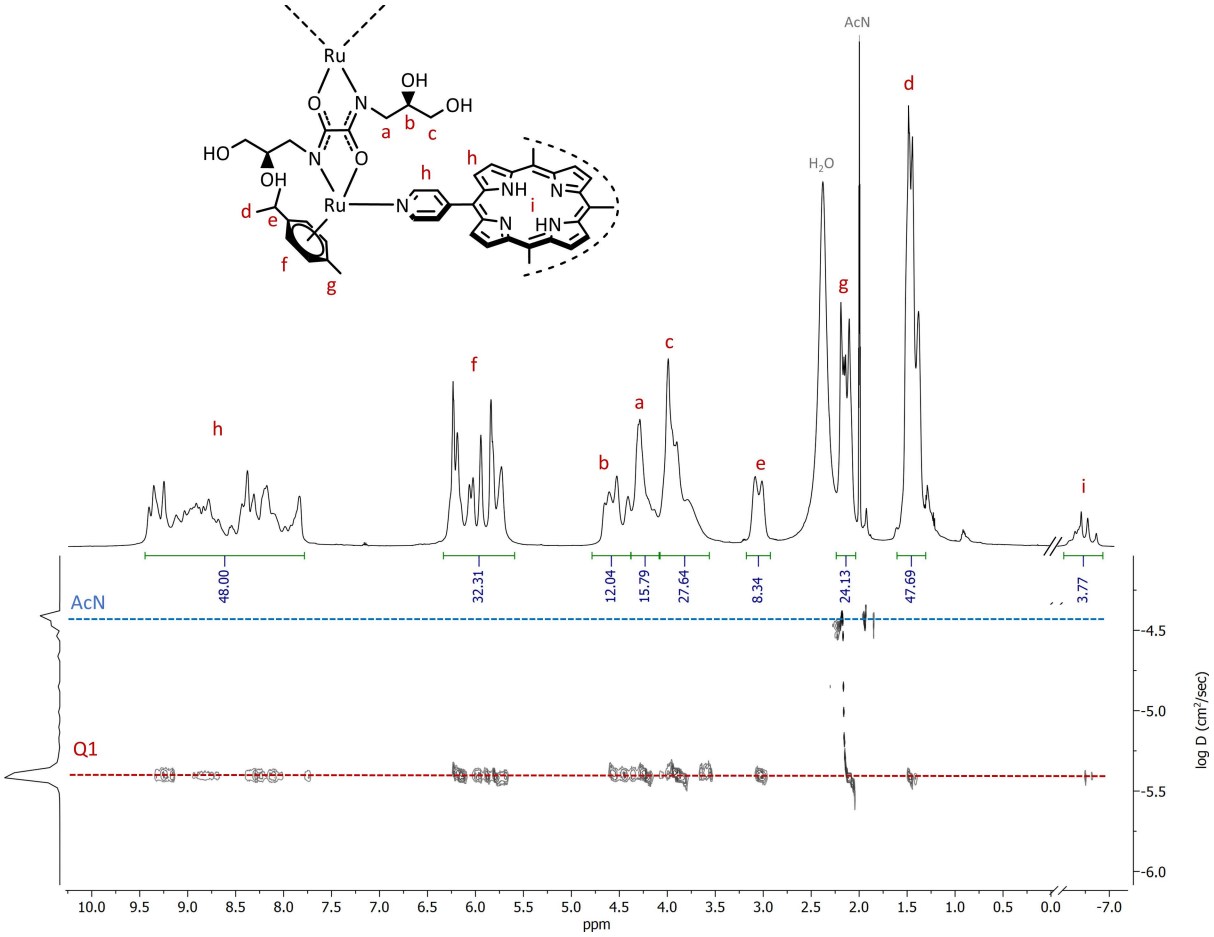

Figure 62. ^{1}H and DOSY NMR spectra of **Q1**.

All signals from tpp (h) appear in the same region, even if they can not be distinguished between them, there is no other building block with protons in the region. Same reasoning can be applied to aromatic CH protons from the *p*-cymene (f). Region containing the signals from the protons of the side-chains (a, b, c), contains as well their OH protons overlapping with them. Alkylic *p*-cymene protons (d, e, g) appear in their expected positions and can be assigned unequivocally. Signal i is specially relevant, as it corresponds to the NH protons of tpp. This signal appears close to -3 ppm for uncoordinated tpp, and when it is coordinated to arene-ruthenium metalla-clips is displaced to -6.5/-7 ppm, representing a very characteristic peak for metalla-cubes.

MS spectra of metalla-cubes are characterized by a main peak assigned to the assembly minus four triflate ions ([**Q1** – $4CF_3SO_3$]$^{4+}$), with fragments containing five ([**Q1** – $3CF_3SO_3$]$^{3+}$) and three ([**Q1** – $5CF_3SO_3$]$^{5+}$) triflates being also present, even if less intense. As an example, analysis for **Q1** is shown in Figure 63.

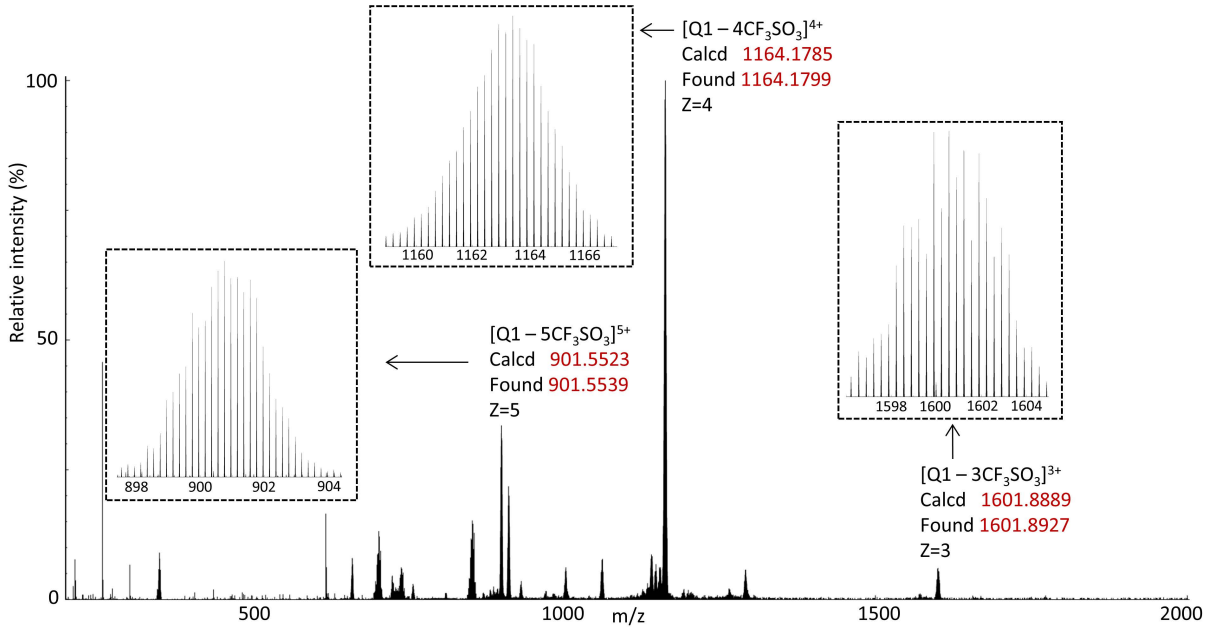

Figure 63. ESI-MS spectrum of **Q1**

Isotopic pattern for octa-nuclear assemblies is very characteristic, similar to what has been described previously for metalla-prisms. In Figure 64, the predicted isotopic pattern for one of the peaks of octa-nuclear cube **Q1** is compared to the experimental pattern. The two patterns are totally overlapped, representing a further confirmation of the formation of the metalla-assembly containing eight ruthenium centers.

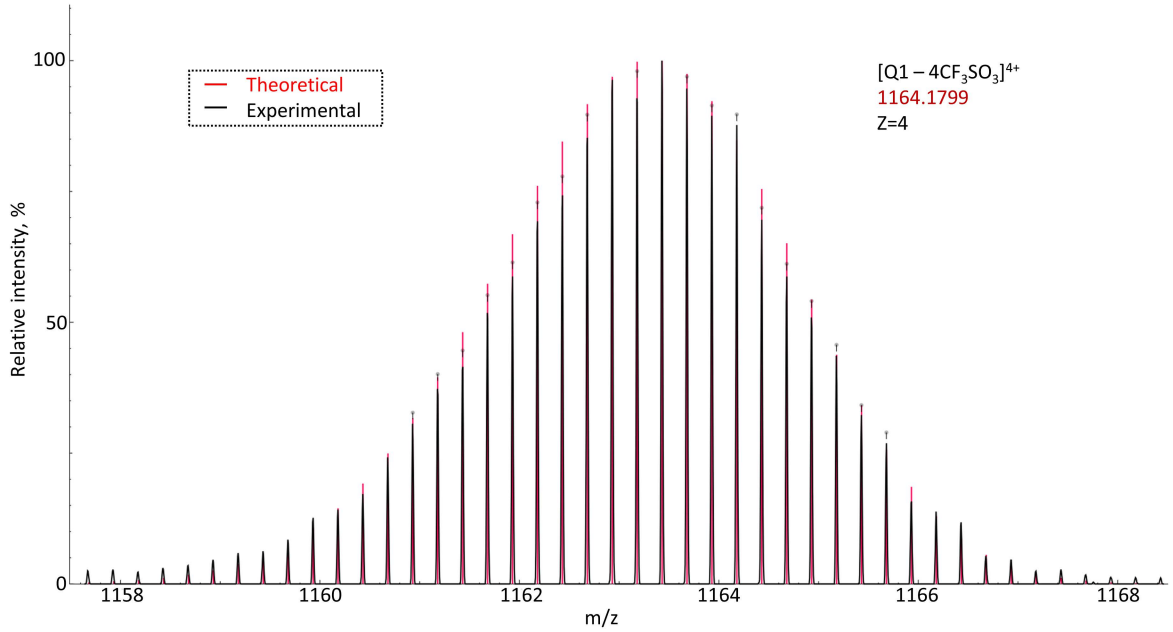

Figure 64. Comparison of predicted (red) and experimental (black) isotopic patterns for [**Q1** – $4CF_3SO_3]^{4+}$

As described above in this chapter for metalla-prisms, lipophilicity of a molecule can be correlated to cellular uptake, which in the context of PDT, may play a role in their efficacy. For this reason, the octanol-water partition coefficient (expressed as log P) was determined by the shake-flask method[168]. Log P is positive for lipophilic molecules and negative for hydrophilic molecules. Results obtained for **Q1-Q6** can be seen in Table 9.

Metalla-cube	Log $P_{o/w}$
Q1	-1.52±0.02
Q2	-1.53±0.02
Q3	-1.52±0.03
Q4	-1.57±0.03
Q5	-1.42±0.02
Q6	0.91±0.05

Table 9. Log P values obtained for **Q1-Q6**

Metalla-cubes **Q1** to **Q4** display a very similar hydrophilic value of log P. Their side-chains are all based on alkylic chains of different lengths with varying amounts of OH groups. This result reveals that in the context of only hydrophilicity, adding a longer chain with more hydroxyl groups presents little to no advantage: the complex with the highest hydrophilicity is **Q4**, which contains a single OH group per side chain. Cube **Q5**, which contains short PEG side chains, has as well a hydrophilic value of log P, slightly smaller but not very far from the first four derivatives. However, complex **Q6** is the only one having a hydrophobic value for log P. This result is not surprising: even if the side chains are based on PEG, they are terminated by the bulky *tert*-butyloxycarbonyl (BOC) protecting group, which is very hydrophobic.

4.3 Conclusion

A new set of arene ruthenium metalla-clips based on functionalized oxamides has been synthesized, containing chains with hydroxyl groups or PEG chains, aiming to tune the hydrophilicity of the metalla-assemblies. They have been used in the synthesis of metalla-prisms (4-tpt as panel) and metalla-cubes (tpp as panel) and their hydrophilicity has been studied by calculation of their octanol-water partition coefficient. Compounds **P1-P5** (prisms) and **Q1-Q5** (cubes) have been found to be highly hydrophilic, with **Q** compounds being less hydrophilic due to the more hydrophobic nature of their porphyrinic panel. On the other hand, compound **P6** has been found to be highly amphiphilic, while **Q6** is hydrophobic: these results are caused by the structure of the clip (**Cx6**) which contains a BOC protecting group at the end of the PEG chains, reducing the general hydrophilicity of the assemblies.

The increased hydrophilicity of these compounds is expected to improve or affect their behavior in biological media. Cytotoxicity of metalla-prisms will be tested on cancer cells, while metalla-cubes will be studied for PDT applications as they contain a porphyrin (a photosensitizer) as a panel.

5. General conclusion and perspectives

5.1 Conclusion

The work presented in this thesis is centered on the functionalization of arene ruthenium metalla-assemblies, with focus on 3D structures (prisms and cubes). Metalla-assemblies are constituted by two main building-blocks: clips and panels, the combination of which determines the geometry and size of the final assembly. In addition, assemblies possess a hydrophobic cavity that is tunable through the modification or selection of the building blocks, in the case of prisms, this cavity has been extensively used to carry hydrophobic guests such as drugs. This modular approach is what makes the functionalization of these systems the most interesting, as different modifications can be introduced at the same time, resulting in a multifunctional platform, a key aspect for new drug delivery systems. In the first chapter of this thesis, the functionalization of trigonal panels, pyrenyl guests and their combinations was studied.

The synthetic strategy for functional panels is based on the structure of 1,3,5-tris(pyridin-4-ylethynyl)benzene, a panel used before to assemble metalla-prisms. In a first step, the desired functional group is added to 2,4,6-triiodophenol through a Williamson ether synthesis reaction, followed by formation of the trigonal panel by Sonogashira coupling with 4-ethynylpyridine. The formation of metalla-prisms is not hindered by the presence of the functional groups on the panels, at least to the extent that has been studied in this thesis. On the other hand, the loss of symmetry on the panel results in the formation of two different isomers: an eclipsed conformation where the two side-chains are one above the other and a staggered conformation, where the two side-chains lay on different sides of the prism. The presence of such isomers complicates the final characterization of the assemblies by NMR, as there is splitting of the signals from the protons that are not anymore equivalent.

Double-arm pyrenyl guests present an opportunity to obtain higher molecular weight systems. In the same chapter, pyrenyl derivatives with arms in their 1 and 6 positions are synthesized through Heck coupling. Then, they are encapsulated inside metalla-prisms with 4-tpt and metalla-prisms with functional 4-tpe panels, proving that the combination of both functionalizing strategies is possible.

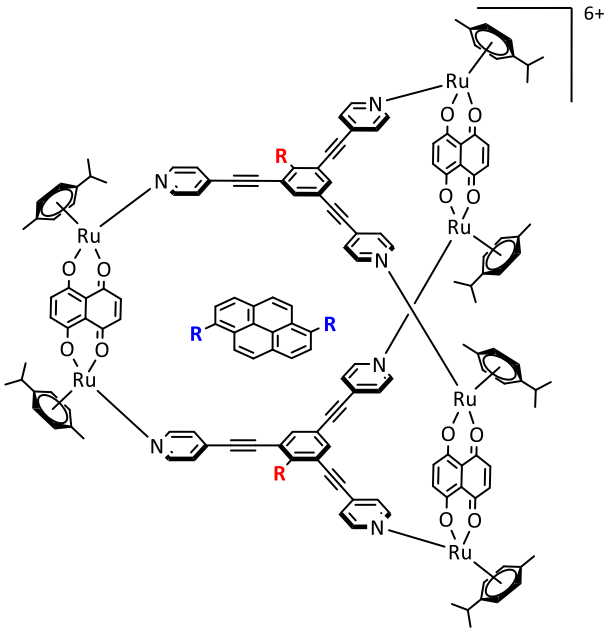

Another strategy investigated to obtain high molecular weight assemblies is based on the use of a porphyrinic core interconnecting up to 4 metalla-prisms after encapsulation. The designed system, has a final Mw of over 16 kDa, which is close to the required size to exploit the EPR effect. The downside of this approach is that the presence of four host-guest systems complicates significantly the study through NMR, in-depth study of the host-guest dynamics should be performed to achieve better understanding of the final products. As it is based on a porphyrin, the phototoxicity of this system on cancer cells could be explored in the future.

The second chapter has focused on the use of the synthetic strategies developed in the first chapter to build a multifunctional metalla-prism to use in PDT. More specifically, the assemblies designed in this work would consist in third generation photosensitizers, as they are the combination of a second-generation photosensitizer and a drug delivery system. Three different photosensitizers (based on tetraphenyl porphyrin, pheophorbide-a and BODIPY) were connected to pyrene through a PEG linker connected by amide bonds. On the other hand, a trigonal panel with a biotinylated side-chain was synthesized, aiming to improve the targeting of cancerous tissues, as those are known to overexpress receptors for biotin. Pyrenyl-PS derivatives were then encapsulated inside metalla-prisms containing functional and non-functional panels, obtaining a total of 8 different assemblies (including the two empty prisms).

Phototoxicity of guests, metalla-prisms and host-guest systems was studied *in vitro* on HCT116 colorectal cancer cells in the laboratory of Prof. Bertrand Liagre at the University of Limoges (France). The cytotoxic activity of the two empty metalla-assemblies is comparable, which does not suggest an improvement of the cytotoxicity by the presence of biotin. Nevertheless, further studies should be performed in order to determine if the accumulation of biotinylated assemblies is higher in cancerous tissues as opposed to healthy tissues. Among the host-guest systems, the most interesting results are those of **Pyrene-PheoA⊂P**, showing a phototoxic index (PI) of 160 and an IC_{50} after irradiation of 10 nM. In opposition, assemblies containing **Pyrene-TPP** as guest do not seem to improve in terms of PI, even if the IC_{50} after irradiation was higher when compared to the guest alone. **Pyrene-BODIPY** and its host-guest systems are studied at the moment using a more adequate irradiation wavelength closer to its absorption maximum. Other tests such as ROS production or cell internalization studies should be performed on these samples to have a better understanding of their phototoxic activity and the role of the metalla-assemblies.

The third and last chapter of the thesis involved the functionalization of clips with oxamide spacers to tune the hydrophilicity of prisms and cubes. Different alkylic chains with varying number of hydroxyl groups or PEG chains have been prepared, obtaining in most cases hydrophilic values of Log $P_{o/w}$. Comparing both sets of samples, prisms are always more hydrophilic compared to the cube with the same clip, due to the nature of the porphyrin used as panel for the cubes which is highly hydrophobic. Differences between clips with more or less hydroxyl groups are small from the point of view of water solubility, a longer chain does not improve significantly the hydrophilicity of the assembly. Assemblies with PEGylated clip **Cx5** show as well hydrophilic behavior, while those with **Cx6** (PEG terminated in BOC protecting group) show hydrophobic (cubes) or amphiphilic (prisms) behavior.

Anticancer activity of prisms will be investigated in the near future, to find out how the increased water solubility affects the cytotoxicity of arene ruthenium metalla-prisms. Moreover, metalla-cubes phototoxicity will be studied under PDT conditions, as the porphyrinic panel possesses photosensitizing properties.

5.2 Perspectives

Metalla-assemblies present an opportunity for the design of specialized drug delivery systems. In this thesis, it has been proved that the combination of different functionalization strategies is possible, resulting in very versatile systems. Many other possibilities remain to be explored, considering the numerous combinations of building blocks and/or guests.

In the case of functional clips, some preliminary tests suggest that clips with oxamide as spacer are not long enough to allow the cavity of the prism to host a guest, similarly to what had been observed before for oxalate spacers. Still, they could be mixed with functional panels to tune their properties. Another strategy would be to use other types of spacers which would increase the length of the clip such as benzoquinones. Metalla-prisms with benzoquinone spacers with alkylic chains have been previously reported in our group[158], which would potentially leave space for a guest.

Pyrenyl derivatives containing two arms have been found to be good guests, as their encapsulation was comparable to that of single arm pyrenes. Having more than one functional site may be useful in many cases, for example, the same Pyrenyl-PS guests used in this work could be bearing two PSs per guest, potentially improving the activity of the assemblies.

Systems containing several assemblies connected are a suitable shortcut to obtain high molecular weight assemblies. To improve the solubility of the system presented here, prisms with functional clips could be used. At the same time, to overcome host-guest problematics, prisms could be attached to central core by other methods such as linking them through their panels, resulting in more tunable systems.

Other synthetic strategies could simplify the obtention of multi-functional assemblies. For instance, a main prismatic scaffold could be synthesized and the final coupling reaction of a functional group could be performed afterwards, at the appropriate moment. Click chemistry is a coupling strategy that could be suited for this purpose, as it is fast and highly selective[170], while at the same time the reaction conditions would not affect the metalla-prisms. Since its introduction by Sharpless and colleagues in 2001[171], it has been extensively used as a bioconjugation strategy for drug delivery systems[172,173].

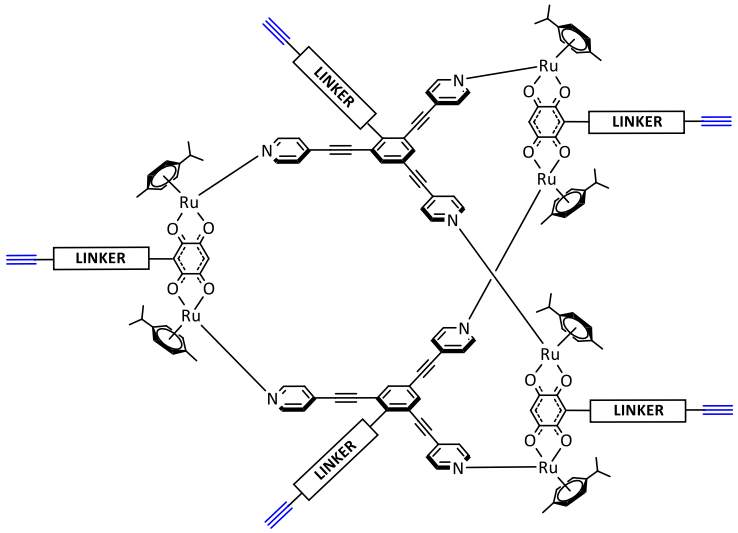

6. Experimental section

6.1 General remarks

6.1.1 Solvents, reagents and products

Solvents of analytical grade were purchased from Fisher Scientific and used as received. Dry/anhydrous level solvents were purchased from ACROS organics. All commercial reagents were purchased from Brunschwig, Merck, Fisher Scientific or Porphychem. The following products were prepared according to published methods:[(*p*-cymene)$_2$Ru$_2$Cl$_2$(μ-Cl)$_2$][174], [Ru$_2$(p-cymene)$_2$(dobq)Cl$_2$][175], [Ru$_2$(p-cymene)$_2$(donq)Cl$_2$][175], 2,4,6-tris(4-pyridyl)-1,3,5-triazine (4-tpt)[176], prism **P**[177], *tert*-butyl 2-(2,4,6-triiodophenoxy)acetate[178], 2-(2,4,6-triiodophenoxy)acetic acid[178], *tert*-butyl (2-(2-(2-(4-(pyren-1-yl)butanamido)ethoxy)ethoxy)ethyl)carbamate[179], N-(2-(2-(2-aminoethoxy)ethoxy)ethyl)-4-(pyren-1-yl)butanamide[179], methyl pheophorbide a[180], BODIPY[181], N,N'-bis(2,3,4,5,6-pentahydroxyhexyl)oxalamide[182], clip **Cx4**[183] and prism **P4**[183].

Flash chromatography was performed on a Biotage® Isolera One instrument equipped with a UV-Vis detector. Biotage® Sfär silica columns of different sizes were obtained as well directly from Biotage (Sweden).

6.1.2 Analytical techniques

NMR spectra were recorded on a Bruker Avance Neo Ascend 600MHz spectrometer using the residual protonated solvent as internal standard.

Absorption spectra were recorded on a Perkin-Elmer Lambda 650 UV-Vis or a Lambda 365 UV-Vis.

Emission spectra were collected with an Edinburgh FLS920 spectrofluorimeter, equipped with a Peltier-cooled Hamamatsu R928 PMT (280-850 nm) at the Institute for Organic Synthesis and Photoreactivity (ISOF) under the supervision of Dr. Barbara Ventura.

ESI-MS studies of the multifunctional metalla-prisms were obtained at the Freie Universität Berlin at Pr. Christoph Schalley's group. Measurements were obtained with a Water's Synapt G2-S travelling wave ion mobility mass spectrometer (Manchester, UK) equipped with a Z-spray electrospray ionisation source. Measurements were performed with a capillary voltage of 2.50 kV and with the sample cone and source offset both set to 10 V. The source and desolvation temperature were 80 °C and 80 °C, respectively. A final sample concentration of 10μM in acetonitrile was used with injection rate of 5 μL/min.

ESI-MS spectra for all other compounds were obtained at EPFL ISIC's mass service with a LTQ Orbitrap ELITE ETD (Thermo fisher) equipped with a nanochiped-based ESI system Advion TriVera Nanomate®, all the data was analyzed using the open access EPFL MStoolbox.

6.1.3 Octanol/water partition coefficient (log P) measurements

Octanol/water partition coefficient was obtained following a published method[168]. Water and octanol were pre-saturated with each other before use and all experiments were performed by triplicates, results are reported as the average log P value and their standard deviation.

In the case of prisms, sample was dissolved in 2 ml of water (around 10^{-5} M) and 2 ml of octanol were added. Then, mixture was vigorously shaken by hand. Layers were allowed to stand and separate for 24 h and concentration in both phases was determined by UV-Vis spectroscopy, further dilution was performed when necessary.

In the case of cubes, a mother solution in 0.5 ml of DMSO was prepared (around 10^{-4} M) and 100 µL of this solution was added into a mixture of 3 ml of water and 3 ml of octanol. All mixtures were shaken vigorously by hand and allowed to separate over 24 h. Concentration in both phases was determined by UV-Vis spectroscopy using appropriate dilutions when needed.

6.1.4 *In vitro* phototoxicity studies

Phototoxicity of guests, metalla-prisms and host-guest systems was studied in the laboratory of Prof. Bertrand Liagre at the University of Limoges (France). Human HCT116 colorectal cancer cells were seeded at 4000 cells/well and were incubated for 24 h prior to exposure to the compounds. Stock solutions of the compounds were prepared in DMSO and then diluted in RPMI medium into the final concentration of interest. Cells were irradiated or not with a 630-660 nm CURElight lamp at 75 J/cm^2. Antiproliferative activity was estimated using an MTT assay 24 h after irradiation and experiments were performed at least in triplicate (for cytotoxicity in the dark, same procedure was used but without irradiation).

6.2 Synthesis and characterization

6.2.1 Investigating the functionalization of metalla-assemblies

bis(*tert*-butyl)-3,3'-(1,6-pyrenediyl)-diacrylate (Pyr1): Under inert conditions, 1,6-dibromopyrene (2 g, 5.55 mmol, 1 eq.) and $Pd(PPh_3)_4$ (642 mg, 0.55 mmol, 0.1 eq.) were dissolved in 5 ml of dry DMF. Then, triethylamine (1.16 ml, 1.5 eq.) and *tert*-butyl acrylate (3.23 ml, 22.22 mmol, 4 eq.) were added and the solution was heated to 90 °C and kept stirring overnight. The product was purified by flash chromatography on a silica column, using a cyclohexane:ethyl acetate gradient to obtain the product as a solid. (Orange solid, 2.1 g, 83% yield).

^{1}H NMR (600 MHz, $CDCl_3$) δ 8.72 (d, *J* = 15.7 Hz, 2H, C*H*=CH), 8.51 (d, *J* = 9.2 Hz, 2H, H_{pyr}), 8.28 (d, *J* = 8.1 Hz, 2H, H_{pyr}), 8.18 (d, *J* = 8.1 Hz, 2H, H_{pyr}), 8.14 (d, *J* = 9.2 Hz, 2H, H_{pyr}), 6.65 (d, *J* = 15.7 Hz, 2H, CH=C*H*), 1.62 (s, 18H, $CH_{3t\text{-}but}$). UV/Vis (DCM): λ_{max} (ε [$M^{-1}cm^{-1}$]) = 255 (54000), 291 (25000), 301 (29000), 393 (48000), 421 (43000).

4-hydroxybutyl-3-(6-bromopyren-1-yl)acrylate (Pyr2): Under inert conditions, 1,6-dibromopyrene (350 mg, 927 µmol) and $Pd(PPh_3)_4$ (56 mg, 49 µmol) were dissolved in 5 ml of dry DMF. Then, triethylamine (203 µL, 1.46 mmol) and 4-hydroxybutyl acrylate (336 µL, 2.43 mmol) were added and the solution was heated to 90 °C and kept stirring overnight. The solution was then diluted with DCM and washed with an aqueous solution of NH_4Cl and twice with water. Organic phase was dried over Na_2SO_4, filtered, and the solvent evaporated to dryness to give an orange solid. The product was purified by flash chromatography on a silica column, using a cyclohexane:ethyl acetate gradient. Both mono and disubstituted products were obtained as solids. (201 mg, 42% yield).

^{1}H NMR (600 MHz, $CDCl_3$) δ 8.77 (d, *J* = 15.8 Hz, 1H, C*H*=CH), 8.43 (dd, *J* = 9.2, 2.0 Hz, 2H, H_{pyr}), 8.24 (dd, *J* = 16.4, 8.1 Hz, 2H, H_{pyr}), 8.14 (d, *J* = 8.1 Hz, 1H, H_{pyr}), 8.08 (dd, *J* = 13.9, 9.2 Hz, 2H, H_{pyr}), 8.00 (d, *J* = 8.2 Hz, 1H, H_{pyr}), 6.70 (d, *J* = 15.7 Hz, 1H, CH=C*H*), 4.35 (t, *J* = 6.5 Hz, 2H, COOC*H*$_2$), 3.77 (q, *J* = 6.0 Hz, 2H, CH_2CH_2OH), 1.89 (p, *J* = 6.9 Hz, 2H, $CH_2CH_2CH_2$), 1.77 (p, *J* = 6.0 Hz, 2H, $CH_2CH_2CH_2$), 1.50 (t, *J* = 5.2 Hz, 1H, CH_2CH_2OH). ^{13}C NMR (151 MHz, $CDCl_3$) δ 167.21 (*C*$OOCH_2$), 141.44 (*C*H=CH), 132.55 (C_{pyr}), 130.84 (C_{pyr}), 130.64 (CH_{pyr}), 130.25 (C_{pyr}), 129.95 (C_{pyr}), 129.78 (C_{pyr}), 129.09 (C_{pyr}), 128.96 (CH_{pyr}), 128.62 (C_{pyr}), 127.21 (CH_{pyr}), 126.36 (CH_{pyr}), 125.94 (C_{pyr}), 125.68 (CH_{pyr}), 124.94 (CH_{pyr}), 124.41 (C_{pyr}), 122.87 (CH_{pyr}), 121.13 (C_{pyr}), 120.84 (CH=*C*H), 64.70 (COO*C*H_2), 62.62 (CH_2CH_2OH), 29.37 ($CH_2CH_2CH_2$), 25.45 ($CH_2CH_2CH_2$). UV/Vis (DCM): λ_{max} (ε [$M^{-1}cm^{-1}$]) = 238 (37000), 288 (22000), 297 (24000), 379 (36000), 405 (19000). HRMS (ESI) m/z: [**Pyr2**+Na]$^+$ Calcd for $C_{23}H_{19}BrNaO_3$ 445.0410; Found 445.0411.

bis(4-hydroxybutyl)-3,3'-(1,6-pyrenediyl)-diacrylate (Pyr3): Obtained from same reaction. (145 mg, 31% yield).

^{1}H NMR (600 MHz, $CDCl_3$) δ 8.83 (d, *J* = 15.7 Hz, 2H, C*H*=CH), 8.54 (d, *J* = 9.2 Hz, 2H, H_{pyr}), 8.31 (d, *J* = 8.1 Hz, 2H, H_{pyr}), 8.20 (dd, *J* = 22.2, 8.6 Hz, 4H, H_{pyr}), 6.73 (d, *J* = 15.7 Hz, 2H, CH=C*H*), 4.35 (t, *J* = 6.5 Hz, 4H, COOC*H*$_2$), 3.77 (q, *J* = 6.1 Hz, 4H, CH_2CH_2OH), 1.89 (p, *J* = 6.4 Hz, 4H, $CH_2CH_2CH_2$), 1.76 (p, *J* = 6.9 Hz, 4H, $CH_2CH_2CH_2$), 1.40 (t, *J* = 5.3 Hz, 2H, CH_2CH_2OH). ^{13}C NMR (151 MHz, $CDCl_3$) δ 167.21 (*C*$OOCH_2$), 141.48 (*C*H=CH), 132.96 (C_{pyr}), 132.28 (CH_{pyr}), 132.22 (CH_{pyr}), 132.11 (C_{pyr}), 130.03 (C_{pyr}), 129.41 (C_{pyr}), 128.70(CH_{pyr}), 128.62 (CH_{pyr}), 126.00 (C_{pyr}), 124.81 (C_{pyr}), 123.75 (C_{pyr}), 120.91 (CH=*C*H), 64.70 (COO*C*H_2), 62.63 (CH_2CH_2OH), 29.38 ($CH_2CH_2CH_2$), 25.45 ($CH_2CH_2CH_2$). UV/Vis (DCM): λ_{max} (ε [$M^{-1}cm^{-1}$]) = 231 (32000), 256 (37000), 291 (17000), 301 (20000), 393 (31000), 424 (29000). HRMS (ESI) m/z: [**Pyr3**]$^+$ Calcd for $C_{30}H_{30}O_6$ 486.2037; Found 486.2036.

3,3'-(pyrene-1,6-diyl)diacrylic acid: To a solution of **Pyr1** (1 g, 2.20 mmol, 1 eq.), TFA was added dropwise (3.37 ml, 44 mmol, 20 eq.), the resulting solution was stirred overnight. Then, solvent was evaporated to give the product as a solid, it was used without further purification. (Orange solid, 641 mg, 1.87 mmol, 85% yield).

^{1}H NMR (600 MHz, D_2O) δ 7.99 (d, *J* = 15.6 Hz, 2H, C*H*=CH), 7.63 (d, *J* = 7.8 Hz, 2H, H_{pyr}), 7.54 (d, *J* = 9.0 Hz, 2H, H_{pyr}), 7.36 (d, *J* = 7.9 Hz, 2H, H_{pyr}), 7.23 (d, *J* = 9.0 Hz, 2H, H_{pyr}), 6.46 (dd, *J* = 15.6, 1.4 Hz, 2H, CH=C*H*).

Pyr4: A solution of EDCl (95 mg, 0.49 mmol, 1.5 eq.), HOBt (67 mg, 0.49 mmol, 1.5 eq.) and 3,3'-(pyrene-1,6-diyl)diacrylic acid (113 mg, 0.33 mmol, 1 eq.) in 15 ml of anhydrous DMF was prepared under inert conditions. After stirring for 30 min, N-Boc-2,2'-(ethylenedioxy)diethylamine (205 mg, 0.83 mmol, 2.5 eq.) and DMAP (40 mg, 0.33 mmol, 1 eq.) were added. The reaction mixture was stirred at room temperature for 96 h. The crude product was then partitioned between DCM and water and washed twice with brine. The organic phase was dried over Na_2SO_4, filtered and evaporated to dryness. Product is further purified by flash chromatography on a silica column, using an ethyl acetate:methanol gradient. (Yellow solid, 116 mg, 44% yield).

^{1}H NMR (600 MHz, DMSO) δ 8.58 – 8.49 (m, 4H, C*H*=CH and H_{pyr}), 8.42 – 8.29 (m, 6H, H_{pyr}), 6.96 (d, *J* = 15.5 Hz, 2H, CH=C*H*), 6.78 (t, *J* = 5.8 Hz, 2H, NH), 3.59 – 3.51 (m, 12H, CH_{2PEG}), 3.41 (dt, *J* = 23.8, 5.9 Hz, 8H, CH_{2PEG}), 3.07 (q, *J* = 6.0 Hz, 4H, CH_{2PEG}), 1.35 (s, 18H, $CH_{3t\text{-but}}$). UV/Vis (DCM): λ_{max} (ε [$M^{-1}cm^{-1}$]) = 256 (66000), 290 (30000), 300 (33000), 395 (58000), 418 (49000).

Standard procedure for the preparation of host-guest metalla-assemblies: A mixture of $AgCF_3SO_3$ (53 mg, 206 µmol, 6 eq.) and $[Ru_2(p\text{-cymene})_2(donq)Cl_2]$ (75 mg, 103 µmol, 3 eq.) in 25 ml of MeOH was stirred at RT for 4 h. Then, the solution was filtered into another MeOH solution containing 4-tpt (21 mg, 68 µmol, 2 eq.) and guest (**Pyr2** or **Pyr3**, 34 µmol, 1 eq.). The solution was heated to 60 °C and kept stirring overnight. After evaporation of solvent, the solid was redissolved in minimum amount of DCM (1-2 ml) and diethyl ether was added dropwise to induce precipitation. The precipitate formed is filtered off and washed with diethyl ether and pentane.

Pyr2⊂Prism: Dark solid, 105 mg, 27 µmol, 78% yield. ^{1}H NMR (600 MHz, CD_2Cl_2) δ 8.54 (s, 12H, H_α), 8.17 (m, 12H, H_β), 7.44 (s, 12H, H_q), 5.67 (d, *J* = 5.8 Hz, 12H, $H_{p\text{-cym}}$), 5.46 (d, *J* = 5.8 Hz, 12H, $H_{p\text{-cym}}$), 4.54 (s, 2H, COOC*H*$_2$), 3.88 (s, 2H, CH_2CH_2OH), 2.79 (sept, *J* = 7.0 Hz, 6H, (C*H*$(CH_3)_2$), 2.00 (s, 18H, CH_3), 1.30 (d, *J* = 7.0 Hz, 36H, (CH(C*H*$_3$)$_2$). ^{13}C NMR (151 MHz, CD_2Cl_2) δ 171.18 (CO), 166.66 (*C*OOCH$_2$), 153.00 (CH_α), 139.80 (*C*H=CH), 138.15 (CH_q) , 131.76 (C_{pyr}), 130.61 (C_{pyr}), 129.78 (C_{pyr}), 129.20 (C_{pyr}), 128.58 (C_{pyr}), 127.89 (CH_{pyr}), 126.50 (CH_{pyr}), 125.97 (C_{pyr}), 124.52 (C_{pyr}), 124.39 (CH_β), 123.29 (C_{pyr}), 122.39 (CH_{pyr}), 120.27 (C_{pyr}), 118.14 (CH=*C*H), 111.71 (C_q), 104.22 ($C_{p\text{-}cym}$), 100.57 ($C_{p\text{-cym}}$), 85.12 ($CH_{p\text{-cym}}$), 83.02 ($CH_{p\text{-cym}}$), 65.73 (COO*C*H$_2$), 62.33 (CH_2CH_2OH), 31.06 (*C*H$(CH_3)_2$), 30.12 ($CH_2CH_2CH_2$), 25.75 ($CH_2CH_2CH_2$), 22.29 (CH(*C*H$_3$)$_2$), 17.37 (CH_3). UV/Vis (DCM): λ_{max} (ε [$M^{-1}cm^{-1}$]) = 234 (176000), 283 (61000), 297 (65000), 320 (53000), 378 (52000), 407 (41000), 454 (28000), 638 (7000), 692 (8000). HRMS (ESI) m/z: [**Pyr2⊂Prism** - $4CF_3SO_3$]$^{4+}$ Calcd for $C_{151}H_{139}BrF_6N_{12}O_{21}Ru_6S_2$ 831.0736; Found 831.0765.

Pyr3⊂Prism: Dark solid, 115 mg, 29 µmol, 84% yield. ^{1}H NMR (600 MHz, CD_2Cl_2) δ 8.57 (d, *J* = 5.6 Hz, 12H, H_α), 8.39 (m, 12H, H_β), 7.31 (s, 12H, H_q), 5.66 (d, *J* = 5.9 Hz, 12H, $H_{p\text{-cym}}$), 5.47 (d, *J* = 5.9 Hz, 12H, $H_{p\text{-cym}}$), 4.36 (s, 4H, COOC*H*$_2$), 3.80 (s, 4H, CH_2CH_2OH), 2.79 (sept, *J* = 7.0 Hz, 6H, (C*H*$(CH_3)_2$), 2.04 (s, 18H, CH_3), 1.30 (d, *J* = 7.0 Hz, 36H, (CH(C*H*$_3$)$_2$). ^{13}C NMR (151 MHz, CD_2Cl_2) δ 171.19 (CO), 169.77 (C_{tpt}), 166.42 (*C*OOCH$_2$), 153.29 (CH_α), 144.37 (C_{tpt}), 139.70 (*C*H=CH), 137.92 (CH_q), 130.76 (C_{pyr}), 128.69 (C_{pyr}), 124.81 (CH_β), 124.52 (C_{pyr}), 123.91 (C_{pyr}), 122.39 (CH_{pyr}), 120.26 (CH_{pyr}), 118.13 (CH=*C*H), 111.82 (C_q), 104.25 ($C_{p\text{-cym}}$), 100.44 ($C_{p\text{-cym}}$), 84.99 ($CH_{p\text{-cym}}$), 83.08 ($CH_{p\text{-cym}}$), 65.38 (COO*C*H$_2$), 62.44 (CH_2CH_2OH), 31.07

(*C*H(CH$_3$)$_2$), 29.95 (CH$_2$*C*H$_2$CH$_2$), 25.92 (CH$_2$*C*H$_2$CH$_2$), 22.30 (CH(*C*H$_3$)$_2$), 17.41 (CH$_3$). UV/Vis (DCM): λ_{max} (ε [M^{-1}cm^{-1}]) = 246 (148000), 292 (54000), 302 (59000), 319 (43000), 394 (52000), 424 (55000), 637 (6000), 694 (7000). HRMS (ESI) m/z: [**Pyr3⊂Prism** - 4CF$_3$SO$_3$]$^{4+}$ Calcd for $C_{158}H_{150}F_6N_{12}O_{24}Ru_6S_2$ 847.1118; Found 847.1148.

Standard procedure for the synthesis of functionalized 1,3,5-triiodobenzenes: Under inert conditions, 1,3,5-triiodophenol (1 eq.), halogenated chain (1 eq.; icosane bromide, 766 mg, 2.12 mmol; tris-ethylene glycol monomethyl ether iodide, 0.57 ml, 2.12 mmol; *tert*-butyl bromoacetate, 1.56 ml, 10.60 mmol) and K_2CO_3 (1.2 eq.) were dissolved in 30 ml of anhydrous DMF. The resulting solution was heated to 50 °C and kept stirring overnight. The mixture was then partitioned between 40 ml of H_2O and 40 ml of DCM, followed by two more extractions with DCM. Combined organic extracts were dried over Na_2SO_4, filtered and evaporated to dryness to give a white solid.

1,3,5-triiodo-2-(icosyloxy)benzene: White solid, 1.52 g, 2.02 mmol, 95% yield. ^{1}H NMR (600 MHz, $CDCl_3$) δ 7.64 (s, 2H), 3.97 (t, *J* = 6.6 Hz, 2H), 1.85 (p, *J* = 7.4 Hz, 2H), 1.51 (p, *J* = 7.8 Hz, 2H), 1.33 (m, 6H), 1.25 (s, 26H), 0.88 (t, *J* = 7.0 Hz, 3H). ^{13}C NMR (151 MHz, $CDCl_3$) δ 153.21 (C_{bz}O), 135.12 (C_{bz}H), 119.25 (C_{bz}), 117.23 (C_{bz}), 73.91 (O*C*H$_2$CH$_2$), 32.08 (OCH$_2$*C*H$_2$), 30.12 (CH$_2$*C*H$_2$CH$_2$), 29.85 (CH$_2$*C*H$_2$CH$_2$), 29.81 (CH$_2$*C*H$_2$CH$_2$), 29.76 (CH$_2$*C*H$_2$CH$_2$), 29.72 (CH$_2$*C*H$_2$CH$_2$), 29.57 (CH$_2$*C*H$_2$CH$_2$), 29.51 (CH$_2$*C*H$_2$CH$_2$), 25.98 (CH$_2$*C*H$_2$CH$_2$), 22.84 (CH$_2$*C*H$_2$CH$_3$), 14.27 (CH$_3$). UV/Vis (DCM): λ_{max} (ε [M^{-1}cm^{-1}]) = 282 (1000), 290 (1000).

tert-butyl 2-(2,4,6-triiodophenoxy)acetate: Yellow oil, 6 g, 96% yield. ^{1}H NMR (600 MHz, $CDCl_3$) δ 8.04 (s, 2H, CH_{bz}), 4.42 (s, 2H, CH_2CO), 1.53 (s, 9H, CH_3).

1,3,5-triiodo-2-(2-(2-(2-methoxyethoxy)ethoxy)ethoxy)benzene: White solid, 807 mg, 1.31 mmol, 62% yield. ^{1}H NMR (600 MHz, $CDCl_3$) δ 7.55 (s, 2H, CH_{bz}), 4.08 (t, *J* = 4.9 Hz, 2H, CH_{2PEG}), 3.82 (t, *J* = 4.9 Hz, 2H, CH_{2PEG}), 3.70 – 3.64 (m, 2H, CH_{2PEG}), 3.60 (dd, *J* = 5.8, 3.8 Hz, 2H, CH_{2PEG}), 3.57 (dt, *J* = 7.4, 2.9 Hz, 2H, CH_{2PEG}), 3.49 – 3.44 (m, 2H, CH_{2PEG}), 3.29 (s, 3H, CH_3).

2-(2,4,6-triiodophenoxy)acetic acid: To a solution of *tert*-butyl 2-(2,4,6-triiodophenoxy)acetate (1.5 g, 2.56 mmol, 1 eq.), TFA was added dropwise (4.38 g, 38.4 mmol, 15 eq.), the resulting clear solution was stirred at RT for 5 h. Then, solvent was evaporated and the resulting solid is filtered and cleaned with water and DCM. (White powder, 1.01 g, 2.56 mmol, 74% yield). ^{1}H NMR (600 MHz, DMSO) δ 12.31 (s, 1H, COOH), 7.30 (s, 2H, H_{bz}), 3.59 (s, 2H, CH_2).

TriPEGboc: A solution of EDCl (160 mg, 0.83 mmol, 1.5 eq.), HOBt (113 mg, 0.83 mmol, 1.5 eq.) and 2-(2,4,6-triiodophenoxy)acetic acid (294 mg, 0.56 mmol, 1 eq.) in 15 ml of anhydrous DMF prepared under inert conditions was cooled to 0 °C. After stirring for 30 min, N-Boc-2,2'-(ethylenedioxy)diethylamine (207 mg, 0.83 mmol, 1.5 eq.) and DMAP (68 mg, 0.56 mmol, 1 eq.) were added. The reaction mixture was stirred at 0 °C for 2 h and at room temperature for 48 h. The crude product was then partitioned between DCM and an aqueous 1M HCl solution, followed by an aqueous solution of $NaHCO_3$ and a final wash with water. The organic phase was then dried over Na_2SO_4, filtered and evaporated to dryness. (Pale brown solid, 292 mg, 69% yield).

^{1}H NMR (600 MHz, $CDCl_3$) δ 8.06 (s, 2H, H_{bz}), 7.23 (s, 1H, NH), 4.97 (s, 1H, NH), 4.46 (s, 2H, CH_2), 3.68 – 3.60 (m, 8H, CH_{2PEG}), 3.54 (t, *J* = 5.2 Hz, 2H, CH_{2PEG}), 3.31 (q, *J* = 5.5 Hz, 2H, CH_{2PEG}), 1.43 (s, 9H, CH_{3boc}).

TriPEGNH$_2$: To a solution of **TriPEGboc** (480 mg, 0.63 mmol, 1 eq.), TFA was added dropwise (1.08 g, 9.47 mmol, 15 eq.), the resulting solution was stirred overnight. Then, solvent was evaporated and the resulting oil was used in the next step without further purification. (Brown oil, 330 mg, 0.5 mmol, 79% yield).

^{1}H NMR (600 MHz, $CDCl_3$) δ 8.07 (s, 2H, H_{bz}), 7.47 (t, *J* = 6.1 Hz, 1H, NH), 4.53 (s, 2H, CH_2), 3.77 (t, *J* = 4.9 Hz, 2H, CH_{2PEG}), 3.74 – 3.62 (m, 8H, CH_{2PEG}), 3.29 (h, *J* = 5.7 Hz, 2H, CH_{2PEG}).

TriPEGAnth: A solution of EDCl (174 mg, 0.91 mmol, 1.5 eq.), HOBt (123 mg, 0.91 mmol, 1.5 eq.) and 3-(anthracen-9-yl)propanoic acid (228 mg, 0.91 mmol, 1.5 eq.) in 15 ml of anhydrous DMF prepared under inert conditions was cooled to 0 °C. After stirring for 30 min, **TriPEGNH₂** (400 mg, 0.61 mmol, 1 eq.) and DMAP (74 mg, 0.61 mmol, 1 eq.) were added. The reaction mixture was stirred at 0 °C for 2 h and at room temperature for 48 h. The crude product was then partitioned between DCM and an aqueous 1 M HCl solution, followed by an aqueous solution of $NaHCO_3$ and a final wash with water. The organic phase was then dried over Na_2SO_4, filtered and evaporated to dryness. (Brown solid, 372 mg, 0.42 mmol, 69% yield).

^{1}H NMR (600 MHz, $CDCl_3$) δ 8.37 (s, 1H, H_{anth}), 8.31 – 8.27 (m, 2H, H_{anth}), 8.00 (s, 2H, H_{bz}), 7.55 – 7.49 (m, 3H, H_{anth}), 7.49 – 7.41 (m, 3H, H_{anth}), 7.10 (t, *J* = 5.6 Hz, 1H, NH), 5.90 (t, *J* = 5.2 Hz, 1H, NH), 4.34 (s, 2H, CH_2), 4.03 – 3.96 (m, 4H, CH_{2PEG}), 3.58 – 3.45 (m, 4H, CH_{2PEG}), 3.43 – 3.30 (m, 4H, CH_{2PEG}), 2.85 – 2.79 (m, 2H, CH_2), 2.67 (t, *J* = 8.1 Hz, 2H, CH_2).

Standard procedure for the synthesis of functionalized panels: Under inert conditions, corresponding triiodo benzene derivative (1 eq.; **L1**: 1,3,5-triiodophenol, 2 g, 4.24 mmol; **L2**: 1,3,5-triiodo-2-(icosyloxy)benzene, 1 g, 1.33 mmol; **L3**: *tert*-butyl 2-(2,4,6-triiodophenoxy)acetate, 850 mg, 1.45 mmol; **L4**: 1,3,5-triiodo-2-(2-(2-(2-methoxyethoxy)ethoxy)ethoxy)benzene, 250 mg, 0.52 mmol; **L5**: 1,3,5-triiodo-2-(PEG3-anthracene)benzene, 300 mg, 0.34 mmol), $Pd(PPh_3)_4$ (0.1 eq.) and CuI (0.1 eq.) were dissolved in a mixture of triethylamine and anhydrous THF (1:1.5). After stirring for 15 min, 4-ethynylpyridine hydrochloride (4 eq.) was added and the solution was heated to 100 °C and kept stirring for 48 h. The solvent was evaporated and the resulting residue was redissolved in DCM, washed with an aqueous solution of NH_4Cl and twice with water. The organic phase was dried over Na_2SO_4, filtered, and the solvent evaporated to dryness. The product was purified by flash chromatography on a silica column, using a DCM:MeOH gradient to obtain the product as a brown solid.

L1: Pale brown solid, 590 mg, 1.48 mmol, 35% yield. ^{1}H NMR (600 MHz, $CDCl_3$) δ 8.74 (m, 2H, H_α), 8.69 (m, 2H, H_α), 8.63 (m, 2H, H_α), 7.86 (d, J = 1.6 Hz, 1H, H_{bz}), 7.76 (m, 3H, H_{bz} + H_β), 7.50 (m, 2H, H_β), 7.40 (m, 2H, H_β). ^{13}C NMR (151 MHz, $CDCl_3$) δ 155.02 (COH), 150.71 (CH_α), 150.09 (CH_α), 149.98 (CH_α), 136.48 ($C_{bz}H$), 132.94, 131.26, 130.87 (C_{bz}), 129.30 (C_{bz}), 126.36 (CH_β), 125.75 (CH_β), 125.62 (CH_β), 119.05 (C_{bz}), 118.02 (C_{bz}), 107.53, 104.82, 92.95 (C≡C), 92.22 (C≡C), 86.91 (C≡C), 86.59 (C≡C). UV/Vis (DCM): λ_{max} (ε [$M^{-1}cm^{-1}$]) = 294 (63000), 305 (65000), 345 (13000). HRMS (ESI) m/z: [**L1** + H]$^+$ Calcd for $C_{27}H_{16}N_3O$ 398.1288; Found 398.1292.

L2: Brown solid, 281 mg, 0.41 mmol, 31% yield. ^{1}H NMR (600 MHz, $CDCl_3$) δ 8.62 (m, 6H, H_α), 7.72 (s, 2H, H_{bz}), 7.38 (m, 6H, H_β), 4.38 (t, J = 6.3 Hz, 2H, OCH_2CH_2), 1.87 (m, 2H, OCH_2CH_2), 1.56 (p, J = 7.7 Hz, 2H, $CH_2CH_2CH_2$), 1.33 (p, J = 7.3 Hz, 2H, $CH_2CH_2CH_2$), 1.22 (m, 30H, $CH_2CH_2CH_2$), 0.86 (t, J = 7.0 Hz, 3H, CH_3). ^{13}C NMR (151 MHz, $CDCl_3$) δ 162.25 ($C_{bz}O$), 150.28 (CH_α), 149.83 (CH_α), 149.76 (CH_α), 137.86 ($C_{bz}H$), 131.18 (C_{bz}), 125.66 (CH_β), 125.56 (CH_β), 120.76 (C_{bz}), 117.77 (C_{bz}), 117.29 (C_{bz}), 91.81 (C≡C), 91.70 (C≡C), 89.02 (C≡C), 87.42 (C≡C), 75.29 (OCH_2CH_2), 32.04 (OCH_2CH_2), 30.64 ($CH_2CH_2CH_2$), 29.83 ($CH_2CH_2CH_2$), 29.78 ($CH_2CH_2CH_2$), 29.76 ($CH_2CH_2CH_2$), 29.75 ($CH_2CH_2CH_2$), 29.63 ($CH_2CH_2CH_2$), 29.48 ($CH_2CH_2CH_2$), 26.35 ($CH_2CH_2CH_2$), 22.81 ($CH_2CH_2CH_3$), 14.25 (CH_3). UV/Vis (DCM): λ_{max} (ε [$M^{-1}cm^{-1}$]) = 287 (72000), 303 (72000) 348 (7000). HRMS (ESI) m/z: [**L2** +H]$^+$ Calcd for $C_{47}H_{56}N_3O$ 678.4418; Found 678.4419.

L3: Brown solid, 580 mg, 1.13 mmol, 78% yield. ^{1}H NMR (600 MHz, $CDCl_3$) δ 8.65 – 8.59 (m, 6H, H_α), 7.72 (s, 2H, H_{bz}), 7.43 – 7.39 (m, 4H, H_β), 7.38 – 7.34 (m, 2H, H_β), 4.97 (s, 2H, CH_2CO), 1.43 (s, 9H, CH_3). UV/Vis (DCM): λ_{max} (ε [$M^{-1}cm^{-1}$]) = 287 (50000), 303 (51000), 347 (4000).

L4: 92 mg, 0.17 mmol, 39% yield. ^{1}H NMR (600 MHz, $CDCl_3$) δ 8.65 (s, 6H, H_α), 7.73 (s, 2H, H_{bz}), 7.42 (d, *J* = 5.0 Hz, 4H, H_β), 7.37 (d, *J* = 5.2 Hz, 2H, H_β), 4.58 – 4.54 (m, 2H, CH_{2PEG}), 3.97 – 3.92 (m, 2H, CH_{2PEG}), 3.76 – 3.69 (m, 2H, CH_{2PEG}), 3.63 – 3.52 (m, 4H, CH_{2PEG}), 3.51 – 3.48 (m, 2H, CH_{2PEG}), 3.35 (s, 3H, CH_3).

L5: 154 mg, 0.19 mmol, 56% yield. ^{1}H NMR (600 MHz, $CDCl_3$) δ 8.70 – 8.55 (m, 6H, H_α), 8.32 (d, *J* = 4.5 Hz, 1H, H_{anth}), 8.27 (d, *J* = 8.8 Hz, 2H, H_{anth}), 7.97 (d, *J* = 8.3 Hz, 2H, H_{anth}), 7.71 (s, 2H, H_{bz}), 7.51 – 7.45 (m, 2H, H_{anth}), 7.45 – 7.41 (m, 2H, H_{anth}), 7.40 – 7.36 (m, 2H, H_β), 7.34 – 7.30 (m, 4H, H_β), 6.12 (t, *J* = 5.4 Hz, 1H, NH), 4.80 (s, 2H, CH_2), 3.96 (t, *J* = 7.9 Hz, 2H, CH_2), 3.43 – 3.38 (m, 2H, CH_{2PEG}), 3.36 – 3.20 (m, 8H, CH_{2PEG}), 2.64 (t, *J* = 7.9 Hz, 2H, CH_2).

Standard procedure for the preparation of metalla-assemblies with functionalized panels: A mixture of $AgCF_3SO_3$ (6 eq.) and [Ru_2(*p*-cymene)$_2$(OO∩OO)Cl_2] (3 eq.; **Pr1**: dobq, 128 mg, 189 µmol; **Pr2**: dobq, 70 mg, 103 µmol; **Pr3**: donq, 75 mg, 103 µmol; **Pr4**: donq, 15 mg, 22 µmol; **Pr5**: donq, 67 mg, 92 µmol) in 25 ml of MeOH was stirred at RT for 4 h. Then, the solution was filtered into another MeOH solution containing the panel (2 eq., **Pr1**: **L1**, 50 mg, 126 µmol; **Pr2**: **L2**, 47 mg, 69 µmol; **Pr3**: **L3**, 35 mg, 68 µmol; **Pr4**: **L4**, 8 mg, 15 µmol; **Pr5**: **L5**, 50 mg, 61 µmol). The solution was heated to 60 °C and kept stirring overnight. After evaporation of solvent, the solid was redissolved in minimum amount of DCM (1-2 ml) and diethyl ether was added dropwise to induce precipitation. The precipitate formed is filtered off and washed with diethyl ether and pentane.

Pr1: Red solid, 150 mg, 43 µmol, 68% yield. ^{1}H NMR (600 MHz, CD_2Cl_2) δ 8.25 (m, 12H, H_α), 7.87 (m, 4H, H_{bz}), 7.56 (m, 12H, H_β), 5.80 (m, 30H, $H_{p\text{-cym}}$ and H_q), 2.85 (m, 6H, (C*H*$(CH_3)_2$), 2.18 (m, 18H, CH_3), 1.33 (m, 36H, (CH(C*H*$_3)_2$). ^{13}C NMR (151 MHz, CD_2Cl_2) δ 184.54 (CO), 184.42 (CO), 153.71 (COH), 153.39 (CH_α), 153.32 (CH_α), 152.87 (CH_α), 129.29 (C_{bz}H), 128.33 (C_{bz}H), 124.50 (C_{bz}), 122.37 (CH_β), 121.57 (CH_β), 120.24 (CH_β), 118.12 (C_{bz}), 117.43 (C_{bz}), 104.47 (CH_q), 104.42 ($C_{p\text{-cym}}$), 102.41 ($C_{p\text{-cym}}$), 99.25 ($C_{p\text{-cym}}$), 84.02 (C≡C), 83.78 (C≡C), 82.26 ($CH_{p\text{-cym}}$), 82.17 ($CH_{p\text{-cym}}$), 31.69 (*C*H$(CH_3)_2$), 31.66 (*C*H$(CH_3)_2$), 31.62 (*C*H$(CH_3)_2$), 22.45 (CH(*C*H$_3)_2$), 22.38 (CH(*C*H$_3)_2$), 22.34 (CH(*C*H$_3)_2$), 18.29 (CH_3), 18.21 (CH_3), 18.14 (CH_3). UV/Vis (DCM): λ_{max} (ε [$M^{-1}cm^{-1}$]) = 322 (230000), 498 (73000). HRMS (ESI) m/z: [**Pr1** - $4CF_3SO_3$]$^{4+}$ Calcd for $C_{134}H_{120}F_6N_6O_{20}Ru_6S_2$ 730.5535; Found 730.5561.

Pr2: Red solid, 113 mg, 28 µmol, 80% yield. ^{1}H NMR (600 MHz, CD_2Cl_2) δ 8.25 (m, 12H, H_α), 7.75 (m, 4H, H_{bz}), 7.47 (m, 12H, H_β), 5.86 (m, 12H, $H_{p\text{-cym}}$), 5.79 (m, 6H, H_q), 5.73 (m, 12H, $H_{p\text{-cym}}$), 4.36 (td, *J* = 6.3, 4.1 Hz, 4H, OC*H*$_2$CH$_2$), 2.84 (sept, *J* = 6.9 Hz, 6H, (C*H*$(CH_3)_2$), 2.18 (s, 12H, CH_3), 2.17 (s, 6H, CH_3), 1.82 (sept, *J* = 6.2 Hz, 4H, OCH$_2$C*H*$_2$), 1.50 (m, 4H, OCH$_2$CH$_2$C*H*$_2$), 1.33 (m, 40H, (CH(C*H*$_3)_2$ and CH$_2$C*H*$_2$CH$_2$), 1.25 (s, 60H, CH$_2$C*H*$_2$CH$_2$), 0.85 (td, *J* = 7.0, 2.6 Hz, 6H, CH$_2$CH$_2$C*H*$_3$). ^{13}C NMR (151 MHz, CD_2Cl_2) δ 184.54 (CO), 163.83 (C_{bz}O), 153.00 (CH_α), 152.91 (CH_α), 140.72 (C_{bz}H), 134.67 (C_{bz}), 134.54 (C_{bz}), 128.31 (CH_β), 128.16 (CH_β), 124.54 (C_{bz}), 122.41 (CH_β), 120.28 (CH_β), 118.15 (C_{bz}), 116.87 (C_{bz}), 116.25 (C_{bz}), 116.19 (C_{bz}), 116.10 (C_{bz}), 104.46 (CH_q), 102.43 (CH_q), 99.22 ($C_{p\text{-cym}}$), 96.31 ($C_{p\text{-cym}}$), 93.83 (C≡C), 90.54 (C≡C), 86.42 , 83.76 ($CH_{p\text{-cym}}$), 82.59 ($CH_{p\text{-cym}}$), 82.51 ($CH_{p\text{-cym}}$), 82.31 ($CH_{p\text{-cym}}$), 76.03 (O*C*H$_2$CH$_2$), 75.89 (O*C*H$_2$CH$_2$), 32.29 (OCH$_2$*C*H$_2$), 31.68 (*C*H$(CH_3)_2$), 30.74 (CH$_2$*C*H$_2$CH$_2$), 30.21 (CH$_2$*C*H$_2$CH$_2$), 30.18 (CH$_2$*C*H$_2$CH$_2$), 30.16 (CH$_2$*C*H$_2$CH$_2$), 30.13 (CH$_2$*C*H$_2$CH$_2$), 30.12 (CH$_2$*C*H$_2$CH$_2$), 30.10 (CH$_2$*C*H$_2$CH$_2$), 30.04 (CH$_2$*C*H$_2$CH$_2$), 30.02 (CH$_2$*C*H$_2$CH$_2$), 29.74 (CH$_2$*C*H$_2$CH$_2$), 26.44 (CH$_2$*C*H$_2$CH$_2$), 23.05 (CH$_2$*C*H$_2$CH$_3$), 22.38 (CH$_2$*C*H$_2$CH$_3$), 18.29 (CH(*C*H$_3)_2$), 14.26 (CH_3). UV/Vis (DCM): λ_{max} (ε [$M^{-1}cm^{-1}$]) = 321 (190000), 497 (53000). HRMS (ESI) m/z: [**Pr2** - $4CF_3SO_3$]$^{4+}$ Calcd for $C_{174}H_{200}F_6N_6O_{20}Ru_6S_2$ 870.7100; Found 870.7144.

Pr3: Dark solid, 85 mg, 22 µmol 64% yield. ^{1}H NMR (600 MHz, Acetone) δ 8.67 – 8.55 (m, 12H, H_α), 7.80 – 7.74 (m, 4H, H_{bz}), 7.63 – 7.51 (m, 12H, H_β), 7.33 – 7.29 (m, 12H, H_q), 6.03 – 5.97 (m, 12H, $H_{p\text{-}cym}$), 5.85 – 5.78 (m, 12H, $H_{p\text{-}cym}$), 5.09 (s, 4H, CH_2CO), 2.93 (hept, *J* = 7.0 Hz, 6H, (C*H*$(CH_3)_2$), 2.19 (s, 18H, CH_3), 1.39 – 1.34 (m, 36H, CH(C*H*$_3)_2$), 1.24 (s, 18H, $CH_{3t\text{-}but}$). UV/Vis (DCM): λ_{max} (ε [$M^{-1}cm^{-1}$]) = 225 (207000), 326 (258000), 642 (10000), 697 (12000).

Pr4: Dark green solid, 17 mg, 5 µmol 66% yield. ^{1}H NMR (600 MHz, Acetone) δ 8.41 – 8.34 (m, 12H, H_α), 7.81 – 7.72 (m, 4H, H_{bz}), 7.64 – 7.53 (m, 12H, H_β), 6.16 – 6.12 (m, 12H, $H_{p\text{-}cym}$), 5.95 – 5.92 (m, 12H, $H_{p\text{-}cym}$), 5.77 (s, 6H, H_q), 4.46 (s, 4H, CH_{2PEG}), 3.86 – 3.81 (m, 4H, CH_{2PEG}), 3.57 – 3.54 (m, 4H, CH_{2PEG}), 3.46 – 3.40 (m, 4H, CH_{2PEG}), 3.38 – 3.31 (m, 4H, CH_{2PEG}), 3.25 – 3.17 (m, 4H, CH_{2PEG}), 2.99 – 2.96 (m, 6H, (C*H*$(CH_3)_2$), 2.21 – 2.19 (m, 18H, $CH_{3p\text{-}cym}$), 1.35 – 1.31 (m, 42H, CH(C*H*$_3)_2$ and CH_{3PEG}).

Pr5: Dark green solid, 102 mg, 23 µmol, 74% yield. ^{1}H NMR (600 MHz, CD_3CN) δ 8.39 – 8.16 (m, 12H, H_α), 8.12 – 7.96 (m, 4H, H_{anth}), 7.85 – 7.78 (m, 4H, H_{bz}), 7.50 (d, *J* = 8.2 Hz, 4H, H_{anth}), 7.39 – 7.13 (m, 24H, H_β and H_{naph}), 7.12 – 6.93 (m, 10H, H_{anth}), 5.72 – 5.58 (m, 12H, $H_{p\text{-}cym}$), 5.53 – 5.39 (m, 12H, $H_{p\text{-}cym}$), 4.37 – 4.20 (m, 4H, CH_{2PEG}), 3.63 (d, *J* = 8.3 Hz, 4H, CH_{2PEG}), 3.47 – 3.24 (m, 8H, CH_{2PEG}), 3.21 – 2.93 (m, 8H, CH_{2PEG}), 2.80 (hept, *J* = 7.4 Hz, 6H, (C*H*$(CH_3)_2$), 2.65 – 2.53 (m, 4H, CH_2), 2.44 (t, *J* = 8.4 Hz, 4H, CH_2), 2.13 – 2.04 (m, 18H, $CH_{3p\text{-}cym}$), 1.35 – 1.26 (m, 36H, CH(C*H*$_3)_2$).

Pyr4⊂Pr6: A mixture of $AgCF_3SO_3$ (38 mg, 149 µmol 6 eq.) and [Ru_2(p-cymene)$_2$(donq)Cl_2] (55 mg, 75 µmol 3 eq.) in 25 ml of MeOH was stirred at RT for 4 h. Then, the solution was filtered into another MeOH solution containing panel **L3** (25 mg, 50 µmol, 2 eq.) and **Pyr4** (20 mg, 25 µmol 1 eq.). The solution was heated to 60 °C and kept stirring overnight. After evaporation of solvent, the solid was redissolved in minimum amount of DCM (1-2 ml) and diethyl ether was added dropwise to induce precipitation. The precipitate formed is filtered off and washed with diethyl ether and pentane. (Dark solid, 90 mg, 19 µmol, 77% yield).

^{1}H NMR (600 MHz, CD_3CN) δ 8.49 – 8.25 (m, 12H, H_α), 8.19 (s, 1H, H_{pyr}), 7.53 (s, 1H, H_{pyr}), 7.31 – 7.17 (m, 24H, H_β and H_{naph}), 6.75 (s, 1H, H_{pyr}), 6.38 (s, 1H, H_{pyr}), 5.71 – 5.65 (m, 12H, $H_{p\text{-}cym}$), 5.50 – 5.46 (m, 12H, $H_{p\text{-}cym}$), 4.78 – 4.69 (m, 4H, CH_2), 3.68 (s, 4H, CH_{2PEG}), 3.63 (s, 4H, CH_{2PEG}), 3.58 (t, *J* = 5.9 Hz, 4H, CH_{2PEG}), 3.37 – 3.27 (m, 6H, CH_{2PEG}), 2.87 – 2.75 (m, 6H, (C*H*$(CH_3)_2$), 2.10 – 2.05 (m, 18H, $CH_{3p\text{-}cym}$), 1.39 (s, 18H, $CH_{3t\text{-}butpyr}$), 1.32 – 1.28 (m, 36H, CH(C*H*$_3)_2$), 1.28 – 1.25 (m, 18H, $CH_{3t\text{-}butpanel}$). UV/Vis (DCM): λ_{max} (ε [$M^{-1}cm^{-1}$]) = 229 (259000), 306 (242000), 326 (275000), 390 (131000), 418 (106000), 640 (10000), 696 (12000).

PPyr$_4$: Under inert conditions, pyrenebutyric acid (451 mg, 1.56 mmol, 6 eq.) and EDCl (450 mg, 3.35 mmol, 9 eq.) were dissolved in 15 mL of anhydrous DMF. After stirring for 30 min at room temperature, a solution of Porphyrin-PEG_4 (342 mg, 0.26 mmol, 1 eq.) and DMAP (318 mg, 2.61 mmol, 10 eq.) in 10 mL of anhydrous DMF was added. The reaction mixture was stirred for 24 h in the dark. Then, solvent was evaporated under vacuum and the resulting residue was partitioned between DCM and a 1 M HCl solution, followed by several water washes. The organic phase was dried over $MgSO_4$, filtered, and evaporated to dryness. The product was further purified by flash chromatography on a silica column, using a DCM:MeOH gradient up to 9:1. (Purple solid, 255 mg, 107 µmol, 41%).

^{1}H NMR (600 MHz, $CDCl_3$) δ 8.71 (s, 8H, $H_{\beta pyrrole}$), 8.16 (d, *J* = 8.3 Hz, 8H, H_{ph}), 8.10 (m, 10H, H_{ph} and H_{pyr}), 8.09 (s, 2H, H_{pyr}), 7.95 (dd, *J* = 7.6, 1.1 Hz, 4H, H_{pyr}), 7.87 (dd, *J* = 7.7, 1.2 Hz, 4H, H_{pyr}), 7.84 (d, *J* = 7.8 Hz, 4H, H_{pyr}), 7.82 (s, 2H, H_{pyr}), 7.78 (m, 14H, H_{pyr}), 7.65 (d, *J* = 7.7 Hz, 4H, H_{pyr}), 6.99 (t, *J* = 5.3 Hz, 4H, $NHCO_{porph}$), 6.02 (t, *J* = 5.5 Hz, 4H, NHCO), 3.74 (dt, *J* = 21.6, 5.1 Hz, 16H, H_{PEG}), 3.65 (m, 16H, H_{PEG}), 3.57 (t, *J* = 5.2 Hz, 8H, H_{PEG}), 3.48 (m, 8H, H_{PEG}), 3.23 (t, *J* = 7.7 Hz, 8H, H_{butyl}), 2.25 (t, *J* = 7.3 Hz, 8H, H_{butyl}), 2.11 (p, *J* = 7.5 Hz, 8H, H_{butyl}). ^{13}C NMR (151 MHz, $CDCl_3$) δ 172.91 (*C*OCH_2), 167.67 (*C*OC_{ph}), 145.18

($C_{ph}C_{porph}$), 135.73 (C_{porph}), 134.63 (C_{porph}), 133.98 ($C_{ph}CO$), 131.15 (C_{pyr}), 130.63 (C_{pyr}), 129.70 (C_{pyr}), 128.56 (C_{pyr}), 127.28 (CH_{ph}), 127.18 (CH_{ph}), 126.52 (CH_{pyr}), 125.68 (CH_{pyr}), 125.56 (CH_{pyr}), 124.83 (CH_{pyr}), 124.75 (CH_{pyr}), 124.70 (CH_{pyr}), 124.63 (CH_{pyr}), 124.58 (CH_{pyr}), 123.18 ($CH_{\beta pyrrole}$), 119.25 ($CH_{\beta pyrrole}$), 70.33 (CH_{2PEG}), 70.31 (CH_{2PEG}), 69.96 (CH_{2PEG}), 69.92 (CH_{2PEG}), 53.55 (DCM), 40.03 (CH_2NH), 39.26 (CH_2NH), 35.99 (CH_2CO), 32.68 (CH_2C_{pyr}), 27.39 ($CH_2CH_2CH_2$). UV/Vis (DCM): λ_{max} (ε [$M^{-1}cm^{-1}$]) = 236 (213000), 244 (288000), 267 (121000), 278 (197000), 315 (64000), 329 (126000), 345 (178000), 421 (427000), 517 (20000), 553 (9000), 592 (6000), 646 (4000). HRMS-ESI m/z: [**$PPyr_4$** + H + Na]$^{+2}$ Calcd for $C_{152}H_{143}N_{12}NaO_{16}$ 1207.5316; Found 1207.5330.

$PPyr_4$⊂$Prism_4$: A mixture of $Ag(CF_3SO_3)$ (71 mg, 275 µmol, 24 eq.) and $[Ru_2(p\text{-cymene})_2(donq)Cl_2]$ (100 mg, 137 µmol, 12 eq.) in 25 ml of MeOH was stirred at RT for 4 h. Then, the solution was filtered and 4-tpt (29 mg, 92 µmol, 8 eq.) and $PPyr_4$ (28 mg, 12 µmol, 1 eq.) were added. The resulting solution was heated to 60 °C and kept stirring overnight. After evaporation of the solvent, the resulting solid was redissolved in minimum amount of DCM (1 to 2 mL) and diethylether (20 mL) was added dropwise to induce precipitation. The product was recovered by filtration, rinsed with diethylether and dried under vacuum to give a dark solid. (Dark solid, 119 mg, 7.27 µmol, 64%).

6.2.2 Design and synthesis of multifunctional metalla-assemblies

Pyrene-TPP: A solution of EDCl (34 mg, 179 µmol), HOBt (24 mg, 179 µmol) and 5-(4-carboxyphenyl)-10,15,20-(triphenyl)porphyrin (79 mg, 119 µmol) in 15 ml of anhydrous DCM prepared under inert conditions was shielded from light and cooled to 0 °C. After stirring for 30 min, **PyrenePEGNH$_2$** (50 mg, 119 µmol) and DMAP (15 mg, 119 µmol) were added. The reaction mixture was stirred at 0 °C for 2 h and at room temperature for 48 h. The crude product was then partitioned between DCM and an aqueous 1 M HCl solution, followed by two water washes. The organic phase was then dried over Na_2SO_4, filtered and evaporated to dryness. The resulting solid was further purified by flash chromatography using a DCM:MeOH gradient up to 95:5. (Shiny purple solid, 115 mg, 91% yield)

^{1}H NMR (600 MHz, $CDCl_3$) δ 8.87 – 8.82 (m, 6H, $H_{\beta pyrrole}$), 8.74 (d, *J* = 4.6 Hz, 2H, $H_{\beta pyrrole}$), 8.26 – 8.15 (m, 9H, H_{pyr} + H_{ph}), 8.12 (d, *J* = 8.1 Hz, 2H, H_{ph}), 8.05 – 7.98 (m, 1H, H_{pyr}), 7.96 (d, *J* = 7.4 Hz, 1H, H_{ph}), 7.92 (t, *J* = 8.2 Hz, 2H, H_{ph}), 7.86 (d, *J* = 1.3 Hz, 2H, H_{ph}), 7.82 (t, *J* = 7.5 Hz, 1H), 7.80 – 7.71 (m, 10H, H_{ph}), 6.90 (t, *J* = 5.3 Hz, 1H, $NHCO_{porph}$), 5.94 (d, *J* = 5.3 Hz, 1H, NHCO), 3.79 – 3.71 (m, 4H, H_{PEG}), 3.71 – 3.64 (m, 4H, H_{PEG}), 3.61 (t, *J* = 5.2 Hz, 2H, H_{PEG}), 3.51 (q, *J* = 5.3 Hz, 2H, H_{PEG}), 3.31 (d, *J* = 7.8 Hz, 2H, H_{butyl}), 2.29 (t, *J* = 7.2 Hz, 2H, H_{butyl}), 2.17 (p, *J* = 7.3 Hz, 2H, H_{butyl}), -2.81 (s, 2H). ^{13}C NMR (151 MHz, $CDCl_3$) δ 172.91 (CO_{but}), 167.77 (CO_{ph}), 145.75 (C_{ph}), 142.16 (C_{ph}), 135.85 (C_{ph}), 134.79 ($CH_{pyrrole}$), 134.70 ($CH_{pyrrole}$), 134.67 ($CH_{pyrrole}$), 133.8 (C_{pyr}), 131.35 (C_{pyr}), 130.82 (C_{pyr}), 129.90 (C_{pyr}), 128.75 (C_{pyr}), 127.91 (CH_{ph}), 127.44 (CH_{ph}), 127.36 (CH_{ph}), 126.85 (CH_{ph}), 126.70 (CH_{pyr}), 125.83 (CH_{pyr}), 125.50 (CH_{pyr}), 125.04 (CH_{pyr}), 124.90 (CH_{pyr}), 124.77 (CH_{pyr}), 124.74 (CH_{pyr}), 123.36 (C_{porph}), 120.66 (C_{porph}), 120.48 (CH_{pyr}), 118.62 (C_{porph}), 70.43 (CH_{2PEG}), 70.38 (CH_{2PEG}), 70.09 (CH_{2PEG}), 70.04 (CH_{2PEG}), 40.05 (CH_2NH), 39.34 (CH_2NH), 36.11 (CH_{2butyl}), 32.79 (CH_{2butyl}), 27.47 (CH_{2butyl}). UV/Vis (DCM): λ_{max} (ε [$M^{-1}cm^{-1}$]) = 235 (72000), 244 (100000), 266 (49000), 277 (78000), 313 (29000), 328 (47000), 344 (69000), 418 (498000), 514 (22000), 549 (9000), 590 (6000), 645 (5000). HRMS (ESI) m/z: [**Pyrene-TPP** + H]$^+$ Calcd. for $C_{71}H_{59}N_6O_4$ 1059.4592; Found 1059.4594.

Pyrene-PheoA: A solution of EDCl (25 mg, 127 µmol), HOBt (17 mg, 127 µmol) and pheophorbide-a (50 mg, 84 µmol) in 15 ml of anhydrous DCM prepared under inert conditions was shielded from light and cooled to 0 °C. After stirring for 30 min, **PyrenePEGNH$_2$** (35 mg, 84 µmol) and DMAP (10 mg, 84 µmol) were added. The reaction mixture was stirred at 0 °C for 2 h and at room temperature for 48 h. The crude product was then partitioned between DCM and an aqueous 1 M HCl solution and washed twice with water. The organic phase was then dried over Na_2SO_4, filtered and evaporated to dryness. The resulting solid was further purified by flash chromatography using a DCM:MeOH gradient up to 90:10. (Dark solid, 60 mg, 72% yield)

^{1}H NMR (600 MHz, $CDCl_3$) δ 9.43 (d, *J* = 16.9 Hz, 1H, H_{pheo}), 9.24 (d, *J* = 74.0 Hz, 1H), 8.48 (d, *J* = 39.6 Hz, 1H, H_{pheo}), 8.04 – 7.90 (m, 4H, H_{pyr}), 7.88 – 7.78 (m, 5H, H_{pyr}), 7.54 (d, *J* = 7.7 Hz, 1H, H_{pheo}), 6.27 (d, *J* = 1.2 Hz, 1H, H_{pheo}), 6.24 (s, 1H, H_{pheo}), 6.16 (dd, *J* = 11.5, 1.2 Hz, 1H, H_{pheo}), 5.77 (s, 1H, NHCO), 5.70 (s, 1H, NHCO), 4.52 – 4.42 (m, 1H, H_{pheo}), 4.19 – 4.14 (m, 1H, H_{pheo}), 3.82 (s, 3H, H_{pheo}), 3.70 – 3.63 (m, 2H, H_{pheo}), 3.62 (s, 3H, H_{pheo}), 3.36 (s, 3H, H_{pheo}), 3.35 – 3.23 (m, 8H, H_{PEG}), 3.21 (s, 3H, H_{pheo}), 3.18 – 3.15 (m, 4H, H_{PEG}), 2.99 (t, *J* = 8.1 Hz, 2H, H_{butyl}), 2.83 – 2.56 (m, 2H, H_{pheo}), 2.48 – 2.20 (m, 2H, H_{pheo}), 2.03 – 1.98 (m, 2H, H_{butyl}), 1.91 (p, *J* = 7.1 Hz, 2H, H_{butyl}), 1.77 (d, *J* = 7.5 Hz, 3H, H_{pheo}), 1.69 (t, *J* = 7.8 Hz, 3H, H_{pheo}), -1.67 (s, 1H, NH_{pheo}). ^{13}C NMR (151 MHz, $CDCl_3$) δ 188.62 (CO_{pheo}), 171.71 (CONH), 171.56 (C_{pheo}), 171.29 (CONH), 168.72 (CO_{pheo}), 136.76 (C_{pheo}), 134.56 (C_{pheo}), 130.08 (C_{pyr}), 129.54 (C_{pyr}), 128.52 (C_{pyr}), 127.84 (C_{pheo}), 127.30 (C_{pheo}), 126.17 (C_{pheo}), 125.93 (C_{pheo}), 125.86 (CH_{pheo}), 125.36 (CH_{pyr}), 124.54 (CH_{pyr}), 123.67 (CH_{pyr}), 123.63 (CH_{pyr}), 123.59 (CH_{pyr}), 123.45 (CH_{pyr}), 123.42 (CH_{pyr}), 122.01 (CH_{pheo}), 103.22 (CH_{pheo}), 96.37 (CH_{pheo}), 92.16 (C_{pheo}), 68.88 (CH_{2PEG}), 68.86 (CH_{2PEG}), 68.58 (CH_{2PEG}), 68.42 (CH_{2PEG}), 63.79 (CH_{pheo}), 52.26, 51.88 (CH_3O_{pheo}), 50.38 (C_{pheo}), 49.90 (C_{pheo}), 49.13 (CH_{pheo}), 37.91 (CH_2NH), 37.83 (CH_2NH), 34.65 (CH_{2pheo}), 31.37 (CH_{2butyl}), 26.06 (CH_{2pheo}), 22.07 (CH_{2pheo}), 18.35 (CH_{3pheo}), 16.31

(CH_{3pheo}), 11.03 (CH_{3pheo}), 10.13 (CH_{3pheo}). UV/Vis (DCM): λ_{max} (ε [$M^{-1}cm^{-1}$]) = 235 (70000), 244 (90000), 266 (45000), 277 (69000), 328 (55000), 344 (69000), 414 (114000), 508 (12000), 538 (11000), 611 (10000), 667 (51000). HRMS (ESI) m/z: [**Pyrene-PheoA** + H]$^+$ Calcd. for $C_{61}H_{65}N_6O_7$ 993.4909; Found 993.4925.

Pyrene-BODIPY: A solution of EDCl (47 mg, 244 µmol), HOBt (33 mg, 244 µmol) and **BODIPY** (60 mg, 163 µmol) in 15 ml of anhydrous DCM prepared under inert conditions was shielded from light and cooled to 0 °C. After stirring for 30 min, **PyrenePEGNH$_2$** (68 mg, 163 µmol) and DMAP (10 mg, 84 µmol) were added. The reaction mixture was stirred at 0 °C for 2 h and at room temperature for 48 h. The crude product was then partitioned between DCM and an aqueous 1 M HCl solution and washed twice with water. The organic phase was then dried over Na_2SO_4, filtered and evaporated to dryness. The resulting semi-solid was further purified by flash chromatography using a DCM:MeOH gradient up to 90:10. (Orange solid, 112 mg, 89% yield)

^{1}H NMR (600 MHz, $CDCl_3$) δ 8.30 (d, *J* = 9.2 Hz, 1H, H_{pyr}), 8.19 – 8.12 (m, 2H, H_{ph}), 8.11 – 8.08 (m, 2H, H_{pyr}), 8.01 (s, 2H, H_{pyr}), 7.98 (t, *J* = 7.6 Hz, 1H, H_{pyr}), 7.86 (dd, *J* = 7.9, 5.9 Hz, 3H, H_{pyr}), 7.31 (d, *J* = 8.2 Hz, 2H, H_{ph}), 6.69 (s, 1H, $NHCO_{bpy}$), 5.95 (s, 2H), 5.87 (s, 1H, NHCO), 3.61 (d, *J* = 5.9 Hz, 8H, H_{PEG}), 3.55 (t, *J* = 5.2 Hz, 2H, H_{PEG}), 3.45 (q, *J* = 5.3 Hz, 2H, H_{PEG}), 3.39 (t, *J* = 7.5 Hz, 2H, H_{butyl}), 2.55 (s, 6H, CH_{3bpy}), 2.29 (t, *J* = 7.1 Hz, 2H, H_{butyl}), 2.21 (p, *J* = 7.1 Hz, 2H, H_{butyl}), 1.30 (s, 6H, CH_{3bpy}). ^{13}C NMR (151 MHz, $CDCl_3$) δ 172.89 (CO_{but}), 166.70 (CO_{ph}), 156.06 (CN_{bodipy}), 142.97 (CN_{bodipy}), 140.35 (CN_{bodipy}), 138.50 (C_{ph}), 135.92 (C_{ph}), 134.97 (C_{pyr}), 131.52 (C_{pyr}), 130.99 (C_{bodipy}), 130.08 (C_{bodipy}), 128.90 (C_{pyr}), 128.56 (CH_{ph}), 127.94 (CH_{ph}), 127.59 , 127.54, 127.50 (CH_{pyr}), 126.89 (CH_{pyr}), 126.04 (CH_{pyr}), 125.20 (CH_{pyr}), 125.11 (CH_{pyr}), 125.07 (C_{pyr}), 124.92 (CH_{pyr}), 123.49 (CH_{pyr}), 121.58 (CH_{pyr}), 70.33 (CH_{2PEG}), 70.04 (CH_{2PEG}), 69.84 (CH_{2PEG}), 39.95 (CH_2NH), 39.28 (CH_2NH), 36.11 (CH_{2butyl}), 32.83 (CH_{2butyl}), 27.47 (CH_{2butyl}), 14.76 ($CH_{3bodipy}$), 14.70 14.76 ($CH_{3bodipy}$). UV/Vis (DCM): λ_{max} (ε [$M^{-1}cm^{-1}$]) = 235 (209000), 244 (255000), 266 (98000), 277 (166000), 314 (56000), 328 (100000), 344 (143000), 502 (242000). HRMS (ESI) m/z: [**Pyrene-BODIPY** + H]$^+$ Calcd. for $C_{46}H_{48}BF_2N_4O_4$ 769.3731; Found 769.3741.

2-(2,4,6-triiodophenoxy)-PEGboc: A solution of EDCl (1.09 g, 5.66 mol), HOBt (765 mg, 5.66 mmol) and 2-(2,4,6-triiodophenoxy)acetic acid (2 g, 3.77 mmol) in 20 ml of anhydrous DMF prepared under inert conditions was shielded from light and cooled to 0 °C. After stirring for 30 min, N-Boc-2,2'-(ethylenedioxy)diethylamine (1.17 g, 4.72 mmol) and DMAP (461 mg, 3.77 mmol) dissolved in 5 ml of anhydrous DMF were added. The reaction mixture was stirred at 0 °C for 2 h and at room temperature for 48 h. The solvent was then removed under vacuum and the resulting residue was partitioned between DCM and an aqueous 1 M HCl solution and washed twice with water. The organic phase was then dried over Na_2SO_4, filtered and evaporated to dryness. The resulting solid was further purified by flash chromatography using a DCM:MeOH gradient up to 90:10. (White solid, 1.97 g, 69% yield).

^{1}H NMR (600 MHz, $CDCl_3$) δ 8.06 (s, 2H, H_{ph}), 7.23 (s, 1H, NHCO), 4.97 (s, 1H, NHCO), 4.46 (s, 2H, H_{CH2}), 3.67 – 3.60 (m, 8H, H_{PEG}), 3.54 (t, *J* = 5.2 Hz, 2H, H_{PEG}), 3.34 – 3.28 (m, 2H, H_{PEG}), 1.43 (s, 9H, H_{tbut}). ^{13}C NMR (151 MHz, $CDCl_3$) δ 167.05 (CO), 156.52 ($C_{ph}O$), 155.94 (CO_{tbut}), 147.54 (CH_{ph}), 91.36 (C_I), 90.53 (C_I), 79.32 (C_{tbut}), 70.75 (CH_{2PEG}), 70.39 (CH_{2PEG}), 70.33 (CH_{2PEG}), 70.27 (CH_{2PEG}), 69.81 (CH_2CO), 40.31 (CH_2NH), 38.97 (CH_2NH), 28.46 (CH_{3tbut}). UV/Vis (DCM): λ_{max} (ε [$M^{-1}cm^{-1}$]) = 234 (49000). HRMS (ESI) m/z: [**2-(2,4,6-triiodophenoxy)-PEGboc** + Na]$^+$ Calcd. for $C_{19}H_{27}I_3N_2NaO_6$ 782.8895; Found 782.8875.

Panel-PEGboc: A solution of **2-(2,4,6-triiodophenoxy)-PEGboc** (1.8 g, 2.37 mmol), $Pd(PPh_3)_4$ (237 mg, 236 µmol) and CuI (23 mg, 118 µmol) in a mixture of previously degassed triethylamine and anhydrous THF (10:15) was prepared under inert conditions. After stirring for 30 min, 4-ethynylpyridine hydrochloride (1.16 g, 8.29 mmol) was added and the resulting mixture was stirred at 75 °C for 48 h. The solvent was then removed under vacuum and the product was purified by flash chromatography

using an EtOAc:MeOH gradient up to 80:20. The resulting solid was washed with water. (Brown solid, 700 mg, 43% yield).

^{1}H NMR (600 MHz, $CDCl_3$) δ 8.70 – 8.61 (m, 6H, H_α), 7.76 (s, 2H, H_{ph}), 7.41 – 7.36 (m, 6H, H_β), 4.96 (s, 1H, NHCO), 4.89 (s, 2H, H_{CH2}), 3.54 – 3.46 (m, 8H, H_{PEG}), 3.44 (t, *J* = 5.2 Hz, 2H, H_{PEG}), 3.27 – 3.21 (m, 2H, H_{PEG}), 1.41 (s, 9H, H_{tbut}). ^{13}C NMR (151 MHz, $CDCl_3$) δ 167.98 (CO), 159.74 ($C_{ph}O$), 156.01 (CO_{tbut}), 150.27 ($CH_{\alpha pyridine}$), 150.18 ($CH_{\alpha pyridine}$), 150.17 ($CH_{\alpha pyridine}$), 150.07 ($CH_{\alpha pyridine}$), 137.91 (CH_{ph}), 136.82 (CH_{ph}), 130.70 ($C_{pyridine}$), 130.25 ($C_{pyridine}$), 129.68 ($C_{pyridine}$), 125.59 ($CH_{\beta pyridine}$), 125.55 ($CH_{\beta pyridine}$), 119.24 (C_{ph}), 116.88 (C_{ph}), 92.95 (C_{alkyne}), 90.88 (C_{alkyne}), 88.14 (C_{alkyne}), 87.58 (C_{alkyne}), 79.38 (C_{tbut}), 72.49 (CH_{2PEG}), 70.40 (CH_{2PEG}), 70.33 (CH_{2PEG}), 70.25 (CH_{2PEG}), 69.72 (CH_2CO), 40.43 (CH_2NH), 39.20 (CH_2NH), 28.52 (CH_{3tbut}). UV/Vis (DCM): λ_{max} (ε [$M^{-1}cm^{-1}$]) = 287 (99000), 303 (92000). HRMS (ESI) m/z: [**Panel-PEGboc** + H]$^+$ Calcd. for $C_{40}H_{40}N_5O_6$ 686.2973; Found 686.2951.

Panel-PEGNH$_2$: Panel-PEGboc (450 mg, 657 µmol) was dissolved in anhydrous DCM under inert conditions. Trifluoroacetic acid (1 ml, 15 eq.) was then added dropwise and the resulting solution was stirred for 4 h. The solvent was removed under vacuum and the resulting oil was dissolved in water, basified using an aqueous solution of $NaHCO_3$ and extracted three times with DCM. Combined organic extracts were dried over Na_2SO_4, filtered and evaporated to dryness. (Brown oil, 352 mg, 92% yield).

^{1}H NMR (600 MHz, $CDCl_3$) δ 8.68 – 8.60 (m, 6H, H_α), 7.76 (s, 2H, H_{ph}), 7.43 – 7.31 (m, 6H, H_β), 4.88 (s, 2H, H_{CH2}), 3.52 (s, 2H, H_{PEG}), 3.47 (s, 8H, H_{PEG}), 2.81 – 2.74 (m, 2H, H_{PEG}). ^{13}C NMR (151 MHz, $CDCl_3$) δ 172.91 (CO) , 150.24 ($CH_{\alpha pyridine}$), 150.16 ($CH_{\alpha pyridine}$), 150.13 ($CH_{\alpha pyridine}$), 150.06 ($CH_{\alpha pyridine}$), 137.89 (CH_{ph}), 136.94 (CH_{ph}), 130.23 ($C_{pyridine}$), 129.67 ($C_{pyridine}$), 125.70 ($CH_{\beta pyridine}$), 125.64 ($CH_{\beta pyridine}$), 125.58 ($CH_{\beta pyridine}$), 124.09 ($CH_{\beta pyridine}$), 124.00 ($CH_{\beta pyridine}$), 93.60 (C_{alkyne}), 90.23 (C_{alkyne}), 89.85 (C_{alkyne}), 87.45 (C_{alkyne}), 70.42 (CH_{2PEG}), 70.23 (CH_{2PEG}), 70.06 (CH_{2PEG}), 68.93 (CH_2CO), 61.13 (CH_{2PEG}), 49.01 (CH_2NH_2), 40.78 (CH_2NH). UV/Vis (DCM): λ_{max} (ε [$M^{-1}cm^{-1}$]) = 287 (447000), 305 (390000) HRMS (ESI) m/z: [**Panel-PEGNH$_2$** + H]$^+$ Calcd. for $C_{35}H_{32}N_5O_4$ 586.2449; Found 586.2431.

Panel-PEG-Biotin: A solution of EDCl (98 mg, 512 µmol), HOBt (69 mg, 512 µmol) and biotin (100 mg, 410 µmol) in 15 ml of anhydrous DMF prepared under inert conditions was shielded from light and cooled to 0 °C. After stirring for 30 min, **Panel-PEGNH$_2$** (200 mg, 341 µmol) and DMAP (42 mg, 341 µmol) dissolved in 5 ml of anhydrous DMF were added. The reaction mixture was stirred at 0 °C for 2 h and at room temperature for 48 h. The solvent was then removed under vacuum and the resulting residue was partitioned between DCM and an aqueous $NaHCO_3$ solution and washed twice with water. The organic phase was then dried over Na_2SO_4, filtered and evaporated to dryness. The resulting oil was further purified by flash chromatography using a DCM:MeOH gradient up to 80:20. (Brown solid, 168 mg, 61% yield).

^{1}H NMR (600 MHz, $CDCl_3$) δ 8.69 – 8.62 (m, 6H, H_α), 7.77 (s, 2H, H_{ph}), 7.44 – 7.34 (m, 6H, H_β), 6.37 (t, *J* = 5.3 Hz, 1H, H_{biotin}), 6.20 – 6.17 (m, 1H, H_{biotin}), 5.70 (s, 1H, NHCO), 4.91 (s, 2H, H_{CH2}), 4.81 (s, 1H, H_{biotin}), 4.51 – 4.44 (m, 1H, H_{biotin}), 4.34 – 4.25 (m, 1H, H_{biotin}), 3.56 – 3.42 (m, 10H, H_{PEG}), 3.43 – 3.33 (m, 2H, H_{PEG}), 3.15 – 3.09 (m, 1H, H_{biotin}), 2.94 – 2.86 (m, 1H, H_{biotin}), 2.19 – 2.13 (m, 2H, H_{biotin}), 1.68 – 1.57 (m, 6H, H_{biotin}). ^{13}C NMR (151 MHz, $CDCl_3$) δ 173.43 (CONH), 172.87 (CONH), 168.06 (CO_{biotin}), 159.72 ($C_{ph}O$), 150.16 ($CH_{\alpha pyridine}$), 150.13 ($CH_{\alpha pyridine}$), 150.06 ($CH_{\alpha pyridine}$), 149.96 ($CH_{\alpha pyridine}$), 137.87 (CH_{ph}), 136.86 (CH_{ph}), 130.64 ($C_{pyridine}$), 130.24 ($C_{pyridine}$), 129.66 ($C_{pyridine}$), 125.62 ($CH_{\beta pyridine}$), 125.57 ($CH_{\beta pyridine}$), 125.54 ($CH_{\beta pyridine}$), 123.88 ($CH_{\beta pyridine}$), 119.15 (C_{ph}), 116.72 (C_{ph}), 106.64 (C_{ph}), 93.51 (C_{alkyne}), 92.87 (C_{alkyne}), 90.83 (C_{alkyne}), 90.21 (C_{alkyne}), 89.80 (C_{alkyne}), 88.11 (C_{alkyne}), 87.65 (C_{alkyne}), 72.42 (CH_{2PEG}), 70.36 (CH_{2PEG}), 70.18 (CH_{2PEG}), 70.06 (CH_{2PEG}), 70.01 (CH_{2PEG}), 69.85 (CH_{2PEG}), 69.58 (CH_{2PEG}), 68.72 (CH_2O), 61.83 (CHN_{biotin}), 60.21 (CHN_{biotin}), 55.67 (CHS), 40.59 (CH_2S), 39.48 (CH_2NH), 39.12 (CH_2NH), 35.94 ($CH_{2biotin}$),

28.29 ($CH_{2biotin}$), 28.15 ($CH_{2biotin}$), 25.66 ($CH_{2biotin}$). UV/Vis (DCM): λ_{max} (ε [$M^{-1}cm^{-1}$]) = 288 (20000), 305 (18000). HRMS (ESI) m/z: [**Panel-PEG-biotin** + H]$^+$ Calcd. for $C_{45}H_{46}N_7O_6S$ 812.3225; Found 812.3232.

Standard procedure for the preparation of empty metalla-assemblies A mixture of $AgCF_3SO_3$ (6 eq.; **P**: 72 mg, 280 µmol; **PB**: 38 mg, 148 µmol) and [Ru_2(*p*-cymene)$_2$(donq)Cl_2] (3 eq.; **P**: 100 mg, 140 µmol; **PB**: 54 mg, 74 µmol) in methanol (15 ml) was stirred at room temperature for 4 h and then filtered to remove the AgCl formed. To the filtrate, panel (2 eq.; **P**: 4-tpe, 36 mg, 93 µmol; **PB**: **Panel-PEG-Biotin**, 40 mg, 49 µmol) was added and the resulting solution was stirred at 60 °C overnight. After evaporation of the solvent, the solid was redissolved in minimum amount of acetonitrile and diethyl ether was added slowly to precipitate the product. The solid formed was recovered by filtration and washed with more diethyl ether.

P: Dark green solid, 140 mg, 83% yield.

PB: Dark green solid, 87 mg, 79% yield. UV/Vis (DCM): λ_{max} (ε [$M^{-1}cm^{-1}$]) = 326 (182000), 640 (11000), 694 (12000). HRMS (ESI) m/z: [**PB** – $3CF_3SO_3$]$^{3+}$ Calcd. for $C_{183}H_{186}F_9N_{14}O_{33}Ru_6S_5$ 1349.8670; Found 1349.8693. [**PB** – $4CF_3SO_3$]$^{4+}$ Calcd. for $C_{182}H_{186}F_6N_{14}O_{30}Ru_6S_4$ 975.1621; Found 975.1621.

Standard procedure for the preparation of host-guest metalla-assemblies: A mixture of $AgCF_3SO_3$ (6 eq.) and [Ru_2(*p*-cymene)$_2$(donq)Cl_2] (3 eq.) in methanol (15 ml) was stirred at room temperature for 4h and then filtered to remove the AgCl formed. To the filtrate, panel (2 eq., 4-tpe in **P** assemblies, **Panel-PEG-Biotin** in **PB** assemblies; **Pyrene-TPP⊂P**: 18 mg, 47 µmol; **Pyrene-PheoA⊂P**: 12 mg, 30 µmol; **Pyrene-BODIPY⊂P**: 20 mg, 52 µmol; **Pyrene-TPP⊂PB**: 23 mg, 28 µmol; **Pyrene-PheoA⊂PB**: 25 mg, 30 µmol; **Pyrene-BODIPY⊂PB**: 32 mg, 39 µmol) and the pyrenyl guest molecule (1 eq.; **Pyrene-TPP⊂P**: 25 mg, 24 µmol; **Pyrene-PheoA⊂P**: 15 mg, 15 µmol; **Pyrene-BODIPY⊂P**: 20 mg, 26 µmol; **Pyrene-TPP⊂PB**: 15 mg, 14 µmol; **Pyrene-PheoA⊂PB**: 15 mg, 15 µmol; **Pyrene-BODIPY⊂PB**: 15 mg, 20 µmol) were added and the resulting solution was stirred at 60 °C overnight. After evaporation of the solvent, the solid was redissolved in minimum amount of acetonitrile and diethyl ether was added slowly to precipitate the product. The solid formed was recovered by filtration and washed with more diethyl ether.

Pyrene-TPP⊂P: Dark green solid, 98 mg, 89% yield. UV/Vis (DCM): λ_{max} (ε [$M^{-1}cm^{-1}$]) = 233 (78000), 243 (67000), 267 (42000), 277 (56000), 314 (82000), 327 (90000), 418 (167000), 513 (11000), 548 (5000), 591 (5000), 645 (5000). HRMS (ESI) m/z: [**Pyrene-TPP⊂P** – $3CF_3SO_3$]$^{3+}$ Calcd. for $C_{218}H_{184}F_9N_{12}O_{25}Ru_6S_3$ 1415.8919; Found 1415.9006. [**Pyrene-TPP⊂P** – $4CF_3SO_3$]$^{4+}$ Calcd. for $C_{217}H_{184}F_6N_{12}O_{22}Ru_6S_2$ 1024.6808; Found 1024.6774.

Pyrene-PheoA⊂P: Dark green solid, 52 mg, 74% yield. UV/Vis (DCM): λ_{max} (ε [$M^{-1}cm^{-1}$]) = 233 (45000), 243 (39000), 267 (25000), 277 (33000), 314 (48000), 327 (54000), 413 (31000), 512 (5000), 543 (4000), 612 (4000), 667 (10000). HRMS (ESI) m/z: [**Pyrene-PheoA⊂P** – $3CF_3SO_3$]$^{3+}$ Calcd. for $C_{208}H_{190}F_9N_{12}O_{28}Ru_6S_3$ 1393.9025; Found 1393.9000. [**Pyrene-PheoA⊂P** – $4CF_3SO_3$]$^{4+}$ Calcd. for $C_{207}H_{190}F_6N_{12}O_{25}Ru_6S_2$ 1008.1888; Found 1008.1863.

Pyrene-BODIPY⊂P: Dark green solid, 105 mg, 91% yield. UV/Vis (DCM): λ_{max} (ε [$M^{-1}cm^{-1}$]) = 234 (162000), 243 (139000), 267 (78000), 277 (107000), 314 (156000), 327 (172000), 503 (70000). HRMS (ESI) m/z: [**Pyrene-BODIPY⊂P** – $3CF_3SO_3$]$^{3+}$ Calcd. for $C_{193}H_{173}BF_{11}N_{10}O_{25}Ru_6S_3$ 1319.1966; Found 1319.1986. [**Pyrene-BODIPY⊂P** – $4CF_3SO_3$]$^{4+}$ Calcd. for $C_{192}H_{173}BF_8N_{10}O_{22}Ru_6S_2$ 952.1593; Found 952.1586.

Pyrene-TPP⊂PB: Dark green solid, 65 mg, 81% yield. UV/Vis (DCM): λ_{max} (ε [$M^{-1}cm^{-1}$]) = 233 (155000), 243 (132000), 267 (89000), 277 (116000), 314 (164000), 327 (173000), 419 (302000), 513 (21000), 548 (11000), 590 (9000), 645 (11000). HRMS (ESI) m/z: [**Pyrene-TPP⊂PB** – $3CF_3SO_3]^{3+}$ Calcd. for $C_{254}H_{244}F_9N_{20}O_{37}Ru_6S_5$ 1702.6843; Found 1702.6851. [**Pyrene-TPP⊂PB** – $4CF_3SO_3]^{4+}$ Calcd. for $C_{253}H_{244}F_6N_{20}O_{34}Ru_6S_4$ 1239.7751; Found 1239.7733.

Pyrene-PheoA⊂PB: Dark green solid, 63 mg, 76% yield. UV/Vis (DCM): λ_{max} (ε [$M^{-1}cm^{-1}$]) = 233 (183000), 243 (160000), 267 (102000), 277 (135000), 314 (191000), 327 (210000), 413 (119000), 502 (23000), 537 (16000), 612 (15000), 668 (48000). HRMS (ESI) m/z: [**Pyrene-PheoA⊂PB** – $3CF_3SO_3]^{3+}$ Calcd. for $C_{244}H_{250}F_9N_{20}O_{40}Ru_6S_5$ 1680.6949; Found 1680.6912. [**Pyrene-PheoA⊂PB** – $4CF_3SO_3]^{4+}$ Calcd. for $C_{243}H_{250}F_6N_{20}O_{37}Ru_6S_4$ 1223.2830; Found 1223.2853.

Pyrene-BODIPY⊂PB: Dark green solid, 81 mg, 79% yield. UV/Vis (DCM): λ_{max} (ε [$M^{-1}cm^{-1}$]) = 233 (148000), 243 (137000), 266 (74000), 277 (103000), 316 (133000), 328 (149000), 503 (79000). HRMS (ESI) m/z: [**Pyrene-BODIPY⊂PB** – $3CF_3SO_3]^{3+}$ Calcd. for $C_{229}H_{233}BF_{11}N_{18}O_{37}Ru_6S_5$ 1605.9890; Found 1605.9894. [**Pyrene-BODIPY⊂PB** – $4CF_3SO_3]^{4+}$ Calcd. for $C_{228}H_{233}BF_8N_{18}O_{34}Ru_6S_4$ 1167.0068; Found 1167.0060.

6.2.3 Synthesis of metalla-assemblies with functionalized metalla-clips

Procedure for the synthesis of substituted oxalamides: To a stirred solution of the appropriate amino derivative (2 eq.; **Ox1**: (*R*)-3-amino-1,2-propanediol, 500 mg, 5.49 mmol; **Ox2**: (*S*)-3-amino-1,2-propanediol, 500 mg, 5.49 mmol; **Ox3**: D-glucamine, 1 g, 5.52 mmol; **Ox4**: 2-[2-(2-aminoethoxy)ethoxy]ethanol, 1 g, 6.70 mmol; **Ox5**: N-Boc-2,2'-(ethylenedioxy)diethylamine, 750 mg, 3.02 mmol) in toluene, diethyl oxalate (1 eq.) was added dropwise. The resulting solution was stirred overnight or for 48 h, until a white precipitate was formed. Then, it was filtered and washed with diethyl ether and pentane.

Ox1: White solid, 544 mg, 2.30 mmol, 84% yield. ^{1}H NMR (600 MHz, DMSO) δ 8.45 (t, *J* = 6.1 Hz, 2H, COONH), 4.87 (d, *J* = 5.0 Hz, 2H, OH), 4.61 (t, *J* = 5.7 Hz, 2H, OH), 3.56 (h, *J* = 5.5 Hz, 2H, CH), 3.33 – 3.24 (m, 6H, CH_2), 3.12 – 3.04 (m, 2H, CH_2). ^{13}C NMR (151 MHz, DMSO) δ 159.93 (CO), 69.71 (COH), 63.89 (COH), 42.63 (CH_2). HRMS (ESI) m/z: [**Ox1** + H]$^+$ Calcd. for $C_8H_{17}N_2O_6$ 237.1081; Found 237.1081.

Ox2: White solid, 550 mg, 2.33 mmol, 85% yield. ^{1}H NMR (600 MHz, DMSO) δ 8.45 (t, *J* = 6.1 Hz, 2H, COONH), 4.87 (d, *J* = 5.1 Hz, 2H, OH), 4.61 (t, *J* = 5.8 Hz, 2H, OH), 3.56 (h, *J* = 5.1 Hz, 2H, CH), 3.34 – 3.24 (m, 6H, CH_2), 3.12 – 3.05 (m, 2H, CH_2). ^{13}C NMR (151 MHz, DMSO) δ 160.07 (CO), 69.85 (COH), 64.03 (COH), 42.77 (CH_2). HRMS (ESI) m/z: [**Ox2** + H]$^+$ Calcd. for $C_8H_{17}N_2O_6$ 237.1081; Found 237.1081.

Ox3: White solid, 1.03 g, 2.48 mmol, 90% yield. ^{1}H NMR (600 MHz, D_2O) δ 3.98 – 3.90 (m, 2H, CHOH), 3.84 – 3.72 (m, 6H, CH_2OH and CHOH), 3.71 – 3.67 (m, 2H, CHOH), 3.67 – 3.61 (m, 2H, CHOH), 3.55 – 3.49 (m, 2H, CH_2NH), 3.45 – 3.38 (m, 2H, CH_2NH). ^{13}C NMR (151 MHz, D_2O) δ 161.07 (CO), 71.25 (CHOH), 70.95 (CHOH), 70.75 (CHOH), 70.20 (CHOH), 62.67 (CH_2OH), 42.10 (CH_2NH). HRMS (ESI) m/z: [**Ox3** + H]$^+$ Calcd. for $C_{14}H_{29}N_2O_{12}$ 417.1715; Found 417.1716.

Ox5: White solid, 991 mg, 2.81 mmol, 84% yield. ^{1}H NMR (600 MHz, D_2O) δ 3.75 – 3.67 (m, 16H, CH_2), 3.64 – 3.60 (m, 4H, CH_2OH), 3.50 (t, *J* = 5.4 Hz, 4H, CH_2NH). ^{13}C NMR (151 MHz, D_2O) δ 160.96 (CO), 71.68 (CH_2), 69.49 (CH_2), 69.42 (CH_2), 68.46 (CH_2), 60.33 (CH_2OH), 39.02 (CHNH). HRMS (ESI) m/z: [**Ox5** + H]$^+$ Calcd. for $C_{14}H_{29}N_2O_8$ 353.1918; Found 353.1919.

Ox6: Flash column chromatography, DCM:MeOH gradient. Waxy white solid, 651 mg, 1.18 mmol, 78% yield. ^{1}H NMR (600 MHz, $CDCl_3$) δ 7.83 (s, 1H, NH), 7.55 (s, 1H, NH), 5.06 (s, 2H, NH), 3.61 – 3.54 (m, 12H, CH_2), 3.53 – 3.46 (m, 8H, CH_2 and CH_2NH), 3.28 (q, *J* = 5.5 Hz, 4H, CH_2NH), 1.39 (s, 18H, CH_3). ^{13}C NMR (151 MHz, $CDCl_3$) δ 160.75 (CO), 156.16 (CO), 79.21 ($C_{t\text{-butyl}}$), 70.50 (CH_2), 70.45 (CH_2), 70.42 (CH_2), 70.30 (CH_2), 69.34 (CH_2), 40.48 (CH_2NH), 39.59 (CH_2NH), 28.53 (CH_3), 28.51 (CH_3). HRMS (ESI) m/z: [**Ox6** + H]$^+$ Calcd. for $C_{24}H_{47}N_4O_{10}$ 551.3287; Found 551.3288.

Procedure for the synthesis of clips: To a solution of [(*p*-cymene)$_2$Ru$_2$Cl$_2$(μ-Cl)$_2$] (1 eq.) in methanol, appropriate oxalamide (1 eq.; **Cx1**: **Ox1**, 200 mg, 847 μmol; **Cx2**: **Ox2**, 200 mg, 847 μmol; **Cx3**: **Ox3**, 300 mg, 720 μmol; **Cx5**: **Ox5**, 300 mg, 851 μmol) and triethylamine (2 eq.) were added. The resulting solution was refluxed overnight. Then, solvent was evaporated partially and the flask cooled to 2 °C for 3 h to induce precipitation. The precipitate formed was filtered and cleaned with diethyl ether and pentane.

Cx1: Orange solid, 317 mg, 409 μmol, 48% yield. ^{1}H NMR (600 MHz, $CDCl_3$) δ 5.41 (m, 4H, $CH_{p\text{-cym}}$), 5.31 (dd, *J* = 20.4, 6.0 Hz, 2H, $CH_{p\text{-cym}}$), 5.01 (dd, *J* = 22.9, 5.7 Hz, 2H, $CH_{p\text{-cym}}$), 4.43 (dd, *J* = 13.1, 3.4 Hz, 1H, CH), 4.28 – 4.23 (m, 2H, CH_2), 3.98 – 3.89 (m, 2H, OH), 3.89 – 3.83 (m, 1H, OH), 3.72 – 3.65 (m, 2H, CH), 3.60 – 3.52 (m, 3H, CH_2), 3.38 – 3.30 (m, 2H, CH_2), 2.75 (hept, *J* = 7.0 Hz, 1H, (C*H*(CH_3)$_2$), 2.65 (hept, *J* = 7.0 Hz, 1H, (C*H*(CH_3)$_2$), 2.61 – 2.55 (m, 1H, OH), 2.22 (d, *J* = 20.0 Hz, 6H, CH_3), 1.23 – 1.14 (m, 12H, CH(C*H*$_3$)$_2$). ^{13}C NMR (151 MHz, $CDCl_3$) δ 170.65 (CO), 170.09 (CO), 101.31 ($C_{p\text{-cym}}$), 101.08 ($C_{p\text{-cym}}$), 98.66

($C_{p\text{-cym}}$), 97.43 ($C_{p\text{-cym}}$), 83.15 ($CH_{p\text{-cym}}$), 82.34 ($CH_{p\text{-cym}}$), 81.47 ($CH_{p\text{-cym}}$), 80.87 ($CH_{p\text{-cym}}$), 80.59 ($CH_{p\text{-cym}}$), 79.77 (COH), 78.36 (COH), 72.84 (COH), 71.14 (COH), 64.51 (CH_2OH), 62.76 (CH_2OH), 54.85 (CH_2N), 52.50 (CH_2N), 31.11 ($CH(CH_3)_2$), 31.08 ($CH(CH_3)_2$), 23.12 ($CH(CH_3)_2$), 22.10 ($CH(CH_3)_2$), 21.80 ($CH(CH_3)_2$), 19.09 (CH_3), 18.93 (CH_3). UV/Vis (AcN): λ_{max} (ε [$M^{-1}cm^{-1}$]) = 313 (12000). HRMS (ESI) m/z: [**Cx1** - Cl]$^+$ Calcd. for $C_{28}H_{42}ClN_2O_6Ru_2$ 741.0813; Found 741.0822.

Cx2: Orange solid, 223 mg, 287 µmol, 34% yield. ^{1}H NMR (600 MHz, $CDCl_3$) δ 5.45 – 5.38 (m, 4H, $CH_{p\text{-cym}}$), 5.31 (dd, *J* = 20.5, 6.0 Hz, 2H, $CH_{p\text{-cym}}$), 5.01 (dd, *J* = 23.7, 5.7 Hz, 2H, $CH_{p\text{-cym}}$), 4.43 (d, *J* = 13.1 Hz, 1H, CH), 4.29 – 4.23 (m, 2H, CH_2), 3.97 – 3.89 (m, 2H, OH), 3.89 – 3.81 (m, 1H, OH), 3.72 – 3.65 (m, 2H, CH), 3.60 – 3.51 (m, 3H, CH_2), 3.38 – 3.30 (m, 2H, CH_2), 2.75 (hept, *J* = 7.1 Hz, 1H, ($CH(CH_3)_2$), 2.65 (hept, *J* = 7.1 Hz, 1H, ($CH(CH_3)_2$), 2.59 – 2.54 (m, 1H, OH), 2.22 (d, *J* = 20.2 Hz, 6H, CH_3), 1.27 – 1.10 (m, 12H, $CH(CH_3)_2$). ^{13}C NMR (151 MHz, $CDCl_3$) δ 170.53 (CO), 101.20 ($C_{p\text{-cym}}$), 100.96 ($C_{p\text{-cym}}$), 98.55 ($C_{p\text{-cym}}$), 97.32 ($C_{p\text{-cym}}$), 83.04 ($CH_{p\text{-cym}}$), 82.22 ($CH_{p\text{-cym}}$), 81.35 ($CH_{p\text{-cym}}$), 80.75 ($CH_{p\text{-cym}}$), 80.47 ($CH_{p\text{-cym}}$), 79.66 (COH), 78.25 (COH), 72.73 (COH), 71.01 (COH), 64.39 (CH_2OH), 62.64 (CH_2OH), 54.73 (CH_2N), 52.38 (CH_2N), 31.00 ($CH(CH_3)_2$), 30.97 ($CH(CH_3)_2$), 23.01 ($CH(CH_3)_2$), 21.99 ($CH(CH_3)_2$), 21.69 ($CH(CH_3)_2$), 18.97 (CH_3), 18.81 (CH_3). UV/Vis (AcN): λ_{max} (ε [$M^{-1}cm^{-1}$]) = 313 (10000). HRMS (ESI) m/z: [**Cx2** - Cl]$^+$ Calcd. for $C_{28}H_{42}ClN_2O_6Ru_2$ 741.0813; Found 741.0824.

Cx3: Orange solid, 259 mg, 271 µmol, 38% yield. ^{1}H NMR (600 MHz, MeOD) δ 5.70 – 5.56 (m, 4H, $CH_{p\text{-cym}}$), 5.45 (dd, *J* = 32.2, 6.1 Hz, 2H, $CH_{p\text{-cym}}$), 5.28 (dd, *J* = 45.1, 5.5 Hz, 2H, $CH_{p\text{-cym}}$), 4.27 (dd, *J* = 12.5, 3.9 Hz, 1H, CHOH), 4.20 – 4.03 (m, 3H, CHOH), 3.93 – 3.87 (m, 1H, CHOH), 3.86 – 3.79 (m, 4H, CH_2OH), 3.78 – 3.75 (m, 2H, CHOH), 3.74 – 3.65 (m, 3H, CH_2N and CHOH), 3.61 – 3.54 (m, 2H, CH_2N), 2.71 (hept, *J* = 6.9 Hz, 2H, ($CH(CH_3)_2$), 2.18 (d, *J* = 13.6 Hz, 6H, CH_3), 1.17 (dd, *J* = 32.6, 7.2 Hz, 12H, $CH(CH_3)_2$). ^{13}C NMR (151 MHz, MeOD) δ 172.24 (CO), 171.94 (CO), 101.98 ($C_{p\text{-cym}}$), 101.68 ($C_{p\text{-cym}}$), 97.88 ($C_{p\text{-cym}}$), 97.71 ($C_{p\text{-cym}}$), 84.27 ($CH_{p\text{-cym}}$), 84.07 ($CH_{p\text{-cym}}$), 83.52 ($CH_{p\text{-cym}}$), 82.89 ($CH_{p\text{-cym}}$), 81.29 ($CH_{p\text{-cym}}$), 80.46 ($CH_{p\text{-cym}}$), 79.75 (COH), 79.30 (COH), 74.49 (COH), 74.22 (COH), 73.17 (COH), 72.99 (COH), 72.40 (COH), 71.69 (COH), 64.88 (CH_2OH), 55.93 (CH_2N), 53.11 (CH_2N), 32.20 ($CH(CH_3)_2$), 31.99 ($CH(CH_3)_2$), 23.43 ($CH(CH_3)_2$), 23.10 ($CH(CH_3)_2$), 22.15 ($CH(CH_3)_2$), 22.04 ($CH(CH_3)_2$), 18.99 (CH_3). UV/Vis (AcN): λ_{max} (ε [$M^{-1}cm^{-1}$]) = 312 (10000). HRMS (ESI) m/z: [**Cx3** - Cl]$^+$ Calcd. for $C_{34}H_{54}ClN_2O_{12}Ru_2$ 921.1447; Found 921.1457.

Cx5: Red solid, 370 mg, 415 µmol, 49% yield. ^{1}H NMR (600 MHz, $CDCl_3$) δ 5.42 (d, *J* = 5.8 Hz, 2H, $CH_{p\text{-cym}}$), 5.39 (d, *J* = 6.0 Hz, 2H, $CH_{p\text{-cym}}$), 5.36 (d, *J* = 5.9 Hz, 2H, $CH_{p\text{-cym}}$), 5.16 (d, *J* = 5.7 Hz, 2H, $CH_{p\text{-cym}}$), 4.00 – 3.89 (m, 2H, CH_2OH), 3.76 – 3.63 (m, 18H, CH_{2PEG}), 3.61 (t, *J* = 4.4 Hz, 4H, CH_2N), 2.77 – 2.67 (m, 4H, ($CH(CH_3)_2$ and OH), 2.13 (s, 6H, CH_3), 1.20 (dd, *J* = 22.4, 6.9 Hz, 12H, $CH(CH_3)_2$). ^{13}C NMR (151 MHz, $CDCl_3$) δ 170.73 (CO), 100.67 ($C_{p\text{-cym}}$), 94.37 ($C_{p\text{-cym}}$), 82.49 ($CH_{p\text{-cym}}$), 81.12 ($CH_{p\text{-cym}}$), 80.41 ($CH_{p\text{-cym}}$), 80.09 ($CH_{p\text{-cym}}$), 72.53 (CH_{2PEG}), 70.69 (CH_{2PEG}), 70.50 (CH_{2PEG}), 70.04 (CH_{2PEG}), 61.91 (CH_2OH), 51.35 (CH_2N), 30.90 ($CH(CH_3)_2$), 22.52 ($CH(CH_3)_2$), 22.32 ($CH(CH_3)_2$), 18.48 (CH_3). UV/Vis (AcN): λ_{max} (ε [$M^{-1}cm^{-1}$]) = 309 (11000). HRMS (ESI) m/z: [**Cx5** - Cl]$^+$ Calcd. for $C_{34}H_{54}ClN_2O_8Ru_2$ 857.1650; Found 857.1659.

Procedure for the synthesis of Cx6: To a solution of [(*p*-cymene)$_2$$Ru_2Cl_2$(µ-Cl)$_2$] (500 mg, 817 µmol, 1 eq.) in methanol, **Ox6** (450 mg, 817 µmol, 1 eq.) and triethylamine (228 µl, 1.63 mmol, 2 eq.) were added. The resulting solution was refluxed overnight. Then, solvent was evaporated partially and diethyl ether was added. Colorless needles are formed (triethylammonium chloride) which were removed by filtration. The filtrate was evaporated to dryness and redissolved in minimum amount of chloroform (2 ml), diethyl ether was added again to precipitate the product as a yellow/orange powder.

Yellow solid, 558 mg, 512 µmol, 62% yield. ^{1}H NMR (600 MHz, $CDCl_3$) δ 5.42 (d, *J* = 5.7 Hz, 2H, $CH_{p\text{-cym}}$), 5.38 (d, *J* = 5.9 Hz, 2H, $CH_{p\text{-cym}}$), 5.34 (d, *J* = 6.0 Hz, 2H, $CH_{p\text{-cym}}$), 5.15 (d, *J* = 5.7 Hz, 2H, $CH_{p\text{-cym}}$), 4.99 (s, 2H, NH), 4.00 – 3.91 (m, 2H, CH_2), 3.77 – 3.59 (m, 14H, CH_{2PEG}), 3.55 (t, *J* = 5.2 Hz, 4H, CH_2N), 3.32 (q, *J*

= 5.6 Hz, 4H, C*H*$_2$NH), 2.72 (hept, *J* = 7.0 Hz, 2H, (C*H*(CH$_3$)$_2$), 2.14 (s, 6H, CH$_3$), 1.43 (s, 18H, CH$_{3t\text{-}butyl}$), 1.22 (d, *J* = 7.1 Hz, 6H, (CH(*C*H$_3$)$_2$), 1.18 (d, *J* = 6.9 Hz, 6H, (CH(*C*H$_3$)$_2$). ^{13}C NMR (151 MHz, CDCl$_3$) δ 170.73 (CO), 100.71 (C$_{p\text{-}cym}$), 94.14 (C$_{p\text{-}cym}$), 82.59 (CH$_{p\text{-}cym}$), 81.41 (CH$_{p\text{-}cym}$), 81.07 (CH$_{p\text{-}cym}$), 80.64 (CH$_{p\text{-}cym}$), 80.25 (CH$_{p\text{-}cym}$), 80.07 (C$_{t\text{-}butyl}$), 70.49 (CH$_{2PEG}$), 70.44 (CH$_{2PEG}$), 70.30 (CH$_{2PEG}$), 70.13 (CH$_{2PEG}$), 51.32 (CH$_2$N), 40.49 (CH$_2$NH), 30.87 (*C*H(CH$_3$)$_2$), 28.54 (CH$_{3t\text{-}butyl}$), 22.54 (CH(*C*H$_3$)$_2$), 22.23 (CH(*C*H$_3$)$_2$), 18.50 (CH$_3$). UV/Vis (AcN): λ$_{max}$ (ε [M^{-1}cm^{-1}]) = 310 (11000). HRMS (ESI) m/z: [**Cx6** - Cl]$^+$ Calcd. for $C_{44}H_{72}ClN_4O_{10}Ru_2$ 1055.3018; Found 1055.3039.

Procedure for the synthesis of metalla-prisms: A mixture of corresponding dinuclear clip (3 eq.; **P1**: **Cx1**, 75 mg, 97 µmol; **P2**: **Cx2**, 75 mg, 97 µmol; **P3**: **Cx3**, 50 mg, 52 µmol; **P5**: **Cx5**, 75 mg, 84 µmol; **P6**: **Cx6**, 50 mg, 46 µmol) and $Ag_3CF_3SO_3$ (6 eq.) in 20 ml of MeOH was stirred at room temperature for 3h. Then, 2,4,6-tris(4-pyridyl)-1,3,5-triazine (2 eq.) was added and the solution was stirred at 70 °C overnight. The mixture was then filtered to remove AgCl and solvent was removed under vacuum. The crude was dissolved in minimum amount of acetonitrile or dichloromethane (2 ml) and diethyl ether (10 ml) was added dropwise. The precipitate formed was filtered off and cleaned with more diethyl ether.

P1: Brown solid, 87 mg, 24 µmol, 74% yield. ^{1}H NMR (600 MHz, MeOD) δ 8.54 (br, 24H, CH$_{tpt}$), 6.23 – 6.17 (m, 6H, CH$_{p\text{-}cym}$), 6.02 – 5.93 (m, 6H, CH$_{p\text{-}cym}$), 5.69 – 5.59 (m, 6H, CH$_{p\text{-}cym}$), 5.51 – 5.41 (m, 6H, CH$_{p\text{-}cym}$), 4.44 – 4.37 (m, 6H, CH), 4.31 – 4.06 (m, 8H, CH$_2$), 3.90 – 3.75 (m, 16H, CH$_2$), 2.88 (hept, *J* = 7.2 Hz, 6H, C*H*(CH$_3$)$_2$), 1.78 (s, 10H, CH$_3$), 1.75 – 1.62 (m, 8H, CH$_3$), 1.39 – 1.34 (m, 18H, CH(C*H*$_3$)$_2$), 1.29 – 1.23 (m, 18H, CH(C*H*$_3$)$_2$). ^{13}C NMR (151 MHz, MeOD) δ 172.69 (CO), 171.77 (CO), 155.70 (CH$_{tpt}$), 144.95 (C$_{tpt}$), 125.89 (CH$_{tpt}$), 125.15 (C$_{tpt}$), 123.03 (C$_{tpt}$), 120.92 (C$_{tpt}$), 118.80 (C$_{tpt}$), 105.84 (C$_{p\text{-}cym}$), 98.80 (C$_{p\text{-}cym}$), 86.79 (CH$_{p\text{-}cym}$), 85.33 (CH$_{p\text{-}cym}$), 84.59 (CH$_{p\text{-}cym}$), 82.35 (CH$_{p\text{-}cym}$), 72.47 (CHOH), 66.45 (CH$_2$OH), 56.88 (CH$_2$N), 32.31 (*C*H(CH$_3$)$_2$), 23.03 (CH(*C*H$_3$)$_2$), 22.34 (CH(*C*H$_3$)$_2$), 17.76 (CH$_3$). UV/Vis (AcN): λ$_{max}$ (ε [M^{-1}cm^{-1}]) = 248 (133000), 307 (51000). HRMS (ESI) m/z: [**P1** – 3CF$_3$SO$_3$]$^{3+}$ Calcd. for $C_{123}H_{150}F_9N_{18}O_{27}Ru_6S_3$ 1063.1393; Found 1063.1406. [**P1** – 4CF$_3$SO$_3$]$^{4+}$ Calcd. for $C_{122}H_{150}F_6N_{18}O_{24}Ru_6S_2$ 760.1164; Found 760.1174.

P2: Brown solid, 100 mg, 28 µmol, 85% yield. ^{1}H NMR (600 MHz, MeOD) δ 8.56 (br, 24H, CH$_{tpt}$), 6.25 – 6.19 (m, 6H, CH$_{p\text{-}cym}$), 6.01 – 5.94 (m, 6H, CH$_{p\text{-}cym}$), 5.68 – 5.62 (m, 6H, CH$_{p\text{-}cym}$), 5.48 – 5.43 (m, 6H, CH$_{p\text{-}cym}$), 4.43 – 4.37 (m, 6H, CH), 4.29 – 4.13 (m, 8H, CH$_2$), 3.87 – 3.78 (m, 16H, CH$_2$), 2.89 (hept, *J* = 7.2 Hz, 6H, C*H*(CH$_3$)$_2$), 1.77 (s, 12H, CH$_3$), 1.74 – 1.63 (m, 6H, CH$_3$), 1.37 (d, *J* = 6.9 Hz, 18H, CH(C*H*$_3$)$_2$), 1.27 (d, *J* = 6.9 Hz, 18H, CH(C*H*$_3$)$_2$). 13C NMR (151 MHz, MeOD) δ 172.69 (CO), 171.77 (CO), 155.70 (CH$_{tpt}$), 144.94 (C$_{tpt}$), 125.91 (C$_{tpt}$), 125.15 (CH$_{tpt}$), 123.03 (C$_{tpt}$), 120.92 (C$_{tpt}$), 118.80 (C$_{tpt}$), 105.83 (C$_{p\text{-}cym}$), 98.82 (C$_{p\text{-}cym}$), 86.80 (CH$_{p\text{-}cym}$), 85.34 (CH$_{p\text{-}cym}$), 84.58 (CH$_{p\text{-}cym}$), 82.34 (CH$_{p\text{-}cym}$), 72.46 (CHOH), 66.45 (CH$_2$OH), 56.88 (CH$_2$N), 32.31 (*C*H(CH$_3$)$_2$), 23.04 (CH(*C*H$_3$)$_2$), 22.35 (CH(*C*H$_3$)$_2$), 17.77 (CH$_3$). UV/Vis (AcN): λ$_{max}$ (ε [M^{-1}cm^{-1}]) = 248 (130000), 307 (49000). HRMS (ESI) m/z: [**P2** – 3CF$_3$SO$_3$]$^{3+}$ Calcd. for $C_{123}H_{150}F_9N_{18}O_{27}Ru_6S_3$ 1063.1394; Found 1063.1409. [**P2** – 4CF$_3$SO$_3$]$^{4+}$ Calcd. for $C_{122}H_{150}F_6N_{18}O_{24}Ru_6S_2$ 760.1164; Found 760.1176.

P3: Dark solid, 65 mg, 16 µmol, 89% yield. ^{1}H NMR (600 MHz, MeOD) δ 8.6 (br, 24H, CH$_{tpt}$), 6.55 – 6.41 (m, 2H, CH$_{p\text{-}cym}$), 6.39 – 6.26 (m, 2H, CH$_{p\text{-}cym}$), 6.22 – 6.15 (m, 2H, CH$_{p\text{-}cym}$), 6.13 – 5.96 (m, 6H, CH$_{p\text{-}cym}$), 5.72 – 5.42 (m, 12H, CH$_{p\text{-}cym}$), 4.46 (s, 6H, CH), 4.30 – 3.72 (m, 42H, CH$_2$ and CH), 3.01 – 2.75 (m, 6H, C*H*(CH$_3$)$_2$), 1.95 – 1.78 (m, 6H, CH$_3$), 1.76 – 1.61 (m, 6H, CH$_3$), 1.54 – 1.39 (m, 6H, CH$_3$), 1.36 – 1.29 (m, 18H, CH(C*H*$_3$)$_2$), 1.27 – 1.19 (m, 18H, CH(C*H*$_3$)$_2$). ^{13}C NMR (151 MHz, MeOD) δ 172.81 (CO), 171.57 (CO), 155.83 (CH$_{tpt}$), 145.11 (C$_{tpt}$), 125.81 (CH$_{tpt}$), 125.06 (C$_{tpt}$), 122.94 (C$_{tpt}$), 120.83 (C$_{tpt}$), 118.71 (C$_{tpt}$), 104.42 (C$_{p\text{-}cym}$), 99.83 (C$_{p\text{-}cym}$), 90.25 (CH$_{p\text{-}cym}$), 89.61 (CH$_{p\text{-}cym}$), 87.67 (CH$_{p\text{-}cym}$), 86.44 (CH$_{p\text{-}cym}$), 84.83 (CH$_{p\text{-}cym}$), 83.81 (CH$_{p\text{-}cym}$), 80.39 (CH$_{p\text{-}cym}$), 74.66 (CHOH), 73.48 (CHOH), 72.69 (CHOH), 64.80 (CH$_2$OH), 59.16 (CH$_2$N), 57.61 (CH$_2$N), 32.30 (*C*H(CH$_3$)$_2$), 32.09 (*C*H(CH$_3$)$_2$), 23.37 (CH(*C*H$_3$)$_2$), 23.01 (CH(*C*H$_3$)$_2$), 22.77 (CH(*C*H$_3$)$_2$), 22.35 (CH(*C*H$_3$)$_2$), 17.95 (CH$_3$), 17.76 (CH$_3$). UV/Vis (AcN): λ$_{max}$ (ε [M^{-1}cm^{-1}]) = 249 (101000),

301 (39000). HRMS (ESI) m/z: [**P3** – $3CF_3SO_3$]$^{3+}$ Calcd. for $C_{141}H_{186}F_9N_{18}O_{45}Ru_6S_3$ 1243.2027; Found 1243.2052. [**P3** – $4CF_3SO_3$]$^{4+}$ Calcd. for $C_{140}H_{186}F_6N_{18}O_{42}Ru_6S_2$ 895.1639; Found 895.1655.

P5: Brown/orange solid, 82 mg, 21 µmol, 73% yield. 1H NMR (600 MHz, MeOD) δ 8.55 (br, 24H, CH_{tpt}), 6.25 – 6.17 (m, 6H, $CH_{p\text{-}cym}$), 6.03 – 5.94 (m, 6H, $CH_{p\text{-}cym}$), 5.76 – 5.59 (m, 6H, $CH_{p\text{-}cym}$), 5.53 – 5.43 (m, 6H, $CH_{p\text{-}cym}$), 4.42 – 4.33 (m, 6H, CH_2N_{PEG}), 4.25 – 4.17 (m, 6H, CH_{2PEG}), 4.07 – 3.84 (m, 36H, CH_{2PEG}), 3.78 – 3.64 (m, 24H, CH_{2PEG} and CH_2OH), 2.90 – 2.80 (m, 6H, C*H*$(CH_3)_2$), 1.77 (s, 6H, CH_3), 1.72 (s, 4H, CH_3), 1.70 (s, 4H, CH_3), 1.68 (s, 4H, CH_3), 1.41 – 1.35 (m, 18H, CH(C*H*$_3)_2$), 1.30 – 1.24 (m, 18H, CH(C*H*$_3)_2$). ^{13}C NMR (151 MHz, MeOD) δ 172.75 (CO), 172.66 (CO), 172.53 (CO), 171.71 (CO), 171.55 (CO), 171.29 (CO), 155.76 (CH_{tpt}), 144.94 (C_{tpt}), 126.00 (C_{tpt}), 125.21 (CH_{tpt}), 123.09 (C_{tpt}), 120.98 (C_{tpt}), 118.87 (C_{tpt}), 105.74 ($C_{p\text{-}cym}$), 105.56 ($C_{p\text{-}cym}$), 105.43 ($C_{p\text{-}cym}$), 98.71 ($C_{p\text{-}cym}$), 98.58 ($C_{p\text{-}cym}$), 98.47 ($C_{p\text{-}cym}$), 87.24 ($CH_{p\text{-}cym}$), 87.08 ($CH_{p\text{-}cym}$), 86.80 ($CH_{p\text{-}cym}$), 85.62 ($CH_{p\text{-}cym}$), 85.54 ($CH_{p\text{-}cym}$), 85.39 ($CH_{p\text{-}cym}$), 84.83 ($CH_{p\text{-}cym}$), 84.73 ($CH_{p\text{-}cym}$), 84.67 ($CH_{p\text{-}cym}$), 82.74 ($CH_{p\text{-}cym}$), 82.52 ($CH_{p\text{-}cym}$), 82.45 ($CH_{p\text{-}cym}$), 73.70 (CH_{2PEG}), 72.09 (CH_{2PEG}), 71.70 (CH_{2PEG}), 71.45 (CH_{2PEG}), 62.22 (CH_2OH), 54.33 (CH_2N), 32.37 (*C*H$(CH_3)_2$), 23.27 (CH(*C*H$_3)_2$), 23.19 (CH(*C*H$_3)_2$), 23.11 (CH(*C*H$_3)_2$), 22.26 (CH(*C*H$_3)_2$), 22.21 (CH(*C*H$_3)_2$), 22.14 (CH(*C*H$_3)_2$), 17.74 (CH_3), 17.70 (CH_3), 17.66 (CH_3). UV/Vis (AcN): λ_{max} (ε [$M^{-1}cm^{-1}$]) = 249 (125000), 306 (55000). HRMS (ESI) m/z: [**P5** – $3CF_3SO_3$]$^{3+}$ Calcd. for $C_{141}H_{186}F_9N_{18}O_{33}Ru_6S_3$ 1179.2231; Found 1179.2265. [**P5** – $4CF_3SO_3$]$^{4+}$ Calcd. for $C_{140}H_{186}F_6N_{18}O_{30}Ru_6S_2$ 847.1792; Found 847.1816.

P6: Green solid, 44 mg, 10 µmol, 63% yield. ^{1}H NMR (600 MHz, MeOD) δ 8.59 (m, 24H, CH_{tpt}), 6.24 (d, *J* = 6.8 Hz, 6H, $CH_{p\text{-}cym}$), 6.10 – 5.94 (m, 6H, $CH_{p\text{-}cym}$), 5.71 – 5.61 (m, 6H, $CH_{p\text{-}cym}$), 5.54 – 5.43 (m, 6H, $CH_{p\text{-}cym}$), 4.47 – 4.28 (m, 6H, CH_{2PEG}), 4.26 – 4.16 (m, 4H, CH_{2PEG}), 4.10 – 3.78 (m, 28H, CH_{2PEG}), 3.63 (d, *J* = 5.5 Hz, 10H, CH_{2PEG}), 3.31 – 3.23 (m, 4H, CH_{2PEG}), 2.90 – 2.82 (m, 6H, C*H*$(CH_3)_2$), 2.08 – 2.00 (m, 4H, CH_3), 1.85 – 1.64 (m, 14H, CH_3), 1.47 – 1.30 (m, 60H, CH_{3tbut} and , CH(C*H*$_3)_2$), 1.29 – 1.20 (m, 18H, CH(C*H*$_3)_2$). ^{13}C NMR (151 MHz, MeOD) δ 178.40 (C_{tpt}), 172.77 (CO), 172.65 (CO), 172.50 (CO), 171.71 (CO), 171.55 (CO), 171.29 (CO), 158.38 (CH_{tpt}), 155.76 (CH_{tpt}), 144.97 (C_{tpt}), 126.26 (C_{tpt}), 125.18 (CH_{tpt}), 123.07 (C_{tpt}), 120.95 (C_{tpt}), 118.84 (C_{tpt}), 105.41 ($C_{p\text{-}cym}$), 104.25 ($C_{p\text{-}cym}$), 98.68 ($C_{p\text{-}cym}$), 87.49 ($CH_{p\text{-}cym}$), 85.71 ($CH_{p\text{-}cym}$), 84.65 ($CH_{p\text{-}cym}$), 82.21 ($CH_{p\text{-}cym}$), 80.08, 72.07 (CH_{2PEG}), 71.48 (CH_{2PEG}), 71.00 (CH_{2PEG}), 54.33 (CH_2N), 47.96, 41.31 (CH_2NH), 32.38 (*C*H$(CH_3)_2$), 28.78 ($CH_{3t\text{-}butyl}$), 23.40 (CH(*C*H$_3)_2$), 23.33 (CH(*C*H$_3)_2$), 23.24 (CH(*C*H$_3)_2$), 22.28 (CH(*C*H$_3)_2$), 22.24 (CH(*C*H$_3)_2$), 22.17 (CH(*C*H$_3)_2$), 17.93 (CH_3), 17.78 (CH_3), 17.74 (CH_3). UV/Vis (AcN): λ_{max} (ε [$M^{-1}cm^{-1}$]) = 249 (169000), 305 (58000). HRMS (ESI) m/z: [**P6** – $3CF_3SO_3$]$^{3+}$ Calcd. for $C_{171}H_{240}F_9N_{24}O_{39}Ru_6S_3$ 1377.3599; Found 1377.3661. [**P6** – $4CF_3SO_3$]$^{4+}$ Calcd. for $C_{170}H_{240}F_6N_{24}O_{36}Ru_6S_2$ 995.7818; Found 995.7858.

Procedure for the synthesis of metalla-cubes: A mixture of the dinuclear clip (4 eq.; **Q1**: **Cx1**, 60 mg, 77 µmol; **Q2**: **Cx2**, 60 mg, 77 µmol; **Q3**: **Cx3**, 75 mg, 78 µmol; **Q4**: **Cx4**, 75 mg, 84 µmol; **Q5**: **Cx5**, 75 mg, 84 µmol; **Q6**: **Cx6**, 75 mg, 69 µmol) and $Ag_3CF_3SO_3$ (8 eq.) in 20 ml of MeOH was stirred at room temperature for 3 h. Then, 5,10,15,20-(tetra-4-pyridyl)porphyrin (2 eq.) was added and the solution was stirred at 70 °C overnight. The mixture was then filtered to remove AgCl and solvent was removed under vacuum. The crude was dissolved in minimum amount of acetonitrile or methanol (2 ml) and diethyl ether (10 ml) was added dropwise. The precipitate formed was filtered off and cleaned with more diethyl ether.

Q1: Brown solid, 82 mg, 16 µmol, 81% yield. ^{1}H NMR (600 MHz, CD_3CN) δ 9.44 – 7.61 (m, 48H, H_{porph}), 6.34 – 5.45 (m, 32H, $CH_{p\text{-}cym}$), 4.67 – 4.30 (m, 12H, CH and OH), 4.29 – 4.01 (m, 16H, CH_2N), 4.00 – 3.62 (m, 28H, C*H*$_2$OH and OH), 3.15 – 2.88 (m, 8H, C*H*$(CH_3)_2$), 2.18 – 1.99 (m, 24H, CH_3), 1.56-1.21 (m, 48H, CH(C*H*$_3)_2$), -6.77 (m, 4H, NH_{porph}). ^{13}C NMR (151 MHz, CD_3CN) δ 173.28 (CO), 171.62 (CO), 155.39 (CH_{porph}), 151.51 (CH_{porph}), 149.15 (CH_{porph}), 132.94 (CH_{porph}), 123.22 (C_{porph}), 121.10 (C_{porph}), 115.72 (C_{porph}), 98.91 ($C_{p\text{-}cym}$), 86.82 ($CH_{p\text{-}cym}$), 84.46 ($CH_{p\text{-}cym}$), 81.34 ($CH_{p\text{-}cym}$), 72.59 (CHOH), 66.06 (CH_2OH), 56.22 (CH_2N), 32.04 (*C*H$(CH_3)_2$), 22.87 (CH(*C*H$_3)_2$), 22.46 (CH(*C*H$_3)_2$), 22.19 (CH(*C*H$_3)_2$), 18.17 (CH_3).

UV/Vis (AcN): λ_{max} (ε [$M^{-1}cm^{-1}$]) = 311 (83000), 410 (487000), 525 (19000), 562 (14000), 597 (8000), 654 (5000). HRMS (ESI) m/z: [**Q1** – $4CF_3SO_3$]$^{4+}$ Calcd. for $C_{196}H_{220}F_{12}N_{24}O_{36}Ru_8S_4$ 1164.1785; Found 1164.1799. [**Q1** – $5CF_3SO_3$]$^{5+}$ Calcd. for $C_{195}H_{220}F_9N_{24}O_{33}Ru_8S_3$ 901.5523; Found 901.5539.

Q2: Brown solid, 78 mg, 15 µmol, 77% yield. ^{1}H NMR (600 MHz, CD_3CN) δ 9.52 – 7.59 (m, 48H, H_{porph}), 6.28 – 5.61 (m, 32H, $CH_{p\text{-}cym}$), 4.66 – 4.31 (m, 12H, CH and OH), 4.31 – 4.01 (m, 16H, CH_2N), 3.99 – 3.78 (m, 20H, CH_2OH and OH), 3.71 – 3.48 (m, 8H, OH), 3.12 – 2.93 (s, 8H, CH(CH_3)$_2$), 2.18 – 2.04 (m, 24H, CH_3), 1.54 – 1.29 (m, 48H, CH(CH_3)$_2$), -6.75 (m, 4H, NH_{porph}). ^{13}C NMR (151 MHz, CD_3CN) δ 171.62 (CO), 151.58 (CH_{porph}), 149.17 (CH_{porph}), 132.94 (CH_{porph}), 125.33 (C_{porph}), 123.21 (C_{porph}), 121.08 (C_{porph}), 118.96 (C_{porph}), 115.68 (C_{porph}), 98.91 ($C_{p\text{-}cym}$), 86.79 ($CH_{p\text{-}cym}$), 84.51 ($CH_{p\text{-}cym}$), 81.17 ($CH_{p\text{-}cym}$), 72.39 (CHOH), 66.05 (CH_2OH), 56.17 (CH_2N), 32.07 (*C*H(CH_3)$_2$), 22.99 (CH(*C*H_3)$_2$), 18.15 (CH_3). UV/Vis (AcN): λ_{max} (ε [$M^{-1}cm^{-1}$]) = 312 (83000), 410 (505000), 524 (19000), 562 (14000), 597 (8000), 654 (5000). HRMS (ESI) m/z: [**Q2** – $4CF_3SO_3$]$^{4+}$ Calcd. for $C_{196}H_{220}F_{12}N_{24}O_{36}Ru_8S_4$ 1164.1785; Found 1164.1796. [**Q2** – $5CF_3SO_3$]$^{5+}$ Calcd. for $C_{195}H_{220}F_9N_{24}O_{33}Ru_8S_3$ 901.5523; Found 901.5538.

Q3: Brown solid, 100 mg, 17 µmol, 85% yield. ^{1}H NMR (600 MHz, MeOD) δ 9.96 – 7.56 (m, 48H, H_{porph}), 6.69 – 6.27 (m, 11H, $CH_{p\text{-}cym}$), 6.26 – 6.12 (m, 5H, $CH_{p\text{-}cym}$), 6.11 – 5.96 (m, 4H, $CH_{p\text{-}cym}$), 5.93 – 5.74 (m, 12H, $CH_{p\text{-}cym}$), 4.79 – 4.49 (m, 10H, CH and CH_2), 4.47 – 4.04 (m, 30H, CH and CH_2), 4.04 – 3.72 (m, 24H, CH and CH_2), 3.24 – 2.96 (m, 8H, C*H*(CH_3)$_2$), 2.25 – 2.01 (m, 24H, CH_3), 1.57 – 1.36 (m, 48H, CH(CH_3)$_2$). ^{13}C NMR (151 MHz, MeOD) δ 173.70 (CO), 172.02 (CO), 155.36* (CH_{porph}), 129.84 (CH_{porph}), 125.19 (C_{porph}), 123.08 (C_{porph}), 120.96 (C_{porph}), 118.85 (C_{porph}), 87.44 ($CH_{p\text{-}cym}$), 84.88 ($CH_{p\text{-}cym}$), 81.87 ($CH_{p\text{-}cym}$), 78.97 ($CH_{p\text{-}cym}$), 73.75 (CHOH), 73.55 (CHOH), 72.24 (CHOH), 64.96 (CH_2OH), 64.72 (CH_2OH), 57.47 (CH_2N), 32.57 (*C*H(CH_3)$_2$), 32.30 (*C*H(CH_3)$_2$), 24.50 (CH(*C*H_3)$_2$), 23.79 (CH(*C*H_3)$_2$), 23.09 (CH(*C*H_3)$_2$), 22.57 (CH(*C*H_3)$_2$), 22.18 (CH(*C*H_3)$_2$), 18.35 (CH_3). UV/Vis (AcN): λ_{max} (ε [$M^{-1}cm^{-1}$]) = 313 (58000), 411 (367000), 524 (15000), 562 (11000), 598 (7000), 654 (4000). HRMS (ESI) m/z: [**Q3** – $4CF_3SO_3$]$^{4+}$ Calcd. for $C_{220}H_{268}F_{12}N_{24}O_{60}Ru_8S_4$ 1344.2419; Found 1344.2441. [**Q3** – $5CF_3SO_3$]$^{5+}$ Calcd. for $C_{219}H_{268}F_9N_{24}O_{57}Ru_8S_3$ 1045.6030; Found 1045.6047.

Q4: Green solid, 110 mg, 22 µmol, 92% yield. ^{1}H NMR (600 MHz, CD_3CN) δ 9.52 – 7.64 (m, 48H, H_{porph}), 6.21 – 5.61 (m, 32H, $CH_{p\text{-}cym}$), 4.54 – 3.79 (m, 40H, CH_2 and OH), 3.06 – 2.91 (m, 8H, C*H*(CH_3)$_2$), 2.19 – 2.01 (m, 24H, CH_3), 1.61 – 1.33 (m, 48H, CH(CH_3)$_2$), -6.73 (m, 4H, NH_{porph}). ^{13}C NMR (151 MHz, CD_3CN) δ 173.41 (CO), 171.59 (CO), 155.39 (CH_{porph}), 151.79 (CH_{porph}), 132.90 (CH_{porph}), 125.41 (C_{porph}), 123.28 (C_{porph}), 121.15 (C_{porph}), 119.03 (C_{porph}), 115.67 (C_{porph}), 105.12 ($C_{p\text{-}cym}$), 100.51 ($C_{p\text{-}cym}$), 86.09 ($CH_{p\text{-}cym}$), 85.00 ($CH_{p\text{-}cym}$), 84.48 ($CH_{p\text{-}cym}$), 82.54 ($CH_{p\text{-}cym}$), 61.47 (CH_2OH), 56.61 (CH_2N), 55.75 (CH_2N), 32.05 (*C*H(CH_3)$_2$), 23.21 (CH(*C*H_3)$_2$), 22.92 (CH(*C*H_3)$_2$), 22.62 (CH(*C*H_3)$_2$), 22.20 (CH(*C*H_3)$_2$), 18.21 (CH_3). UV/Vis (AcN): λ_{max} (ε [$M^{-1}cm^{-1}$]) = 312 (78000), 410 (480000), 525 (17000), 562 (13000), 598 (8000), 654 (5000). HRMS (ESI) m/z: [**Q4** – $4CF_3SO_3$]$^{4+}$ Calcd. for $C_{188}H_{204}F_{12}N_{24}O_{28}Ru_8S_4$ 1104.1573; Found 1104.1609. [**Q4** – $5CF_3SO_3$]$^{5+}$ Calcd. for $C_{187}H_{204}F_9N_{24}O_{25}Ru_8S_3$ 853.5354; Found 853.5364.

Q5: Purple solid, 105 mg, 18 µmol, 87% yield. ^{1}H NMR (600 MHz, MeOD) δ 9.74 – 7.57 (m, 48H, H_{porph}), 6.67 – 6.32 (m, 8H, $CH_{p\text{-}cym}$), 6.25 – 5.75 (m, 24H, $CH_{p\text{-}cym}$), 4.68 – 4.39 (m, 16H, CH_{2PEG}), 4.26 – 3.64 (m, 80H, CH_{2PEG}), 3.25 – 2.97 (m, 8H, C*H*(CH_3)$_2$), 2.31 – 1.90 (m, 24H, CH_3), 1.63 – 1.27 (m, 48H, CH(CH_3)$_2$), -6.82 (m, 4H, NH_{porph}). ^{13}C NMR (151 MHz, CD_3CN) δ 171.29 (CO), 147.15 (CH_{porph}), 132.98* (CH_{porph}), 125.40 (C_{porph}), 123.27 (C_{porph}), 121.14 (C_{porph}), 119.02 (C_{porph}), 86.08*($CH_{p\text{-}cym}$), 84.79* ($CH_{p\text{-}cym}$), 83.18* ($CH_{p\text{-}cym}$), 81.41* ($CH_{p\text{-}cym}$), 73.41 (CH_{2PEG}), 71.68 (CH_{2PEG}), 71.26 (CH_{2PEG}), 70.78 (CH_{2PEG}), 62.07 (CH_2OH), 32.10 (*C*H(CH_3)$_2$), 23.28 (CH(*C*H_3)$_2$), 22.62 (CH(*C*H_3)$_2$), 21.87 (CH(*C*H_3)$_2$), 18.13 (CH_3). UV/Vis (AcN): λ_{max} (ε [$M^{-1}cm^{-1}$]) = 313 (119000), 411 (579000), 529 (22000), 566 (18000), 597 (8000), 601 (10000). HRMS

* Extracted from HSQC data

(ESI) m/z: [**Q5** – $4CF_3SO_3]^{4+}$ Calcd. for $C_{220}H_{268}F_{12}N_{24}O_{44}Ru_8S_4$ 1280.2622; Found 1280.2631. [**Q5** – $5CF_3SO_3]^{5+}$ Calcd. for $C_{219}H_{268}F_9N_{24}O_{41}Ru_8S_3$ 994.4193; Found 994.4203.

Q6: Purple solid, 58 mg, 9 µmol, 52% yield. ^{1}H NMR (600 MHz, CD_3CN) δ 9.57 – 7.65 (m, 48H , H_{porph}), 6.55 – 6.20 (m, 8H, $CH_{p\text{-}cym}$), 6.17 – 5.65 (m, 16H, $CH_{p\text{-}cym}$), 5.56 – 5.32 (m, 8H, $CH_{p\text{-}cym}$), 4.73 – 4.30 (m, 14H, CH_{2PEG}), 4.26 – 3.76 (m, 44H, CH_{2PEG}), 3.73 – 3.51 (m, 18H, CH_{2PEG}), 3.39 – 3.20 (m, 14H, CH_{2PEG}), 3.15 – 2.95 (m, 8H, $CH(CH_3)_2$), 2.43 – 2.31 (m, 4H, CH_{2PEG}), 2.16 – 2.03 (m, 16H, CH_3), 1.63 – 1.19 (m, 120H $CH_{3t\text{-}butyl}$ and $CH(CH_3)_2$), -6.82 (m, 4H, NH_{porph}). ^{13}C NMR (151 MHz, CD_3CN) δ 171.36 (CO), 156.91 (CH_{porph}), 132.81* (CH_{porph}), 125.47 (C_{porph}), 123.34 (C_{porph}), 121.21 (C_{porph}), 119.08 (C_{porph}), 115.65 (C_{porph}), 86.24* ($CH_{p\text{-}cym}$), 84.79* ($CH_{p\text{-}cym}$), 82.86* ($CH_{p\text{-}cym}$), 82.05* ($CH_{p\text{-}cym}$), 79.23 ($C_{t\text{-}butyl}$), 71.69 (CH_{2PEG}), 71.18 (CH_{2PEG}), 70.73 (CH_{2PEG}), 54.53 (CH_2N), 41.09 (CH_2NH), 32.31 ($CH(CH_3)_2$), 32.20 ($CH(CH_3)_2$), 32.04 ($CH(CH_3)_2$), 28.77 ($CH_{3t\text{-}butyl}$), 28.70 ($CH_{3t\text{-}butyl}$), 28.58 ($CH_{3t\text{-}butyl}$), 23.42 ($CH(CH_3)_2$), 22.98 ($CH(CH_3)_2$), 22.80 ($CH(CH_3)_2$), 18.20 (CH_3). UV/Vis (AcN): λ_{max} (ε [$M^{-1}cm^{-1}$]) = 313 (80000), 411 (489000), 526 (18000), 565 (13000), 599 (8000), 656 (5000). HRMS (ESI) m/z: [**Q6** – $4CF_3SO_3]^{4+}$ Calcd. for $C_{260}H_{340}F_{12}N_{32}O_{52}Ru_8S_4$ 1478.3990; Found 1478.4022. [**Q6** – $5CF_3SO_3]^{5+}$ Calcd. for $C_{259}H_{340}F_9N_{32}O_{49}Ru_8S_3$ 1152.9287; Found 1152.9307.

* Extracted from HSQC data

7. References

(1) Lawrence, M. A. W.; Bullock, J. L.; Holder, A. A. Basic Coordination Chemistry of Ruthenium. In *Ruthenium Complexes*; Browne, W. R., Holder, A. A., Lawrence, M. A., Bullock Jr, J. L., Lilge, L., Eds.; Wiley, 2018; pp 25–41. https://doi.org/10.1002/9783527695225.ch2.

(2) Clarke, M. J.; Bitler, S.; Rennert, D.; Buchbinder, M.; Kelman, A. D. Reduction and Subsequent Binding of Ruthenium Ions Catalyzed by Subcellular Components. *J. Inorg. Biochem.* **1980**, *12* (1), 79–87. https://doi.org/10.1016/S0162-0134(00)80045-8.

(3) Melchart, M.; Sadler, P. J. Ruthenium Arene Anticancer Complexes. In *Bioorganometallics*; John Wiley & Sons, Ltd, 2005; pp 39–64. https://doi.org/10.1002/3527607692.ch2.

(4) Therrien, B. Biologically Relevant Arene Ruthenium Metalla-Assemblies. *CrystEngComm* **2015**, *17* (3), 484–491. https://doi.org/10.1039/C4CE02146K.

(5) Winkhaus, G.; Singer, H. Ruthen(II)-Komplexe Mit Zweizähnigem Cycloheptatrien Und Benzol. *J. Organomet. Chem.* **1967**, *7* (3), 487–491. https://doi.org/10.1016/S0022-328X(00)85370-X.

(6) Bennett, M. A.; Smith, A. K. Arene Ruthenium(II) Complexes Formed by Dehydrogenation of Cyclohexadienes with Ruthenium(III) Trichloride. *J. Chem. Soc. Dalton Trans.* **1974**, No. 2, 233–241. https://doi.org/10.1039/DT9740000233.

(7) Kuehl, C. J.; Yamamoto, T.; Seidel, S. R.; Stang, Peter. J. Self-Assembly of Molecular Prisms via an Organometallic "Clip." *Org. Lett.* **2002**, *4* (6), 913–915. https://doi.org/10.1021/ol017296d.

(8) Kuehl, C. J.; Kryschenko, Y. K.; Radhakrishnan, U.; Seidel, S. R.; Huang, S. D.; Stang, P. J. Self-Assembly of Nanoscopic Coordination Cages of D_{3h} Symmetry. *Proc. Natl. Acad. Sci.* **2002**, *99* (8), 4932–4936. https://doi.org/10.1073/pnas.012540799.

(9) Yang, H.-B.; Ghosh, K.; Northrop, B. H.; Stang, P. J. Self-Recognition in the Coordination-Driven Self-Assembly of Three-Dimensional M_3L_2 Polyhedra. *Org. Lett.* **2007**, *9* (8), 1561–1564. https://doi.org/10.1021/ol070371l.

(10) Kumazawa, K.; Biradha, K.; Kusukawa, T.; Okano, T.; Fujita, M. Multicomponent Assembly of a Pyrazine-Pillared Coordination Cage That Selectively Binds Planar Guests by Intercalation. *Angew. Chem. Int. Ed.* **2003**, *42* (33), 3909–3913. https://doi.org/10.1002/anie.200351797.

(11) Kumazawa, K.; Yamanoi, Y.; Yoshizawa, M.; Kusukawa, T.; Fujita, M. A Palladium(II)-Clipped Aromatic Sandwich. *Angew. Chem. Int. Ed.* **2004**, *43* (44), 5936–5940. https://doi.org/10.1002/anie.200460868.

(12) Yoshizawa, M.; Nakagawa, J.; Kumazawa, K.; Nagao, M.; Kawano, M.; Ozeki, T.; Fujita, M. Discrete Stacking of Large Aromatic Molecules within Organic-Pillared Coordination Cages. *Angew. Chem. Int. Ed.* **2005**, *44* (12), 1810–1813. https://doi.org/10.1002/anie.200462171.

(13) Fujita, M.; Tominaga, M.; Hori, A.; Therrien, B. Coordination Assemblies from a Pd(II)-Cornered Square Complex. *Acc. Chem. Res.* **2005**, *38* (4), 369–378. https://doi.org/10.1021/ar040153h.

(14) Yan, H.; Süss-Fink, G.; Neels, A.; Stoeckli-Evans, H. Mono-, Di- and Tetra-Nuclear p-Cymeneruthenium Complexes Containing Oxalato Ligands. *J. Chem. Soc. Dalton Trans.* **1997**, No. 22, 4345–4350. https://doi.org/10.1039/A704658H.

(15) Mattsson, J.; Govindaswamy, P.; Furrer, J.; Sei, Y.; Yamaguchi, K.; Süss-Fink, G.; Therrien, B. Encapsulation of Aromatic Molecules in Hexanuclear Arene Ruthenium Cages: A Strategy to Build Up Organometallic Carceplex Prisms with a Dangling Arm Standing Out. *Organometallics* **2008**, *27* (17), 4346–4356. https://doi.org/10.1021/om800419s.

(16) Barry, N. P. E.; Therrien, B. Host–Guest Chemistry in the Hexanuclear (Arene)Ruthenium Metalla-Prismatic Cage [Ru6(p-Cymene)6(Tpt)2(Dhnq)3]6+. *Eur. J. Inorg. Chem.* **2009**, *2009* (31), 4695–4700. https://doi.org/10.1002/ejic.200900649.

(17) Barry, N. P. E.; Furrer, J.; Therrien, B. In- and Out-of-Cavity Interactions by Modulating the Size of Ruthenium Metallarectangles. *Helv. Chim. Acta* **2010**, *93* (7), 1313–1328. https://doi.org/10.1002/hlca.200900422.

(18) Barry, N. P. E.; Edafe, F.; Therrien, B. Anticancer Activity of Tetracationic Arene Ruthenium Metalla-Cycles. *Dalton Trans.* **2011**, *40* (27), 7172. https://doi.org/10.1039/c1dt10489f.

(19) Garci, A.; Dobrov, A. A.; Riedel, T.; Orhan, E.; Dyson, P. J.; Arion, V. B.; Therrien, B. Strategy to Optimize the Biological Activity of Arene Ruthenium Metalla-Assemblies. *Organometallics* **2014**, *33* (14), 3813–3822. https://doi.org/10.1021/om5005176.
(20) Barry, N. P. E.; Therrien, B. Host–Guest Chemistry in the Hexanuclear (Arene)Ruthenium Metalla-Prismatic Cage [Ru6(p-Cymene)6(Tpt)2(Dhnq)3]6+. *Eur. J. Inorg. Chem.* **2009**, *2009* (31), 4695–4700. https://doi.org/10.1002/ejic.200900649.
(21) Freudenreich, J.; Barry, N. P. E.; Süss-Fink, G.; Therrien, B. Permanent Encapsulation or Host–Guest Behavior of Aromatic Molecules in Hexanuclear Arene Ruthenium Prisms. *Eur. J. Inorg. Chem.* **2010**, *2010* (16), 2400–2405. https://doi.org/10.1002/ejic.201000191.
(22) Bennett, M. A.; Huang, T.-N.; Matheson, T. W.; Smith, A. K.; Ittel, S.; Nickerson, W. 16. (H6-Hexamethylbenzene)Ruthenium Complexes. In *Inorganic Syntheses*; John Wiley & Sons, Ltd, 1982; pp 74–78. https://doi.org/10.1002/9780470132524.ch16.
(23) Therrien, B.; Ward, T. R.; Pilkington, M.; Hoffmann, C.; Gilardoni, F.; Weber, J. Synthesis and Reactivity of Tethered H1:H6-(Phosphinoarene)Ruthenium Dichlorides. *Organometallics* **1998**, *17* (3), 330–337. https://doi.org/10.1021/om970735l.
(24) Pinto, P.; Marconi, G.; Heinemann, F. W.; Zenneck, U. Chiral Arene Ruthenium Complexes. 6. Diastereoselective Formation of Chiral-At-Metal P-Tethered Arene Ruthenium(II) Complexes. *Organometallics* **2004**, *23* (3), 374–380. https://doi.org/10.1021/om0305768.
(25) Therrien, B.; Süss-Fink, G. New Mono and Dinuclear Arene Ruthenium Chloro Complexes Containing Ester Substituents. *Inorganica Chim. Acta* **2006**, *359* (13), 4350–4354. https://doi.org/10.1016/j.ica.2006.06.006.
(26) Dyson, P. J. Systematic Design of a Targeted Organometallic Antitumour Drug in Pre-Clinical Development. *CHIMIA* **2007**, *61* (11), 698–698. https://doi.org/10.2533/chimia.2007.698.
(27) Dougan, S. J.; Sadler, P. J. The Design of Organometallic Ruthenium Arene Anticancer Agents. *CHIMIA* **2007**, *61* (11), 704–704. https://doi.org/10.2533/chimia.2007.704.
(28) Allardyce, C. S.; Dyson, P. J.; Ellis, D. J.; Heath, S. L. [Ru(H6-p-Cymene)Cl2(Pta)] (Pta = 1,3,5-Triaza-7-Phosphatricyclo- [3.3.1.1]Decane): A Water Soluble Compound That Exhibits pH Dependent DNA Binding Providing Selectivity for Diseased Cells. *Chem. Commun.* **2001**, No. 15, 1396–1397. https://doi.org/10.1039/B104021A.
(29) Ang, W. H.; Casini, A.; Sava, G.; Dyson, P. J. Organometallic Ruthenium-Based Antitumor Compounds with Novel Modes of Action. *J. Organomet. Chem.* **2011**, *696* (5), 989–998. https://doi.org/10.1016/j.jorganchem.2010.11.009.
(30) Scolaro, C.; Chaplin, A. B.; Hartinger, C. G.; Bergamo, A.; Cocchietto, M.; Keppler, B. K.; Sava, G.; Dyson, P. J. Tuning the Hydrophobicity of Ruthenium(II)–Arene (RAPTA) Drugs to Modify Uptake, Biomolecular Interactions and Efficacy. *Dalton Trans.* **2007**, No. 43, 5065–5072. https://doi.org/10.1039/B705449A.
(31) Ang, W. H.; Daldini, E.; Juillerat-Jeanneret, L.; Dyson, P. J. Strategy To Tether Organometallic Ruthenium−Arene Anticancer Compounds to Recombinant Human Serum Albumin. *Inorg. Chem.* **2007**, *46* (22), 9048–9050. https://doi.org/10.1021/ic701474m.
(32) Ang, W. H.; Parker, L. J.; De Luca, A.; Juillerat-Jeanneret, L.; Morton, C. J.; Lo Bello, M.; Parker, M. W.; Dyson, P. J. Rational Design of an Organometallic Glutathione Transferase Inhibitor. *Angew. Chem. Int. Ed.* **2009**, *48* (21), 3854–3857. https://doi.org/10.1002/anie.200900185.
(33) Anca Furrer, M.; Schmitt, F.; Wiederkehr, M.; Juillerat-Jeanneret, L.; Therrien, B. Cellular Delivery of Pyrenyl-Arene Ruthenium Complexes by a Water-Soluble Arene Ruthenium Metalla-Cage. *Dalton Trans.* **2012**, *41* (24), 7201–7211. https://doi.org/10.1039/C2DT30193H.
(34) Garci, A.; Mbakidi, J.-P.; Chaleix, V.; Sol, V.; Orhan, E.; Therrien, B. Tunable Arene Ruthenium Metallaprisms to Transport, Shield, and Release Porphin in Cancer Cells. *Organometallics* **2015**, *34* (16), 4138–4146. https://doi.org/10.1021/acs.organomet.5b00555.
(35) Garci, A.; Dobrov, A. A.; Riedel, T.; Orhan, E.; Dyson, P. J.; Arion, V. B.; Therrien, B. Strategy to Optimize the Biological Activity of Arene Ruthenium Metalla-Assemblies. *Organometallics* **2014**, *33* (14), 3813–3822. https://doi.org/10.1021/om5005176.

(36) Mannancherril, V.; Therrien, B. Strategies toward the Enhanced Permeability and Retention Effect by Increasing the Molecular Weight of Arene Ruthenium Metallaassemblies. *Inorg. Chem.* **2018**, *57* (7), 3626–3633. https://doi.org/10.1021/acs.inorgchem.7b02668.
(37) Gras, M.; Therrien, B.; Süss-Fink, G.; Zava, O.; Dyson, P. J. Thiophenolato-Bridged Dinuclear Arene Ruthenium Complexes: A New Family of Highly Cytotoxic Anticancer Agents. *Dalton Trans.* **2010**, *39* (42), 10305–10313. https://doi.org/10.1039/C0DT00887G.
(38) Furrer, M. A.; Garci, A.; Denoyelle-Di-Muro, E.; Trouillas, P.; Giannini, F.; Furrer, J.; Clavel, C. M.; Dyson, P. J.; Süss-Fink, G.; Therrien, B. Synthesis, Characterisation and In Vitro Anticancer Activity of Hexanuclear Thiolato-Bridged Arene Ruthenium Metalla-Prisms. *Chem. – Eur. J.* **2013**, *19* (9), 3198–3203. https://doi.org/10.1002/chem.201203712.
(39) Dubey, A.; Mishra, A.; Min, J. W.; Lee, M. H.; Kim, H.; Stang, P. J.; Chi, K.-W. Self-Assembly of New Arene-Ruthenium Rectangles Containing Triptycene Building Block and Their Application in Fluorescent Detection of Nitro Aromatics. *Inorganica Chim. Acta* **2014**, *423*, 326–331. https://doi.org/10.1016/j.ica.2014.08.037.
(40) Vajpayee, V.; Song, Y. H.; Lee, M. H.; Kim, H.; Wang, M.; Stang, P. J.; Chi, K.-W. Self-Assembled Arene–Ruthenium-Based Rectangles for the Selective Sensing of Multi-Carboxylate Anions. *Chem. – Eur. J.* **2011**, *17* (28), 7837–7844. https://doi.org/10.1002/chem.201100242.
(41) Mishra, A.; Vajpayee, V.; Kim, H.; Lee, M. H.; Jung, H.; Wang, M.; Stang, P. J.; Chi, K.-W. Self-Assembled Metalla-Bowls for Selective Sensing of Multi-Carboxylate Anions. *Dalton Trans.* **2012**, *41* (4), 1195–1201. https://doi.org/10.1039/C1DT11612F.
(42) Mishra, A.; Ravikumar, S.; Song, Y. H.; Prabhu, N. S.; Kim, H.; Hong, S. H.; Cheon, S.; Noh, J.; Chi, K.-W. A New Arene–Ru Based Supramolecular Coordination Complex for Efficient Binding and Selective Sensing of Green Fluorescent Protein. *Dalton Trans.* **2014**, *43* (16), 6032–6040. https://doi.org/10.1039/C3DT53186D.
(43) Mishra, A.; Jeong, Y. J.; Jo, J.-H.; Kang, S. C.; Kim, H.; Chi, K.-W. Coordination-Driven Self-Assembly and Anticancer Potency Studies of Arene–Ruthenium-Based Molecular Metalla-Rectangles. *Organometallics* **2014**, *33* (5), 1144–1151. https://doi.org/10.1021/om401042m.
(44) Gupta, G.; Das, A.; Panja, S.; Ryu, J. Y.; Lee, J.; Mandal, N.; Lee, C. Y. Self-Assembly of Novel Thiophene-Based BODIPY RuII Rectangles: Potential Antiproliferative Agents Selective Against Cancer Cells. *Chem. – Eur. J.* **2017**, *23* (68), 17199–17203. https://doi.org/10.1002/chem.201704368.
(45) Liu, H.-W.; Xu, S.; Wang, P.; Hu, X.-X.; Zhang, J.; Yuan, L.; Zhang, X.-B.; Tan, W. An Efficient Two-Photon Fluorescent Probe for Monitoring Mitochondrial Singlet Oxygen in Tissues during Photodynamic Therapy. *Chem. Commun.* **2016**, *52* (83), 12330–12333. https://doi.org/10.1039/C6CC05880A.
(46) Klaper, M.; Linker, T. Evidence for an Oxygen Anthracene Sandwich Complex. *Angew. Chem. Int. Ed.* **2013**, *52* (45), 11896–11899. https://doi.org/10.1002/anie.201304768.
(47) Mahmoud Asadirad, A.; Erno, Z.; R. Branda, N. Photothermal Release of Singlet Oxygen from Gold Nanoparticles. *Chem. Commun.* **2013**, *49* (50), 5639–5641. https://doi.org/10.1039/C3CC42217H.
(48) Gaschard, M.; Nehzat, F.; Cheminel, T.; Therrien, B. Arene Ruthenium Metalla-Assemblies with Anthracene Moieties for PDT Applications. *Inorganics* **2018**, *6* (3), 97. https://doi.org/10.3390/inorganics6030097.
(49) Alvariño, C.; Heinrich, B.; Donnio, B.; Deschenaux, R.; Therrien, B. Supramolecular Arene-Ruthenium Metallacycle with Thermotropic Liquid-Crystalline Properties. *Inorg. Chem.* **2019**, *58* (14), 9505–9512. https://doi.org/10.1021/acs.inorgchem.9b01532.
(50) Murugesan, S.; Shetty, S. J.; Srivastava, T. S.; Noronha, O. P. D.; Samuel, A. M. A Technetium-99m-Labelled Cyclam Acid Porphyrin (CAP) for Tumour Imaging. *Appl. Radiat. Isot.* **2001**, *55* (5), 641–646. https://doi.org/10.1016/S0969-8043(01)00113-0.
(51) Simões, J. C. S.; Wagnières, G.; Sarpaki, S.; Sol, V.; Therrien, B. Porphyrin Metalla-Assemblies Coupled to Cellulose Nanocrystals for PDT and Imaging Applications. *J. Porphyr. Phthalocyanines* **2023**, *27* (05), 797–810. https://doi.org/10.1142/S1088424623500499.

(52) Werner, A. Über Die Raumisomeren Kobaltverbindungen. *Justus Liebigs Ann. Chem.* **1912**, *386* (1–2), 1–272. https://doi.org/10.1002/jlac.19123860102.
(53) Liu, W.; Das, P. J.; Colquhoun, H. M.; Stoddart, J. F. Whither Second-Sphere Coordination? *CCS Chem.* **2021**, *4* (3), 755–784. https://doi.org/10.31635/ccschem.021.202101286.
(54) Allocati, N.; Masulli, M.; Di Ilio, C.; Federici, L. Glutathione Transferases: Substrates, Inihibitors and pro-Drugs in Cancer and Neurodegenerative Diseases. *Oncogenesis* **2018**, *7* (1), 1–15. https://doi.org/10.1038/s41389-017-0025-3.
(55) Townsend, D. M.; Findlay, V. L.; Tew, K. D. Glutathione S-Transferases as Regulators of Kinase Pathways and Anticancer Drug Targets. *Methods Enzymol.* **2005**, *401*, 287–307. https://doi.org/10.1016/S0076-6879(05)01019-0.
(56) Barry, N. P. E.; Abd Karim, N. H.; Vilar, R.; Therrien, B. Interactions of Ruthenium Coordination Cubes with DNA. *Dalton Trans.* **2009**, No. 48, 10717. https://doi.org/10.1039/b913642h.
(57) Therrien, B. The Role of the Second Coordination Sphere in the Biological Activity of Arene Ruthenium Metalla-Assemblies. *Front. Chem.* **2018**, *6*, 602. https://doi.org/10.3389/fchem.2018.00602.
(58) Vereshchuk, N.; Matheu, R.; Benet-Buchholz, J.; Pipelier, M.; Lebreton, J.; Dubreuil, D.; Tessier, A.; Gimbert-Suriñach, C.; Ertem, M.; Llobet, A. Second Coordination Sphere Effects in an Evolved Ru Complex Based on Highly Adaptable Ligand Results in Rapid Water Oxidation Catalysis. *J. Am. Chem. Soc.* **2020**, *142* (11), 5068–5077. https://doi.org/10.1021/jacs.9b11935.
(59) Ma, H.-C.; Hsiao, S.-C.; Wang, Y.-H. Tuning Primary and Secondary Coordination Spheres of Ruthenium Complexes for the Homogeneous Water Oxidation Reaction: A Perspective from Catalytic Activity and Overpotential. *Catal. Sci. Technol.* **2023**, *13* (6), 1598–1622. https://doi.org/10.1039/D2CY02109A.
(60) Ghosh, A.; Dasgupta, S.; Kundu, A.; Mandal, S. The Impact of Secondary Coordination Sphere Engineering on Water Oxidation Reactivity Catalysed by Molecular Ruthenium Complexes: A next-Generation Approach to Develop Advanced Catalysts. *Dalton Trans.* **2022**, *51* (27), 10320–10337. https://doi.org/10.1039/D2DT01124G.
(61) Shook, R. L.; Borovik, A. S. Role of the Secondary Coordination Sphere in Metal-Mediated Dioxygen Activation. *Inorg. Chem.* **2010**, *49* (8), 3646–3660. https://doi.org/10.1021/ic901550k.
(62) Matsumura, Y.; Maeda, H. A New Concept for Macromolecular Therapeutics in Cancer Chemotherapy: Mechanism of Tumoritropic Accumulation of Proteins and the Antitumor Agent Smancs. *Cancer Res* **1986**, *46*, 6387–6392.
(63) Hashida, M. Advocation and Advancements of EPR Effect Theory in Drug Delivery Science: A Commentary. *J. Controlled Release* **2022**, *346*, 355–357. https://doi.org/10.1016/j.jconrel.2022.04.031.
(64) Majidpoor, J.; Mortezaee, K. Angiogenesis as a Hallmark of Solid Tumors - Clinical Perspectives. *Cell. Oncol.* **2021**, *44* (4), 715–737. https://doi.org/10.1007/s13402-021-00602-3.
(65) Makrilia, N.; Lappa, T.; Xyla, V.; Nikolaidis, I.; Syrigos, K. The Role of Angiogenesis in Solid Tumours: An Overview. *Eur. J. Intern. Med.* **2009**, *20* (7), 663–671. https://doi.org/10.1016/j.ejim.2009.07.009.
(66) Dvorak, H. F.; Nagy, J. A.; Dvorak, J. T.; Dvorak, A. M. Identification and Characterization of the Blood Vessels of Solid Tumors That Are Leaky to Circulating Macromolecules. *Am. J. Pathol.* **1988**, *133* (1), 95–109.
(67) Sindhwani, S.; Syed, A. M.; Ngai, J.; Kingston, B. R.; Maiorino, L.; Rothschild, J.; MacMillan, P.; Zhang, Y.; Rajesh, N. U.; Hoang, T.; Wu, J. L. Y.; Wilhelm, S.; Zilman, A.; Gadde, S.; Sulaiman, A.; Ouyang, B.; Lin, Z.; Wang, L.; Egeblad, M.; Chan, W. C. W. The Entry of Nanoparticles into Solid Tumours. *Nat. Mater.* **2020**, *19* (5), 566–575. https://doi.org/10.1038/s41563-019-0566-2.
(68) Leu, A. J.; Berk, D. A.; Lymboussaki, A.; Alitalo, K.; Jain, R. K. Absence of Functional Lymphatics within a Murine Sarcoma: A Molecular and Functional Evaluation1. *Cancer Res.* **2000**, *60* (16), 4324–4327.

(69) Maeda, H.; Wu, J.; Sawa, T.; Matsumura, Y.; Hori, K. Tumor Vascular Permeability and the EPR Effect in Macromolecular Therapeutics: A Review. *J. Controlled Release* **2000**, *65* (1), 271–284. https://doi.org/10.1016/S0168-3659(99)00248-5.
(70) Wu, J.; Akaike, T.; Hayashida, K.; Okamoto, T.; Okuyama, A.; Maeda, H. Enhanced Vascular Permeability in Solid Tumor Involving Peroxynitrite and Matrix Metalloproteinases. *Jpn. J. Cancer Res.* **2001**, *92* (4), 439–451. https://doi.org/10.1111/j.1349-7006.2001.tb01114.x.
(71) Wu, J.; Akaike, T.; Hayashida, K.; Miyamoto, Y.; Nakagawa, T.; Miyakawa, K.; Müller-Esterl, W.; Maeda, H. Identification of Bradykinin Receptors in Clinical Cancer Specimens and Murine Tumor Tissues. *Int. J. Cancer* **2002**, *98* (1), 29–35. https://doi.org/10.1002/ijc.10142.
(72) Wu, J.; Akaike, T.; Maeda, H. Modulation of Enhanced Vascular Permeability in Tumors by a Bradykinin Antagonist, a Cyclooxygenase Inhibitor, and a Nitric Oxide Scavenger1. *Cancer Res.* **1998**, *58* (1), 159–165.
(73) Hamed, E. A.; El-Noweihi, A. M.; Mohamed, A. Z.; Mahmoud, A. Vasoactive Mediators (VEGF and TNF-Alpha) in Patients with Malignant and Tuberculous Pleural Effusions. *Respirol. Carlton Vic* **2004**, *9* (1), 81–86. https://doi.org/10.1111/j.1440-1843.2003.00529.x.
(74) Stockhofe, K.; Postema, J. M.; Schieferstein, H.; Ross, T. L. Radiolabeling of Nanoparticles and Polymers for PET Imaging. *Pharmaceuticals* **2014**, *7* (4), 392–418. https://doi.org/10.3390/ph7040392.
(75) Acharya, S.; Sahoo, S. K. PLGA Nanoparticles Containing Various Anticancer Agents and Tumour Delivery by EPR Effect. *Adv. Drug Deliv. Rev.* **2011**, *63* (3), 170–183. https://doi.org/10.1016/j.addr.2010.10.008.
(76) Maruyama, K. Intracellular Targeting Delivery of Liposomal Drugs to Solid Tumors Based on EPR Effects. *Adv. Drug Deliv. Rev.* **2011**, *63* (3), 161–169. https://doi.org/10.1016/j.addr.2010.09.003.
(77) Ishima, Y.; Chen, D.; Fang, J.; Maeda, H.; Minomo, A.; Kragh-Hansen, U.; Kai, T.; Maruyama, T.; Otagiri, M. S-Nitrosated Human Serum Albumin Dimer Is Not Only a Novel Anti-Tumor Drug but Also a Potentiator for Anti-Tumor Drugs with Augmented EPR Effects. *Bioconjug. Chem.* **2012**, *23* (2), 264–271. https://doi.org/10.1021/bc2005363.
(78) Yamamoto, M.; Kurino, T.; Matsuda, R.; Jones, H. S.; Nakamura, Y.; Kanamori, T.; Tsuji, A. B.; Sugyo, A.; Tsuda, R.; Matsumoto, Y.; Sakurai, Y.; Suzuki, H.; Sano, M.; Osada, K.; Uehara, T.; Ishii, Y.; Akita, H.; Arano, Y.; Hisaka, A.; Hatakeyama, H. Delivery of aPD-L1 Antibody to i.p. Tumors via Direct Penetration by i.p. Route: Beyond EPR Effect. *J. Controlled Release* **2022**, *352*, 328–337. https://doi.org/10.1016/j.jconrel.2022.10.032.
(79) Maeda, H.; Nakamura, H.; Fang, J. The EPR Effect for Macromolecular Drug Delivery to Solid Tumors: Improvement of Tumor Uptake, Lowering of Systemic Toxicity, and Distinct Tumor Imaging in Vivo. *Adv. Drug Deliv. Rev.* **2013**, *65* (1), 71–79. https://doi.org/10.1016/j.addr.2012.10.002.
(80) Maeda, H. The 35th Anniversary of the Discovery of EPR Effect: A New Wave of Nanomedicines for Tumor-Targeted Drug Delivery—Personal Remarks and Future Prospects. *J. Pers. Med.* **2021**, *11* (3), 229. https://doi.org/10.3390/jpm11030229.
(81) Kang, H.; Rho, S.; Stiles, W. R.; Hu, S.; Baek, Y.; Hwang, D. W.; Kashiwagi, S.; Kim, M. S.; Choi, H. S. Size-Dependent EPR Effect of Polymeric Nanoparticles on Tumor Targeting. *Adv. Healthc. Mater.* **2020**, *9* (1), 1901223. https://doi.org/10.1002/adhm.201901223.
(82) Therrien, B.; Süss-Fink, G.; Govindaswamy, P.; Renfrew, A. K.; Dyson, P. J. The "Complex-in-a-Complex" Cations [(Acac)2M⊂Ru6(p-iPrC6H4Me)6(Tpt)2(Dhbq)3]6+: A Trojan Horse for Cancer Cells. *Angew. Chem. Int. Ed.* **2008**, *47* (20), 3773–3776. https://doi.org/10.1002/anie.200800186.
(83) Cram, D. J. Cavitands: Organic Hosts with Enforced Cavities. *Science* **1983**, *219* (4589), 1177–1183. https://doi.org/10.1126/science.219.4589.1177.
(84) Mattsson, J.; Govindaswamy, P.; Furrer, J.; Sei, Y.; Yamaguchi, K.; Süss-Fink, G.; Therrien, B. Encapsulation of Aromatic Molecules in Hexanuclear Arene Ruthenium Cages: A Strategy to Build Up Organometallic Carceplex Prisms with a Dangling Arm Standing Out. *Organometallics* **2008**, *27* (17), 4346–4356. https://doi.org/10.1021/om800419s.

(85) Yi, J. W.; Barry, N. P. E.; Furrer, M. A.; Zava, O.; Dyson, P. J.; Therrien, B.; Kim, B. H. Delivery of Floxuridine Derivatives to Cancer Cells by Water-Soluble Organometallic Cages. *Bioconjug. Chem.* **2012**, *23* (3), 461–471. https://doi.org/10.1021/bc200472n.

(86) Pitto-Barry, A.; Barry, N. P. E.; Russo, V.; Heinrich, B.; Donnio, B.; Therrien, B.; Deschenaux, R. Designing Supramolecular Liquid-Crystalline Hybrids from Pyrenyl-Containing Dendrimers and Arene Ruthenium Metallacycles. *J. Am. Chem. Soc.* **2014**, *136* (50), 17616–17625. https://doi.org/10.1021/ja510338r.

(87) Pitto-Barry, A.; Barry, N. P. E.; Zava, O.; Deschenaux, R.; Dyson, P. J.; Therrien, B. Double Targeting of Tumours with Pyrenyl-Modified Dendrimers Encapsulated in an Arene-Ruthenium Metallaprism. *Chem. - Eur. J.* **2011**, *17* (6), 1966–1971. https://doi.org/10.1002/chem.201002634.

(88) Pitto-Barry, A.; Barry, N. P. E.; Zava, O.; Deschenaux, R.; Therrien, B. Encapsulation of Pyrene-Functionalized Poly(Benzyl Ether) Dendrons into a Water-Soluble Organometallic Cage. *Chem. - Asian J.* **2011**, *6* (6), 1595–1603. https://doi.org/10.1002/asia.201100136.

(89) Pitto-Barry, A.; Zava, O.; Dyson, P. J.; Deschenaux, R.; Therrien, B. Enhancement of Cytotoxicity by Combining Pyrenyl-Dendrimers and Arene Ruthenium Metallacages. *Inorg. Chem.* **2012**, *51* (13), 7119–7124. https://doi.org/10.1021/ic202739d.

(90) Furrer, M. A.; Schmitt, F.; Wiederkehr, M.; Juillerat-Jeanneret, L.; Therrien, B. Cellular Delivery of Pyrenyl-Arene Ruthenium Complexes by a Water-Soluble Arene Ruthenium Metalla-Cage. *Dalton Trans.* **2012**, *41* (24), 7201. https://doi.org/10.1039/c2dt30193h.

(91) Mattsson, J.; Zava, O.; Renfrew, A. K.; Sei, Y.; Yamaguchi, K.; Dyson, P. J.; Therrien, B. Drug Delivery of Lipophilic Pyrenyl Derivatives by Encapsulation in a Water Soluble Metalla-Cage. *Dalton Trans.* **2010**, *39* (35), 8248. https://doi.org/10.1039/c0dt00436g.

(92) Mohajer, F.; M. Heravi, M.; Zadsirjan, V.; Poormohammad, N. Copper-Free Sonogashira Cross-Coupling Reactions: An Overview. *RSC Adv.* **2021**, *11* (12), 6885–6925. https://doi.org/10.1039/D0RA10575A.

(93) Baba, M.; Saitoh, M.; Kowaka, Y.; Taguma, K.; Yoshida, K.; Semba, Y.; Kasahara, S.; Yamanaka, T.; Ohshima, Y.; Hsu, Y.-C.; Lin, S. H. Vibrational and Rotational Structure and Excited-State Dynamics of Pyrene. *J. Chem. Phys.* **2009**, *131* (22), 224318. https://doi.org/10.1063/1.3270136.

(94) Groves, P. Diffusion Ordered Spectroscopy (DOSY) as Applied to Polymers. *Polym. Chem.* **2017**, *8* (44), 6700–6708. https://doi.org/10.1039/C7PY01577A.

(95) Freudenreich, J.; Furrer, J.; Süss-Fink, G.; Therrien, B. Template-Directed Synthesis of Hexanuclear Arene Ruthenium Complexes with Trigonal-Prismatic Architecture Based on 2,4,6-Tris(3-Pyridyl)Triazine Ligands. *Organometallics* **2011**, *30* (5), 942–951. https://doi.org/10.1021/om100920v.

(96) Furrer, M. A.; Schmitt, F.; Wiederkehr, M.; Juillerat-Jeanneret, L.; Therrien, B. Cellular Delivery of Pyrenyl-Arene Ruthenium Complexes by a Water-Soluble Arene Ruthenium Metalla-Cage. *Dalton Trans.* **2012**, *41* (24), 7201. https://doi.org/10.1039/c2dt30193h.

(97) Pitto-Barry, A.; Barry, N. P. E.; Zava, O.; Deschenaux, R.; Dyson, P. J.; Therrien, B. Double Targeting of Tumours with Pyrenyl-Modified Dendrimers Encapsulated in an Arene–Ruthenium Metallaprism. *Chem. – Eur. J.* **2011**, *17* (6), 1966–1971. https://doi.org/10.1002/chem.201002634.

(98) Mattsson, J.; Govindaswamy, P.; Renfrew, A. K.; Dyson, P. J.; Štěpnička, P.; Süss-Fink, G.; Therrien, B. Synthesis, Molecular Structure, and Anticancer Activity of Cationic Arene Ruthenium Metallarectangles. *Organometallics* **2009**, *28* (15), 4350–4357. https://doi.org/10.1021/om900359j.

(99) Vajpayee, V.; Yang, Y. J.; Kang, S. C.; Kim, H.; Kim, I. S.; Wang, M.; Stang, P. J.; Chi, K.-W. Hexanuclear Self-Assembled Arene-Ruthenium Nano-Prismatic Cages: Potential Anticancer Agents. *Chem. Commun.* **2011**, *47* (18), 5184. https://doi.org/10.1039/c1cc10167f.

(100) Barry, N. P. E.; Therrien, B. Host–Guest Chemistry in the Hexanuclear (Arene)Ruthenium Metalla-Prismatic Cage $[Ru_6(p\text{-cymene})_6(Tpt)_2(Dhnq)_3]^{6+}$. *Eur. J. Inorg. Chem.* **2009**, *2009* (31), 4695–4700. https://doi.org/10.1002/ejic.200900649.

(101) Schmitt, F.; Freudenreich, J.; Barry, N. P. E.; Juillerat-Jeanneret, L.; Süss-Fink, G.; Therrien, B. Organometallic Cages as Vehicles for Intracellular Release of Photosensitizers. *J. Am. Chem. Soc.* **2012**, *134* (2), 754–757. https://doi.org/10.1021/ja207784t.

(102) Gallardo-Villagrán, M.; Paulus, L.; Charissoux, J.-L.; Leger, D. Y.; Vergne-Salle, P.; Therrien, B.; Liagre, B. Ruthenium-Based Assemblies Incorporating Tetrapyridylporphyrin Panels: A Photosensitizer Delivery Strategy for the Treatment of Rheumatoid Arthritis by Photodynamic Therapy. *Dalton Trans.* **2022**, *51* (25), 9673–9680. https://doi.org/10.1039/D2DT00917J.

(103) Mannancherril, V.; Therrien, B. Strategies toward the Enhanced Permeability and Retention Effect by Increasing the Molecular Weight of Arene Ruthenium Metallaassemblies. *Inorg. Chem.* **2018**, *57* (7), 3626–3633. https://doi.org/10.1021/acs.inorgchem.7b02668.

(104) Wang, M.; Vajpayee, V.; Shanmugaraju, S.; Zheng, Y.-R.; Zhao, Z.; Kim, H.; Mukherjee, P. S.; Chi, K.-W.; Stang, P. J. Coordination-Driven Self-Assembly of M3L2 Trigonal Cages from Preorganized Metalloligands Incorporating Octahedral Metal Centers and Fluorescent Detection of Nitroaromatics. *Inorg. Chem.* **2011**, *50* (4), 1506–1512. https://doi.org/10.1021/ic1020719.

(105) Gianferrara, T.; Bergamo, A.; Bratsos, I.; Milani, B.; Spagnul, C.; Sava, G.; Alessio, E. Ruthenium−Porphyrin Conjugates with Cytotoxic and Phototoxic Antitumor Activity. *J. Med. Chem.* **2010**, *53* (12), 4678–4690. https://doi.org/10.1021/jm1002588.

(106) Kamkaew, A.; Lim, S. H.; Lee, H. B.; Kiew, L. V.; Chung, L. Y.; Burgess, K. BODIPY Dyes in Photodynamic Therapy. *Chem Soc Rev* **2013**, *42* (1), 77–88. https://doi.org/10.1039/C2CS35216H.

(107) Gallardo-Villagrán, M.; Paulus, L.; Champavier, Y.; Leger, D. Y.; Therrien, B.; Liagre, B. Combination of Tetrapyridylporphyrins and Arene Ruthenium(II) Complexes to Treat Synovial Sarcoma by Photodynamic Therapy. *J. Porphyr. Phthalocyanines* **2022**, *26* (08n09), 533–541. https://doi.org/10.1142/S1088424622500018.

(108) Berlman, I. B. *Handbook of Fluorescence Spectra of Aromatic Molecules*, 2nd ed.; Academic Press, 1971.

(109) Seybold, P. G.; Gouterman, M. Porphyrins: XIII: Fluorescence Spectra and Quantum Yields. *J. Mol. Spectrosc.* **1969**, *31* (1), 1–13. https://doi.org/10.1016/0022-2852(69)90335-X.

(110) Shirdel, J.; Penzkofer, A.; Procházka, R.; Shen, Z.; Strauss, J.; Daub, J. Absorption and Emission Spectroscopic Characterisation of a Pyrene-Flavin Dyad. *Chem. Phys.* **2007**, *331* (2–3), 427–437. https://doi.org/10.1016/j.chemphys.2006.11.014.

(111) Ojima, I.; Geng, X.; Wu, X.; Qu, C.; Borella, C. P.; Xie, H.; Wilhelm, S. D.; Leece, B. A.; Bartle, L. M.; Goldmacher, V. S.; Chari, R. V. J. Tumor-Specific Novel Taxoid−Monoclonal Antibody Conjugates. *J. Med. Chem.* **2002**, *45* (26), 5620–5623. https://doi.org/10.1021/jm025540g.

(112) Leamon, C. P.; Reddy, J. A. Folate-Targeted Chemotherapy. *Adv. Drug Deliv. Rev.* **2004**, *56* (8), 1127–1141. https://doi.org/10.1016/j.addr.2004.01.008.

(113) Wei, L.; He, X.; Shang, X.; Kandawa-Shultz, M.; Shao, G.; Wang, Y. Biotin-Modified Cyclometalated Iridium-Based Photosensitizers as Mitochondria-Targeted Theranostic Agents for Tumor Photodynamic Therapy in Vitro and in Vivo. *Dyes Pigments* **2023**, *219*, 111641. https://doi.org/10.1016/j.dyepig.2023.111641.

(114) Bradley, M. O.; Webb, N. L.; Anthony, F. H.; Devanesan, P.; Witman, P. A.; Hemamalini, S.; Chander, M. C.; Baker, S. D.; He, L.; Horwitz, S. B.; Swindell, C. S. Tumor Targeting by Covalent Conjugation of a Natural Fatty Acid to Paclitaxel. *Clin. Cancer Res. Off. J. Am. Assoc. Cancer Res.* **2001**, *7* (10), 3229–3238.

(115) Chu, T. C.; Marks, J. W.; Lavery, L. A.; Faulkner, S.; Rosenblum, M. G.; Ellington, A. D.; Levy, M. Aptamer:Toxin Conjugates That Specifically Target Prostate Tumor Cells. *Cancer Res.* **2006**, *66* (12), 5989–5992. https://doi.org/10.1158/0008-5472.CAN-05-4583.

(116) Nagy, A.; Schally, A. V.; Halmos, G.; Armatis, P.; Cai, R.-Z.; Csernus, V.; Kovács, M.; Koppán, M.; Szepesházi, K.; Kahán, Z. Synthesis and Biological Evaluation of Cytotoxic Analogs of Somatostatin Containing Doxorubicin or Its Intensely Potent Derivative, 2-Pyrrolinodoxorubicin. *Proc. Natl. Acad. Sci.* **1998**, *95* (4), 1794–1799. https://doi.org/10.1073/pnas.95.4.1794.

(117) Russell-Jones, G.; McTavish, K.; McEwan, J.; Rice, J.; Nowotnik, D. Vitamin-Mediated Targeting as a Potential Mechanism to Increase Drug Uptake by Tumours. *J. Inorg. Biochem.* **2004**, *98* (10), 1625–1633. https://doi.org/10.1016/j.jinorgbio.2004.07.009.
(118) Bildstein, L.; Dubernet, C.; Couvreur, P. Prodrug-Based Intracellular Delivery of Anticancer Agents. *Adv. Drug Deliv. Rev.* **2011**, *63* (1–2), 3–23. https://doi.org/10.1016/j.addr.2010.12.005.
(119) Pelegri-O'Day, E. M.; Lin, E.-W.; Maynard, H. D. Therapeutic Protein–Polymer Conjugates: Advancing Beyond PEGylation. *J. Am. Chem. Soc.* **2014**, *136* (41), 14323–14332. https://doi.org/10.1021/ja504390x.
(120) Owens, D. E.; Peppas, N. A. Opsonization, Biodistribution, and Pharmacokinetics of Polymeric Nanoparticles. *Int. J. Pharm.* **2006**, *307* (1), 93–102. https://doi.org/10.1016/j.ijpharm.2005.10.010.
(121) Bukowski, K.; Kciuk, M.; Kontek, R. Mechanisms of Multidrug Resistance in Cancer Chemotherapy. *Int. J. Mol. Sci.* **2020**, *21* (9), 3233. https://doi.org/10.3390/ijms21093233.
(122) Robey, R. W.; Pluchino, K. M.; Hall, M. D.; Fojo, A. T.; Bates, S. E.; Gottesman, M. M. Revisiting the Role of ABC Transporters in Multidrug-Resistant Cancer. *Nat. Rev. Cancer* **2018**, *18* (7), 452–464. https://doi.org/10.1038/s41568-018-0005-8.
(123) Castano, A. P.; Mroz, P.; Hamblin, M. R. Photodynamic Therapy and Anti-Tumour Immunity. *Nat. Rev. Cancer* **2006**, *6* (7), 535–545. https://doi.org/10.1038/nrc1894.
(124) McFarland, S. A.; Mandel, A.; Dumoulin-White, R.; Gasser, G. Metal-Based Photosensitizers for Photodynamic Therapy: The Future of Multimodal Oncology? *Curr. Opin. Chem. Biol.* **2020**, *56*, 23–27. https://doi.org/10.1016/j.cbpa.2019.10.004.
(125) Karges, J.; Basu, U.; Blacque, O.; Chao, H.; Gasser, G. Polymeric Encapsulation of Novel Homoleptic Bis(Dipyrrinato) Zinc(II) Complexes with Long Lifetimes for Applications as Photodynamic Therapy Photosensitisers. *Angew. Chem. Int. Ed Engl.* **2019**, *58* (40), 14334–14340. https://doi.org/10.1002/anie.201907856.
(126) Zhang, J.; Jiang, C.; Figueiró Longo, J. P.; Azevedo, R. B.; Zhang, H.; Muehlmann, L. A. An Updated Overview on the Development of New Photosensitizers for Anticancer Photodynamic Therapy. *Acta Pharm. Sin. B* **2018**, *8* (2), 137–146. https://doi.org/10.1016/j.apsb.2017.09.003.
(127) Niculescu, A.-G.; Grumezescu, A. M. Photodynamic Therapy—An Up-to-Date Review. *Appl. Sci.* **2021**, *11* (8), 3626. https://doi.org/10.3390/app11083626.
(128) Setaro, F.; Wennink, J. W. H.; Mäkinen, P. I.; Holappa, L.; Trohopoulos, P. N.; Ylä-Herttuala, S.; Nostrum, C. F. van; Escosura, A. de la; Torres, T. Amphiphilic Phthalocyanines in Polymeric Micelles: A Supramolecular Approach toward Efficient Third-Generation Photosensitizers. *J. Mater. Chem. B* **2020**, *8* (2), 282–289. https://doi.org/10.1039/C9TB02014D.
(129) Gualdesi, M. S.; Vara, J.; Aiassa, V.; Alvarez Igarzabal, C. I.; Ortiz, C. S. New Poly(Acrylamide) Nanoparticles in the Development of Third Generation Photosensitizers. *Dyes Pigments* **2021**, *184*, 108856. https://doi.org/10.1016/j.dyepig.2020.108856.
(130) Kou, J.; Dou, D.; Yang, L. Porphyrin Photosensitizers in Photodynamic Therapy and Its Applications. *Oncotarget* **2017**, *8* (46), 81591–81603. https://doi.org/10.18632/oncotarget.20189.
(131) Saide, A.; Lauritano, C.; Ianora, A. Pheophorbide a: State of the Art. *Mar. Drugs* **2020**, *18* (5), 257. https://doi.org/10.3390/md18050257.
(132) Ruggiero, E.; Castro, S. A.; Habtemariam, A.; Salassa, L. Upconverting Nanoparticles for the near Infrared Photoactivation of Transition Metal Complexes: New Opportunities and Challenges in Medicinal Inorganic Photochemistry. *Dalton Trans.* **2016**, *45* (33), 13012–13020. https://doi.org/10.1039/C6DT01428C.
(133) Banfi, S.; Caruso, E.; Zaza, S.; Mancini, M.; Gariboldi, M. B.; Monti, E. Synthesis and Photodynamic Activity of a Panel of BODIPY Dyes. *J. Photochem. Photobiol. B* **2012**, *114*, 52–60. https://doi.org/10.1016/j.jphotobiol.2012.05.010.
(134) Wittmershaus, B. P.; Skibicki, J. J.; McLafferty, J. B.; Zhang, Y.-Z.; Swan, S. Spectral Properties of Single BODIPY Dyes in Polystyrene Microspheres and in Solutions. *J. Fluoresc.* **2001**, *11* (2), 119–128. https://doi.org/10.1023/A:1016629518660.

(135) Yi, J. W.; Barry, N. P. E.; Furrer, M. A.; Zava, O.; Dyson, P. J.; Therrien, B.; Kim, B. H. Delivery of Floxuridine Derivatives to Cancer Cells by Water-Soluble Organometallic Cages. *Bioconjug. Chem.* **2012**, *23* (3), 461–471. https://doi.org/10.1021/bc200472n.

(136) Pitto-Barry, A.; Barry, N. P. E.; Zava, O.; Deschenaux, R.; Dyson, P. J.; Therrien, B. Double Targeting of Tumours with Pyrenyl-Modified Dendrimers Encapsulated in an Arene-Ruthenium Metallaprism. *Chem. - Eur. J.* **2011**, *17* (6), 1966–1971. https://doi.org/10.1002/chem.201002634.

(137) Zava, O.; Mattsson, J.; Therrien, B.; Dyson, P. J. Evidence for Drug Release from a Metalla-Cage Delivery Vector Following Cellular Internalisation. *Chem. - Eur. J.* **2010**, *16* (5), 1428–1431. https://doi.org/10.1002/chem.200903216.

(138) Monro, S.; Colón, K. L.; Yin, H.; Roque, J. I.; Konda, P.; Gujar, S.; Thummel, R. P.; Lilge, L.; Cameron, C. G.; McFarland, S. A. Transition Metal Complexes and Photodynamic Therapy from a Tumor-Centered Approach: Challenges, Opportunities, and Highlights from the Development of TLD1433. *Chem. Rev.* **2019**, *119* (2), 797–828. https://doi.org/10.1021/acs.chemrev.8b00211.

(139) Zeng, L.; Gupta, P.; Chen, Y.; Wang, E.; Ji, L.; Chao, H.; Chen, Z.-S. The Development of Anticancer Ruthenium(II) Complexes: From Single Molecule Compounds to Nanomaterials. *Chem. Soc. Rev.* **2017**, *46* (19), 5771–5804. https://doi.org/10.1039/C7CS00195A.

(140) Mahesh, S.; Tang, K.-C.; Raj, M. Amide Bond Activation of Biological Molecules. *Mol. Basel Switz.* **2018**, *23* (10), 2615. https://doi.org/10.3390/molecules23102615.

(141) Rampazzo, E.; Bonacchi, S.; Genovese, D.; Juris, R.; Montalti, M.; Paterlini, V.; Zaccheroni, N.; Dumas-Verdes, C.; Clavier, G.; Méallet-Renault, R.; Prodi, L. Pluronic-Silica (PluS) Nanoparticles Doped with Multiple Dyes Featuring Complete Energy Transfer. *J. Phys. Chem. C* **2014**, *118* (17), 9261–9267. https://doi.org/10.1021/jp501345f.

(142) Otvagin, V. F.; Nyuchev, A. V.; Kuzmina, N. S.; Grishin, I. D.; Gavryushin, A. E.; Romanenko, Y. V.; Koifman, O. I.; Belykh, D. V.; Peskova, N. N.; Shilyagina, N. Y.; Balalaeva, I. V.; Fedorov, A. Yu. Synthesis and Biological Evaluation of New Water-Soluble Photoactive Chlorin Conjugate for Targeted Delivery. *Eur. J. Med. Chem.* **2018**, *144*, 740–750. https://doi.org/10.1016/j.ejmech.2017.12.062.

(143) Pitto-Barry, A.; Zava, O.; Dyson, P. J.; Deschenaux, R.; Therrien, B. Enhancement of Cytotoxicity by Combining Pyrenyl-Dendrimers and Arene Ruthenium Metallacages. *Inorg. Chem.* **2012**, *51* (13), 7119–7124. https://doi.org/10.1021/ic202739d.

(144) Sagara, Y.; Mutai, T.; Yoshikawa, I.; Araki, K. Material Design for Piezochromic Luminescence: Hydrogen-Bond-Directed Assemblies of a Pyrene Derivative. *J. Am. Chem. Soc.* **2007**, *129* (6), 1520–1521. https://doi.org/10.1021/ja0677362.

(145) Kue, C. S.; Ng, S. Y.; Voon, S. H.; Kamkaew, A.; Chung, L. Y.; Kiew, L. V.; Lee, H. B. Recent Strategies to Improve Boron Dipyrromethene (BODIPY) for Photodynamic Cancer Therapy: An Updated Review. *Photochem. Photobiol. Sci.* **2018**, *17* (11), 1691–1708. https://doi.org/10.1039/c8pp00113h.

(146) Freudenreich, J.; Furrer, J.; Süss-Fink, G.; Therrien, B. Template-Directed Synthesis of Hexanuclear Arene Ruthenium Complexes with Trigonal-Prismatic Architecture Based on 2,4,6-Tris(3-Pyridyl)Triazine Ligands. *Organometallics* **2011**, *30* (5), 942–951. https://doi.org/10.1021/om100920v.

(147) Barry, N. P. E.; Furrer, J.; Therrien, B. In- and Out-of-Cavity Interactions by Modulating the Size of Ruthenium Metallarectangles. *Helv. Chim. Acta* **2010**, *93* (7), 1313–1328. https://doi.org/10.1002/hlca.200900422.

(148) Ruggiero, E.; Castro, S. A.; Habtemariam, A.; Salassa, L. Upconverting Nanoparticles for the near Infrared Photoactivation of Transition Metal Complexes: New Opportunities and Challenges in Medicinal Inorganic Photochemistry. *Dalton Trans.* **2016**, *45* (33), 13012–13020. https://doi.org/10.1039/C6DT01428C.

(149) Stolik, S.; Delgado, J. A.; Pérez, A.; Anasagasti, L. Measurement of the Penetration Depths of Red and near Infrared Light in Human “Ex Vivo” Tissues. *J. Photochem. Photobiol. B* **2000**, *57* (2), 90–93. https://doi.org/10.1016/S1011-1344(00)00082-8.

(150) Vajpayee, V.; Yang, Y. J.; Kang, S. C.; Kim, H.; Kim, I. S.; Wang, M.; Stang, P. J.; Chi, K.-W. Hexanuclear Self-Assembled Arene-Ruthenium Nano-Prismatic Cages: Potential Anticancer Agents. *Chem. Commun.* **2011**, *47* (18), 5184. https://doi.org/10.1039/c1cc10167f.

(151) Yildiz, E. A.; Ünlü, B. A.; Karatay, A.; Bozkurt, Y.; Özler, M. E.; Sözmen, F.; Yabaş, E.; Boyacioglu, B.; Ünver, H.; Elmali, A. Two-Photon Absorption Response of Functionalized BODIPY Dyes in Near-IR Region by Tuning Conjugation Length and Meso-Substituents. *ACS Omega* **2023**, *8* (34), 30939–30948. https://doi.org/10.1021/acsomega.3c02314.

(152) Zhang, T.; Lan, R.; Gong, L.; Wu, B.; Wang, Y.; Kwong, D. W. J.; Wong, W.-K.; Wong, K.-L.; Xing, D. An Amphiphilic BODIPY-Porphyrin Conjugate: Intense Two-Photon Absorption and Rapid Cellular Uptake for Two-Photon-Induced Imaging and Photodynamic Therapy. *ChemBioChem* **2015**, *16* (16), 2357–2364. https://doi.org/10.1002/cbic.201500349.

(153) Yan, H.; Süss-Fink, G.; Neels, A.; Stoeckli-Evans, H. Mono-, Di- and Tetra-Nuclear p-Cymeneruthenium Complexes Containing Oxalato Ligands. *J. Chem. Soc. Dalton Trans.* **1997**, No. 22, 4345–4350. https://doi.org/10.1039/a704658h.

(154) Barry, N. P. E.; Edafe, F.; Therrien, B. Anticancer Activity of Tetracationic Arene Ruthenium Metalla-Cycles. *Dalton Trans.* **2011**, *40* (27), 7172. https://doi.org/10.1039/c1dt10489f.

(155) Therrien, B.; Süss-Fink, G.; Govindaswamy, P.; Renfrew, A. K.; Dyson, P. J. The “Complex-in-a-Complex” Cations [(Acac)2M⊂Ru6(p-iPrC6H4Me)6(Tpt)2(Dhbq)3]6+: A Trojan Horse for Cancer Cells. *Angew. Chem. Int. Ed.* **2008**, *47* (20), 3773–3776. https://doi.org/10.1002/anie.200800186.

(156) Barry, N. P. E.; Therrien, B. Host–Guest Chemistry in the Hexanuclear (Arene)Ruthenium Metalla-Prismatic Cage $[Ru_6(p\text{-cymene})_6(Tpt)_2(Dhnq)_3]^{6+}$. *Eur. J. Inorg. Chem.* **2009**, *2009* (31), 4695–4700. https://doi.org/10.1002/ejic.200900649.

(157) Stasiuk, M.; Kozubek, A. Embelin - a Promising Bioactive Compound from the Myrsinaceae Family. *Glob. J. Biochem.* **2011**, *2*, 262–270.

(158) Furrer, M. A.; Furrer, J.; Therrien, B. Physical and Physicochemical Stimuli-Responsive Arene Ruthenium Metallaprism. *Organometallics* **2012**, *31* (8), 3149–3154. https://doi.org/10.1021/om300038g.

(159) Garci, A.; Mbakidi, J.-P.; Chaleix, V.; Sol, V.; Orhan, E.; Therrien, B. Tunable Arene Ruthenium Metallaprisms to Transport, Shield, and Release Porphin in Cancer Cells. *Organometallics* **2015**, *34* (16), 4138–4146. https://doi.org/10.1021/acs.organomet.5b00555.

(160) Yi, J. W.; Barry, N. P. E.; Furrer, M. A.; Zava, O.; Dyson, P. J.; Therrien, B.; Kim, B. H. Delivery of Floxuridine Derivatives to Cancer Cells by Water-Soluble Organometallic Cages. *Bioconjug. Chem.* **2012**, *23* (3), 461–471. https://doi.org/10.1021/bc200472n.

(161) Pitto-Barry, A.; Zava, O.; Dyson, P. J.; Deschenaux, R.; Therrien, B. Enhancement of Cytotoxicity by Combining Pyrenyl-Dendrimers and Arene Ruthenium Metallacages. *Inorg. Chem.* **2012**, *51* (13), 7119–7124. https://doi.org/10.1021/ic202739d.

(162) Schmitt, F.; Barry, N. P. E.; Juillerat-Jeanneret, L.; Therrien, B. Efficient Photodynamic Therapy of Cancer Using Chemotherapeutic Porphyrin–Ruthenium Metalla-Cubes. *Bioorg. Med. Chem. Lett.* **2012**, *22* (1), 178–180. https://doi.org/10.1016/j.bmcl.2011.11.058.

(163) Barry, N. P. E.; Zava, O.; Furrer, J.; Dyson, P. J.; Therrien, B. Anticancer Activity of Opened Arene Ruthenium Metalla-Assemblies. *Dalton Trans.* **2010**, *39* (22), 5272. https://doi.org/10.1039/c001521k.

(164) Gallardo-Villagrán, M.; Paulus, L.; Charissoux, J.-L.; Leger, D. Y.; Vergne-Salle, P.; Therrien, B.; Liagre, B. Ruthenium-Based Assemblies Incorporating Tetrapyridylporphyrin Panels: A Photosensitizer Delivery Strategy for the Treatment of Rheumatoid Arthritis by Photodynamic Therapy. *Dalton Trans.* **2022**, *51* (25), 9673–9680. https://doi.org/10.1039/D2DT00917J.

(165) Testa, M. L.; Zaballos, E.; Zaragozá, R. J. Reactivity of β-Amino Alcohols against Dialkyl Oxalate: Synthesis and Mechanism Study in the Formation of Substituted Oxalamide and/or Morpholine-2,3-Dione Derivatives. *Tetrahedron* **2012**, *68* (47), 9583–9591. https://doi.org/10.1016/j.tet.2012.09.067.

(166) Garci, A.; Dobrov, A. A.; Riedel, T.; Orhan, E.; Dyson, P. J.; Arion, V. B.; Therrien, B. Strategy to Optimize the Biological Activity of Arene Ruthenium Metalla-Assemblies. *Organometallics* **2014**, *33* (14), 3813–3822. https://doi.org/10.1021/om5005176.

(167) Govindaswamy, P.; Linder, D.; Lacour, J.; Süss-Fink, G.; Therrien, B. Self-Assembled Hexanuclear Arene Ruthenium Metallo-Prisms with Unexpected Double Helical Chirality. *Chem Commun* **2006**, No. 45, 4691–4693. https://doi.org/10.1039/B610155K.

(168) Ryan, R. T.; Havrylyuk, D.; Stevens, K. C.; Moore, L. H.; Parkin, S.; Blackburn, J. S.; Heidary, D. K.; Selegue, J. P.; Glazer, E. C. Biological Investigations of Ru(II) Complexes with Diverse β-Diketone Ligands. *Eur. J. Inorg. Chem.* **2021**, *2021* (35), 3611–3621. https://doi.org/10.1002/ejic.202100468.

(169) Barry, N. P. E.; Austeri, M.; Lacour, J.; Therrien, B. Highly Efficient NMR Enantiodiscrimination of Chiral Octanuclear Metalla-Boxes in Polar Solvent. *Organometallics* **2009**, *28* (16), 4894–4897. https://doi.org/10.1021/om900461s.

(170) Devaraj, N. K.; Finn, M. G. Introduction: Click Chemistry. *Chem. Rev.* **2021**, *121* (12), 6697–6698. https://doi.org/10.1021/acs.chemrev.1c00469.

(171) Kolb, H. C.; Finn, M. G.; Sharpless, K. B. Click Chemistry: Diverse Chemical Function from a Few Good Reactions. *Angew. Chem. Int. Ed.* **2001**, *40* (11), 2004–2021. https://doi.org/10.1002/1521-3773(20010601)40:11<2004::AID-ANIE2004>3.0.CO;2-5.

(172) Fantoni, N. Z.; El-Sagheer, A. H.; Brown, T. A Hitchhiker's Guide to Click-Chemistry with Nucleic Acids. *Chem. Rev.* **2021**, *121* (12), 7122–7154. https://doi.org/10.1021/acs.chemrev.0c00928.

(173) Hein, C. D.; Liu, X.-M.; Wang, D. Click Chemistry, a Powerful Tool for Pharmaceutical Sciences. *Pharm. Res.* **2008**, *25* (10), 2216–2230. https://doi.org/10.1007/s11095-008-9616-1.

(174) Bennett, M. A.; Smith, A. K. Arene Ruthenium(II) Complexes Formed by Dehydrogenation of Cyclohexadienes with Ruthenium(III) Trichloride. *J. Chem. Soc. Dalton Trans.* **1974**, No. 2, 233–241. https://doi.org/10.1039/DT9740000233.

(175) Barry, N. P. E.; Edafe, F.; Therrien, B. Anticancer Activity of Tetracationic Arene Ruthenium Metalla-Cycles. *Dalton Trans.* **2011**, *40* (27), 7172. https://doi.org/10.1039/c1dt10489f.

(176) Anderson, H. L.; Anderson, S.; Sanders, J. K. M. Ligand Binding by Butadiyne-Linked Porphyrin Dimers, Trimers and Tetramers. *J. Chem. Soc. Perkin 1* **1995**, No. 18, 2231. https://doi.org/10.1039/p19950002231.

(177) Vajpayee, V.; Yang, Y. J.; Kang, S. C.; Kim, H.; Kim, I. S.; Wang, M.; Stang, P. J.; Chi, K.-W. Hexanuclear Self-Assembled Arene-Ruthenium Nano-Prismatic Cages: Potential Anticancer Agents. *Chem. Commun.* **2011**, *47* (18), 5184. https://doi.org/10.1039/c1cc10167f.

(178) Andresen, T. L.; Jolck, R. I.; Albrechtsen, M. Gel Formulations for Guiding Radiotherapy. WO 2014/187962 Al, November 27, 2014.

(179) Kim, Y.-K.; Na, H.-K.; Lee, Y. W.; Jang, H.; Han, S. W.; Min, D.-H. The Direct Growth of Gold Rods on Graphene Thin Films. *Chem. Commun.* **2010**, *46* (18), 3185. https://doi.org/10.1039/c002002h.

(180) Otvagin, V. F.; Nyuchev, A. V.; Kuzmina, N. S.; Grishin, I. D.; Gavryushin, A. E.; Romanenko, Y. V.; Koifman, O. I.; Belykh, D. V.; Peskova, N. N.; Shilyagina, N. Y.; Balalaeva, I. V.; Fedorov, A. Yu. Synthesis and Biological Evaluation of New Water-Soluble Photoactive Chlorin Conjugate for Targeted Delivery. *Eur. J. Med. Chem.* **2018**, *144*, 740–750. https://doi.org/10.1016/j.ejmech.2017.12.062.

(181) Rampazzo, E.; Bonacchi, S.; Genovese, D.; Juris, R.; Montalti, M.; Paterlini, V.; Zaccheroni, N.; Dumas-Verdes, C.; Clavier, G.; Méallet-Renault, R.; Prodi, L. Pluronic-Silica (PluS) Nanoparticles Doped with Multiple Dyes Featuring Complete Energy Transfer. *J. Phys. Chem. C* **2014**, *118* (17), 9261–9267. https://doi.org/10.1021/jp501345f.

(182) Rammo, J.; Schneider, H. Ligand and Cosubstrate Effects on the Hydrolysis of Phosphate Esters and DNA with Lanthanoids. *Liebigs Ann.* **1996**, *1996* (11), 1757–1767. https://doi.org/10.1002/jlac.199619961109.

(183) Garci, A.; Dobrov, A. A.; Riedel, T.; Orhan, E.; Dyson, P. J.; Arion, V. B.; Therrien, B. Strategy to Optimize the Biological Activity of Arene Ruthenium Metalla-Assemblies. *Organometallics* **2014**, *33* (14), 3813–3822. https://doi.org/10.1021/om5005176.

8. Annexes

8.1 Abbreviations

4-tpe	1,3,5-tris(pyridin-4-ylethynyl)benzene
4-tpt	2,4,6-tris(4-pyridyl)-1,3,5-triazine
BOC	*tert*-butyloxycarbonyl
BODIPY	Boron-dipyrromethene
DCM	Dichloromethane, methylene chloride
DMAP	4-Dimethylaminopyridine
DMF	Dimethylformamide
DMSO	Dimethyl sulfoxide
dobq	2,5-dioxydo-1,4-benzoquinonato
donq	5,8-dioxydo-1,4-naphtoquinonato
DOSY	Diffusion ordered spectroscopy
dotq	6,11-dioxydo-5,12-naphtacenedionato
EDCI	1-Ethyl-3-(3-dimethylaminopropyl)carbodiimide
EPR	Enhanced permeability and retention
ESI-MS	Electrospray ionization mass spectrometry
Et_3N	Triethylamine
EtOAc	Ethyl acetate
FCS	First coordination sphere
HOBt	1-Hydroxybenzotriazole
HSQC	Heteronuclear Single Quantum Coherence
MeOH	Methanol
PDT	Photodynamic therapy
PEG	Polyethylene glycol
PI	Phototoxic index
PS	Photosensitizer
ROS	Reactive oxygen species
RT	Room temperature
SCS	Second coordination sphere
TFA	Trifluoroacetic acid
THF	Tetrahydrofuran
tpp	5,10,15,20-tetra(4-pyridyl)-21H,23H-porphyrin

8.2 List of structures

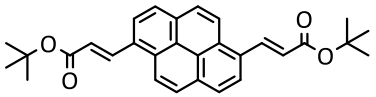

Pyr1

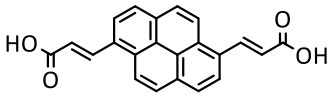

3,3'-(pyrene-1,6-diyl)diacrylic acid

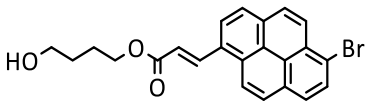

Pyr2

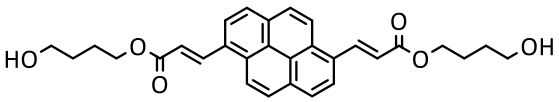

Pyr3

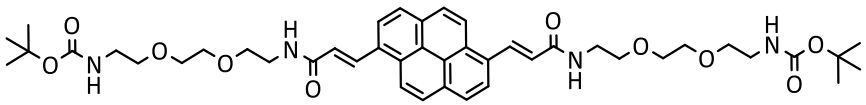

Pyr4

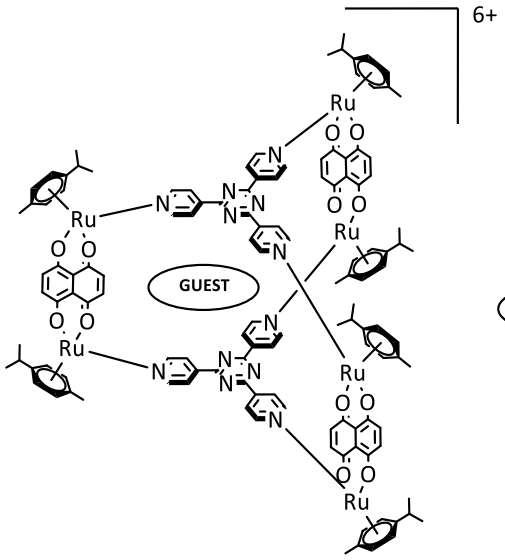

Guest⊂Prism

GUEST =

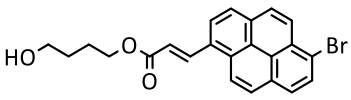

Pyr2

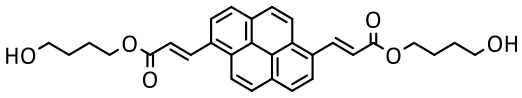

Pyr3

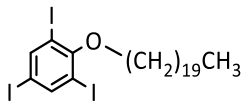

1,3,5-triiodo-2-(icosyloxy)benzene

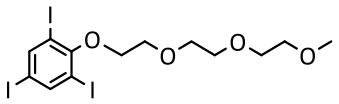

1,3,5-triiodo-2-(2-(2-(2-methoxyethoxy)ethoxy)ethoxy)benzene

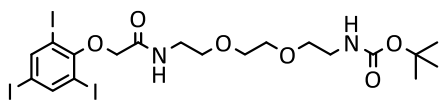

TriPEGboc

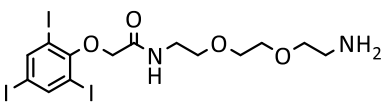

TriPEGNH$_2$

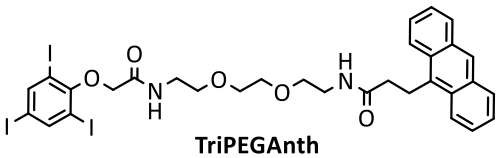

TriPEGAnth

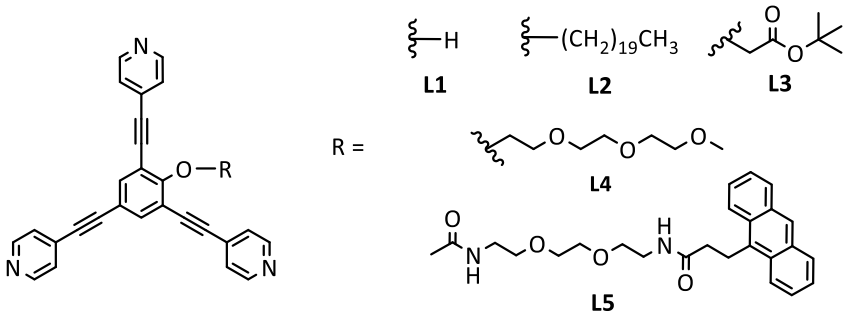

L1 **L2** **L3**

R =

L4

L5

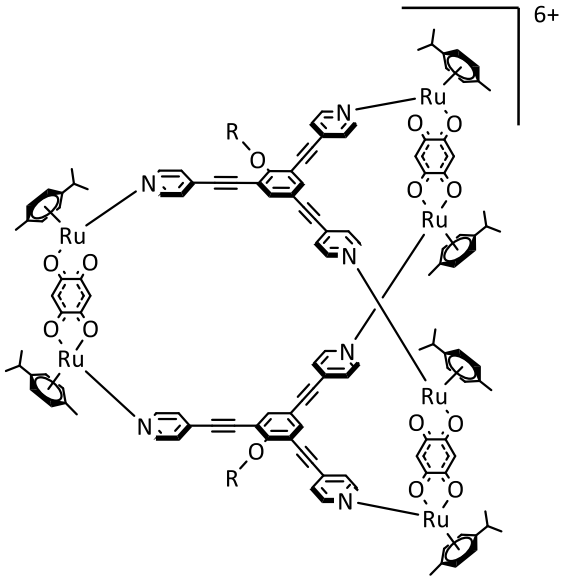

R =

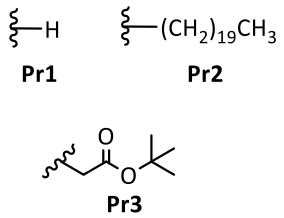

Pr1 **Pr2**

Pr3

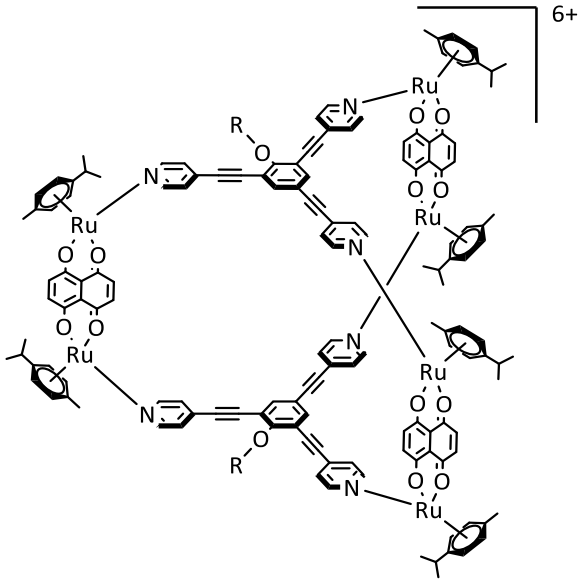

R =

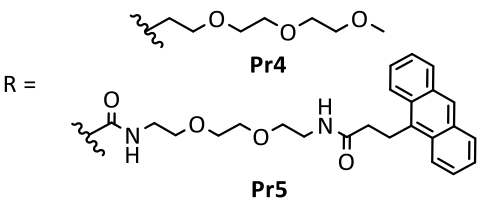

Pr4

Pr5

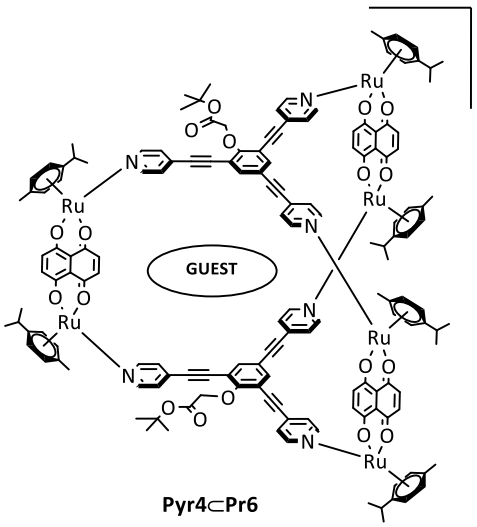

Pyr4⊂Pr6

GUEST =

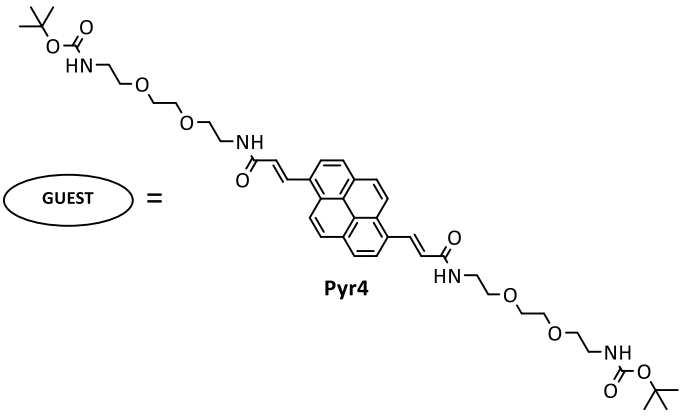

Pyr4

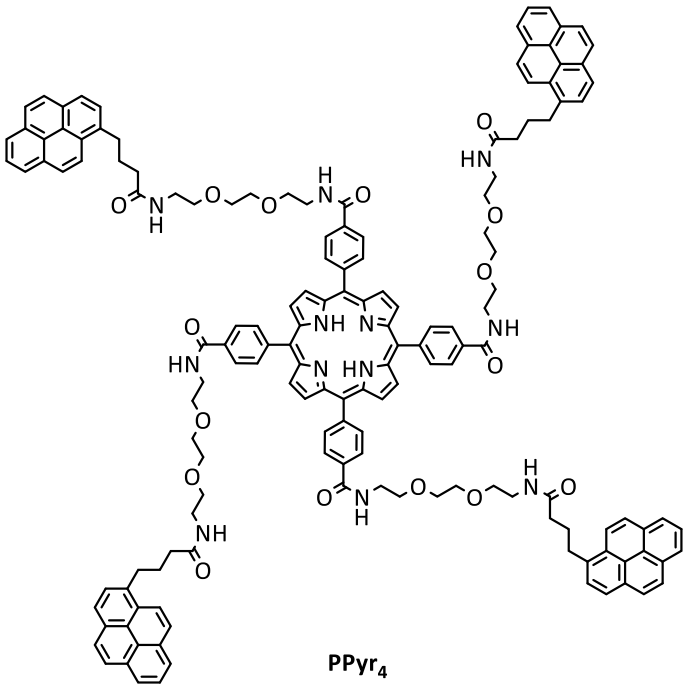

PPyr$_4$

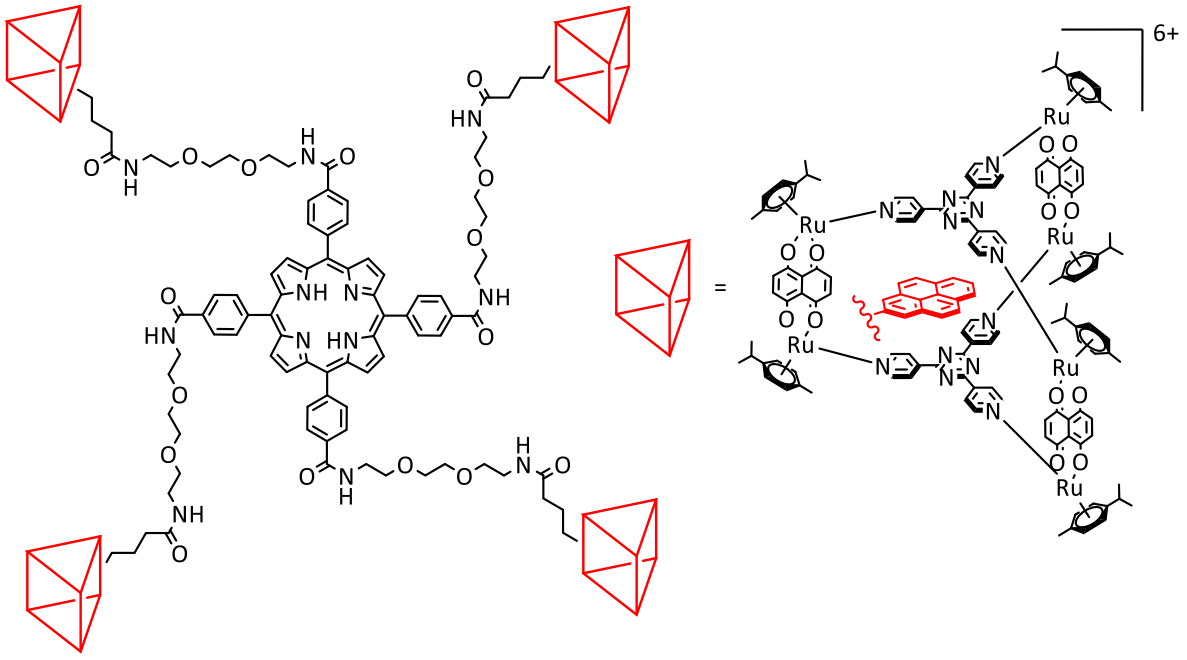

PPyr$_4$⊂Prism$_4$

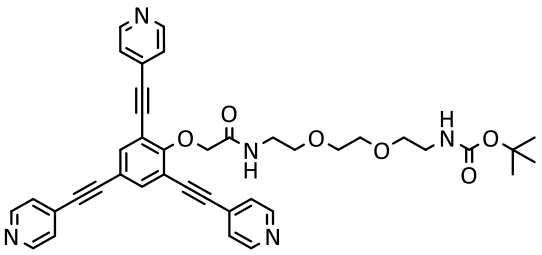

Panel-PEGtert

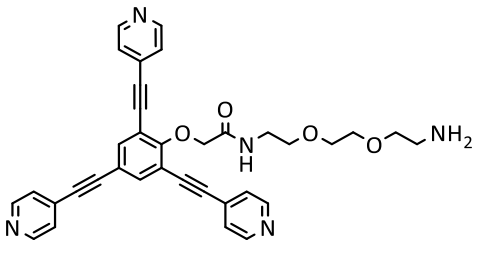

Panel-PEGNH$_2$

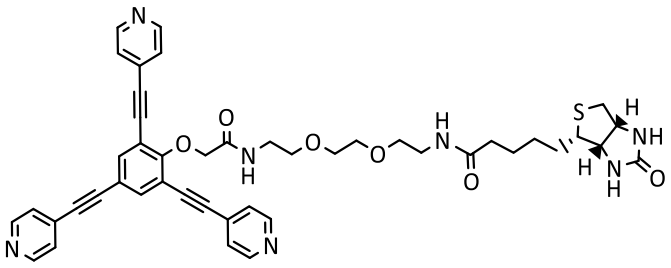

Panel-PEG-Biotin

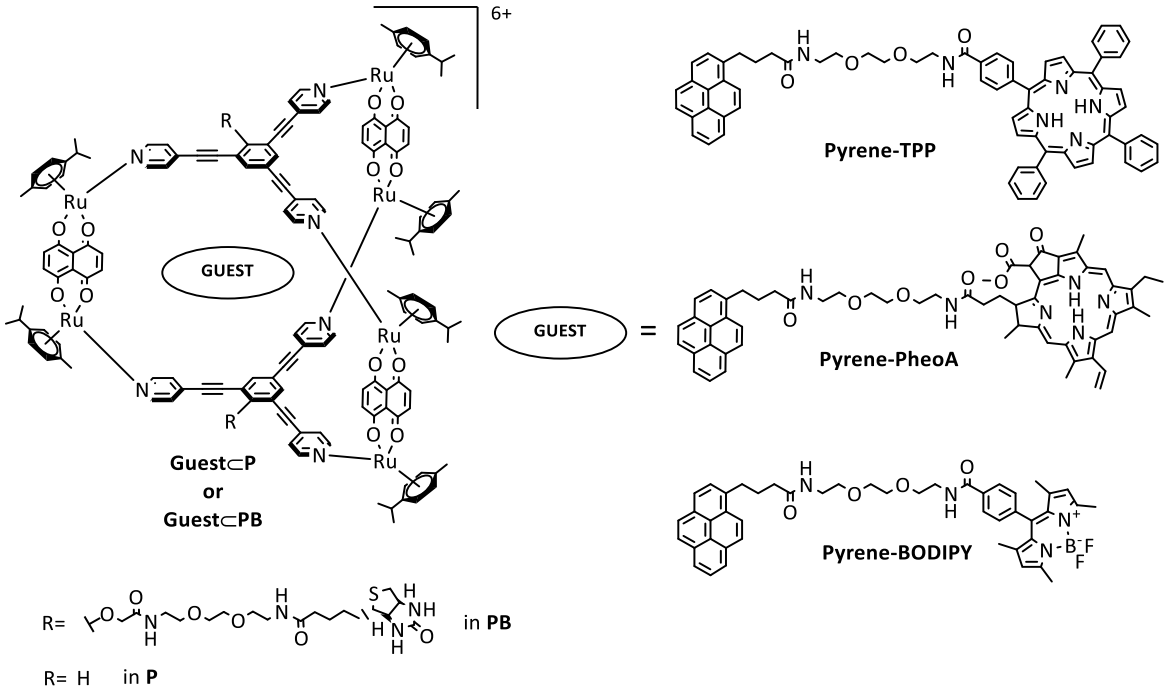

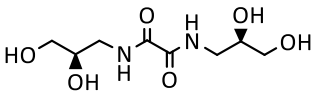

Ox1

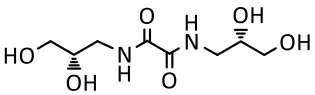

Ox2

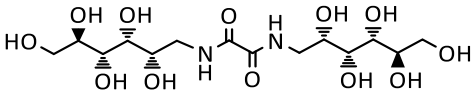

Ox3

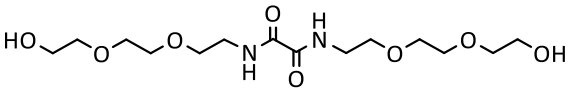

Ox5

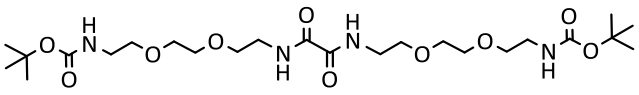

Ox6

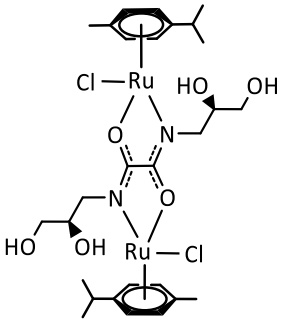

Cx1

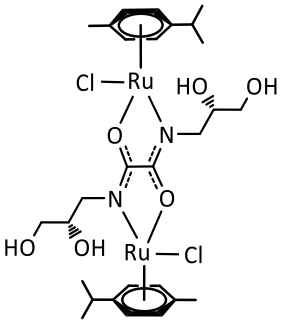

Cx2

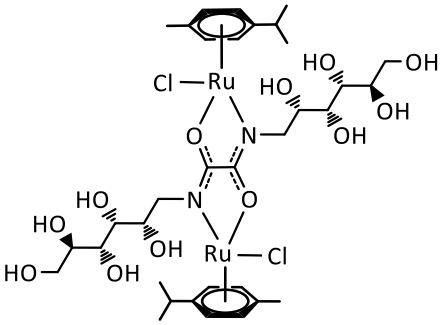

Cx3

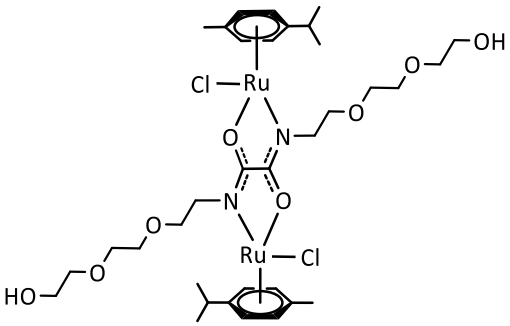

Cx5

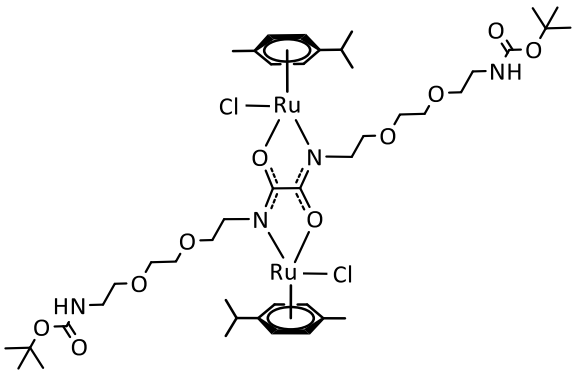

Cx6

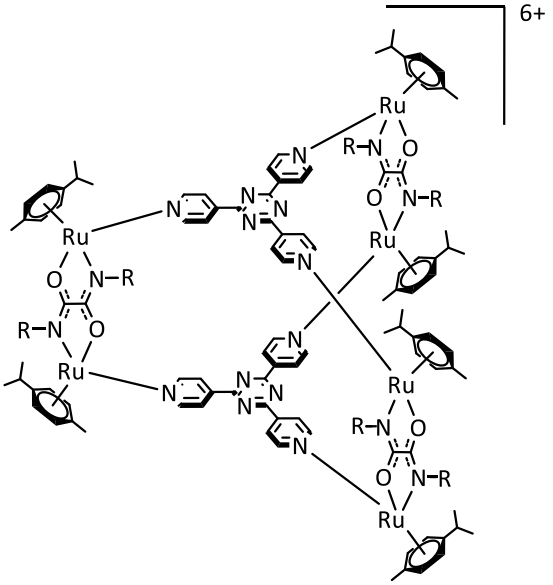
6+
Ru
N
R–N
O
N–R

R =

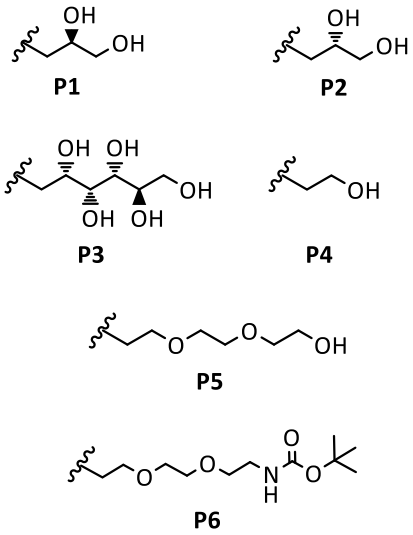
OH
P1
P2
P3
P4
P5
P6

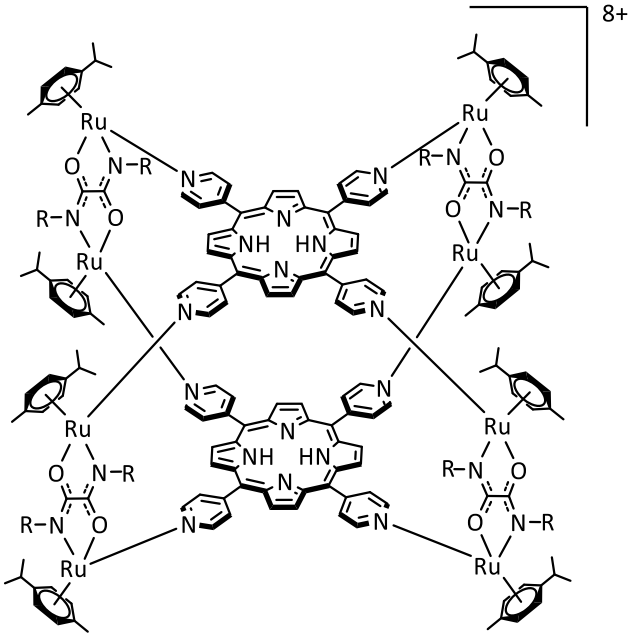
8+
Ru
N
NH
HN
R–N
O
N–R

R =

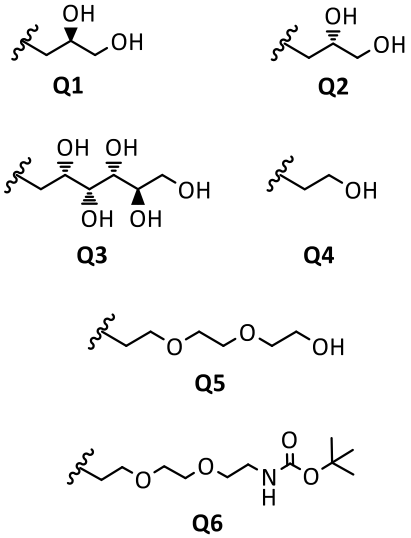
OH
Q1
Q2
Q3
Q4
Q5
Q6